Universidad de la República
Facultad de Ciencias

Majorana neutrinos in an effective lagrangian approach

M.Sc. Lucía Duarte

Tesis presentada para completar los requerimientos del grado de Doctor en Física

Orientador: Dr. Oscar Alfredo Sampayo
Co-Orientador: Dr. Gabriel González Sprinberg

defendida el 24 de marzo de 2017 ante el tribunal integrado por

Dr. Nicolás Wschebor (presidente)
Dr. Pablo Mora
Dr. Esteban Roulet
Dr. Martín Reiris
Dr. O. Alfredo Sampayo (orientador)
Dr. Ernesto Blanco (suplente)

A mi abuelo, Alfredo Pastorino. Un optimista.

Agradecimientos

En primer lugar quiero agradecer a mi orientador Fredy por su gran dedicación y permanente apoyo y a mi coorientador Gabriel por ayudar a viabilizar este proyecto. He aprendido mucho de ustedes en estos años de trabajo.

Agradezco también a mis amigos. A las chicas: a mi hermana Mariana Duarte, Gabriela Tabárez, Lucía Fernández, Ana Inés Zambrana, Amparo Pitier, Mercedes Moltini. A Rodrigo Eyheralde, Andrés Vallejo y Javier Cóppola. Y a todos los amigos que durante los años me ayudaron a aprender cosas.

Gracias a mi novio el franchute. Una inspiración para el trabajo, y una alegría para la vida.

Gracias a toda mi familia, en especial a mis padres por obligarme a desarrollar mi tenacidad.

Agradezco mucho a mis compañeros de trabajo. A los físicos: Rodrigo Eyheralde, Marcela Peláez, Esteban Mato, Nahuel Barrios y Florencia Benítez, gracias por los cursos que tomamos juntos en este tiempo, me divertí mucho. Gracias al resto de los compañeros del IFFI: en la sala alfa Gastón Ayubí, Magdalena Fuentes, Virginia Feldman (e Ignacio Duarte) y a Nicolás Casaballe, Julia Alonso, Ariel Fernández, Javier Pereyra, Agustín Laguarda y Daniel Gau. Y a todos los que de alguna forma u otra me acompañaron en este proceso: profesores, compañeros de clase y estudiantes en la Facultad de Ciencias y en Ingeniería. Y por supuesto también agradezco a las secretarias de Pedeciba-Física y el IFFI: Ana Inés Zambrana, Jimena Rodríguez y Amelia Ferrari, por toda su ayuda con la operativa del doctorado.

Gracias a la gente de Mar del Plata, a todos en el IFIMAR y el Departamento de Física de la Facultad de Ciencias Exactas y Naturales de la UNMDP.

Agradezco también la financiación: a Pedeciba-Física, a la Agencia Nacional de Innovación e Investigación por la beca de doctorado y a la Comisión Acadámica de Posgrado (CAP-UdelaR) por la beca de finalización. Al programa Pasantías en el exterior de CSIC que financió los viajes a Mar del Plata, junto con una beca de la AUGM en 2014. Al Instituto de Física de la Facultad de Ingeniería, por apoyarme con tiempo libre durante este último semestre para dedicarme a la redacción de este trabajo.

Lucía, febrero de 2017.

Resumen

El Modelo Estándar de física de partículas ha logrado explicar con asombrosa precisión las interacciones de los componentes fundamentales del universo conocido. Sin embargo, a partir del descubrimiento del fenómeno de las oscilaciones de neutrinos, sabemos que los neutrinos estándar tienen una masa no nula, del orden de 0,1 eV (seis órdenes de magnitud menor que la masa de los electrones[1]). Ésta es la primer evidencia convincente de física más allá del Modelo Estándar. Para explicar la presencia de masas de los neutrinos el Modelo Estándar puede ser extendido agregando neutrinos derechos singletes del grupo de simetría electrodébil $SU(2)$, que permiten generar términos de masa de Dirac y de Majorana al existir la posibilidad de que estos neutrinos sean su propia antipartícula. Así se generan auto estados de masa livianos (los ya conocidos) y pesados (los neutrinos de Majorana pesados) mediante el mecanismo llamado seesaw (subibaja). Sin embargo, en su versión clásica el mecanismo seesaw sólo logra explicar los pequeñísimos valores de las masas de los neutrinos livianos requiriendo que la mezcla entre estos y los neutrinos pesados sea prácticamente despreciable, haciendo muy difícil la detección de los efectos de los neutrinos de Majorana pesados en diversos experimentos. En estas condiciones cualquier observación de efectos físicos atribuibles a neutrinos de Majorana correspondería a física más allá del mecanismo seesaw. En vista de este escenario, se han propuesto teorías de campos efectivas que introducen neutrinos de Majorana pesados como nuevos grados de libertad, pero modelando sus interacciones con las partículas estándar mediante operadores efectivos que preservan las simetrías de gauge del Modelo Estándar. En esta tesis se estudia la fenomenología de este modelo efectivo en diversos procesos que evidenciarían la existencia de neutrinos de Majorana pesados: se investigaron las predicciones para el ancho de decaimiento total de los neutrinos de Majorana pesados y las fracciones de los distintos canales para masas bajas [2] y altas [3], la producción de neutrinos de Majorana en el propuesto colisionador electrón-protón LHeC (CERN) [4] y la posibilidad de observar procesos mediados por neutrinos de Majorana de masas de algunos GeV en el LHC (CERN) explotando observables de vértices desplazados [5]. Además se estudiaron los efectos sobre la propagación en la Tierra de neutrinos del tau de ultra alta energía, que se pueden observar en el telescopio de neutrinos IceCube [6].

Palabras clave: Neutrinos, Neutrinos de Majorana, Neutrinos estériles, Nueva Física, Teorías de campos efectivas.

[1] El Particle Data Group toma como valor límite indicativo $\frac{m_\nu}{m_\ell} \lesssim 10^{-6}$ para $\ell = e$ [1].

Abstract

The Standard Model of particle physics has been able to explain with overwhelming precision the interactions between the fundamental constituents of the known universe. However, since the discovery of the neutrino oscillation phenomenon, we know standard neutrinos have a non-zero mass, of the order of 0.1 eV (six orders of magnitude below the electron mass[2]). This is the first compelling evidence of physics beyond the Standard Model. In order to explain the presence of neutrino masses the Standard Model can be extended by incorporating right-handed neutrinos, which are singlets under the electroweak symmetry group $SU(2)$ and allow to generate Dirac and Majorana mass terms, as they can be their own antiparticle. This generates light (the known neutrinos) and heavy mass eigenstates (the heavy Majorana neutrinos) by the seesaw mechanism. However, in its classic version the seesaw mechanism can only explain the tiny values for light neutrino masses by requiring the mixing between them and the heavy states to be almost negligible. The detection of any physical effect ascribable to Majorana neutrinos would signal the presence of physics beyond the minimal seesaw mechanism. In view of this scenario, effective field theories have been proposed, incorporating heavy Majorana neutrinos as new degrees of freedom and modeling their interactions with the standard particles by effective operators preserving the Standard Model gauge symmetries. This thesis studies the phenomenology of the effective model in different processes that would indicate the existence of heavy Majorana neutrinos. We studied the predictions for the total decay width of heavy Majorana neutrinos and the branching fractions for the different decay channels for low [2] and high [3] masses, the production of heavy Majorana neutrinos in the proposed electron-proton collider LHeC (CERN) [4] and the possibility to observe Majorana neutrino-mediated processes in the LHC (CERN) for masses around a few GeV exploiting displaced vertices observables [5]. Moreover, we studied the effects on the ultra high energy tau neutrinos propagation through the Earth, that can be observed in the IceCube neutrino telescope [6].

Keywords: Neutrinos, Majorana neutrinos, Sterile neutrinos, New physics, Effective field theories.

[2]The Particle Data Group takes as indicative value $\frac{m_\nu}{m_\ell} \lesssim 10^{-6}$ for $\ell = e$ [1].

Contents

Introduction

The history[3] of neutrinos dates back to the discovery of the nuclear radioactive beta decay, in which a nucleus A decays into another emitting a "beta particle" ($A \to A' + e^-$) and the continuous beta spectrum observation in 1914 by Chadwick. This was a challenging fact, because the momentum and energy conservation in two-body decays determines that all the emitted beta particles -electrons- should have the same energy[4]. This totally unexpected phenomenon led Bohr and Dirac to consider the extreme possibility that energy was not conserved. By the time of 1930, Pauli proposed a remedy for this serious problem: the existence of an electrically neutral, very weakly interacting spin 1/2 particle, which he called the *neutron*. His "neutrons" could solve the problem: being emitted together with the electrons, they would make their spectrum not to be monochromatic ($A \to A' + e^- + n$). The "neutrons" mass had to be less than one percent of the proton mass, in order to be consistent with the measured spectrum.

In 1932 Chadwick discovered the particles we today call neutrons -the companions of the protons forming nuclei- which were found to be the nuclear constituents decaying in the beta process. In 1934 Fermi reformulated Pauli's idea of a very light weakly interacting particle involved in nuclear radioactive decays, renaming it as *neutrino*: "the little neutral one" in Italian. Fermi's famous theory of nuclear beta decay invoked Dirac's antiparticles and Pauli's neutrinos in the form of a quantum field theory, in analogy to quantum electrodynamics. In this theory -today known as Fermi's theory- in the weak interaction neutrons decay to protons via a non-renormalizable four-fermion interaction $n \to p + e^- + \bar{\nu}$, where $\bar{\nu}$ is the electron antineutrino. The electron and the antineutrino are created as a pair, rather than being emitted from the nucleus. Since parity violation was unthinkable at the moment soon the theory was extended by introducing vector and axial-vector parity conserving currents, but also scalar, pseudoscalar and tensor couplings were soon realized to be viable in the Gamow and Teller's extension of Fermi's theory.

Reines and Cowan conducted the Savannah River reactor experiment in 1956 and observed the inverse beta decay, in which an antineutrino (emitted by the reactor in beta decay) gets captured by a proton producing a positron and a neutron. Thus the antineutrinos got detected and this finally settled the existence of Pauli's neutrinos.

First indicated by cosmic rays and accelerator experiments with kaons (the "$\theta - \tau$

[3] This historical introduction is based on several review articles, from which I have mostly followed [7]. The citations to all the classical papers I mention here can be found in references therein.

[4] The kinematics of the final two-body phase-space are discussed in the appendix A.1

puzzle") and then observed in the beta decay of polarized ^{60}Co in 1956, parity violation in weak interactions was confirmed. The possible weak interaction lagrangian became more uncertain until the arrival of the maximal parity violating $V-A$ (vector minus axial vector) chiral coupling theory, formulated in 1958 by Feynman and Gell-Mann, and simultaneously by Sudarshan and Marshak. It could easily be realized in the lepton sector using the two-component theory of a massless neutrino proposed in 1957 by L.Landau, T.D. Lee and C.N. Yang, and Salam (the idea had been developed by Weyl in the 1930s, but Pauli rejected it on the ground that it violated parity). In this theory, as the "two-component" name suggests, neutrinos are left-handed and antineutrinos are right-handed, leading automatically to $V-A$ couplings. Many thought parity violation in weak interactions was due to neutrino's nature: a massless neutrino only has one helicity state. This was experimentally confirmed 1958 in polarized electron capture experiments: the polarization of the neutrino was in the opposite direction to its motion.

The concept of lepton number (L) was introduced in 1953 by Konopinski and Mahmoud to explain certain missing decay modes, assigning distinct lepton numbers to leptons and their antiparticles. While the radiative muon decay process $\mu^- \to e^-\gamma$ is not forbidden by lepton number conservation its experimental limits are very tight and this suggested a *lepton flavor* conservation law, or an independent lepton number for each lepton family. This assignment predicted that if the muon neutrino produced in pion decay $\pi^+ \to \mu^+ + \nu_\mu$ cannot induce e^- then the ν_e and ν_μ are different particles. This idea led to the muon neutrino discovery in 1962. Nowadays the leptons are assigned $L=1$ and antileptons $L=-1$ (for each family $\ell = e,\ \mu,\ \tau$ and including neutrinos). Due to the conservation of the lepton number, for example, in the beta decay of the neutron an electron and an antineutrino are produced.

However, there exist in nature also neutral particles with all charges equal to zero. Examples are the photon, the π^0 meson, etc. In the case of such particles there is no notion of antiparticles (or particles and antiparticles are identical). In 1937 the Italian physicist E. Majorana proposed a theory of truly neutral particles with spin equal to 1/2 (which today are called Majorana particles). Majorana was not satisfied with the existing at that time theory of electrons and positrons in which positrons were considered as holes in the Dirac sea of the states of electrons with negative energies. He wanted to formulate the symmetrical theory in which there is no notion of negative energy states. In the paper "Symmetrical theory of electron and positron" he came also to a theory of spin 1/2 particles in which particles and antiparticles are identical. It is an open problem if the neutrino is a truly neutral Majorana particle or a Dirac particle which possesses a lepton number.

All the experimental findings about the weak interactions were condensed in the formulation of the Glashow-Weinberg-Salam Standard Model (SM) in 1967. Based on an $SU(2)\times U(1)$ gauge symmetry model mixing the weak and electromagnetic interactions and incorporating the Higgs mechanism of mass generation, the theory predicted that the charged current weak interactions took place due to the exchange of massive W bosons coupled to left-handed fields, replacing the four-fermion description of Fermi's theory of beta decay. Another new ingredient was the neutral weak current mediated by the

massive Z boson. The SM neutrinos are left-handed, they do not interact with the Higgs field at all, and thus are massless. The experimental success of the SM was affirmed in 1974 with the discovery of neutral-current neutrino interactions in the Gargamelle bubble chamber experiment at CERN, and the following discovery of the W and Z bosons in the Super Proton Synchrotron (SPS, CERN) in 1983 and 1984. Its last missing piece -the Higgs boson- seems to have been found in the LHC in 2012.

Neutrinos are copiously produced in natural sources: in the burning of the stars, in the interaction of cosmic rays and also as relics of the Big Bang. Starting from the 1960s neutrinos produced in the Sun and in the atmosphere were observed. In 1987 neutrinos from a supernova in the Large Magellanic Cloud were also detected. Indeed an important leading role in this story was played by the neutrinos produced in the Sun and in the atmosphere. The experiments that measured the flux of atmospheric neutrinos found results that suggested the disappearance of muon neutrinos when propagating over distances of the order of hundreds (or more) kilometers. Experiments that measured the flux of solar neutrinos found results that suggested the disappearance of electron neutrinos while propagating within the Sun or between the Sun and the Earth. These results called back to 1968 when Gribov and Pontecorvo realized that flavor oscillations -a change of neutrinos flavor during their propagation- arise if neutrinos are massive and mixed.

The disappearance of both atmospheric ν_μ's and solar ν_e's was most easily explained in terms of neutrino oscillations. The emerging picture was that at least two neutrinos were massive and mixed, unlike what it is predicted in the SM. In the two last decades this picture became fully established with the upcome of a set of precise experiments. In particular, the results obtained with solar and atmospheric neutrinos have been confirmed in experiments using terrestrial beams in which neutrinos produced in nuclear reactors and accelerator facilities have been detected at distances of the order of hundred kilometers. These huge experimental efforts were awarded with the Nobel prize in 2015 to the directors of the SNO and Super-Kamiokande experiments for the discovery of neutrino oscillations. Neutrinos in the SM are truly massless fermions for which no gauge invariant renormalizable mass term can be constructed. Therefore, the experimental evidence for neutrino masses and mixing provided an unambiguous signal of new physics and remains until now as compelling experimental evidence of physics beyond the SM.

From the theoretical point of view, well before the neutrino oscillations discovery, the situation concerning neutrino masses and the mixing problem changed at the end of the 1970s with the appearance of the grand unification theories (GUT). In these models leptons and quarks enter into the same symmetry multiplets and the generation of masses of quarks and charged leptons in some models naturally lead to non-zero neutrino masses. At that time the famous seesaw mechanism of the neutrino mass generation -which could explain the smallness of the neutrino masses with respect to the masses of quarks and charged leptons- was proposed and masses and mixing of neutrinos started to be considered as a signature of the physics beyond the SM.

If one wishes to account for neutrino masses with only the SM degrees of freedom,

one needs Weinberg's dimension five effective operator

$$\mathcal{L}^5 = -\frac{\lambda}{2\Lambda} L_L L_L \phi\ \phi + h.c. \tag{1}$$

where L_L stands for the SM lepton doublet and ϕ is the Higgs field. This operator generates neutrino Majorana masses, and massive neutrino states which are Majorana particles. The non-renormalizable nature of the above operator signals the appearance of new physics through the scale Λ. Its main consequence is the $\Delta L = 2$ violation of lepton number through neutrinoless double beta decay ($0\nu\beta\beta$-decay) -suggested soon after Majorana's classical work by Racah an Furry- and by the production of same-sign lepton pairs in colliders, first suggested in the early eighties by Keung and Senjanovič. With the arrival of the LHC at CERN the same-sign dilepton signal started to receive wide attention.

In the seesaw mechanism neutrino masses are given by the seesaw formula: $m_\nu \sim \frac{Y^2 v^2}{\Lambda}$, where Y is a dimensionless Yukawa constant and $v \sim 250\ GeV$ is the Higgs vacuum expectation value, which characterizes the scale of the violation of the electroweak symmetry. The scale of the lepton number violation (LNV) Λ depends on the value of the Yukawa constants Y which are unknown, but need to be fixed to accommodate the known tiny values of the neutrino masses $m_\nu \sim 0.1\ eV$.

In the most popular renormalizable realization for the Weinberg operator, called Type I seesaw [8–11], the seesaw mechanism takes place by the introduction of right-handed sterile neutrinos that -as they do not have distinct particle and antiparticle degrees of freedom- can have a Majorana mass term leading to the tiny known masses for the standard neutrinos, as long as the Yukawa couplings between the right-handed Majorana neutrinos and the standard ones remain small. For Yukawa couplings of order $Y \sim 1$, we need a Majorana mass scale of order $M_N \sim 10^{15} GeV$ to account for a light ν mass compatible with the current neutrino data, and this fact leads to the decoupling of the Majorana neutrinos. On the other hand, for smaller Yukawa couplings of the order $Y \sim 10^{-8} - 10^{-6}$, sterile neutrinos with masses around $M_N \sim (1 - 1000)\ GeV$ could exist, but in the simplest Type-I seesaw this leads to a negligible left-right neutrino mixing $U_{lN}^2 \sim m_\nu / M_N \sim 10^{-14} - 10^{-10}$. As this mixing parameter is assumed to govern all the Majorana neutrino interactions with the standard particles, this in fact leads to the decoupling of the Majorana physics and makes it almost undetectable in experiments.

This situation has been accommodated in several proposals [12–14] increasing the mixings value to be of order $U_{\ell N} \sim \mathcal{O}(0.1)$ by introducing specific textures to the Majorana mass matrices in the seesaw formula, generally imposing additional symmetries or fine tunning the entries. Many works in the past decade have been devoted to probe the existence of Majorana particles with masses $\simeq 1\ TeV$ through the observation of the mentioned LNV process of same-sign leptons in proton-proton collisions at the LHC in the Type I seesaw scenario [15–23].

On the other hand, currently almost all neutrino oscillations data can be described with the mixing of three flavor neutrino states, implying the existence of three light massive neutrinos ν_j having masses which do not exceed approximately $0.1\ eV$. But since 2001 there have been possible hints on the presence in the mixing of one or more

additional sterile neutrinos with masses at the eV scale. These hints have been obtained in the LSND and MiniBooNE experiments and in short baseline reactor neutrino oscillation data. There are two possible "minimal" phenomenological schemes widely discussed in the literature giving explanations to this anomalies. These are the so called "3+1" and "3+2" models [24], introducing neutrinos which should be Majorana particles, but there exist other proposed explanations. These light sterile neutrino hypotheses are being tested in many experiments, with reactor and accelerator neutrinos and in colliders, but also in the field of neutrino astronomy. Cosmic rays offer an opportunity to study the properties of elementary particles, and a main objective in experiments like IceCube in Antarctica or Auger in Argentina is to determine a flux of neutrinos or cosmic ray nuclei as they interact with terrestrial matter. These interactions involve energies not explored so far at particle colliders, so their study should lead us to a better understanding of that physics, specially concerning neutrino interactions.

In a paper by F.del Águila, S.Bar-Shalom, A.Soni and J.Wudka [15] an alternative effective lagrangian approach for the Majorana neutrinos is proposed. Arguing that the detection of Majorana neutrinos through LNV in colliders would be a signal of physics beyond the minimal seesaw mechanism, the authors propose to describe its interactions in a model-independent approach based on an effective theory, considering the addition of only one relatively light Majorana neutrino with mass $m_N \lesssim 1\ TeV$ and negligible mixing with the left-handed standard neutrinos ν_L. A set of dimension six effective operators preserving the SM symmetries with the Majorana neutrino field as an active degree of freedom is introduced. The study of the phenomenological consequences of these new interactions in high energy colliders and in neutrino telescopes is the purpose of this thesis.

The text is organized as follows. In chapter 1 I introduce the most relevant features of the SM focusing on the electroweak sector and how fermion masses are generated through the Higgs mechanism leading to the Yukawa lagrangian and electroweak currents. The different spinorial field representations are reviewed, in order to introduce Majorana fermions and Majorana masses, which will be the tool for neutrino mass generation. Also, a brief introduction to the effective field theories framework is included. Chapter 2 is devoted to the discussion of massive neutrino physics. It starts with a brief introduction on the discovery of neutrino oscillations and how they are interpreted in terms of non-vanishing neutrino masses. The seesaw mechanism of neutrino mass generation is thoroughly discussed. In particular the Type I seesaw scenario is presented and its shortcomings discussed, in order to motivate the introduction of the new effective lagrangian approach introduced in chapter 3. The goal of this chapter is the derivation of the complete effective lagrangian from the dimension six effective operators introduced in [15] and a discussion on how the existing experimental bounds can be translated to the effective couplings. The original results are presented in the following.

Chapter 4 is devoted to the study of the Majorana neutrino decays, joining the results published in the papers [2, 3]. In particular, it is found that in the low mass region a dominant decay channel to a neutrino and a photon leads to a very interesting phenomenology and can be invoked to explain some well known neutrino-related puzzles

as the mentioned MiniBooNE anomaly. The phenomenology of Majorana neutrinos in colliders is introduced in chapter 5, where we study the possibilities for their production in the proposed electron-proton collider LHeC at CERN, presenting the results obtained in [4]. In chapter 6 we study the phenomenology of the effective Majorana interactions in the LHC focusing on two new features: Majorana neutrinos lead to the well known same-sign dilepton signal mentioned above but in this work we propose to investigate the possibility of detecting it with the aid of observables exploiting the separation between the production and decay vertices, given that Majorana neutrinos with a mass of a few GeV have a measurable decay length. Also, as in the low mass region we have a dominant neutrino plus photon decay channel, a possible search with displaced photon observables is considered [5]. Chapter 7 is dedicated to the study of the effects of the existence of the Majorana neutrino on the propagation of ultra high energy tau neutrinos trough the Earth and the possible detection of these effects in the IceCube neutrino telescope, presenting the results obtained in [6]. The conclusions and future work perspectives are included in chapter 8.

Chapter 1

The Standard Model

In this chapter I introduce the most relevant characteristics of the Standard Model of particle physics, focusing on the scalar and electroweak sector and how fermion masses appear in the Yukawa lagrangian. I include a brief discussion on the different possible spinor fields in order to deepen in the properties of Majorana fermions, which I will introduce later as a tool for generating non-zero masses for the neutrinos. In the end of the chapter I comment on the renormalization procedure to introduce the effective field theories framework, which is the approach taken throughout this thesis.

The contents of this first introductory chapter are based on the treatments made in quantum field theory (QFT) introductory books and lecture notes, among which I have chosen [25–29] and on specialized classic textbooks on neutrino physics as [30].

1.1. Introduction

The SM is a quantum field theory describing the electroweak (EW) and strong interactions between the quarks and leptons. These constitute the fermionic matter content in the theory and are replicated in three copies (families) only distinguished by their masses and the flavor quantum number, as well as the baryon and lepton numbers. To first order, the strong interaction is only existent between quarks, while quarks and leptons have weak and electromagnetic interactions.

The free physical states can be classified by the Poincaré group representations in a one-particle Hilbert base space with definite momentum, leading to massive (or massless) particles characterized by their spin. These particles are created out of the Fock space vacuum by field operators, which are functions of the space-time coordinates with well defined transformation properties under Poincaré transformations. Depending on their transformation properties under Lorentz symmetries they are scalar fields, Weyl, Dirac or Majorana spinor fields, vector fields, etc. There are also other properties beyond the energy, momentum and spin which characterize physical states and identify their interactions, as the electric charges. The interactions can be determined by internal symmetries in the theories beyond the Poincaré group. These are incorporated by means of the local gauge symmetry, whose conserved charge is the corresponding interaction

charge, and its generators give the number of required mediating particles, the spin 1 bosonic fields: eight massless gluons for QCD, the massive $W^{\pm}$ and Z for the weak force, and one massless photon for electromagnetism. This makes the SM a local gauge theory based on the $G \equiv SU(3)_{QCD} \times [SU(2)_L \times U(1)_Y]_{EW}$ symmetry group.

The mass terms for the fields in the SM lagrangian break this local gauge symmetry. This forces us to incorporate an ad-hoc mechanism which brings non symmetrical results preserving the symmetries at the lagrangian level to include massive particles. The Higgs mechanism -which is associated to the Goldstone theorem in the frame of the EW theory- introduces the idea of spontaneous symmetry breaking (SSB), assuming a gauge-invariant lagrangian with a non-invariant vacuum breaking the electroweak part of the symmetry group G into the electromagnetic $G \to SU(3)_{QCD} \times U(1)_{EM}$ subgroup. The breaking is implemented by incorporating a scalar field with zero electric charge, and a non-zero interaction with the vacuum (it acquires a vacuum expectation value $\langle\phi\rangle = v$). The scalar field, once the gauge symmetry is broken, generates the Higgs particle as an excitation of its fundamental state. The Higgs interaction with fermions, with gauge bosons by means of the covariant derivative, and with itself is what brings in the masses, defined by the corresponding interaction coupling and the non-zero vacuum expectation value.

1.2. The fundamental ingredients

As I mentioned in the introduction, the SM building blocks are field operators creating and destroying particles in a Fock-space. As we want these fields to describe the properties of particles in Nature they must be described by Lorentz invariant equations. Having a collection of fields φ and a differential operator $\mathcal{D}$, the statement "$\mathcal{D}\varphi = 0$ is relativistically invariant" means that if $\varphi(x)$ satisfies this equation and we perform a rotation or boost to a different reference frame, the transformed field must satisfy the same equation. This is guaranteed if the φ dynamics is described by an equation of motion coming from a lagrangian that is a Lorentz scalar. These can be built by systematically finding Lorentz transformation laws for fields: restricting to linear transformation laws leads us to the fact that they must form an n-dimensional representation of the Lorentz group. As we also need to include space-time translations invariance, the valid quantum field operators provide representations of the Poincaré group (space-time translations plus Lorentz transformations).

I will focus on the spinorial field representations in order to describe the SM fermions. Spinorial representations describe half-integer spin quantities. For spatial rotations, the physically relevant group is not $SO(3)$ but rather $SU(2)$, besides both groups have the same Lie algebras.

The Lorentz algebra, given by commutation rules between the angular momentum J^i and the boost K^i generators

$$[J^i, J^j] = i\epsilon^{ijk} J^k \tag{1.1}$$

$$[J^i, K^j] = i\epsilon^{ijk} K^k \tag{1.2}$$

$$[K^i, K^j] = -i\epsilon^{ijk} J^k \tag{1.3}$$

can be disentangled by defining the combinations

$$J^{\pm,i} = \frac{J^i \pm iK^i}{2} \tag{1.4}$$

which give the commutators:

$$[J^{+,i}, J^{+,j}] = i\epsilon^{ijk} J^{+,k} \tag{1.5}$$

$$[J^{-,i}, J^{-,j}] = i\epsilon^{ijk} J^{-,k} \tag{1.6}$$

$$[J^{+,i}, J^{-,j}] = 0. \tag{1.7}$$

Equations (1.5) and (1.6) give two copies of the $SU(2)$ angular momentum algebra which commute with themselves. In order to include spinorial representations we take all solutions of the algebra (1.5)-(1.7) including spinor representations, and find that the representations of the the Lorenz algebra can be labeled by two half-integers: $(\mathbf{j}_-, \mathbf{j}_+)$. The dimension of the representation $(\mathbf{j}_-, \mathbf{j}_+)$ is $(2j_- + 1)(2j_+ + 1)$ and as the generator of rotations J^i is related to $J^\pm$ by $J^i = J^+ + J^-$, by the usual addition of angular momenta in quantum mechanics in the representation $(\mathbf{j}_-, \mathbf{j}_+)$ we find states with all possible spin j integer steps from $|j_+ - j_-|$ to $j_+ + j_-$.

The $(\mathbf{0}, \mathbf{0})$ representation is the dimension one scalar representation. On it $J^{i,\pm} = 0$ and also $J^i = 0$ and $K^i = 0$.

1.2.1. Weyl spinors

The $(\mathbf{1/2}, \mathbf{0})$ and $(\mathbf{0}, \mathbf{1/2})$ representations both have dimension two and spin 1/2, so they are spinorial representations. We denote $(\psi_L)_\alpha$ with $\alpha = 1, 2$ a spinor in $(\mathbf{1/2}, \mathbf{0})$ and $(\psi_R)_\alpha$ a spinor in $(\mathbf{0}, \mathbf{1/2})$. Now ψ_L is called a *left-handed Weyl spinor* and ψ_R a *right-handed Weyl spinor*.

Let's find the explicit form of the rotation and boost generators $\mathbf{J}$ and $\mathbf{K}$ in the spinor representation $(\mathbf{1/2}, \mathbf{0})$: by definition the $\mathbf{J}^-$ is represented by a 2×2 matrix, while $\mathbf{J}^+ = \mathbf{0}$. The solution of (1.6) in terms of 2×2 matrices is $\mathbf{J}^- = \boldsymbol{\sigma}/2$, with $\boldsymbol{\sigma} = \sigma^i$ the Pauli matrices, and therefore

$$\mathbf{J} = \mathbf{J}^+ + \mathbf{J}^- = \frac{\boldsymbol{\sigma}}{2} \tag{1.8}$$

$$\mathbf{K} = -i(\mathbf{J}^+ - \mathbf{J}^-) = i\frac{\boldsymbol{\sigma}}{2}. \tag{1.9}$$

Then, under rotations, the spinor ψ_L transforms as $\psi_L \to e^{-\frac{i}{2}\boldsymbol{\sigma}.\boldsymbol{\theta}}\psi_L$ and under a boost with rapidity $\boldsymbol{\eta} = \tanh^{-1}(\boldsymbol{\beta})$ it transforms as $\psi_L \to e^{-\frac{1}{2}\boldsymbol{\sigma}.\boldsymbol{\eta}}\psi_L$, in an "active" viewpoint.

Analogously, it can be seen that ψ_R transforms in the same way under rotations but changes sign under boosts. Summarizing:

$$\psi_L \to \Lambda_L \psi_L = exp\left\{(-i\boldsymbol{\theta} - \boldsymbol{\eta}).\frac{\boldsymbol{\sigma}}{2}\right\}\psi_L, \tag{1.10}$$

$$\psi_R \to \Lambda_R \psi_R = exp\left\{(-i\boldsymbol{\theta} + \boldsymbol{\eta}).\frac{\boldsymbol{\sigma}}{2}\right\}\psi_R. \tag{1.11}$$

With spinors ξ_L and ξ_R also transforming in the representations $(\mathbf{1/2}, \mathbf{0})$ and $(\mathbf{0}, \mathbf{1/2})$ respectively, and defining $\sigma^\mu = (\mathbf{1}, \boldsymbol{\sigma})$ and $\bar{\sigma}^\mu = (\mathbf{1}, -\boldsymbol{\sigma})$, we can write the following four-vector quantities:

$$\xi_L^\dagger \bar{\sigma}^\mu \psi_L \qquad \xi_R^\dagger \sigma^\mu \psi_R. \tag{1.12}$$

We can construct now a free lagrangian for the Weyl spinor fields looking for quadratic combinations that are Lorentz scalars. If one asks also for invariance under global phase transformations $\psi_{L,R} \to e^{i\phi}\psi_{L,R}$, we are left with one possibility (up to a sign)

$$\mathcal{L}_L^{Weyl} = i\psi_L^\dagger \bar{\sigma}^\mu \partial_\mu \psi_L \tag{1.13}$$

for left-handed, and

$$\mathcal{L}_R^{Weyl} = i\psi_R^\dagger \sigma^\mu \partial_\mu \psi_R \tag{1.14}$$

for right-handed Weyl fields. This is the Weyl lagrangian.

The spinor ψ_L is subject to the equation of motion $(\partial_0 - \sigma^i \partial_i)\psi_L = 0$ and therefore to the massless Klein-Gordon equation $(\partial_0^2 - \partial_i^2)\psi_L = 0$. Then a solution is $\psi_L(x) = u_L(k)e^{-ikx}$ with $k^0 = |\vec{k}|$ and we find $(k^0 + k^i\sigma^i)\psi_L = 0$, which implies that for the left-handed Weyl field ψ_L the product $\frac{k^i.\sigma^i}{k^0} = -1$. Recalling that the spin operator is defined as $s^i = \frac{\sigma^i}{2}$, this means the projection of spin along the momentum of a particle created by a left-handed Weyl field is $-1/2$: left-handed massless Weyl spinors have helicity $-1/2$ (massless particles are helicity eigenstates). In the same way a right-handed massless Weyl spinor is an $h = +1/2$ helicity eigenstate.

The Weyl lagrangians (1.13) and (1.14) where constructed with the vector bilinears in (1.12), which correspond to the product representations $(\mathbf{1/2}, \mathbf{1/2}) = (\mathbf{1/2}, \mathbf{0}) \otimes (\mathbf{0}, \mathbf{1/2})$ and $(\mathbf{1/2}, \mathbf{1/2}) = (\mathbf{0}, \mathbf{1/2}) \otimes (\mathbf{1/2}, \mathbf{0})$. In particular, our insistence in demanding the lagrangian to be invariant under a global $U(1)$ symmetry ruled out the scalar term that appears in the product representations $(\mathbf{1/2}, \mathbf{0}) \otimes (\mathbf{1/2}, \mathbf{0}) = (\mathbf{1}, \mathbf{0}) \oplus (\mathbf{0}, \mathbf{0})$ and $(\mathbf{0}, \mathbf{1/2}) \otimes (\mathbf{0}, \mathbf{1/2}) = (\mathbf{0}, \mathbf{1}) \oplus (\mathbf{0}, \mathbf{0})$. The singlet representations correspond to the antisymmetric combinations $\epsilon_{ab}(\psi_{L,R}^a)^T \psi_{L,R}^b$, where ϵ_{ab} is the antisymmetric symbol. Here we should keep in mind that fields with half-integer spin obey the spin-statistics theorem, and the fields $\psi_{L,R}$ satisfy anti-commutation relations, so the combinations do not identically vanish. The antisymmetric symbol ϵ_{ab} can be explicitly written in a 2×2 matrix representation suitable for two-component Weyl spinors as

$$\epsilon = i\sigma^2 = i\begin{pmatrix} 0 & -i \\ i & 0 \end{pmatrix} = \begin{pmatrix} 0 & 1 \\ -1 & 0 \end{pmatrix}. \tag{1.15}$$

Majorana masses

We can now write a Weyl lagrangian including a mass term

$$\mathcal{L}_L^{Weyl} = i\psi_L^\dagger \bar{\sigma}^\mu \partial_\mu \psi_L + \frac{1}{2} m (\psi_L)^T \epsilon \psi_L + h.c. \tag{1.16}$$

$$\mathcal{L}_R^{Weyl} = i\psi_R^\dagger \sigma^\mu \partial_\mu \psi_R + \frac{1}{2} m (\psi_R)^T \epsilon \psi_R + h.c. \tag{1.17}$$

These mass terms -called of Majorana type- are allowed if we do not worry about breaking the global $U(1)$ symmetry $\psi_{L,R} \to e^{i\phi}\psi_{L,R}$. If we consider electrically charged fermions a Majorana mass term is forbidden as it violates the conservation of electric charge or any other $U(1)$ gauge charge. Let's note that Majorana mass terms are constructed out of a single Weyl spinor ψ_L or ψ_R.

Parity

If one performs a Parity transformation $P \quad (t, \vec{x}) \to (t, -\vec{x})$ on the Lorentz $SO(3,1)$ group rotation J^i and boost K^i generators, they transform as pseudo-vectors and vectors respectively:

$$P : J^i \to J^i \qquad P : K^i \to -K^i, \tag{1.18}$$

meaning that $P : J^{\pm,i} \to J^{\mp,i}$ and therefore a representation $(\mathbf{j}_-, \mathbf{j}_+)$ changes to $(\mathbf{j}_+, \mathbf{j}_-)$ under parity. Thus a left-handed Weyl spinor in the representation $(\mathbf{1/2}, \mathbf{0})$ transforms into a right-handed Weyl spinor in $(\mathbf{0}, \mathbf{1/2})$ and vice versa. A vector representation $(\mathbf{1/2}, \mathbf{1/2})$ is invariant under parity.

1.2.2. Dirac spinors

We have seen that parity interchanges left-handed with right-handed Weyl spinors. So an easy way to construct a parity invariant theory for fermions (which will be needed for describing the parity-conserving electromagnetic and strong interactions) is to introduce a pair of Weyl fermions ψ_L and ψ_R combined into a single four-component spinor

$$\psi = \begin{pmatrix} \psi_L \\ \psi_R \end{pmatrix} \tag{1.19}$$

transforming in the $(\mathbf{1/2}, \mathbf{0}) \oplus (\mathbf{0}, \mathbf{1/2})$ reducible representation. This is a *Dirac spinor*. The equations of motion for $\psi_{L,R}$, $i\bar{\sigma}^\mu \partial_\mu \psi_L$ and $\sigma^\mu \partial_\mu \psi_R$ derived respectively from (1.13) and (1.14) can be modified -while being kept linear- to

$$\left.\begin{array}{l} i\sigma^\mu \partial_\mu \psi_R = m\psi_L \\ i\bar{\sigma}^\mu \partial_\mu \psi_L = m\psi_R \end{array}\right\} \Longrightarrow i \begin{pmatrix} 0 & \sigma^\mu \\ \bar{\sigma}^\mu & 0 \end{pmatrix} \partial_\mu \psi = m \begin{pmatrix} \mathbf{1} & 0 \\ 0 & \mathbf{1} \end{pmatrix} \psi. \tag{1.20}$$

These equations of motion can be derived from the lagrangian

$$\mathcal{L}^{Dirac} = i\psi^\dagger \begin{pmatrix} 0 & \sigma^\mu \\ \bar{\sigma}^\mu & 0 \end{pmatrix} \partial_\mu \psi - m\psi^\dagger \begin{pmatrix} 0 & \mathbf{1} \\ \mathbf{1} & 0 \end{pmatrix} \psi \tag{1.21}$$

which can be written in the well-known compact form

$$\mathcal{L}^{Dirac} = \bar{\psi}(i\gamma^\mu \partial_\mu - m)\psi \tag{1.22}$$

defining the Dirac γ-matrices as [1]

$$\gamma^\mu = \begin{pmatrix} 0 & \sigma^\mu \\ \bar{\sigma}^\mu & 0 \end{pmatrix} \tag{1.23}$$

and the conjugate spinor $\bar{\psi}$

$$\bar{\psi} \equiv \psi^\dagger \gamma^0 = \psi^\dagger \begin{pmatrix} 0 & \mathbf{1} \\ \mathbf{1} & 0 \end{pmatrix}. \tag{1.24}$$

The γ-matrices satisfy the Clifford algebra $\{\gamma^\mu, \gamma^\nu\} = 2\eta^{\mu\nu}$, which in D dimensions admits representations of dimension $2^{[D/2]}$. When D es even, the Dirac fermions ψ transform in a reducible representation of the Lorentz group. Defining the matrix

$$\gamma^5 = -i\gamma^0\gamma^1\gamma^2\gamma^3 = \begin{pmatrix} -\mathbf{1} & 0 \\ 0 & \mathbf{1} \end{pmatrix}, \tag{1.25}$$

we see that it anti-commutes with all other γ-matrices, implying the relation $[\gamma^5, \sigma^{\mu\nu}] = 0$, with $\sigma^{\mu\nu} = \frac{-i}{2}[\gamma^\mu, \gamma^\nu]$. Because of Schur's lemma, this implies that the representation of the Lorentz group provided by the $\sigma^{\mu\nu}$ matrices is reducible into subspaces spanned by the eigenvectors of γ^5 with the same eigenvalue. If we define the projectors $P_{R,L} = \frac{1}{2}(1 \pm \gamma^5)$ these subspaces correspond to

$$P_L\psi = \begin{pmatrix} \psi_L \\ 0 \end{pmatrix} \qquad P_R\psi = \begin{pmatrix} 0 \\ \psi_R \end{pmatrix} \tag{1.26}$$

which are precisely the four-component Dirac-spinor versions of the left-handed and right-handed (two-component) Weyl spinors.

1.2.3. Charge conjugation and the Majorana condition

We can define the operation of charge conjugation on Weyl spinors as an operation transforming ψ_L into a new spinor ψ_L^c, defined as

$$\psi_L^c = i\sigma^2\psi_L^* = \epsilon\psi_L^*, \tag{1.27}$$

using the definition given in (1.15).

Recalling the explicit form of the Lorentz group generators $\Lambda_{L,R}$ on Weyl spinors given in (1.10) and (1.11) and using the property of the Pauli matrices $\sigma^2\sigma^i\sigma^2 = -\sigma^{i*}$, one can show that $\sigma^2\Lambda_L^*\sigma^2 = \Lambda_R$, so under a Lorentz transformation $\sigma^2\psi_L^*$ transforms as a right-handed Weyl spinor:

$$\sigma^2\psi_L^* \to \sigma^2(\Lambda_L\psi_L)^* = (\sigma^2\Lambda_L^*\sigma^2)\sigma^2\psi_L^* = \Lambda_R(\sigma^2\psi_L^*) \tag{1.28}$$

[1] This is called the Chiral representation for the γ-matrices.

(using $\sigma^2\sigma^2 = 1$). If $\psi_L \in (\mathbf{1/2}, \mathbf{0})$ then $\sigma^2\psi_L^* \in (\mathbf{0}, \mathbf{1/2})$. This means that the charge conjugation operation in (1.27) converts a left-handed Weyl spinor into a right-handed one and analogously, defining $\psi_R^c = -i\sigma^2\psi_R^*$ the charge conjugate of a right-handed Weyl spinor is a left-handed one.

On a Dirac field, charge conjugation is defined as

$$\psi^c = \begin{pmatrix} -i\sigma^2\psi_R^* \\ i\sigma^2\psi_L^* \end{pmatrix} = -i \begin{pmatrix} 0 & \sigma^2 \\ -\sigma^2 & 0 \end{pmatrix} \psi^* = \begin{pmatrix} -\epsilon & 0 \\ 0 & \epsilon \end{pmatrix} \begin{pmatrix} 0 & 1 \\ 1 & 0 \end{pmatrix} \psi^*. \tag{1.29}$$

If we define the charge conjugation matrix in the chiral basis as

$$\mathcal{C} = \begin{pmatrix} -i\sigma^2 & 0 \\ 0 & i\sigma^2 \end{pmatrix} = \begin{pmatrix} -\epsilon & 0 \\ 0 & \epsilon \end{pmatrix} \tag{1.30}$$

we can write the charge conjugation operation on Dirac spinors as $\psi^c = \mathcal{C}\gamma^0\psi^*$. This relation can also be written as $\psi^c = \mathcal{C}(\psi^\dagger\gamma^0)^T = \mathcal{C}(\bar{\psi})^T$, given that $(\gamma^0)^T = \gamma^0$.

Summarizing:

$$\psi^c = \mathcal{C}\gamma^0\psi^* \qquad \psi^c = \mathcal{C}(\bar{\psi})^T. \tag{1.31}$$

Finally, we get to define a Majorana spinor: this is a Dirac spinor in which ψ_L and ψ_R are not independent, but rather $\psi_R = i\sigma^2\psi_L^*$

$$\psi_M = \begin{pmatrix} \psi_L \\ i\sigma^2\psi_L^* \end{pmatrix}, \tag{1.32}$$

so it has the same number of degrees of freedom as a Weyl spinor, although it is written in the form of a Dirac spinor. From this definition it follows that the Majorana field is its own charge conjugate:

$$\psi_M^c = \psi_M. \tag{1.33}$$

This is called the Majorana condition, and is the defining property of a Majorana fermion. Majorana fermions admit Majorana masses as those in (1.16) and (1.17).

When one writes down the quantized Majorana fields in terms of creation and annihilation operators the Majorana condition implies that a Majorana field describes particles which are their own antiparticles.

1.2.4. Matter content and flavor symmetries

In table 1.1 a list of the fermion content is shown, including the gauge numbers. Here the fields are Dirac spinors, so -for example- one should think of u_L in the first row as

$$u_L = \begin{pmatrix} (\psi_u)_L \\ 0 \end{pmatrix} \tag{1.34}$$

with $(\psi_u)_L$ the Weyl spinor representing the up quark left-handed field.

The lagrangian is the sum of the gauge, matter, Yukawa and Higgs terms

$$\mathcal{L}_{SM} = \mathcal{L}_{gauge} + \mathcal{L}_{matter} + \mathcal{L}_{Yukawa} + \mathcal{L}_{Higgs}. \tag{1.35}$$

				Gauge group $SU(3)_c$	$SU(2)_L$	$U(1)_Y$
$Q_L^i =$	$\begin{pmatrix} u \\ d \end{pmatrix}_L$	$\begin{pmatrix} c \\ s \end{pmatrix}_L$	$\begin{pmatrix} t \\ b \end{pmatrix}_L$	3	2	$\frac{1}{6}$
$u_R^i =$	u_R	c_R	t_R	3	1	$\frac{2}{3}$
$d_R^i =$	d_R	s_R	b_R	3	1	$-\frac{1}{3}$
$L_L^i =$	$\begin{pmatrix} \nu_e \\ e \end{pmatrix}_L$	$\begin{pmatrix} \nu_\mu \\ \mu \end{pmatrix}_L$	$\begin{pmatrix} \nu_\tau \\ \tau \end{pmatrix}_L$	1	2	$-\frac{1}{2}$
$\ell_R^{-i} =$	e_R^-	μ_R^-	τ_R^-	1	1	-1

Table 1.1: The fermion fields in the SM and their gauge quantum numbers.

The matter lagrangian contents the kinetic and gauge interactions of the fermion fields,

$$\mathcal{L}_{matter} = i\bar{Q}_L^i \not{D} Q_L^i + i\bar{u}_R^i \not{D} u_R^i + i\bar{d}_R^i \not{D} d_R^i + \bar{L}_L^i \not{D} L_L^i + \bar{e}_R^{-i} \not{D} e_R^{-i}, \tag{1.36}$$

with the indices $i, j = 1, 2, 3$ representing the three fermion families.

At this stage the fermions are still massless and the covariant derivatives are those presented below[2] (see (1.44)) . Majorana masses are forbidden by the fact that all fermions carry hypercharge. Dirac masses are forbidden by the fact that no fermion transforms under the complex-conjugate representation of another fermion. It is important to notice that there are no right-handed neutrino fields: neutrinos only appear as the upper component in the leptonic $SU(2)_L$ doublets in the fourth row of table 1.1.

The absence of fermion masses implies that $\mathcal{L}_{matter}$ has many *accidental* global symmetries:

$$\begin{aligned} Q_L^i &\to U_{Q_L}^{ij} Q_L^j \\ u_R^i &\to U_{u_R}^{ij} u_R^j \\ d_R^i &\to U_{d_R}^{ij} d_R^j \\ L_L^i &\to U_{L_L}^{ij} L_L^j \\ \ell_R^i &\to U_{\ell_R}^{ij} \ell_R^j. \end{aligned} \tag{1.37}$$

This symmetry is accidental in the sense that it is not imposed, but rather follows from the fermion content, the renormalizability and the gauge symmetries of the model. Since

[2]Without taking into account the $SU(3)_C$ strong gauge interactions. To include them, one must add the gluon terms.

there are five independent $U(3)$ symmetries, the global flavor symmetry in $\mathcal{L}_{matter}$ is $[U(3)]^5$. After the Yukawa couplings of fermions to the Higgs field are introduced (see sect. 1.4.2), this symmetries will be violated.

We now need to implement the local gauge invariance and spontaneous symmetry breaking ideas in order to introduce gauge invariant masses for the fermions and the massive vector gauge bosons mediating the weak interactions. This will be done in the next section.

1.3. The fundamental ideas

The two central ideas sustaining the SM success are the extension of the gauge invariance principle as a local concept (inspired in classical electrodynamics) and the implementation of the spontaneous symmetry breaking phenomenon. The introduction of the local gauge invariance generates the so called gauge bosons and their interactions with matter (fermions) and among themselves (only for non-abelian gauge groups). In turn, the combination of local gauge invariance with spontaneous symmetry breaking leads naturally to the Higgs mechanism, providing the mass terms for the vector weak gauge bosons ($W^{\pm}$ and Z) and the fermions while keeping the invariance under the gauge group at the original lagrangian level.

In this section I introduce both ideas emphasizing the Higgs mechanism that leads to the leptonic mass sector in the lagrangian.

1.3.1. Local gauge invariance

Beginning with classical electrodynamics it is known that Maxwell equations are invariant under a local gauge transformation of the form $A_\mu \to \partial_\mu \lambda(x) + A_\mu$, where A_μ is the four-vector potential. Also, taking the Dirac free lagrangian in (1.22) we can see it is invariant under the global phase shift $\psi \to e^{i\theta}\psi$. However, inspired by the local gauge symmetry in electrodynamics, could we extend the global symmetry and ask it to be local? If it is so, which are the physical consequences of that extension? It is easy to prove that such "locality" could be achieved by replacing the usual derivative ∂_μ with a covariant derivative $D_\mu \equiv \partial_\mu + iqA_\mu$, where A_μ is a field transforming as $A_\mu \to \partial_\mu \lambda(x) + A_\mu$ when the local gauge transformation $\psi \to e^{-iq\lambda(x)}\psi$ is performed. In doing so, the lagrangian (1.22) is changed to

$$\mathcal{L}^{Dirac} = \bar{\psi}(i\gamma^\mu D_\mu - m)\psi = \bar{\psi}(i\gamma^\mu \partial_\mu - m)\psi - qA_\mu \bar{\psi}\gamma^\mu \psi = \mathcal{L}^{Dirac} - J^\mu A_\mu. \qquad (1.38)$$

One can see this new lagrangian is invariant under the combined transformations $\psi \to e^{-iq\lambda(x)}\psi$ and $A_\mu \to \partial_\mu \lambda(x) + A_\mu$. $J^\mu = q\bar{\psi}\gamma^\mu\psi$ is the electromagnetic-current four-vector. To complete the Quantum Electrodynamics (QED) lagrangian we add the kinetic term describing the free photon's propagation

$$\mathcal{L}^{QED} = \mathcal{L}^{Dirac} - J^\mu A_\mu - \frac{1}{4}F^{\mu\nu}F_{\mu\nu}, \qquad F_{\mu\nu} \equiv \partial_\mu A_\nu - \partial_\nu A_\mu. \qquad (1.39)$$

This kinetic term -from which the free Maxwell equations can be derived- is also locally gauge invariant. Therefore, the coupling between matter and radiation is generated by imposing locality. Moreover, to preserve locality we have introduced in the covariant derivative a vector field A_μ called *gauge field* and a q parameter acting as the generator of the local transformations group $\hat{U}(x) = e^{-iq\lambda(x)}$. In this case, in order to analyze the symmetries we have used the one-dimensional rotations group in the complex space $U(1)$, the group of unitary 1×1 "matrices". In the electroweak sector of the SM we will take the $SU(2)$ group, which is a non-abelian group whose generators obey the Lie algebra of the three-dimensional rotations group. After applying the local gauge invariance to the whole electroweak group $[SU(2)\times U(1)]_{EW}$, they will appear four gauge fields, generating -after some additional transformations- the three vectorial bosons of the weak force: $W^\pm, Z$ and the photon.

1.3.2. Spontaneous symmetry breaking and the Higgs mechanism

The use of local gauge invariance as a dynamical principle is not enough to predict the particle physics phenomenology, as it leads to massless gauge bosons which do not correspond to the physical observations. In the SM these bosons acquire their masses by means of the phenomenon of spontaneous symmetry breaking (SSB).

With the aim of generating masses, we have to somehow break the gauge symmetry. However, we need a totally symmetric lagrangian in order to preserve its renormalizability and unitarity. This dilemma can be solved thanks to the possibility of obtaining non-symmetric results starting out of a symmetric lagrangian.

Consider a lagrangian which is invariant under a symmetry group G, with a degenerate set of minimal energy states which transform under G as the members of a given multiplet. If one of these states is arbitrarily realized as the system's fundamental state one says the symmetry is spontaneously broken.

When the spontaneous symmetry breaking mechanism occurs other particles called Goldstone bosons appear in the theory's spectrum [31–33]. However, if the lagrangian has a local gauge symmetry an interrelationship between gauge bosons and Goldstone bosons gives the first a physical mass, while the last disappear from the spectrum. The degrees of freedom corresponding to the massless Goldstone bosons are converted into a longitudinal polarization for the massive vector bosons. That is why it is generically said that the gauge bosons have "eaten" the Goldstone bosons in order to acquire their mass. This is the *Higgs mechanism* [34–37]. However, it is worth noting that besides massive vector bosons, the Higgs mechanism provides us with an additional physical degree of freedom corresponding to a massive scalar field, which describes the Higgs particle.

We can remark that the Higgs mechanism is possible due to the spontaneous symmetry breaking and the local gauge invariance. For instance, if we implement a spontaneous symmetry breaking with a global symmetry, we obtain a certain number of massless (physical) Goldstone bosons, given that a global symmetry does not provide vector bosons to "eat" these extra degrees of freedom. Technically, the number of Goldstone bosons produced by the SSB equals the number of broken generators of the symmetry group in question [31,38].

1.4. The Standard Model (as we know it)

The SM of particle physics [39–41] takes the ideas of local gauge invariance and spontaneous symmetry breaking to implement the Higgs mechanism. The local gauge symmetry of the electroweak sector is given by the group $SU(2)_L \times U(1)_Y$ and the SSB obeys the scheme $SU(2)_L \times U(1)_Y \to U(1)_Q$, where the subindex L indicates that the $SU(2)$ group only acts on fermion left-handed doublets. Y is the original hypercharge $U(1)$ group generator and Q corresponds to a non-broken generator's combination (the electromagnetic charge).

Specifically, the SSB is implemented introducing an $SU(2)_L$ doublet, which is a Lorentz scalar:

$$\phi = \begin{pmatrix} \phi^+ \\ \phi^0 \end{pmatrix} = \begin{pmatrix} \phi_1 + i\phi_2 \\ \phi_3 + i\phi_4 \end{pmatrix}. \tag{1.40}$$

To produce the breaking the scalar doublet[3] must acquire a non-zero vacuum expectation value (VEV)

$$\langle\phi\rangle = \begin{pmatrix} 0 \\ v/\sqrt{2} \end{pmatrix}. \tag{1.41}$$

The original local symmetry group $SU(2)_L \times U(1)_Y$ is non-abelian, leading to gauge boson's self-interactions. They appear when the kinetic term for the gauge bosons is introduced. The generators are called τ_i and Y, corresponding to $SU(2)_L$ and $U(1)_Y$ respectively. The τ_i are defined using the Pauli matrices as $\tau_i \equiv \frac{\sigma_i}{2}$ and they obey the Lie algebra

$$[\tau_i, \tau_j] = i\varepsilon_{ijk}\tau_k, \qquad [\tau_i, Y] = 0. \tag{1.42}$$

When the symmetry is spontaneously broken in the scalar potential the ϕ doublet acquires a VEV and we see all the $SU(2)_L \times U(1)_Y$ generators are broken

$$\tau_1\langle\phi\rangle = \frac{1}{2}\begin{pmatrix} v/\sqrt{2} \\ 0 \end{pmatrix} \neq 0, \qquad \tau_2\langle\phi\rangle = \frac{1}{2}\begin{pmatrix} -iv/\sqrt{2} \\ 0 \end{pmatrix} \neq 0$$

$$\tau_3\langle\phi\rangle = \frac{1}{2}\begin{pmatrix} 0 \\ -v/\sqrt{2} \end{pmatrix} \neq 0, \qquad Y\langle\phi\rangle = \begin{pmatrix} 0 \\ v/\sqrt{2} \end{pmatrix} \neq 0.$$

However, we can define a non-broken combination using the Gell-Mann-Nishijima relation:

$$Q = (\tau_3 + Y) \qquad Q\langle\phi\rangle = 0$$

This definition of the electric charge operator Q fixes the Y hypercharge of the Higgs scalar to be $Y_\phi = \frac{1}{2}$.

The SSB scheme is given by $SU(2)_L \times U(1)_Y \to U(1)_Q$. In agreement with the Goldstone theorem, the number of the would-be Goldstone bosons equals the number of broken generators (which in turn equals the number of massive gauge bosons in the

[3] It is common to refer to the Higgs field as a scalar (Lorentz space-time transformations) doublet ($SU(2)_L$ weak force gauge symmetry). We leave the name Higgs field for the h excitations around the VEV after the SSB.

case of local symmetries). Thus instead of working with four broken generators, we will have three broken generators and a non-broken one Q. This scheme assures the photon remains massless, while the other three gauge bosons acquire their masses by this mechanism, and everything with a gauge invariant lagrangian [42].

1.4.1. The kinetic term

The kinetic term gives the interactions between the scalar particles and the four-vector bosons and generates their masses when the Higgs field acquires a VEV. The kinetic lagrangian is written introducing the gauge fields in the covariant derivative as we did in sec.1.3.1

$$\mathcal{L}_{Kin} = (D_\mu \phi)^\dagger (D^\mu \phi), \tag{1.43}$$

$$D_\mu \equiv \partial_\mu - ig' Y B_\mu - ig \tau_i W_\mu^i \tag{1.44}$$

where W_μ^i with $i = 1, 2, 3$ are the four-vector boson gauge eigenstates associated to the three $SU(2)_L$ generators τ_i. On the other hand B_μ is the vector field associated with the Y generator of the hypercharge symmetry $U(1)_Y$. The constants g and g' correspond to the W_μ^i and B_μ couplings, respectively.

After diagonalizing the gauge boson's mass matrix we obtain the following mass eigenstates:

$$W_\mu^\pm = \frac{W_\mu^1 \mp i W_\mu^2}{\sqrt{2}} \quad ; \quad m_{W^\pm}^2 = \frac{1}{4} g^2 v^2 \tag{1.45}$$

$$\begin{pmatrix} Z_\mu \\ A_\mu \end{pmatrix} = \begin{pmatrix} \cos\theta_W & -\sin\theta_W \\ \sin\theta_W & \cos\theta_W \end{pmatrix} \begin{pmatrix} W_\mu^3 \\ B_\mu \end{pmatrix} \tag{1.46}$$

$$m_Z^2 = \frac{1}{4} v^2 (g^2 + g'^2) = \frac{m_W^2}{\cos^2\theta_W} \quad ; \quad m_A = 0. \tag{1.47}$$

The photon A_μ remains massless, as it is the gauge boson associated to the unbroken generator Q (the electromagnetic charge) of the surviving symmetry $U(1)_Q$. Other important relation follows for the coupling of the unbroken symmetry: the electric charge e is related to the $SU(2)_L$ coupling g and the $U(1)_Y$ coupling g' as:

$$e = \frac{g g'}{\sqrt{g^2 + g'^2}} = g \sin(\theta_W) = g' \cos(\theta_W), \tag{1.48}$$

using the definition of the *weak-mixing angle* θ_W in (1.47).

1.4.2. The Yukawa lagrangian

The SM organizes the observed fermions in three families which are copies of the same $SU(2)_L \times U(1)_Y$ structure, only distinguished by their masses and flavor. The left-handed fields transform as $SU(2)_L$ doublets, whereas the right-handed fields are singlets,

as indicated in table 1.1. I will start putting a "prime" in all the fields, indicating that I am referring to gauge eigenstates, which are the fields that transform as stated under the gauge group:

$$\begin{pmatrix} u' \\ d' \end{pmatrix}_L \quad , \quad \begin{pmatrix} \nu'_\ell \\ \ell' \end{pmatrix}_L \quad ; \quad u'_R \quad , \quad d'_R \quad , \quad \ell'_R. \tag{1.49}$$

Here u', d' and ℓ' are three-entries vectors in the flavor space, as was fully displayed in table 1.1.

The most general renormalizable Yukawa lagrangian is given by

$$\mathcal{L}_{Yukawa} = -\Gamma_u^{ij} \bar{Q'}^i{}_L \tilde{\phi} u'^j_R - \Gamma_d^{ij} \bar{Q'}^i{}_L \phi d'^j_R - \Gamma_\ell^{ij} \bar{L'}^i{}_L \phi \ell'^j_R + h.c. \tag{1.50}$$

Here, the conjugate scalar doublet $\tilde{\phi}$ in the first term is defined as $\tilde{\phi} = i\sigma^2\phi^* = \epsilon\phi^*$, and it can be seen it also transforms as an $SU(2)$ doublet. In order to keep the gauge invariance in the Yukawa term with up-type quarks $\tilde{\phi}$ has hypercharge[4] $Y_{\tilde{\phi}} = -\frac{1}{2}$. The matrices $\Gamma^{ij}_{u,d,\ell}$ are general Yukawa matrices corresponding to the couplings of the scalar doublet with the up, down and charged leptons fermion sectors.

After the SSB the scalar doublet can be written as:

$$\phi = \begin{pmatrix} \phi^+ \\ \phi^0 \end{pmatrix} \quad \xrightarrow{SSB} \quad e^{i\tau_i\theta_i} \begin{pmatrix} 0 \\ \frac{(v+h)}{\sqrt{2}} \end{pmatrix} \tag{1.51}$$

where the θ_i can be rotated out thanks to the $SU(2)_L$ invariance in the lagrangian, and h is the Higgs field. When all the θ_i are rotated away we are in the unitary gauge, in which the physical spectrum is explicit and no Goldstone bosons are present. The Yukawa lagrangian can be written as

$$\mathcal{L}_Y = -\left(1 + \frac{h}{v}\right) \left[\bar{d'}_L M'_d d'_R + \bar{u'}_L M'_u u'_R + \bar{\ell'}_L M'_l \ell'_R\right] \tag{1.52}$$

with $M'_f = \frac{v}{\sqrt{2}}\Gamma_f$, $f = u, d, \ell$. The M'_f matrices can be decomposed as $M'_f = H_f U_f = S_f^\dagger M_f S_f U_f$, with U_f unitary, H_f hermitian, S_f unitary and M_f diagonal, hermitian and positive definite.

The matrices $M_f = S_f M'_f U_f^\dagger S_f^\dagger$ are diagonal, with masses corresponding to the three fermionic sectors:

$$M_u = diag(m_u, m_c, m_t), \qquad M_d = diag(m_d, m_s, m_b), \qquad M_\ell = diag(m_e, m_\mu, m_\tau). \tag{1.53}$$

The resulting fermionic mass eigenstates $f_L = S_f f'_L$ and $f_R = S_f U_f f'_R$ allow to write the Yukawa lagrangian as

$$\mathcal{L}_Y = -\left(1 + \frac{h}{v}\right) \left(\bar{d}_L M_d d_R + \bar{u}_L M_u u_R + \bar{\ell}_L M_\ell \ell_R\right) + h.c. \tag{1.54}$$

[4] All the terms must meet the constraint $\sum_k Y_k = 0$ in order to preserve the gauge invariance.

This expression shows that all the Higgs couplings with fermions are proportional to their masses and are flavor diagonal (different flavors do not mix by the exchange of a scalar particle). Also, one should notice that the masses in (1.54) are Dirac masses: the left-handed and right-handed Weyl neutrinos we had introduced, are now paired up to make Dirac masses for the quarks and charged leptons.

1.4.3. Electroweak currents

Let's now see how the electroweak currents are affected by the fact that the fermions acquire masses.

The Dirac lagrangian, written with the covariant derivative in terms of the massive weak bosons, gives us the charged and neutral interaction terms:

$$\mathcal{L}_{Dirac} = \sum_{j=1}^{3} i\overline{\psi'_j}(x)\gamma^\mu D_\mu \psi'_j \tag{1.55}$$

where the fields ψ'_j represent the quark or lepton fermion fields. The lagrangian (1.55) contains the interaction terms with the gauge bosons, and written in the mass eigenstates from equations (1.45) and (1.46) can be separated in a part describing the charged-currents (CC) and other describing the neutral-currents (NC), depending on weather the fermions interact with the charged gauge bosons $W^\pm$ or the Z neutral boson and the photon.

The charged-current lagrangian only couples the left-handed components of the fermions to the $SU(2)_L$ gauge fields, and can be written as

$$\mathcal{L}_{CC} = -\frac{g}{\sqrt{2}} W^+_\mu J^\mu_{CC} + h.c. \tag{1.56}$$

where

$$J^\mu_{CC} = J^\mu_{lep} + J^\mu_{had} \tag{1.57}$$

with the leptonic and hadronic currents being

$$J^\mu_{lep} = \bar{\nu}'_{\ell,L}\gamma^\mu \ell'_L, \qquad J^\mu_{had} = \bar{u}'_L \gamma^\mu d'_L. \tag{1.58}$$

Let's start with the leptonic charged-current: as the charged lepton field gauge state is rewritten in terms of the mass state $\ell'_L = S^\dagger_\ell \ell_L$, we can redefine the neutrino $\bar{\nu}'_{\ell,L}$ field to be $\bar{\nu}'_{\ell,L} = S_\ell \nu_{\ell,L}$, and the charged-current for the leptons is written

$$J^\mu_{lep} = \bar{\nu}'_{\ell,L}\gamma^\mu \ell'_L = \bar{\nu}_{\ell,L} S_\ell S^\dagger_\ell \gamma^\mu \ell_L = \bar{\nu}_{\ell,L}\gamma^\mu \ell_L. \tag{1.59}$$

Thus we find the leptonic charged-current is written in terms of charged lepton fields with definite mass ℓ_L, with $\ell = e, \mu, \tau$. The neutrino fields $\nu_{\ell,L}$ are called *flavor neutrino fields*, because each of them couples only with the corresponding charged lepton field in the weak current (1.59). In the SM, the flavor neutrino fields are also mass eigenstates, because the linear combination of massless fields is also massless.

Fermions	g_L	g_R
ν_ℓ	$g_L^\nu = 1/2$	$g_R^\nu = 0$
$\ell = e, \mu, \tau$	$g_L^\ell = -1/2 + \sin^2\theta_W$	$g_R^\ell = \sin^2\theta_W$
u, c, t	$g_L^u = 1/2 - 2/3\sin^2\theta_W$	$g_R^u = -2/3\sin^2\theta_W$
d, s, b	$g_L^d = -1/2 + 1/3\sin^2\theta_W$	$g_R^d = 1/3\sin^2\theta_W$

Table 1.2: The fermion's NC couplings to the Z boson.

The hadronic CC is affected by the basis change, given that $\overline{u'_L} d'_L = \overline{u_L} S_u S_d^\dagger d_L \equiv \overline{u_L} V d_L$. In general, $S_u \neq S_d$, and a unitary mixing matrix V appears. This is the Cabibbo-Kobayashi-Masakawa matrix V_{CKM} [43, 44] that couples every type-up quark with all down-type quarks. Then the charged hadronic current is written as

$$J^\mu_{had} = \bar{u'}_L \, \gamma^\mu \, d'_L = \bar{u}_{\alpha,L} \, \gamma^\mu \, V^{\alpha,\beta}_{CKM} \, d_{\beta,L}. \tag{1.60}$$

The charged-current interactions for quarks mix flavors between families: the indices α and β indicate the quark family $\alpha = u, c, t$ and $\beta = d, s, b$.

In the case of the neutral-currents the lagrangian can be written as

$$\mathcal{L}_{NC} = -\frac{g}{\cos\theta_W} J^\mu_Z Z_\mu - e J^\mu_\gamma A_\mu \tag{1.61}$$

with

$$J^\mu_Z = J^\mu_{Z,lep} + J^\mu_{Z,had}, \qquad J^\mu_\gamma = J^\mu_{\gamma,lep} + J^\mu_{\gamma,had}. \tag{1.62}$$

Here the electromagnetic current is

$$J^\mu_{\gamma,lep} = \bar{\ell'}\gamma^\mu \ell', \qquad J^\mu_{\gamma,had} = \frac{2}{3}\bar{u'}\gamma^\mu u' - \frac{1}{3}\bar{d'}\gamma^\mu d' \tag{1.63}$$

and the Z current is

$$J^\mu_{Z,lep} = g_L^\nu \, \bar{\nu}'_{\ell,L} \, \gamma^\mu \, \nu_{\ell,L} + g_L^\ell \, \bar{\ell}'_L \, \gamma^\mu \, \ell_L + g_R^\ell \, \bar{\ell}'_R \, \gamma^\mu \, \ell_R \tag{1.64}$$

$$J^\mu_{Z,had} = g_L^u \, \bar{u}'_L \, \gamma^\mu \, u'_L + g_R^u \, \bar{u}'_R \, \gamma^\mu \, u'_R + g_L^d \, \bar{d}'_L \, \gamma^\mu \, d'_L + g_R^d \, \bar{d}'_R \, \gamma^\mu \, d'_R. \tag{1.65}$$

The couplings $g_{L,R}$ of the Z boson to quarks and leptons are shown in table 1.2. Here e is the proton's electric charge.

When changing to the fermion's mass eigenstate basis, the NC lagrangian (1.61) keeps its shape, as $\overline{f'_L} f'_L = \overline{f_L} f_L$ and $\overline{f'_R} f'_R = \overline{f_R} f_R$ for every fermion f. Therefore in the SM there are no *flavor changing neutral-currents*. This phenomenon is known as the GIM mechanism (for Glashow, Iliopoulos and Maiani) [45] and it is a consequence of treating equally every fermion with the same electric charge.

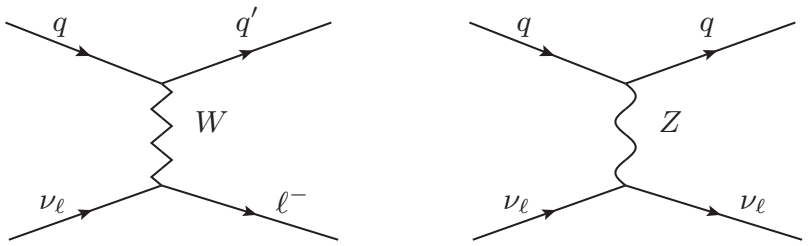

(a) Neutrino SM Charged Current (CC) (b) Neutrino SM Neutral Current (NC)

Figure 1.1: Example of charged (W) and neutral (Z) neutrino-quark currents in the SM. The diagram (a) is produced by the interactions in (1.59) and (1.60). The diagram (b) is produced by the interactions in (1.64) and (1.65).

1.4.4. Anomalies and B-L conservation

As a consequence of mass generation, only a very small subgroup of the $[U(3)]^5$ symmetries we had found in (1.37) remain valid, corresponding to *baryon number*

$$\begin{aligned} Q_L^i &\to e^{i\theta/3} Q_L^i \\ u_R^i &\to e^{i\theta/3} u_R^i \\ d_R^i &\to e^{i\theta/3} d_R^i \end{aligned} \tag{1.66}$$

and *lepton number*

$$\begin{aligned} L_L^i &\to e^{i\phi} L_L^i \\ \ell_R^i &\to e^{i\phi} \ell_R^i. \end{aligned} \tag{1.67}$$

Baryon and lepton number are accidental global symmetries of the SM, in the sense discussed in sec.1.2.4.

Baryon number conservation implies that in every process the quantity $B = \frac{1}{3}(n_q - n_{\bar{q}})$ must be the same in the initial and final states, with n_q representing the number of quarks, and $n_{\bar{q}}$ of anti-quarks. A baryon -made of three quarks (like the proton)- has baryon number $B = 1$. The lepton number is defined analogously as $L = n_l - n_{\bar{l}}$, but also, as lepton flavors do not mix in SM electroweak interactions, leptonic family numbers can be defined: L_e, L_μ, L_τ.

However, none of these classical global symmetries is carried over to the quantum theory: when a symmetry present at the classical lagrangian level is not present upon quantization, we say it is *anomalous*. It was pointed out by Adler, Bell and Jackiw [46,47] that in chiral theories (those involving γ^5 currents) of fermions one-loop triangular diagrams in general destroy the current conservation which was true at the tree-level.

In the case of the SM, the conserved quantum number is $B - L$, the difference between baryon and lepton number.

The gauge anomalies are also very important for the SM. A quantum mechanical violation of gauge symmetry leads to the non-decoupling of negative norm states, because the gauge-fixing constraints cannot be consistently implemented and unphysical states that would be eliminated classically by the gauge symmetry become propagating, spoiling the quantum theory's consistency. Anomalies in a gauge symmetry can be expected only in chiral theories where left and right-handed fermions transform in different representations of the gauge group.

The cancellation of anomalies emerging in triangle diagrams in the SM requires that leptons and quarks appear in complete multiplets with the structure $(L_L, \ell_R, Q_L, u_R, d_R)$ as given in table 1.1, also fixing their quantum numbers as electric charges, hypercharges and the existent number of quark colors. This set of fields is called a family of quarks and leptons. The consistency of the theory requires that quarks and leptons appear in Nature organizing themselves into families in this way. It is remarkable that all the known elementary fermions can be accommodated in appropriate representations of the symmetry group of the SM with exact cancellation of quantum anomalies.

1.5. Neutrino mass and the Standard Model: perspectives

So far we have discussed how particle masses are generated in the SM framework: the Higgs mechanism is introduced in order to give masses to the weak bosons, quarks and charged leptons, because adding explicit mass terms for fermions and gauge bosons to the lagrangian breaks gauge invariance, which is necessary for the renormalizability of the theory.

For the neutrinos the situation is somewhat special: neutrinos in the SM are massless because only one left-handed helicity state is included per fermion family. Therefore, it cannot acquire a mass though the Yukawa interaction with the Higgs VEV. This is in contrast with the masslessness of the photon: it is due to a gauge symmetry, which in turn governs the dynamics of the electromagnetic interaction.

There is no reason why neutrinos should have no mass, and in fact the discovery of neutrino oscillations implies they have very tiny masses. In the next chapter I will introduce the most popular mechanism to bring in neutrino masses: the seesaw mechanism emerging from the addition of the Weinberg dimension five operator, which as we will discuss in the following, leads to a non-renormalizable lagrangian.

In the end of this chapter I will comment on the renormalization procedure, and how it leads to our current use and understanding of effective field theories for describing phenomena occurring in Nature at different scales.

1.5.1. Renormalization

The physical observables we are concerned with in particle physics are (most of the time) computed from quantum mechanical amplitudes evaluated using perturbative QFT,

with the aid of the Feynman diagrams tool, which helps us to compute the different terms in a series expansion over the coupling constants appearing in the classical lagrangian of the theory. When we calculate physical quantities in perturbation theory, infinities may emerge as the result of taking into account higher order terms in the expansion (loop corrections).

In the traditional renormalization procedure one first regularizes the divergent integrals in the computation of Feynman diagrams with loops, subtracting the infinities either by putting a cutoff in the momentum dependence of the integrals, or using dimensional regularization. The integrals now depend on an energy (momentum) scale. When this energy scale is set to infinity the integral diverges. To fix that behavior, one adds a "counterterm" in the classical lagrangian for each divergent lagrangian term in order to cancel the infinity, and derives new Feynman rules which lead to finite results order by order in the perturbative expansion. In removing the ambiguities associated with infinities we introduce a dependence of the couplings on the energy scale at which a process takes place. One can study how this dependence changes: this is done calculating the differential equations giving the evolution of the couplings with the energy scale.

One can count how many divergent quantities are present in the theory: this can be done by counting the number of external legs and vertices a Feynman diagram has, relative to the space-time dimension considered. The theory will be *super-renormalizable* if only a finite number of amplitudes diverge, and *renormalizable* if one has a finite number of diverging amplitudes but divergences occur at all orders in perturbation theory. In these cases the counterterms needed to cancel the divergences have the same structure as the operators (the interaction terms) already present in the original lagrangian. *Non-renormalizable* theories are those in which all amplitudes are divergent at a sufficiently high order in perturbation theory. Also, this criterion can be translated to the mass dimensionality of the coupling constant: if it has positive or zero mass dimension (dimensionless), the theory is renormalizable. If the coupling constant has negative mass dimension, then the theory is non-renormalizable.

In spite of its successes the renormalization procedure presented above can be seen as some kind of prescription or recipe to get rid of the divergences in an ordered way. However, the work of Wilson [48–50] allows us to understand the process of renormalization in a very profound way as a procedure to incorporate the effects of physics at high energies by modifying the value of the parameters that appear in the lagrangian.

In this framework one assumes a particular theory (with a certain lagrangian, leading to a certain action including certain interactions between the fields) is valid up to some energy scale Λ, such that beyond it one needs to include new fields or new interactions in order to describe physics at that new high energy scale. We can regularize the diverging integrals taking this energy scale Λ as a regulator cutoff.

If we would like to compute the effective dynamics of the theory at an energy scale $\mu < \Lambda$, we only have to integrate out all physical modes with energies between the cutoff Λ and the scale of interest μ. One begins with a QFT defined by the lagrangian for the

fields φ_a

$$\mathcal{L}[\varphi_a] = \mathcal{L}_0[\varphi_a] + \sum_i g_i \mathcal{O}_i[\varphi_a] \tag{1.68}$$

where $\mathcal{L}_0[\varphi_a]$ is the kinetic term, and g_i are the couplings associated with the interaction operators $\mathcal{O}_i[\varphi_a]$. In principle we include all the operators $\mathcal{O}_i$ compatible with the symmetries of the theory.

The effective action $S[\varphi'_a, \mu]$ at the scale μ can be written in the language of functional integration as

$$e^{iS[\varphi'_a,\mu]} = \int_{\mu<p<\Lambda} \Pi_a \; \mathcal{D}\varphi_a \; e^{iS[\varphi_a,\Lambda]}. \tag{1.69}$$

Here $S[\varphi_a, \Lambda]$ is the action at the cutoff scale:

$$S[\varphi_a, \Lambda] = \int d^4x \left\{ \mathcal{L}_0[\varphi_a] + \sum_i g_i(\Lambda) \mathcal{O}_i[\varphi_a] \right\} \tag{1.70}$$

and the functional integral in (1.69) is carried only over the field modes with momenta in the range $\mu < p < \Lambda$. The action resulting from integrating out the physics at the intermediate scales between Λ and μ depends not on the original field variables φ_a but on some renormalized fields φ'_a. At the same time, the couplings $g_i(\mu)$ differ from their values at the cutoff scale $g_i(\Lambda)$. Therefore the resulting action at scale μ can be written as

$$S[\varphi'_a, \mu] = \int d^4x \left\{ \mathcal{L}_0[\varphi'_a] + \sum_i g_i(\mu) \mathcal{O}_i[\varphi'_a] \right\}. \tag{1.71}$$

The consequence for physics at low momentum is that we have to replace our action by a new one with different values for the couplings. Our ignorance of the details of the physics going on at high momentum results in a renormalization of the couplings of the action describing the long range physical processes.

In this procedure the running of the coupling with the energy scale can be understood as a way of incorporating into an effective action at scale μ the effects of field excitations at higher energies $E > \mu$. This dependence of the couplings with the momentum scale is the equivalent to the *renormalization group flow* in the Wilsonian approach. We can picture the action of the renormalization group transformation as a flow in the space of couplings, and thus as a flow in the space of different quantum field theories.

There are QFTs that are fixed points of the renormalization group flow, i.e. whose properly adimensionalized coupling constants do not change with the energy-momentum scale. When a scale invariant theory is perturbed with some operator: i.e. if we include some operator in the lagrangian perturbing an action that is already at a fixed point in the renormalization group flow, the perturbed theory is not scale invariant anymore but we may wonder whether the perturbed theory flows at low energies towards or away the fixed point theory. This can be decided by looking at the scaling dimension [5] d of the operator $\mathcal{O}$ used to perturb the theory at the fixed point. In four dimensions the three possibilities are:

[5] At tree-level the scaling dimension coincides with the canonical dimension.

- $d > 4$: irrelevant perturbation. The running of the coupling constants takes the theory back to the fixed point.
- $d < 4$: relevant perturbation. At low energies the theory flows away from the scale-invariant theory.
- $d = 4$: marginal deformation. The direction of the flow cannot be decided only on dimensional grounds.

The coefficient associated with an irrelevant operator dies away during the recursion of the integration to lower and lower momentum scales. Instead, the coefficients of the relevant operators grow. Relevant and marginal operators dominate the dynamics in the infrared, while irrelevant operators become suppressed in this limit.

One can interpret the relevant and marginal perturbing operators about a free lagrangian $\mathcal{L}_0$ as the super-renormalizable and renormalizable interaction terms described in the power-counting analysis we discussed above. The irrelevant operators are associated with non-renormalizable theories.

Since in the Wilsonian approach the quantum theory is always defined with a physical cutoff, there is no fundamental difference between renormalizable and non-renormalizable theories. A renormalizable field theory, like the Standard Model, can generate non-renormalizable operators at low energies such as the effective four-fermion interaction of Fermi's theory of nuclear beta decay. They are not sources of any trouble if we are interested in the physics at scales much below the cutoff $E \ll \Lambda$, since their contribution to the amplitudes is suppressed by powers of[6] E/Λ.

1.5.2. Effective field theories: a foreword

One of the main reasons behind the progress in the understanding of physical processes is the fact that at a given length scale and using the correct variables, our description of the physical phenomena is to a large extent independent of the physics at much shorter distances. The basic ingredients in the building of effective field theories (EFTs) are the light degrees of freedom and the relevant symmetries of the problem. The latter provide the guiding principle to write a lagrangian that would be the starting point for the calculation of physical observables.

A lagrangian constructed using only relevant and marginal operators defines a renormalizable theory, such as the SM, and these operators dominate infrared physics. Observables can then be computed in terms of a limited number of parameters associated to the renormalized couplings of the relevant and marginal operators in the action, but while this description is very accurate in the deep infrared (low energy) region, if we want to include the corrections due to new physics above an energy scale Λ we have to include higher dimension irrelevant operators. These, generically, will appear in the action suppressed by the necessary powers of the scale Λ at which the new degrees of freedom become excited.

[6] To preserve gauge invariance one has to use another method to regularize the integrals, as dimensional regularization.

As we go to higher energies effective theories are replaced by a more complete description. In general this process is repeated as we increase the energy. In EFTs we are interested in physical phenomena taking place in a range of energies much below the scale of new physics $E \ll \Lambda$, and the contributions of the non-renormalizable counterterms to a physical processes are weighted by powers of E/Λ. As it turns out, to a given degree of accuracy, there are only a few irrelevant operators that need to be taken into account in the computations. Therefore, non-renormalizable theories are predictive. Frequently it is experimental information that forces us to introduce higher-dimensional operators in a renormalizable theory, as is the case with the experimental fact that neutrinos have non-zero masses, as we will study in the following chapter 2.

The EFT approach has been widely used in order to facilitate the computation of observables in low energy regimes for theories in which the full ultraviolet renormalizable theory is well known (such as the Fermi's four-fermion interaction theory replacing the full electroweak SM interaction mediated by the vector bosons W, or the treatment of the interactions of mesons like pions or kaons, with masses well below the scale of QCD, etc.). In those cases the heavy fields are integrated out to bring the effective operators by means of the Euler-Lagrange equations of motion. We will present an example of this procedure for the neutrino mass generation in sec.2.6.

Many examples are worked out in reviews and lecture notes such as those in [51–53]. In those cases, the coefficients accompanying the distinct effective operators, and containing the information about the high energy physics, are calculated by the *matching* procedure: they are fixed to make the observables calculated with the full high energy theory equal to the effective lagrangian calculation, and then run down back to the low-energy scale using the renormalization group equations.

In this picture, the physics is described by a chain of different EFTs, with different particle content, which match each other at the corresponding boundary (heavy threshold). Each theory is the low–energy EFT of the previous underlying theory. Going backwards in this evolution, one goes from an effective to a more fundamental theory containing heavier scales.

From now on I will comment on the effective lagrangian extension of the SM, regarded as a low-energy effective theory deriving from some yet unknown ultraviolet theory involving new physics at an unknown high scale Λ.

1.5.3. Effective lagrangian extension of the Standard Model

The SM can be extended considering an effective lagrangian with irrelevant effective operators including just the known SM fields as degrees of freedom (the fermion fields in table 1.1, the four gauge bosons, and the Higgs field), and preserving the $SU(3)_c \times SU(2)_L \times U(1)_Y$ invariance, forming the following series:

$$\mathcal{L}_{eff} = \mathcal{L}_{SM} + \sum_{d=5}^{\infty} \left(\frac{1}{\Lambda^{d-4}} \sum_{\mathcal{J}} c_{\mathcal{J}} \mathcal{O}^d_{\mathcal{J}} + h.c \right) \tag{1.72}$$

where d indicates the canonical dimension of the operator $\mathcal{O}^d_{\mathcal{J}}$, $\mathcal{J}$ labels the distinct operators of the same dimension and Λ is the new physics scale.

The canonical dimension d for the operators is obtained from its field and derivatives content. The different field's canonical dimensions are fixed in the following way: the SM action $S = \int \mathcal{L}\, d^4x$ is dimensionless. Then working in natural units[7] x has dimensions of $[mass]^{-1}$ and the lagrangian density (which I will be just calling lagrangian throughout the thesis) has dimension $[mass]^4$ or just $d = 4$. Thus derivatives $\partial_\mu \equiv \frac{\partial}{\partial x^\mu}$ have canonical mass dimension 1 as well as scalar and vector boson fields, as can be checked from the terms (1.43) and (1.44). It can be seen from (1.55) that fermion fields have dimension $d = 3/2$. Written as in (1.72) the so called "Wilson coefficients" $c_{\mathcal{J}}$ are dimensionless.

The only dimension five operator containing the SM fields and invariant under the SM gauge group is the lepton number violating Weinberg operator [54] we will be considering in detail in section 2.5, as it provides a mass term for neutrinos. Next come dimension six operators, which have been thoroughly studied in the literature. A classical paper containing a pretty redundant but complete operator's list is [55], later revised by [56]. As one moves forward to higher mass dimension, the calculations of observable quantities with the use of the effective lagrangian (1.72) are proportional to a factor $(E/\Lambda)^{d-4}$, so for calculations of scattering cross sections or decay rates at a given energy $E \ll \Lambda$, which is usually given by the energy scale at which certain experiment is performed, the contribution of each term comes with a suppression factor and one needs to consider only the lowest dimension operators for a given desired accuracy.

The idea behind the use of effective lagrangian methods in the case one does not know the underlying ultraviolet theory is to *estimate our ignorance* by bounding the coefficients $c_{\mathcal{J}}$ with knowledge from experiments at the low-energy scale, where the effective lagrangian use is valid. This allows to get a hint of what kind of new physics is responsible for the low energy measured effects.

1.5.4. Perspectives

Until now I have reviewed the main features of the SM we will be concerned with in the rest of the thesis. Although this theory gives a spectacularly accurate description of most measured high energy physics phenomena, many issues remain unexplained. Neutrino mass is a conclusive experimental evidence of the need to include beyond the SM physics. In the following chapter we will be concerned with the problem of neutrino mass. It starts with a brief description of the neutrino oscillation phenomenon and how it is interpreted in terms of non-zero masses for the neutrinos, introducing various possibilities for generating neutrino masses in effective extensions of the SM.

The Dark Matter and the baryon asymmetry problems are frequently addressed in building new neutrino mass-generating models, as the *leptogenesis* scenario connects the neutrino mass mechanism with the matter-antimatter asymmetry of the universe. I will

[7] These units are defined by $\hbar = 1,\ c = 1$ for the Planck constant and the velocity of light in vacuum. In this system $[lenght] = [time] = [energy]^{-1} = [mass]^{-1}$.

not deepen on these and many other open and very interesting possibilities, but it is good to keep them in mind, as another motivation for studying neutrino physics nowadays.

Chapter 2

Massive neutrinos

This chapter is devoted to the introduction of the physics of massive neutrinos. I start with a very brief introduction of neutrino oscillations, moving to a detailed discussion of the typical neutrino mass generation mechanisms, in order to understand the modern view in which some lepton number violating new physics beyond the Standard Model, present at higher energies, is invoked to explain the observed neutrino masses.

The presentation of the basic theoretical aspects is mostly based on neutrino physics textbooks as [30,57,58] and more recent lecture notes and reviews as [59]. An introduction to the experimental aspects concerning neutrino oscillations can be found in [60].

2.1. Invitation: neutrino oscillations

It is well established experimentally that the neutrinos and antineutrinos taking part in the SM charged-current and neutral-current interactions reviewed in sec.1.4.3 are of three varieties of flavors. The electron-neutrino ν_e was discovered in 1956 by Cowan and Reines in the Savannah River reactor experiment [61]. The muon-neutrino ν_μ was discovered by Lederman, Schwartz and Steinberger in the Brookhaven National Laboratory (BNL) in 1962 [62] and the tau-neutrino ν_τ discovery was claimed by the DONuT Collaboration at Fermilab in 2001.

It is also well known that relativistic flavor neutrinos ν_ℓ are produced in weak interaction processes in a state that is predominantly left-handed. To account for this fact is that the ν_ℓ are described in the SM with a left-handed flavor neutrino field $\nu_{\ell,L}$ and -as there is yet not compelling evidence for the existence of states of relativistic neutrinos which are predominantly right-handed- no mass term is written in the SM lagrangian for the neutrinos, as we discussed in the previous chapter. However, the discovery of neutrino oscillations has led to the fact that neutrinos have a mass.

Neutrino oscillation is a quantum mechanical phenomenon proposed in the late 1950s by Pontecorvo [63,64]: neutrinos change flavor as they propagate through the vacuum and matter. The oscillations are generated by the interference of different massive neutrinos, which are produced and detected coherently because of their very small mass differences. In 1962 Maki, Nakagawa and Sakata represented the mixing of two neutrinos by a 2×2

matrix [65], and thus nowadays the matrix describing the oscillations is called PMNS (Pontecorvo-Maki-Nakagawa-Sakata).

The first indication that neutrino oscillations may in fact occur was an apparent deficit in the flux of electron-neutrinos with MeV energies that originate from the nuclear fusion chain in the core of the Sun (called solar neutrinos) detected via the charged-current interactions in (1.56)-(1.58). In 1968 [66] an experiment proposed by R. Davies in the Homestake Mine in South Dakota reported an upper bound for solar neutrinos that was a factor of two or three times smaller than predicted by the Standard Solar Model, developed by J.N. Bahcall in [67,68] and explaining the expected neutrino fluxes due to the nuclear reaction chains in the Sun. Already in 1968 Pontecorvo and Gribov suggested that the deficit could be due to electron into muon-neutrino oscillations $\nu_e \to \nu_\mu$ [69]. This *solar neutrino problem* persisted in many experiments until the neutral-current measurements made in the Sudbury Neutrino Observatory (SNO) first presented in 2001 confirmed the oscillation hypothesis [70–72]. There the combined flux of the three flavor neutrinos could be measured, exploiting the neutral-current interactions in (1.61).

The first confirmed oscillations were of GeV-energy neutrinos originated in the weak decays of pions e.g. $\pi^+ \to \mu^+ + \nu_\mu$, kaons and muons produced by the interactions of cosmic rays with the Earth's atmosphere: the so called *atmospheric neutrinos*. In the early studies of atmospheric neutrino events by the Kamiokande [73, 74] and IMB experiments [75, 76], after 1988, the ν_e/ν_μ rate was a factor of two above expectations: a deficit of ν_μ produced in the atmosphere on the other side of the Earth and detected from the underground direction (upward events) was found, but not for those produced on the same side (downward events). In 1998 the Super-Kamiokande experiment [77, 78] discovered that muon-neutrinos were oscillating into tau-neutrinos during their journey through the Earth, consistently matching the dependence with the energy and distance traveled to the $\nu_\mu \to \nu_\tau$ oscillation predictions.

The spectacular discovery of neutrino oscillations[1] is a compelling experimental evidence of physics beyond the Standard Model. In this section I will discuss the basic aspect of this phenomenon: the implication that neutrinos have mass.

Oscillation formula for mono-energetic neutrinos in vacuum

If we consider a neutrino beam created in a charged interaction together with a charged lepton ℓ^-, by definition, the created neutrino has flavor ℓ, thus it is called ν_ℓ. One can consider that this is not a physically propagating particle, but is rather a superposition of propagating fields ν_α with masses m_α:

$$|\nu_\ell\rangle = \sum_\alpha U_{\ell\alpha} |\nu_\alpha\rangle \tag{2.1}$$

where U is a unitary matrix.

[1] In 2015 the Nobel Prize in Physics was given to the directors of the SNO and Super-Kamiokande experiments, Arthur B. Mc. Donald and Takaaki Kajita "for the discovery of neutrino oscillations, which shows that neutrinos have mass".

Although the momentum $\vec{p}$ of the different components in the beam are the same and determined by momentum conservation in the process in which neutrinos are created, the energies of the components are not the same -given that they have distinct masses- and $E_\alpha = \sqrt{\vec{p}^{\,2} + m_\alpha^2}$. After a time t, the evolution of the initial beam is given by the Schrödinger equation

$$|\nu_\ell(t)\rangle = \sum_\alpha e^{-iE_\alpha t} U_{\ell\alpha} |\nu_\alpha\rangle. \tag{2.2}$$

Since the E_α's are not equal, this state represents a different superposition of the physical states $|\nu_\alpha\rangle$ compared to (2.1) and in general this state has not only the properties of a ν_ℓ, but also those of other flavor states. The amplitude for finding a $\nu_{\ell'}$ in the original ν_ℓ beam is

$$\langle \nu_{\ell'} \mid \nu_\ell(t)\rangle = \sum_{\alpha\beta} \langle \nu_\beta \mid U^\dagger_{\beta\ell'} e^{-iE_\alpha t} U_{\ell\alpha} |\nu_\alpha\rangle = \sum_\alpha e^{-iE_\alpha t} U_{\ell\alpha} U^*_{\ell'\alpha}, \tag{2.3}$$

where we have used the fact that the mass eigenstates are orthonormal: $\langle \nu_\beta \mid \nu_\alpha\rangle = \delta_{\beta\alpha}$. At $t = 0$ the amplitude is just $\delta_{\ell\ell'}$, due to the unitarity of U. At time t the probability of finding a $\nu_{\ell'}$ in an originally ν_ℓ beam is

$$P_{\nu_\ell\nu_{\ell'}}(t) = |\langle \nu_{\ell'} \mid \nu_\ell(t)\rangle|^2 = \sum_{\alpha\beta} |U_{\ell\alpha} U^*_{\ell'\alpha} U^*_{\ell\beta} U_{\ell'\beta}| \cos[(E_\alpha - E_\beta)t - \varphi_{\ell\ell'\alpha\beta}], \tag{2.4}$$

where $\varphi_{\ell\ell'\alpha\beta} = \arg(U_{\ell\alpha} U^*_{\ell'\alpha} U^*_{\ell\beta} U_{\ell'\beta})$. In all practical situations neutrinos are extremely relativistic, so we can approximate the energy-momentum relation as

$$E_\alpha \simeq |\vec{p}\,| + \frac{m_\alpha^2}{2|\vec{p}\,|}, \qquad |\vec{p}\,| = E \tag{2.5}$$

and we can also replace the time t for the distance traveled by the beam[2] L, thus we get

$$P_{\nu_\ell\nu_{\ell'}}(t) = \sum_{\alpha\beta} |U_{\ell\alpha} U^*_{\ell'\alpha} U^*_{\ell\beta} U_{\ell'\beta}| \cos\left[\frac{2\pi L}{L_{\alpha\beta}} - \varphi_{\ell\ell'\alpha\beta}\right], \tag{2.6}$$

with

$$L_{\alpha\beta} \equiv \frac{4\pi E}{\Delta m^2_{\alpha\beta}}, \qquad \Delta m^2_{\alpha\beta} \equiv m^2_\alpha - m^2_\beta. \tag{2.7}$$

The quantities $|L_{\alpha\beta}|$ are called *oscillation lengths*. These give a distance scale over which the oscillation effects are appreciable. If the distance L is an integer multiple of all $L_{\alpha\beta}$ one has $P_{\nu_\ell\nu_{\ell'}} = \delta_{\ell\ell'}$ as in the original beam, but at other distances the effects of the mixing can be detected. In particular, the dependence of the probability with the distance is probed in experiments. It can also be rewritten in the usual form

$$P_{\nu_\ell\nu_{\ell'}}(t) = \sum_{\alpha\beta} |U_{\ell\alpha} U^*_{\ell'\alpha} U^*_{\ell\beta} U_{\ell'\beta}| \cos\left[\frac{\Delta m^2_{\alpha\beta} L}{2E} - \varphi_{\ell\ell'\alpha\beta}\right]. \tag{2.8}$$

[2]We work with natural units, in which the speed of light is $c = 1$, and then $c = \frac{L}{t}$, so that $t = L$.

So neutrino oscillations, i.e. the flavor change during propagation, imply that neutrinos have a mass: the squared mass differences $\Delta m^2 \neq 0$ are needed in order to have a non-zero oscillation probability. In the several current and past experiments on neutrino oscillations the oscillation lengths, squared mass parameters and the L/E dependence, as well as the mixing matrix U_{PMNS} parameters are measured with great accuracy.

All existing compelling data on neutrino oscillations can be described assuming 3-flavor neutrino mixing in vacuum. This is the minimal mixing scheme which can account for the available data on the oscillations of the solar (mostly ν_e), atmospheric (mostly ν_μ and $\bar{\nu}_\mu$), reactor ($\bar{\nu}_e$) and accelerator (ν_μ and $\bar{\nu}_\mu$) neutrinos[3]. The existing data allow the determination of the values of the squared mass differences between the mass states $\Delta m^2_{\alpha\beta}$. For instance, the best fit value for Δm^2_{12} is $7.37 \times 10^{-5}\ eV^2$ [1]. Data on the absolute scale of neutrino masses can be obtained by measuring the spectrum of the electrons in tritium ^3H β-decay experiments, and from cosmological and astrophysical data. The most stringent upper bound $m_{\bar{\nu}_e} < 2.05\ eV$ is given by the Troitzk experiment [79]. The Planck Collaboration obtained a constraint on the sum of the neutrino masses, assuming the existence of three light massive neutrinos -and other model dependent information- which added to baryon acoustic oscillations (BAO) and supernovae data give the limit $\sum_j m_j < 0.23\ eV$ [80].

I will not deepen into the neutrino oscillations phenomenology, but start discussing different historically relevant theoretical models that predict masses for the neutrinos.

2.2. A Dirac mass

A Dirac neutrino mass can be generated with the same Higgs mechanism that gives masses to quarks and charged leptons in the SM, as we saw in sec.1.4. The only extension of the SM that is needed is the introduction of right-handed neutrino components $\nu_{\ell,R}$ for $\ell = e, \mu, \tau$. Let's recall, however, that right-handed neutrino fields are fundamentally different from the other elementary fermion fields, because they are invariant under the symmetries of the SM: they are singlets of the $SU(3)_C \times SU(2)_L$ symmetry group and have zero-hypercharge ($Y = 0$). This is in order to be compatible with the experimental non-finding of right-handed neutrino states. The right-handed neutrino fields are called *sterile*[4] because they don't participate in weak interactions, as well as strong or electromagnetic interactions, like any neutrino. Their only interaction is gravitational[5]. The usual neutrinos, participating in weak interactions, are called *active*.

Also, it is important to notice that the introduction of right-handed neutrino fields is completely irrelevant for the cancellation of quantum anomalies constraining the fermion content in the SM mentioned in sec.1.4.4. So the number of right-handed neutrinos

[3]There have been possible hints for the presence in mixing of one or more additional sterile massive states, obtained by the LSND and MiniBooNe experiments, and short baseline (SBL) reactor neutrino oscillation data. We will discuss them in chapter 4.

[4]The name was first introduced by Pontecorvo in [81].

[5]Let's emphasize that right-handedness is not an essential quality of the new chiral fields, because we could work as well with left-handed chiral fields $\tilde{\nu}_{\ell,L} = \nu^c_{\ell,R}$ as we saw in 1.2.3. The essential characteristic is that the fields are SM singlets, and hence sterile.

is unconstrained by the theory, although it is usual to introduce three right-handed neutrinos (one for each fermion family), but in fact, the presence of only one sterile right-handed neutrino cannot be excluded.

Thus one can extend the SM with three right-handed neutrino fields $\nu'_{\ell,R}$ (the primes indicating it is not a mass eigenstate) -completing the fermion content in (1.49)- and generating a Yukawa term that can be added to (1.50)

$$\mathcal{L}_{Yukawa} = -\Gamma_u^{ij}\bar{Q'}^i_L\tilde{\Phi}u'^j_R - \Gamma_d^{ij}\bar{Q'}^i_L\Phi d'^j_R - \Gamma_\ell^{ij}\bar{L'}^i_L\Phi\ell'^j_R - \Gamma_\nu^{ij}\bar{L'}^i_L\tilde{\Phi}\nu'^j_{\ell,R} + h.c. \tag{2.9}$$

which in the unitary gauge can be written as in (1.52)

$$\mathcal{L}_Y = -\left(1+\frac{h}{v}\right)\left[\bar{d'}_L M'_d d'_R + \bar{u}'_L M'_u u'_R + \bar{\ell}'_L M'_\ell \ell'_R + \bar{\nu}'_{\ell,L} M'_{\nu_\ell}\nu'_{\ell,R}\right]. \tag{2.10}$$

This lagrangian can be diagonalized in the same way we did in sec.1.4.2, generating a mixing between the three Dirac neutrinos in the same way the Cabibbo-Kobayashi-Masakawa V_{CKM} matrix allows for quark flavor-mixing. Recalling from sec.1.4.2 that the matrices $M_\nu = S_{\nu_\ell} M'_{\nu_\ell} U^\dagger_{\nu_\ell} S^\dagger_{\nu_\ell}$ are diagonal, with the neutrino's masses as entries, the massive chiral neutrino arrays are written in terms of the gauge eigenstates as $\nu_{i,L} = S_{\nu_\ell}\nu'_{\ell,L}$ and $\nu_{i,R} = S_{\nu_\ell} U_{\nu_\ell}\nu'_{\ell,R}$, so the mass terms for the neutrinos can be written as

$$\mathcal{L}^D = -\bar{\nu}_{i,L} m_i^D \nu_{i,R} + h.c. \tag{2.11}$$

Here it is made explicit that the massive chiral eigenstates are identified with an index $i = 1, 2, 3$. The superscript D indicates that these mass terms are of the Dirac type.

The neutrino masses we obtain with this mechanism are proportional to the scalar VEV v and the Yukawa couplings Γ_ν, just as the masses of the charged leptons and the quarks. However, it is known that the masses of the neutrinos are much smaller than those of charged leptons and quarks. In the mechanism just described, there is no explanation of the very small values of the Yukawa neutrino couplings. In fact, this question is also left open in the framework of the SM. For example, for the particles in the third fermion family the mass values are:

$$m_t \simeq 173\ GeV, \quad m_b \simeq 4.2\ GeV \quad m_\tau \simeq 1.78\ GeV \quad m_3 \lesssim 0.2\times 10^{-9}\ GeV, \tag{2.12}$$

so the neutrino mass in the third family is 10 orders of magnitude smaller than the corresponding charged lepton mass, and this concrete cold fact is left unexplained if we only extend the SM with sterile neutrinos leading to a Dirac neutrino mass term.

As the massive chiral neutrino states are written in the form $\nu_{i,L} = S_{\nu_\ell}\nu'_{\ell,L}$, this mechanism provides us with a mixing relation between the flavor neutrino left-handed fields $\nu_{\ell,L}$ and the left-handed component of the Dirac massive neutrino fields $\nu_{i,L}$:

$$\nu_{\ell,L} = \sum_{i=1}^{3} S^\dagger_{\nu_\ell}\nu_{i,L}. \tag{2.13}$$

This mixing changes the neutrinos electroweak currents we found in sec.1.4.2. The leptonic charged current coupling neutrinos and charged leptons to the charged $W^{\pm}$ bosons in (1.59) is now written in terms of the massive chiral neutrino states $\nu_{i,L}$ as

$$J^{\mu}_{lep} = \bar{\nu}'_{\ell,L}\gamma^{\mu}\ell'_L = \bar{\nu}_{i,L}S_{\nu_\ell}\gamma^{\mu}S^{\dagger}_{\ell}\ell_L = \bar{\nu}_{\ell,L}\gamma^{\mu}S_{\nu_\ell}S^{\dagger}_{\ell}\ell_L = \bar{\nu}_{\ell,L}\gamma^{\mu}U^{\dagger}_{\ell i}\ell_L. \tag{2.14}$$

Here, in the last step we define the neutrino mixing matrix

$$U_{\ell i} = S_{\ell}S^{\dagger}_{\nu_\ell}. \tag{2.15}$$

This definition allows us to write, as is customary, the left-handed flavor neutrino fields:

$$\nu_{\ell,L} = U_{\ell i}\nu_{i,\ell} \qquad \nu_{\ell,L} = \begin{pmatrix} \nu_{e,L} \\ \nu_{\mu,L} \\ \nu_{\tau,L} \end{pmatrix} \tag{2.16}$$

and the charged current can be written as in the SM:

$$J^{\mu}_{lep} = \bar{\nu}_{i,L}U^{\dagger}_{\ell i}\gamma^{\mu}\ell_L. \tag{2.17}$$

It should be stressed that the flavor neutrino fields must be treated with caution: in practice they are useful only for calculations in which the effects of neutrino masses are neglected, i.e. in the SM limit.

As in the SM, the unitarity of the charged lepton and neutrino mixing matrices leads to the GIM mechanism we saw in (1.61).

The right-handed components of the massive neutrinos $\nu_{i,R}$ do not enter in the weak charged-current in (2.17). Hence, they represent sterile degrees of freedom, not participating in weak interactions. That is why we do not define superpositions of right-handed neutrino fields as in (2.13). In the presence of Dirac mixing, the active and sterile degrees of freedom remain decoupled, and in particular, oscillation between active and sterile states is not possible in this formalism.

Total lepton number conservation

For massive Dirac neutrinos the flavor lepton numbers L_e, L_μ, L_τ defined in sec. 1.4.4 are not conserved, as there is no global $U(1)$ transformation on the charged leptons and neutrino flavor fields leaving invariant the Yukawa and kinetic lagrangians for neutrinos. But -assuming baryon number is conserved- total lepton number $L = n_l - n_{\bar{l}}$ is conserved, as the lagrangian is still invariant under the global $U(1)$ transformations

$$\begin{aligned} \nu_{i,L} &\to e^{i\varphi}\nu_{i,L}, \qquad \nu_{i,R} \to e^{i\varphi}\nu_{i,R} \quad (i = 1,2,3) \\ \ell_{\alpha,L} &\to e^{i\varphi}\ell_{\alpha,L}, \qquad \ell_{\alpha,R} \to e^{i\varphi}\ell_{\alpha,R} \quad (\alpha = e,\mu,\tau) \end{aligned} \tag{2.18}$$

with the same phase φ for the independent chiral neutrino and charged lepton fields. Neutrinos and negatively charged leptons have $L = +1$, whereas anti-neutrinos and anti-charged leptons (with positive electric charge) have $L = -1$. The lepton quantum number

is different for neutrinos and anti-neutrinos. Here, the Dirac character of neutrinos -which implies that neutrinos and anti-neutrinos are different particles- is closely related to the invariance of the total lagrangian under the transformations in (2.18)[6].

2.3. Majorana masses

As we saw in sec.1.2.1, one can write fermion mass terms using only one Weyl spinor, as in equations (1.16) and (1.17). There we introduced the Majorana mass terms as those made out of only a left-handed or right-handed Weyl spinor. We saw those mass terms are allowed only for fields that do not carry any charge, as they are not invariant under, in particular, global $U(1)$ transformations.

The right-handed sterile neutrino $\nu_{\ell,R}$ we introduced in sec.2.2 carries no SM charge, so we can construct a Majorana mass term out of it if we drop the possibility of lepton number conservation. In fact, if we do not consider lepton number as an exact symmetry in the theory there is no reason why a Majorana mass term is forbidden for $\nu_{\ell,R}$ and, thus, we must include it in the lagrangian.

We saw in sec.1.2.3 that we can use the charge conjugation operation to construct the left-handed field

$$\nu^c_{\ell,R} = \mathcal{C}\gamma^0 \nu^*_{\ell,R} = \mathcal{C}(\bar{\nu}_{\ell,R})^T, \tag{2.19}$$

using the relation given in (1.31). The Majorana mass term for $\nu_{\ell,R}$ can then be written as

$$\mathcal{L}^M_R = -\frac{1}{2} m^M_R \bar{\nu}_{\ell,R}\, \mathcal{C}\, (\bar{\nu}_{\ell,R})^T + h.c. = -\frac{1}{2} m^M_R \bar{\nu}_{\ell,R}\, \nu^c_{\ell,R} + h.c. \tag{2.20}$$

So if we incorporate sterile neutrinos to the SM (this is already physics *beyond the Standard Model*) and we do not promote the accidental lepton number conservation to an exact symmetry in our new extended theory, we are obliged to incorporate both Dirac and Majorana mass terms in the lagrangian giving mass to neutrinos. This theory preserves all the SM gauge symmetry. However, if we include both the Dirac and Majorana terms in our neutrino mass lagrangian, then the $\nu_{\ell,L}$ and $\nu_{\ell,R}$ do not pair up to form one Dirac neutrino field, and we will see soon that in fact massive neutrinos are Majorana particles, following the definition given in (1.33).

We could also construct a Majorana mass term with the known SM left-handed $\nu_{\ell,L}$. A term of this kind is strictly forbidden in the SM, as it is not invariant under $SU(2)_L \times U(1)_Y$ gauge symmetry transformations. However, as we will see later, a term like this could be generated by new physics beyond the SM.

With the aid of the charge conjugation operator we can construct the right-handed field

$$\nu^c_{\ell,L} = \mathcal{C}\gamma^0 \nu^*_{\ell,L} = \mathcal{C}(\bar{\nu}_{\ell,L})^T, \tag{2.21}$$

[6] As in the SM, the conserved quantum number is indeed $B - L$, as we argued in sec.1.4.4.

as we did in (2.19). Thus we can now write a Majorana mass only using the standard neutrino field $\nu_{\ell,L}$:

$$\mathcal{L}_L^M = -\frac{1}{2} m_L^M \bar{\nu}_{\ell,L} \mathcal{C} (\bar{\nu}_{\ell,L})^T + h.c. = -\frac{1}{2} m^M \bar{\nu}_{\ell,L} \nu_{\ell,L}^c + h.c. \tag{2.22}$$

2.4. Dirac-Majorana mass term

The most general neutrino mass term which can be built from the flavor left-handed fields $\nu_{\ell,L}$ and sterile fields $\nu_{\ell,R}$ has the form

$$\mathcal{L}^{D+M} = -\frac{1}{2} \bar{\nu}_{\ell,L}\ m_L^M\ \nu_{\ell,L}^c - \bar{\nu}_{\ell,L}\ m^D\ \nu_{\ell,R} - \frac{1}{2} \bar{\nu^c}_{\ell,R}\ m_R^M\ \nu_{\ell,R} + h.c. \tag{2.23}$$

One should notice here that the 1/2 factors in both Majorana terms avoid double counting, as $\nu_{\ell,L}^c$ and $\bar{\nu}_{\ell,L}$ are not independent, but $\nu_{\ell,L}^c = \mathcal{C} \bar{\nu}_{\ell,L}^T$ and the same holds for $\nu_{\ell,R}$. This distinguishes the Majorana from the Dirac mass terms. The lagrangian in (2.23) is usually called *the Dirac and Majorana neutrino mass term* [82, 83].

The matrices m_L^M, m^D and m_R^M are non-diagonal, complex 3×3 matrices. One can see the Majorana $m_{L,R}^M$ matrices are symmetrical[7] -taking into account that spinor fields anti-commute- and that $\mathcal{C}^T = -\mathcal{C}$ (carrying no flavor indices):

$$\bar{\nu}_L\ m_{L,R}^M\ \mathcal{C}\ \bar{\nu}_{L,R}^T = -\bar{\nu}_{L,R} (m_{L,R}^M)^T \mathcal{C}^T \bar{\nu}_{L,R}^T = \bar{\nu}_{L,R} (m_{L,R}^M)^T\ \mathcal{C}\ \bar{\nu}_{L,R}^T. \tag{2.24}$$

Let's now show that the neutrinos with definite masses generated by (2.23) are Majorana particles, i.e. they obey the Majorana condition given in (1.33).

Defining the column vector of left-handed fields

$$n_L = \begin{pmatrix} \nu_{\ell,L} \\ \nu_{\ell,R}^c \end{pmatrix} \tag{2.25}$$

and the symmetrical 6×6 mass matrix

$$M^{D+M} = \begin{pmatrix} m_L^M & m^D \\ (m^D)^T & m_R^M \end{pmatrix} \tag{2.26}$$

the mass lagrangian can be written as

$$\mathcal{L}^{D+M} = -\frac{1}{2} \bar{n}_L M^{D+M} n_L^c + h.c. \tag{2.27}$$

A symmetrical matrix can be diagonalized by a unitary matrix U, giving $M^{D+M} = U\ m\ U^T$, with m a diagonal matrix with positive elements. So, we can write

$$\mathcal{L}^{D+M} = -\frac{1}{2} \overline{U^\dagger n_L}\ m\ (U^\dagger n_L)^c - \frac{1}{2} \overline{(U^\dagger n_L)^C}\ m\ U^\dagger n_L = -\frac{1}{2} \bar{\nu}^m \nu^m = -\frac{1}{2} \sum_{i=1}^{i=6} m_i \bar{\nu}_i \nu_i. \tag{2.28}$$

[7] Here I drop the flavor ℓ subindex, for simplicity.

Here the mass eigenstates are

$$\nu^m = U^\dagger n_L + (U^\dagger n_L)^c = \begin{pmatrix} \nu_1 \\ . \\ . \\ . \\ \nu_6 \end{pmatrix}. \tag{2.29}$$

Then each field ν_i has mass m_i and satisfies the Majorana condition $\nu_i = \nu_i^c = \mathcal{C}\bar{\nu}_i^T$.

So far we have seen that in the case we generate the neutrino masses with a lagrangian including Dirac and Majorana mass terms the resulting massive fields are Majorana particles: they are their own antiparticle. Also, we should keep in mind that as we have included a Majorana mass term this theory violates both individual family and total lepton numbers. These are both general features taking place every time we include Majorana mass terms in the lagrangian of our theory.

2.4.1. One generation seesaw mechanism

The seesaw mechanism is the most popular mechanism of (very) small neutrino masses generation [8–11]. In this section I will introduce the main idea behind the seesaw mechanism in the simple case of just one fermion generation.

The Dirac and Majorana lagrangian mass terms are given by the expression

$$\mathcal{L}^{D+M} = -\frac{1}{2} m_L \bar{\nu}_L \nu_L^c - m_D \bar{\nu}_L \nu_R - \frac{1}{2} m_R \bar{\nu}_R^c \nu_R + h.c. \tag{2.30}$$

where we will assume m_L, m_D and m_R are real parameters. As we did in (2.28), we can write the lagrangian as

$$\mathcal{L}^{D+M} = -\frac{1}{2} \bar{n}_L M^{D+M} n_L^c + h.c. \tag{2.31}$$

now with a two row n_L, and a 2×2 matrix M^{D+M} which is real and symmetric. So, it can be easily diagonalized by an orthogonal matrix O, giving $M^{D+M} = O\ m'\ O^T$. Here $m'_{ij} = m'_i \delta_{ij}$ is a diagonal matrix with eigenvalues $m'_1 < m'_2$

$$m'_{1,2} = \frac{1}{2}(m_R + m_L) \mp \frac{1}{2}\sqrt{(m_R - m_L)^2 + 4m_D^2}. \tag{2.32}$$

From the relation

$$M^{D+M} = O\ m'\ O^T = \tag{2.33}$$
$$\begin{pmatrix} m_L & m_D \\ m_D & m_R \end{pmatrix} = \begin{pmatrix} \cos\theta & \sin\theta \\ -\sin\theta & \cos\theta \end{pmatrix} \begin{pmatrix} m'_1 & 0 \\ 0 & m'_2 \end{pmatrix} \begin{pmatrix} \cos\theta & -\sin\theta \\ \sin\theta & \cos\theta \end{pmatrix}$$

one finds the mixing angle θ is defined by

$$\cos(2\theta) = \frac{m_R - m_L}{\sqrt{(m_R - m_L)^2 + 4m_D^2}}, \quad \tan(2\theta) = \frac{2m_D}{(m_R - m_L)}. \tag{2.34}$$

As the eigenvalues $m'_{1,2}$ can be positive or negative, we can write down $m'_i = m_i\eta_i$, with $m_i = |m'_i|$ and $\eta_i = \pm 1$. Taking the unitary matrix $U = O\sqrt{\eta}$ one diagonalizes $M^{D+M} = U\ m\ U^T$ bringing the mass lagrangian to the usual form

$$\mathcal{L}^{D+M} = -\frac{1}{2}\ m\ \bar{\nu}^m \nu^m \tag{2.35}$$

with

$$\nu^m = U^\dagger n_L + (U^\dagger n_L)^c = \begin{pmatrix} \nu_1 \\ \nu_2 \end{pmatrix}. \tag{2.36}$$

Thus, the fields ν_L and ν_R^c are connected with the massive ν_{1L} and ν_{2L} by the following mixing relations

$$\begin{aligned} \nu_L &= \cos\theta\sqrt{\eta_1}\nu_{1L} + \sin\theta\sqrt{\eta_2}\nu_{2L} \\ \nu_R^c &= -\sin\theta\sqrt{\eta_1}\nu_{1L} + \cos\theta\sqrt{\eta_2}\nu_{2L}. \end{aligned} \tag{2.37}$$

We have seen that neutrino masses are many orders of magnitude smaller than the masses of the charged leptons and quarks, which as we saw in sec. 1.4.2 are all generated by the standard Higgs mechanism of electroweak symmetry breaking. This has been considered as evidence in favor of a non-standard mechanism for neutrino mass generation. Now we will see how the seesaw mechanism connects the smallness of the observed neutrino masses with the violation of total lepton number at a new high energy scale.

The standard (Type I) seesaw mechanism [8–11], is based on the following assumptions:

- The Dirac mass term is generated by the Higgs mechanism, so m_D is of the order of the mass of a charged lepton.
- There is no left-handed Majorana mass term in the lagrangian: $m_L = 0$.
- The constant m_R -which characterizes the right-handed Majorana mass term for the sterile ν_R- is much larger than m_D:

$$m_R \gg m_D. \tag{2.38}$$

From (2.32), (2.34) and (2.38), we have:

$$m'_1 \simeq -\frac{m_D}{m_R} m_D, \quad m'_2 \simeq m_R \quad \tan(2\theta) \simeq \frac{m_D}{m_R} \ll 1. \tag{2.39}$$

Since m'_1 is negative, we have $\eta_1^2 = -1$ and thus $m_1 \simeq \frac{m_D}{m_R} m_D$ and $m_2 \simeq m_R$.

Then we find the seesaw mechanism generates a light neutrino mass m_1 which is much smaller than the Dirac charged lepton masses. In fact, this mass m_1 gets smaller the bigger is the heavy Majorana particle's mass $m_2 \simeq m_R$. The heavy mass m_2 of ν_2

is responsible for the lightness of ν_1, and hence the name seesaw for the mechanism. Summarizing, the Type I seesaw mechanism gives the relations

$$m_1 \simeq \frac{m_D}{m_R} m_D \tag{2.40}$$

$$m_2 \simeq m_R \tag{2.41}$$

In the seesaw limit, the mixing matrix $U = O\sqrt{\eta}$ takes the form

$$U = \begin{pmatrix} \cos\theta & \sin\theta \\ -\sin\theta & \cos\theta \end{pmatrix} \sqrt{\eta} \simeq \begin{pmatrix} 1 & m_D/m_R \\ -m_D/m_R & 1 \end{pmatrix} \sqrt{\eta} \tag{2.42}$$

if we just keep terms up to linear in $m_D/m_R \ll 1$.

The mixing angle given by (2.39) is very small, thus ν_1 is mainly composed of the active ν_L, and the heavy ν_2 is mainly composed of the sterile ν_R^c, as can be seen from (2.37).

The seesaw mechanism is very important, because it provides a very plausible explanation of the smallness of neutrino masses with respect to the SM charged leptons. The assumption $m_L = 0$ is natural, since a Majorana mass term for the chiral field ν_L is forbidden by the SM gauge symmetries and renormalizability. The Dirac mass m_D -which can be generated through the SM Higgs mechanism- is expected to be of the order of the charged leptons mass, or of the order of the type-up quark mass of the same generation. In any case, the order of magnitude of m_D cannot be much larger than the electroweak scale (which is $10^2\ GeV$) because a Dirac mass term is forbidden by the unbroken symmetries of the SM. This fact is summarized by saying that m_D is *protected* by the SM symmetries. It can only arise as the result of spontaneous symmetry breaking, as for the other particles in the SM. On the other hand, since the Majorana mass term in (2.20) is a singlet of the SM symmetries, the Majorana mass m_R of the right-handed chiral neutrino field ν_R is not protected by SM symmetries, and can be very big.

2.5. Effective Majorana mass and seesaw mechanism

The Majorana mass term for the left-handed standard chiral field $\nu_{\ell,L}$ considered in (2.20) is forbidden by the SM gauge symmetries, as we already mentioned in sec.2.3.

However, if one considers the SM as a low-energy effective field theory as we discussed in sec.1.5.2, given the field content and the gauge symmetries of the SM there is only one dimension five operator first introduced by Weinberg [54] which leads to neutrino masses after the electroweak symmetry breaking:

$$\mathcal{L}^5 = -\frac{\lambda^{\ell\ell'}}{2\Lambda} L_{\ell,L} L_{\ell',L} \phi\ \phi + h.c. \tag{2.43}$$

Here $\lambda^{\ell\ell'}$ is a symmetric matrix, and Λ represents an unknown high energy lepton number violating scale. This effective operator has only three renormalizable tree-level high-energy realizations: all of them lead to a *seesaw relation* similar to (2.40). They are called respectively Type I, II an III seesaw mechanisms [84].

- In the Type I seesaw mechanism, the scalar doublet ϕ and the lepton doublet $L_{\ell,L}$ combine into an $SU(2)_L$ scalar, and the intermediate heavy particles are fermion singlets: sterile Majorana neutrinos.

- In the Type II seesaw mechanism, the product of $L_{\ell,L}$ and $L_{\ell',L}$ forms as scalar $SU(2)_L$ triplet $(L^T_{\ell,L}\sigma^i L_{\ell',L})(\phi^T\sigma^i\phi)/2\Lambda$. The intermediate heavy particle is a scalar triplet [83, 85–88].

- In the Type III seesaw mechanism $L_{\ell,L}$ and ϕ form a fermion triplet: $(L^T_{\ell,L}\sigma^i\phi)(L^T_{\ell',L}\sigma^i\phi)/2\Lambda$. The intermediate particle is also a fermion triplet [89].

Type I seesaw

In the Type I seesaw mechanism, the Weinberg operator in (2.43) can be explicitly written as

$$\mathcal{L}^5 = \frac{1}{2\Lambda}\lambda^{\ell\ell'}(L^T_{\ell,L}\epsilon\phi)\ \mathcal{C}\ (\phi^T\epsilon\ L_{\ell',L}) + h.c. \tag{2.44}$$

When the electroweak spontaneous symmetry breaking takes place, as in (1.41), the Weinberg operator generates the Majorana mass term

$$\mathcal{L}_M = -\frac{m^{\ell\ell'}v^2}{2}\nu^T_{\ell,L}\ \mathcal{C}\ \nu_{\ell',L} + h.c. \tag{2.45}$$

with the Majorana mass matrix of the neutrinos given by the relation

$$\frac{m^{\ell\ell'}}{2} = \frac{\lambda^{\ell\ell'}v^2}{\Lambda}. \tag{2.46}$$

2.6. "Vanilla" Type I seesaw model

The most popular realization of the Type I seesaw mechanism is usually called the *vanilla seesaw*. It is implemented by the addition of three sterile right-handed neutrinos[8] $N_{i,R}$ to the SM fields, and writing the most general dimension four renormalizable lagrangian with Dirac and Majorana mass terms, above the electroweak scale:

$$\mathcal{L}_\nu = -\Gamma_{\ell,j}\overline{L_{\ell,L}}\epsilon\phi^* N_{j,R} - \frac{1}{2}(N_{i,R})^T\mathcal{C}M_{ij}N_{j,R} + h.c. \tag{2.47}$$

Here, the first term is the Yukawa interaction that will lead to the Dirac mass term, as we saw in (2.2).

If we consider the mass of the sterile fields $N_{i,R}$ to be very heavy we can integrate out these fields by solving their Euler-Lagrange equations of motion taking into account that in this limit they behave as classical, non-dynamical static fields [90]. Thus we can

[8] I distinguish the $N_{i,R}$ fields from the $\nu_{\ell,R}$ presented before in order to stress that these new fields are not related to the standard $\nu_{\ell,L}$ by charge conjugation.

neglect the kinetic term in the lagrangian and the equation of motion reads $\frac{\partial \mathcal{L}_\nu}{\partial N_{j,R}} \simeq 0$, which, switching to an index free notation for simplicity, can be written as

$$\frac{\partial \mathcal{L}_\nu}{\partial N_R} = -\bar{L}_L \Gamma \epsilon \phi^* - N_R^T M \mathcal{C} + h.c. \tag{2.48}$$

Solving for N_R [28] gives $N_R = \phi^\dagger \epsilon \ \mathcal{C} \ \gamma^0 (\Gamma M^{-1})^T L_L^*$. Plugging this expression back in $\mathcal{L}_\nu$ (2.47) gives the hermitian conjugate part of the $\mathcal{L}^5$ Weinberg lagrangian in (2.44) [9]

$$\mathcal{L}_\nu = -\frac{1}{2\Lambda} (L^\dagger \epsilon \phi^*) \ \mathcal{C} \ (\phi^\dagger \epsilon L_L^*) + h.c. \tag{2.49}$$

where we must identify the couplings in (2.44) and (2.47):

$$\frac{\lambda}{\Lambda} = -(\Gamma (M^{-1})^T \Gamma^T)^\dagger. \tag{2.50}$$

In the end, we find the lagrangian $\mathcal{L}_\nu$ of the vanilla model with right-handed sterile neutrinos given in (2.47) reduces to the Weinberg operator and thus generates a Majorana mass term for the $N_{i,R}$ neutrino fields, as shown in (2.45).

The vanilla seesaw model is the most popular high-energy renormalizable theory leading to the Weinberg operator, which, as we mentioned in sec.1.5.3, is the only dimension five operator compatible with the SM gauge symmetry.

2.6.1. Masses and mixing

Taking into account that we have been dealing with flavor neutrino eigenstates, it is convenient to see how the massive neutrino states appear in this formalism and the seesaw mechanism takes place. The treatment will be similar to what we did in sec.2.4.

Once the electroweak SSB takes place, the lagrangian $\mathcal{L}_\nu$ in (2.47) generates a Dirac and a Majorana mass term and can be written as

$$\mathcal{L}_\nu = -\bar{\nu}_{\ell,L} M^D_{\ell j} N_{j,R} - \frac{1}{2} \overline{N^c_{i,R}} M^N_{ij} N_{j,R}, \tag{2.51}$$

with the Dirac mass given in terms of the Yukawa couplings matrix and the scalar VEV as $(M^D)_{\ell j} = \Gamma_{\ell j} v/\sqrt{2}$.

Expressed in the flavor basis n defined as

$$n = \begin{pmatrix} \nu_{\ell,L} \\ N^c_{i,R} \end{pmatrix} \tag{2.52}$$

the neutrino lagrangian can be written in matrix notation as

$$\mathcal{L}_\nu = \frac{1}{2} \bar{n} \begin{pmatrix} 0 & M^D \\ (M^D)^T & M^N \end{pmatrix} n + h.c. \tag{2.53}$$

[9] I have used the following relations: $\mathcal{C}^T = \mathcal{C}^{-1} = -\mathcal{C}$, $\mathcal{C}\gamma^0 = -\gamma^0 \mathcal{C}$, $\epsilon^T = -\epsilon = \epsilon\dagger$, and the definition of the conjugate spinor given in (1.24).

The above mass matrix M_{seesaw} can be diagonalized as we did in sec.2.4 with the aid of a unitary matrix U.

If we recall that in the seesaw limit the one-generation mixing matrix took the form in (2.42) we can now try to diagonalize the mass matrix considering a mixing matrix U as

$$U \simeq \begin{pmatrix} 1 & A \\ -A^\dagger & 1 \end{pmatrix} \tag{2.54}$$

where A is a 3×3 matrix with elements $A_{j,k} << 1$. One can see that (up to linear terms in A) $U^\dagger U \simeq 1$ and the non-diagonal element of the symmetrical matrix $U^T M_{seesaw} U$ in the linear over A approximation is equal to

$$(M^D)^T - M^N A^\dagger. \tag{2.55}$$

So if we choose $A^\dagger = (M^N)^{-1}(M^D)^T$ the matrix $U^T M_{seesaw} U$ takes the block-diagonal form

$$U^T M_{seesaw} U \simeq \begin{pmatrix} -M^D(M^N)^{-1}(M^D)^T & 0 \\ 0 & M^N \end{pmatrix} \tag{2.56}$$

and the mixing matrix U can be written approximately as

$$U \simeq \begin{pmatrix} 1 & M^{D*}(M^N)^{-1\dagger} \\ -(M^N)^{-1}(M^D)^T & 1 \end{pmatrix}. \tag{2.57}$$

Thus we find that the spectrum has three light Majorana neutrino masses, given by the seesaw relation $M^D(M^N)^{-1}(M^D)^T$ after taking into account the phases[10] η and three heavy Majorana neutrino masses characterized by the scale M^N of the total lepton number violating phenomena associated with the existence of the $N_{i,R}$ fields.

If we call the light neutrino eigenstates ν_m and the heavy ones N, the left-handed neutrinos of flavor ℓ $\nu_{\ell,L}$ can be written in terms of mass eigenstates as

$$\nu_{\ell,L} = U_{\ell m}\nu_m + U_{\ell N} N. \tag{2.58}$$

The matrix $U_{\ell m}$ rules the mixing between the flavor-definite $\nu_{\ell,L}$ neutrino states (the well known standard neutrinos) and the light mass eigenstates ν_m. This mixing describes the neutrino oscillation phenomena: it is the U_{PMNS} matrix we encountered in sec.2.1.

On the other hand, the matrix $U_{\ell N}$ describes the *only* interaction of the heavy Majorana neutrinos N with the standard particles: this mixing rules all the heavy N interactions, as they only take place by the mixing with the standard light neutrinos. Recalling the approximate form for the mixing matrix U in (2.57) we find the $N - \nu_{\ell,L}$ mixings $U_{\ell N}$ take values of order $U_{\ell N} \sim M^D(M^N)^{-1}$. The electroweak interactions of the mostly sterile Majorana neutrinos N are then governed by the mixings $U_{\ell N}$, which enter in the electroweak charged- and neutral-currents, equivalently to what we saw in sec.2.2.

The leptonic charged-current in (2.17) now takes the form $J^\mu_{lep} = U_{\ell N}\bar{N}\gamma^\mu \ell_L$ giving a charged-current lagrangian term for the heavy Majorana neutrinos N:

$$\mathcal{L}^N_{CC} = -\frac{g}{\sqrt{2}} U_{\ell N}\bar{N}\gamma^\mu \ell_L W^+_\mu + h.c. \tag{2.59}$$

[10] This is the same we did in the one-family seesaw case.

Here I am not explicitly writing the charged leptons mixing matrix S_ℓ we considered in (1.59), as this can be absorbed in the definition of the standard neutrino flavor eigenstates $\nu_{\ell,L}$ exactly as we did in sec. 1.4.3.

The neutral-current term is given by the substitution of the mixed expression for $\nu_{\ell,L}$ we have in (2.58) in the corresponding SM Z-boson current in the first term of (1.64)[11]:

$$\mathcal{L}^N_{NC} = -\frac{g}{2\cos\theta_W} U_{\ell N} \bar{N} \gamma^\mu \ \nu_{\ell,L} Z_\mu + h.c. \tag{2.60}$$

From the relation above it can be seen that again the GIM mechanism [45] does not work anymore, as there can be neutral-current transitions between different massive neutrinos and thus flavor changing neutral-currents.

In the literature many authors consider this same "vanilla" Type I seesaw, but introducing a different number of sterile neutrinos often called N_s, with $s = 1, ...S$. The light massive states ν_m are still three but the heavy neutrino states are $S = 1, 2....$ This leads us to a $S \times S$ matrix M^N, and a $3 \times S$ A matrix in (2.54). Reference papers for this kind of treatment focusing on collider phenomenology are [23] and [91]. Also, in a bottom-up approach the right-handed neutrinos can just be introduced "by hand" as the only new particles beyond the SM as it is done in the so called *neutrino standard model* νSM [92].

2.6.2. Phenomenological consequences and shortcomings

The most important phenomenological consequence of the presented Type I seesaw models comes from the prediction of massive Majorana states. One should stress that the Dirac or Majorana descriptions of a neutrino have different phenomenological consequences only if the neutrino is massive. If the neutrino is massless, since the left-handed chiral component of the neutrino fields obeys the Weyl equation (1.13) in both Dirac and Majorana descriptions, and the right-handed chiral component is irrelevant for neutrino interactions, both descriptions are equivalent. One can distinguish a Dirac or Majorana neutrino only by measuring some effect due to the neutrino mass not of kinematical nature: the neutrino oscillations cannot reveal the Majorana or Dirac nature of neutrinos.

The other striking effect is lepton number violation: the presence of Majorana neutrinos induces processes with $\Delta L = 2$. The most promising way to find the Majorana character of neutrinos is the search for neutrinoless double beta decay -that I will introduce in sec.2.6.3- which is possible only if the massive neutrinos are of Majorana nature. Also many other $\Delta L = 2$ processes are being tested experimentally. In this thesis we will be especially concerned with LNV processes taking place at high energy colliders.

However, one of the major shortcomings of the vanilla Type I seesaw mechanism is that it in fact predicts an almost negligible interaction between the heavy massive neutrinos N and the flavor eigenstates $\nu_{\ell,L}$. As we found in (2.57) the mixings $U_{\ell N}$ take values of order $U_{\ell N} \sim M^D (M^N)^{-1}$. As the light mass eigenstates ν_m predicted by the seesaw mechanism have masses given by the seesaw relation $m_\nu = M^D (M^N)^{-1} (M^D)^T$

[11] The expression I am writing is indeed the hermitian conjugate of the neutral-current shown in (1.64).

it is found that the $N - \nu_{\ell,L}$ mixings take the values

$$U_{\ell N} \simeq \sqrt{\frac{m_\nu}{M^N}}. \tag{2.61}$$

Taking for instance the bound $m_\nu \leq 0.1\ eV$, the current bound for the mixing in order to fit this tiny light neutrino mass is

$$U_{\ell N} \lesssim 1 \times 10^{-6} \sqrt{\frac{100\ GeV}{M^N}}. \tag{2.62}$$

This relation tells us that the observation of lepton number violating phenomena -which are suppressed by this factor- is practically impossible for M_N above the EW scale. This leads one to the conclusion that any LNV signal of a massive Majorana state N at the electroweak scale would strongly indicate the existence of new physics beyond the minimal seesaw framework we have reviewed until now.

2.6.3. Current bounds on neutrino mixings

From the above description it is clear that there are two key aspects of Type I seesaw mechanism that can be probed experimentally: the Majorana mass M_N of the mostly sterile neutrinos N and their mixing with the active neutrinos $U_{\ell N}$.

In the literature scenarios with sizable light-heavy neutrino mixings are made possible by assigning specific textures[12] to the Dirac and Majorana mass matrices in the seesaw formula in (2.57). The stability of these textures can in principle be guaranteed by enforcing some additional symmetries in the leptonic sector. But the current approaches do not assume any relations between the mixing matrix elements, and bounds on the mixings $U_{\ell N}$ are generally imposed considering the contributions of the existence of a single heavy Majorana neutrino N (with mass M_N) to various processes [23, 93–95].

The heavy neutrino interactions with the standard particles are assumed to be governed exclusively by their mixing with active light neutrinos via the charged- and neutral-currents in (2.59) and (2.60), as well as the corresponding interaction with the Higgs field obtained from the Yukawa lagrangian in (2.47). Although the production of the N is always considered to happen via the mentioned interactions, some observables depend explicitly on the possible decay modes and can be severely altered if the N has other interactions than those obtained from the mixing with active neutrinos, or can decay to invisible particles like dark matter particles.

Depending on the mass M_N distinct processes can test or put bounds on the existence of the N and its mixing couplings.

[12] This means: they put zeros, or impose relations between some specific matrix entries, in order to make the mixings small enough to satisfy the constrains imposed by the active neutrino tiny masses in (2.62).

- Tests of lepton universality.

  In the SM charged-current interactions couple to the three lepton families e, μ, τ with a universal constant: $g = g_e = g_\mu = g_\tau$, as we saw in (1.56). Such universality can be studied at the percent and sub-percent level by measuring the ratios of decay rates of charged leptons, pseudo-scalar mesons and the W boson. If a heavy neutrino exists then the measured values of $\frac{g_\mu}{g_e}$, $\frac{g_\tau}{g_\mu}$ and $\frac{g_\tau}{g_e}$ can deviate from unity. We will be specifically interested in flavor conserving charged lepton decays as $\tau^- \to e^- \bar{\nu}_e \nu_\tau$, $\tau^- \to \mu^- \bar{\nu}_\mu \nu_\tau$ and $\mu^- \to e^- \bar{\nu}_e \nu_\mu$. The current bounds on lepton universality tests are summarized in e.g. [93].

- Invisible Z boson decays.

  Precision measurements of the decay rates of the Z boson into invisible particles (such as neutrinos) and to charged leptons were made in the e^+e^- collider LEP by the DELPHI and ALEPH Collaborations [96, 97]. These experiments can bound the number of active neutrinos and also give bounds on the mixings for a Majorana neutrino mass $M_N < m_Z$.

- Lepton flavor violating decays.

  The presence of a heavy N participating in the loop level contributions to lepton flavor violating processes -which as we already discussed are very restricted in the SM- can bound the mixing products $|U_{\ell N} U_{\ell' N}|$. This set of processes includes radiative $\ell \to \ell' \gamma$ and three-body, i.e. $\ell \to \ell'^+ \ell'^- \ell^-$ charged lepton decays, $\mu - e$ conversion in nuclei, etc. The most stringent bounds from this group are given by the $\mu \to e\gamma$ radiative decay [13, 98].

This group of measurements together with constraints coming form the unitarity of the quark mixing matrix V_{CKM} (CKM-unitarity bounds) -usually referred as Electroweak Precision Data (EWPD)- are considered in global fits and give bounds on the mixings $U_{\ell N}$. Early works can be found in [13, 99–102], updated to the available data at the time in [103] and recent (2016) fits can be found in [93, 104].

In this thesis we will take this constraints into account by following the treatment made in [91, 105, 106] and consider the bounds on the quantities

$$\Omega_{\ell\ell'} = U_{\ell N} U_{\ell' N}. \tag{2.63}$$

The most stringent bounds for a heavy Majorana neutrino with mass $M_N > m_Z = 91.2\ GeV$ up to date are yet given by the $\mu \to e\gamma$ radiative decay bounds $Br(\mu \to e\gamma) < 5.7 \times 10^{-13}$ [107] giving $|\Omega_{e\mu}| \leq 1 \times 10^{-4}$. These bounds are very weak for masses $M_N < m_W = 80.4\ GeV$ [13]. In the mass range $M_N < m_Z$ the DELPHI bounds on Z decays [97] give a constraint $|U_{\ell N}|^2 \leq 5 \times 10^{-3}$.

In sec.3.4 we will discuss how this constraint is taken into account in the results of this thesis work.

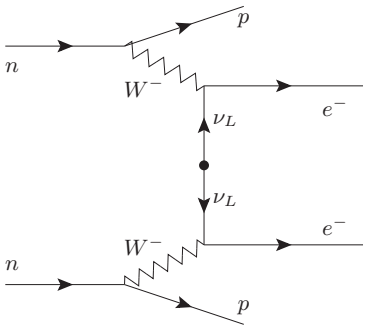

Figure 2.1: The $0\nu\beta\beta$- decay process diagram in the Type I seesaw framework. Each neutron $n = udd$ undergoes a beta decay through the SM process $d \to W^- u$, becoming a proton $p = uud$, and each W decays as $W^- \to e^- \nu_{eL}$, where, if neutrinos are Majorana particles, they can unite to form a Majorana $\nu_L \bar{\nu}_L$ mass term.

- Kinematic constraints.

  One can use the energy spectra of visible final-state particles in beta decay, pion, kaon and muon decays, etc. to search for an invisible massive particle in the final state. These experiments search for peaks in the final charged leptons spectra, corresponding to the mass of the expected particle if it is lower than the originally decaying particle's mass [108, 109]. Other kinematical tests include the decay of heavier mesons like B decays in the Belle and LHCb experiments [110, 111]. The kinematic constraints put bounds on the square product $|U_{\ell N}|^2$.

- Neutrinoless double beta decay.

  The single beta decay is the process by which a neutron decays into a proton emitting an electron (*beta particle*) and an electron-antineutrino $n \to p + e^+ + \bar{\nu}_e$. Double beta decay occurs when two neutrons undergo a beta decay $n + n \to p + p + e^- + e^- + \bar{\nu}_e + \bar{\nu}_e$.

  Neutrinoless double beta decay ($0\nu\beta\beta$) is the two-unit lepton number violating process in which there are no final state neutrinos[13]: $n + n \to p + p + e^- + e^-$. It is only possible if massive neutrinos are Majorana particles, and in the Type I seesaw framework it is interpreted to happen as depicted in fig.2.1.

  Experiments searching for $0\nu\beta\beta$-decay measure the half-life $\tau_{0\nu\beta\beta}$ of the process waiting for it to happen in Germanium, Xenon or other nuclei. From the bounds on the half-life for the decay, bounds can be obtained for the mixing of the first family leptons $|U_{eN}|^2$. The most stringent bounds for $\tau_{0\nu\beta\beta} \gtrsim 1.1 \times 10^{26}$ years are given by the KamLAND-Zen Collaboration [112]. In sec. 3.4 I discuss how this bound is taken into account in our work.

- Neutrino oscillations, cosmology.

  Neutrino oscillations provide information on the light mass mixing parameters $U_{\ell m}$ in (2.58) usually called U_{PMNS} as we discussed in sec.2.1. However, a heavy neutrino with a mass of the order of $M_N \gtrsim 10\ eV$ would alter the oscillation pattern,

[13] For a review see the work by Bilenky and Giunti [59]

and the oscillations of the three light neutrinos would be "non-unitary", meaning the oscillation probability for only three light neutrinos is distinctly different from the oscillation probability for three light neutrinos and one heavy neutrino.

If a heavy neutrino is in thermal equilibrium in the early Universe, it can have an effect on cosmological observables, e.g. the Hubble constant, the primordial abundance of light nuclei, the cosmic microwave background (CMB), supernova luminosities, baryon acoustic oscillations (BAOs), and the large-scale distribution of galaxies, as I commented in sec.2.1.

2.6.4. Perspectives

So far we have discussed the different ways to implement neutrino masses: nowadays neutrino masses are considered to be the first compelling evidence of physics beyond the Standard Model. The modern treatment considers neutrino mass is generated by some unknown new physics at a high-energy lepton number violating scale, with the Weinberg operator we studied in 2.5 as its low-energy signature.

The vanilla Type I seesaw model presented here -which is widely studied in the literature- seems to be the most "economic" renormalizable tree-level realization of the Weinberg operator. However, the heavy, mostly sterile Majorana neutrino (or neutrinos) introduced by the model are predicted to have negligible mixing with the active neutrinos, as we found in (2.62), if one takes into account the bounds put by the actually tiny masses active neutrinos are found to have. As the heavy neutrinos interaction with the standard particles takes place only by their mixing with the active neutrinos these models indeed predict the *decoupling* of the sterile neutrinos they introduce.

In the following chapter I will present an alternative effective lagrangian approach by del Águila, Bar-Shalom, Soni and Wudka [15] which takes into account the possible non-decoupling of the sterile heavy neutrinos. The study of various phenomenological predictions given by this effective lagrangian, which introduces new effective interactions, constitute the original work developed in this thesis.

Chapter 3

Majorana neutrino effective lagrangian

In this chapter I introduce the effective lagrangian approach constituting the case of study in this thesis. It includes the derivation of the lagrangian terms emerging from the introduction of the Majorana neutrino effective operators made by del Águila, Bar-Shalom, Soni and Wudka in their work [15], and a discussion on how the existing experimental knowledge is taken into account to introduce bounds on the effective couplings.

3.1. An alternative approach

The discovery of neutrino oscillations in the end of the 2oth century -and its interpretation in terms non-vanishing neutrino masses- claims for the extension of the SM in order to incorporate them. Meanwhile, the discovery in 2012 at the CERN's Large Hadron Collider of the SM Higgs boson favors the extensions including the Higgs scalar doublet. This scenario has favored the Type I seesaw mechanism as a possible explanation for the tiny but still non-zero neutrino masses.

However, as we saw in the last chapter, the naive "vanilla" Type I seesaw completion of the dimension five Weinberg operator given by the $\mathcal{L}_\nu$ lagrangian in (2.47) predicts an almost vanishing interaction of the heavy Majorana neutrino with the standard fields, in order to accommodate the tiny light neutrino masses, characterized by a $\nu_L - N$ mixing

$$U_{\ell N} \lesssim 1 \times 10^{-6} \sqrt{\frac{100\ GeV}{M^N}}. \tag{3.1}$$

This mixing governs all the interactions of the N with the standard particles, via the charged and neutral currents

$$\mathcal{L}^N_{CC} = -\frac{g}{\sqrt{2}} U_{\ell N} \bar{N} \gamma^\mu \ell_L W^+_\mu + h.c. \tag{3.2}$$

$$\mathcal{L}_{NC}^{N} = -\frac{g}{2\cos\theta_W} U_{\ell N} \bar{N} \gamma^{\mu} \, \nu_{\ell,L} Z_{\mu} + h.c. \tag{3.3}$$

Thus, as stated by the authors in [15], any lepton number violating signal of a sterile N at or below the electroweak scale would strongly indicate the existence of new physics beyond the minimal seesaw framework encoded in the $\mathcal{L}_{\nu}$ lagrangian presented in sec.2.6.

The proposal is to adopt an alternative approach, considering a Majorana neutrino scenario with a relatively light N with mass $m_N \lesssim 1 \; TeV$ and negligible mixing with the left handed standard neutrinos ν_L. The purpose is to present a natural and model-independent formalism that allows a broader view of the expected physics for heavy Majorana neutrinos, motivated principally by the study of N-mediated lepton number violating processes at high energy colliders.

This approach departs from the customary viewpoint [23, 91], in which the couplings in (3.2) and (3.3) are taken to determine the rate of N-mediated LNV signals, and to satisfy a fine-tuned value for the mixings $U_{\ell N} \lesssim \mathcal{O}(0.1)$, many orders of magnitude larger than the value derived from the seesaw mechanism.

3.1.1. New physics parameterization

In view of the discussion above, the authors in [15] choose to depart from the traditional viewpoint and incorporate an effective lagrangian including the SM fields *and* the heavy Majorana neutrino N as the effective degrees of freedom.

The new physics underlying neutrino masses and interactions can be parameterized as a series of effective operators $\mathcal{O}_{\mathcal{J}}$ constructed with the N and the SM fields and preserving the $SU(2)_L \times U(1)_Y$ electroweak symmetry of the Standard Model. These operators have coefficients suppressed by inverse powers of the new physics scale Λ, in a similar way to the SM effective operator extension presented in sec.1.5.3.

So the effective lagrangian we will consider can be written as

$$\mathcal{L}_{eff} = \mathcal{L}_{SM} + \mathcal{L}_{\nu} + \sum_{d=5}^{\infty} \left(\frac{1}{\Lambda^{d-4}} \sum_{\mathcal{J}} \alpha_{\mathcal{J}} \mathcal{O}_{\mathcal{J}}^{d} + h.c. \right) \tag{3.4}$$

with the difference that now the operators include the Majorana neutrino N in their composition. The term $\mathcal{L}_{\nu}$ is the dimension four lagrangian of the "vanilla" Type I seesaw realization of the Weinberg operator in (2.47), which is considered to be the only contribution to this operator.

The dominating new physics effects are generated by the contribution of the operators of the lowest canonical dimension that can be generated at tree-level in the underlying unknown ultraviolet theory. Here the new physics responsible for the effective interactions is assumed to be *weakly coupled*, meaning that radiative (quantum loop level) corrections are smaller than tree-level contributions, and *decoupling*, meaning that the unknown particles responsible for the effective interactions decouple from low-energy physics in the limit in which their masses become large. The expansion in (3.4) is useful when the new physics scale Λ is larger than all the experimentally available energies and the

masses of all the new physics spectrum except m_N, the Majorana neutrino's mass. In particular this requires $\Lambda \gg m_N$ and E, where E is the typical energy of the considered process. One should notice that there is no compelling argument suggesting m_N must be of order Λ: the new physics scale can be set by the symmetry breaking scale in some ultraviolet model, completely independent of the Majorana mass scale.

As introduced in sec.1.5.3, the complete list of dimension six operators only including the SM fields can be found in the classic work by Buchmüller and Wyler re-analyzed in the more recent work by Grzadkowski et.al. [55, 56]. Also, some operators constructed only with the SM fields but allowing for lepton number violation were presented in the works by Babu and Leung [113] and de Gouvêa and Jenkins [114].

There is only one dimension five N-operator contributing to $\mathcal{L}_{eff}$: it can be written as

$$\mathcal{O}_N^5 = (\overline{N^c}N)(\phi^\dagger\phi). \tag{3.5}$$

The contribution of this operator can be included in the renormalization of the Majorana mass matrix M^N. In fact, considering explicitly the contribution of the $\mathcal{L}_\nu$ lagrangian from (2.47), the part of the effective lagrangian in (3.4) contributing at tree-level to the neutrinos mass, after the spontaneous electroweak symmetry breaking, takes the form

$$\mathcal{L}_{eff-mass} = -\bar{\nu}_{\ell,R}M^D_{\ell j}N_R - \frac{1}{2}\overline{N^c_R}M^N N_R - \frac{v^2}{2\Lambda}\alpha_N^{(5)}\overline{N^c_R}N_R \tag{3.6}$$

where the first two terms are the contributions from the seesaw lagrangian $\mathcal{L}_\nu$ we found in (2.51). Thus we find the effect of this operator can be absorbed in a renormalization of the Majorana mass matrix[1] M^N.

Another dimension five operator can be constructed at one-loop level in a fully renormalizable theory. It is $\mathcal{O}^{(5)}_{NNB} = \bar{N}\sigma^{\mu\nu}N^c B_{\mu\nu}$ [115], where the antisymmetric field strength is $B_{\mu\nu} = \partial_\mu B_\nu - \partial_\nu B_\mu$. However, it vanishes in the case N represents one sterile singlet. Eq.(1.31) implies that $N^c = \mathcal{C}\bar{N}^T$ and $(N^c)^T = (\mathcal{C}\bar{N}^T)^T = \bar{N}\mathcal{C}^T = \bar{N}\mathcal{C}^{-1}$. Thus, $\bar{N} = (N^c)^T\mathcal{C}$. Then, using the relation $\mathcal{C}\sigma^{\mu\nu}\mathcal{C} = (\sigma^{\mu\nu})^T$[2], one can write

$$\bar{N}\sigma^{\mu\nu}N^c = (N^c)^T\mathcal{C}\sigma^{\mu\nu}\mathcal{C}(\bar{N})^T = (N^c)^T(\sigma^{\mu\nu})^T(\bar{N})^T = (\bar{N}\sigma^{\mu\nu}N^c)^T.$$

On the other hand

$$\begin{aligned}(\bar{N}\sigma^{\mu\nu}N^c)^T &= -(N^c)^T(\sigma^{\mu\nu})^T\bar{N}^T = -\bar{N}\mathcal{C}^T(\sigma^{\mu\nu})^T\mathcal{C}^{-1}N^c = \\ &\quad -\bar{N}\mathcal{C}(\sigma^{\mu\nu})^T\mathcal{C}N^c = -\bar{N}\sigma^{\mu\nu}N^c,\end{aligned}$$

where the minus sign in the first equality comes from the transposition of two fermion fields. Finally $\bar{N}\sigma^{\mu\nu}N^c = -\bar{N}\sigma^{\mu\nu}N^c = 0$ and the operator vanishes.

Our proposal for this thesis is to consider only the operators leading to new N interactions, and study the possible observable effects of these operators in different scenarios: electron-proton (ep) and proton-proton (pp) colliders as well as the propagation of tau neutrinos ν_τ through the Earth.

[1] We are neglecting the $NNhh$ interaction given by this operator.

[2] It can be obtained from the relations in 1.2.

3.2. Dimension six effective operators

Following the proposed alternative approach, we will consider that the sterile neutrino N interacts with the light neutrinos by higher dimension operators, and take this interaction to be dominant in comparison with the mixing through the Yukawa couplings. The dominating effects come from dimension six operators that can be generated at tree-level in the unknown underlying renormalizable theory.

Following [15] we start with a rather general effective lagrangian density for the interaction of right handed Majorana neutrinos N with leptons and quarks, including dimension six operators. The first subset includes operators with scalar and vector bosons (SVB)

$$\mathcal{O}_{LN\phi} = (\phi^\dagger\phi)(\bar{L}_i N\tilde{\phi}),\ \ \mathcal{O}_{NN\phi} = i(\phi^\dagger D_\mu\phi)(\bar{N}\gamma^\mu N),\ \ \mathcal{O}_{N\ell\phi} = i(\phi^T\epsilon D_\mu\phi)(\bar{N}\gamma^\mu\ell_i) \quad (3.7)$$

and a second subset includes the baryon-number conserving four-fermion contact terms:

$$\begin{aligned}
\mathcal{O}_{duN\ell} &= (\bar{d}_i\gamma^\mu u_i)(\bar{N}\gamma_\mu\ell_i),\ \ \mathcal{O}_{fNN} = (\bar{f}_i\gamma^\mu f_i)(\bar{N}\gamma_\mu N),\ \ \mathcal{O}_{LNL\ell} = (\bar{L}_i N)\epsilon(\bar{L}_i\ell_i),\\
\mathcal{O}_{LNQd} &= (\bar{L}_i N)\epsilon(\bar{Q}_i d_i),\ \ \mathcal{O}_{QuNL} = (\bar{Q}_i u_i)(\bar{N}L_i),\ \ \mathcal{O}_{QNLd} = (\bar{Q}_i N)\epsilon(\bar{L}_i d_i),\\
\mathcal{O}_{LN} &= |\bar{N}L_i|^2,\ \ \mathcal{O}_{QN} = |\bar{Q}N|^2,\ \ \mathcal{O}_{NN} = (\overline{N^c}N)^2,\ \ \mathcal{O}'_{NN} = |\overline{N^c}N|^2
\end{aligned} \quad (3.8)$$

where ℓ_i, u_i, d_i and L_i, Q_i denote, for the family labeled i, the right handed $SU(2)$ singlets and the left-handed $SU(2)$ doublets, respectively, as introduced in sec.1.1, and f_i represents any of these fields. The antisymmetric symbol ϵ is defined as in (1.15).

One can also consider operators generated at one-loop level in the underlying full theory, whose coefficients are naturally suppressed by a factor $1/16\pi^2$ [15, 116]:

$$\begin{aligned}
\mathcal{O}_{NB} &= (\bar{L}_i\sigma^{\mu\nu}N)\tilde{\phi}B_{\mu\nu}, \qquad \mathcal{O}_{NW} = (\bar{L}_i\sigma^{\mu\nu}\tau^I N)\tilde{\phi}W^I_{\mu\nu},\\
\mathcal{O}_{DN} &= (\bar{L}_i D^\mu N)D_\mu\tilde{\phi}, \qquad \mathcal{O}_{\bar{D}N} = (\overline{D^\mu L_i}N)D_\mu\tilde{\phi}\ .
\end{aligned} \quad (3.9)$$

Here the field strength $B_{\mu\nu}$ is defined as in the last section, and $W^I_{\mu\nu} = \partial_\mu W^I_\nu - \partial_\nu W^I_\mu + g\varepsilon^{IJK}W^J_\mu W^K_\nu$, where the indices I, J, K run as $I, J, K = 1, 2, 3$ and the τ^I are the $SU(2)$ generators introduced in sec.1.4.

We start by writing the effective operators in terms of the scalar, fermion and vector fields, in order to write explicitly the dimension six lagrangian to extract the Feynman rules for calculating the different observables we will be interested in.

3.3. Effective lagrangian

We present here the complete effective lagrangian obtained from the operators listed in (3.7), (3.8) and (3.9).

Standard vector bosons operators

The first operators subset presented in (3.7) involves the SM vector bosons, which appear as part of the covariant derivative for the electroweak sector as given in (1.44). Here

we explicitly write the hypercharge of the scalar doublet as $Y_\phi = \frac{1}{2}$, and the derivative takes the form $D_\mu = \partial_\mu - i\frac{g'}{2}B_\mu - ig\tau_i W^i_\mu$. After the electroweak symmetry breaking, the term[3] $D_\mu\phi$ is written as in the SM. It depends explicitly on the massive vector bosons $W^\pm$ and Z, the scalar VEV v and the Higgs field h as:

$$D_\mu\phi = \begin{pmatrix} \frac{-ig}{2}W^+_\mu(v+h) \\ \frac{\partial_\mu h}{\sqrt{2}} + \frac{iev}{m_Z\sqrt{2}}(v+h)Z_\mu \end{pmatrix}, \tag{3.10}$$

where the definitions for the weak boson's masses and the electric charge given in (1.47) and (1.48) are used.

We have also used the Feynman rule for field derivatives (which can be resumed in substituting a derivative for the momentum entering the interaction vertex $\partial_\mu\varphi \to -iP^{(\varphi)}_\mu\varphi$) writing explicitly the momentum dependence in the lagrangian.

Labelling the effective coupling for the operator $\mathcal{O}_{LN\phi} = (\phi^\dagger\phi)(\bar{L}_i N\tilde{\phi})$ as $\alpha_{LN\phi} \equiv \alpha_\phi$, the one for $\mathcal{O}_{NN\phi} = i(\phi^\dagger D_\mu\phi)(\bar{N}\gamma^\mu N)$ as $\alpha_{NN\phi} \equiv \alpha_Z$, and the one for $\mathcal{O}_{N\ell\phi} = i(\phi^T\epsilon D_\mu\phi)(\bar{N}\gamma^\mu\ell_i)$ as $\alpha_{N\ell\phi} \equiv \alpha_W$, the SVB part of the effective lagrangian is written as

$$\begin{aligned}
\mathcal{L}^{tree}_{SVB} = \frac{1}{\Lambda^2}\Bigg\{ & \alpha^{(i)}_\phi\left(\frac{3v^2}{2\sqrt{2}}\,\bar{\nu}_{L,i}N_R\,h + \frac{3v}{2\sqrt{2}}\,\bar{\nu}_{L,i}N_R\,hh + \frac{1}{2\sqrt{2}}\,\bar{\nu}_{L,i}N_R\,hhh\right) \\
& -\alpha_Z\left(-(\bar{N}_R\gamma^\mu N_R)\left(\frac{m_Z}{v}Z_\mu\right)\left(\frac{v^2}{2} + vh + \frac{1}{2}hh\right)\right. \\
& \left. +(\bar{N}_R\gamma^\mu N_R)\left(\frac{v}{2}P^{(h)}_\mu h + \frac{1}{2}P^{(h)}_\mu hh\right)\right) \\
& -\alpha^{(i)}_W(\bar{N}_R\gamma^\mu\ell_{R,i})\left(\frac{vm_W}{\sqrt{2}}W^+_\mu + \sqrt{2}m_W W^+_\mu h + \frac{g}{2\sqrt{2}}W^+_\mu hh\right)\Bigg\} + h.c.
\end{aligned} \tag{3.11}$$

where a sum over the fermions family (or generation) index i is understood. Here one can see the presence of *vectorial* interactions in the terms corresponding to the α_Z and $\alpha^{(i)}_W$ couplings, due to the presence of the γ^μ Dirac matrices.

[3] Taking $\phi = \begin{pmatrix} 0 \\ \frac{v+h}{\sqrt{2}} \end{pmatrix}$.

Four-fermion contact operators

The four-fermion contact operators presented in (3.8) lead in a straightforward manner to the tree-level lagrangian:

$$\begin{aligned}
\mathcal{L}^{tree}_{4-f} = \frac{1}{\Lambda^2}\Big\{ & \alpha^{(i)}_{V_0}\bar{d}_{R,i}\gamma^\mu u_{R,i}\bar{N}_R\gamma_\mu\ell_{R,i} + \alpha^{(i)}_{V_1}\bar{\ell}_{R,i}\gamma^\mu\ell_{R,i}\bar{N}_R\gamma_\mu N_R \\
& +\alpha^{(i)}_{V_2}(\bar{\nu}_{L,i}\gamma^\mu\nu_{L,i}\bar{N}_R\gamma_\mu N_R + \bar{\ell}_{L,i}\gamma^\mu\ell_{L,i}N_R\gamma_\mu N_R) \\
& +\alpha^{(i)}_{V_3}\bar{u}_{R,i}\gamma^\mu u_{R,i}\bar{N}_R\gamma_\mu N_R + \alpha^{(i)}_{V_4}\bar{d}_{R,i}\gamma^\mu d_{R,i}\bar{N}_R\gamma_\mu N_R \\
& +\alpha^{(i)}_{V_5}(\bar{u}_{L,i}\gamma^\mu u_{L,i}\bar{N}_R\gamma_\mu N_R + \bar{d}_{L,i}\gamma^\mu d_{L,i}\bar{N}_R\gamma_\mu N_R) \\
& +\alpha^{(i)}_{S_0}(\bar{\nu}_{L,i}N_R\bar{\ell}_{L,i}\ell_{R,i} - \bar{\ell}_{L,i}N_R\bar{\nu}_{L,i}\ell_{R,i}) + \alpha^{(i)}_{S_1}(\bar{u}_{L,i}u_{R,i}\bar{N}\nu_{L,i} + \bar{d}_{L,i}u_{R,i}\bar{N}\ell_{L,i}) \\
& +\alpha^{(i)}_{S_2}(\bar{\nu}_{L,i}N_R\bar{d}_{L,i}d_{R,i} - \bar{\ell}_{L,i}N_R\bar{u}_{L,i}d_{R,i}) + \alpha^{(i)}_{S_3}(\bar{u}_{L,i}N_R\bar{\ell}_{L,i}d_{R,i} - \bar{d}_{L,i}N_R\bar{\nu}_{L,i}d_{R,i}) \\
& +\alpha^{(i)}_{S_4}(\bar{N}_R\nu_{L,i}\ \bar{\ell}_{L,i}N_R\ + \bar{N}_R\ell_{L,i}\bar{\ell}_{L,i}N_R) + \alpha^{(i)}_{S_5}(\bar{N}_R u_{L,i}\bar{u}_{L,i}N_R + \bar{N}_R d_{L,i}\bar{d}_{L,i}N_R) \\
& +\alpha^{(i)}_{S_6}(\overline{N^c}N_R)(\overline{N^c}N_R) + \alpha^{(i)}_{S_7}|\overline{N^c}N_R||\overline{N^c}N_R|\Big\} + h.c.
\end{aligned} \tag{3.12}$$

In (3.12) a sum over the family index i is understood, and the constants $\alpha^{(i)}_{\mathcal{O}}$ are associated to the specific operators:

$$\begin{aligned}
&\alpha^{(i)}_{V_0} = \alpha^{(i)}_{duN\ell},\ \alpha^{(i)}_{V_1} = \alpha^{(i)}_{\ell NN},\ \alpha^{(i)}_{V_2} = \alpha^{(i)}_{LNN},\ \alpha^{(i)}_{V_3} = \alpha^{(i)}_{uNN},\ \alpha^{(i)}_{V_4} = \alpha^{(i)}_{dNN},\ \alpha^{(i)}_{V_5} = \alpha^{(i)}_{QNN}, \\
&\alpha^{(i)}_{S_0} = \alpha^{(i)}_{LN\ell},\ \alpha^{(i)}_{S_1} = \alpha^{(i)}_{QuNL},\ \alpha^{(i)}_{S_2} = \alpha^{(i)}_{LNQd},\ \alpha^{(i)}_{S_3} = \alpha^{(i)}_{QNLd},\ \alpha^{(i)}_{S_4} = \alpha^{(i)}_{LN},\ \alpha^{(i)}_{S_5} = \alpha^{(i)}_{QN}, \\
&\alpha^{(i)}_{S_6} = \alpha^{(i)}_{NN}\ \alpha^{(i)}_{S_7} = \alpha^{'(i)}_{NN}.
\end{aligned}$$

As the notation suggests, one can classify the distinct four fermion operators by their Lorentz structure in *vectorial* (those involving the Dirac γ^μ) and *scalar*.

One-loop level generated operators

The last operators subset, presented in (3.9), includes the operators that can only be generated at one-loop level in the unknown underlying high energy renormalizable theory, as is proven in [116] for operators with SM fields only. This means this operators cannot be produced by dimension four vertices preserving the SM gauge symmetry, and must be generated by loop graphs in the full theory. Therefore, their couplings are suppressed by a loop factor $\frac{1}{16\pi^2}$ arising from the proper normalization of the loop four-momentum integral in comparison with the operators generated at tree-level.

The operator $\mathcal{O}_{NB} = (\bar{L}_i\sigma^{\mu\nu}N)\tilde{\phi}B_{\mu\nu}$ involves the antisymmetric field strength $B_{\mu\nu}$ and the antisymmetric Dirac tensor $\sigma^{\mu\nu} = \frac{i}{2}[\gamma^\mu,\gamma^\nu]$. The field strength $B_{\mu\nu}$ can be written as

$$B_{\mu\nu} = c_W(\partial_\mu A_\nu - \partial_\nu A_\mu) - s_W(\partial_\mu Z_\nu - \partial_\nu Z_\mu), \tag{3.13}$$

using (1.46), and where $c_W \equiv \cos(\theta_W)$ and $s_W \equiv \sin(\theta_W)$. Replacing the derivatives for the incoming photon and Z momenta, and recalling the definition of $\tilde{\phi} = \epsilon\phi^*$, after the

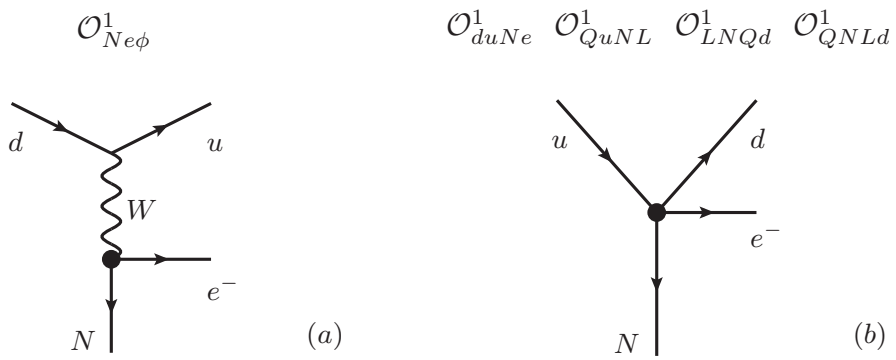

Figure 3.1: Contribution to $0\nu_{\beta\beta}$-decay. In the diagram (a) the solid dot represents the operator $\mathcal{O}^1_{Ne\phi}$ and in the diagram (b) the four-fermion operators $\mathcal{O}^1_{duNe}$, $\mathcal{O}^1_{QuNL}$, $\mathcal{O}^1_{LNQd}$ and $\mathcal{O}^1_{QNLd}$.

SSB the operator $\mathcal{O}_{NB}$ gives the terms in the one loop lagrangian with the coupling we have called $\alpha^{(i)}_{L_1} = \alpha^{(i)}_{NB}$.

The operator $\mathcal{O}_{NW} = (\bar{L}_i \sigma^{\mu\nu} \tau^I N)\tilde{\phi} W^I_{\mu\nu}$ leads to the combination

$$\sigma^{\mu\nu}\tau^I W^I_{\mu\nu} = 2\sigma^{\mu\nu}\partial_\mu(\tau^I W^I_\nu) - ig\sigma^{\mu\nu}(\tau^J W^J_\nu)(\tau^K W^K_\nu). \tag{3.14}$$

Here the product $\tau^I W^I_\nu$ can be written, using eqs. (1.45) and (1.46) as:

$$\tau^I W^I_\nu = \frac{1}{2}\begin{pmatrix} W^3_\nu & \sqrt{2}W^+_\nu \\ \sqrt{2}W^-_\nu & -W^3_\nu \end{pmatrix} = \frac{1}{2}\begin{pmatrix} c_W Z_\nu + s_W A_\nu & \sqrt{2}W^+_\nu \\ \sqrt{2}W^-_\nu & -c_W Z_\nu - s_W A_\nu \end{pmatrix}. \tag{3.15}$$

The terms in the lagrangian (3.18) with coupling $\alpha^{(i)}_{L_3} = \alpha^{(i)}_{NW}$ are the ones generated by this operator.

The remaining two operators are $\mathcal{O}_{DN} = (\bar{L}_i D^\mu N) D_\mu \tilde{\phi}$ and $\mathcal{O}_{\bar{D}N} = (\overline{D^\mu L_i} N) D_\mu \tilde{\phi}$. These can be written using the following expressions for the covariant derivatives, derived from the definition in[4] (1.44):

$$D_\mu \tilde{\phi} = \begin{pmatrix} \frac{\partial_\mu h}{\sqrt{2}} - i\frac{m_Z}{\sqrt{2}} Z_\mu - i\frac{e}{\sqrt{2}s_{2W}} Z_\mu h \\ -im_W W^-_\mu - i\frac{g}{2} W^-_\mu h \end{pmatrix}, \tag{3.16}$$

$$D^\mu L_i = \begin{pmatrix} \partial^\mu \nu_{L,i} - i\frac{e}{s_{2W}} Z^\mu - i\frac{g}{\sqrt{2}} W^{+\mu} \\ -i\frac{g}{\sqrt{2}} W^{-\mu} + \partial^\mu \ell_{L,i} + ie\frac{c_W}{s_W} Z^\mu \ell_{L,i} + ieA^\mu \ell_{L,i} \end{pmatrix} \tag{3.17}$$

and $D^\mu N = \partial^\mu N \to -iP^{\mu(N)} N$.

[4]Here we take the hypercharge values $Y_{\tilde{\phi}} = -\frac{1}{2}$, $Y_L = -\frac{1}{2}$ and $Y_N = 0$.

Their lagrangian parts in (3.18) correspond to those with couplings $\alpha^{(i)}_{L_2} = \alpha^{(i)}_{DN}$ and $\alpha^{(i)}_{L_4} = \alpha^{(i)}_{\bar{D}N}$ respectively.

Then the complete one-loop level lagrangian is the following:

$$
\begin{aligned}
\mathcal{L}^{1-loop}_{eff} = {} & \frac{\alpha^{(i)}_{L_1}}{\Lambda^2}\Big(-i\sqrt{2}vc_W P^{(A)}_\mu\ \bar{\nu}_{L,i}\sigma^{\mu\nu}N_R\ A_\nu + i\sqrt{2}vs_W P^{(Z)}_\mu\ \bar{\nu}_{L,i}\sigma^{\mu\nu}N_R\ Z_\nu + \\
& -i\sqrt{2}c_W P^{(A)}_\mu\ \bar{\nu}_{L,i}\sigma^{\mu\nu}N_R\ A_\nu h + i\sqrt{2}s_W P^{(Z)}_\mu\ \bar{\nu}_{L,i}\sigma^{\mu\nu}N_R\ Z_\nu h\Big) \\
& -\frac{\alpha^{(i)}_{L_2}}{\Lambda^2}\left(\frac{m_Z}{\sqrt{2}}P^{(N)}_\mu\ \bar{\nu}_{L,i}N_R\ Z^\mu + \frac{m_z}{\sqrt{2}v}P^{(N)}_\mu\ \bar{\nu}_{L,i}N_R\ Z^\mu h + m_W P^{(N)}_\mu\ \bar{\ell}_{L,i}N_R\ W^{-\mu}\right. \\
& \left. + \frac{\sqrt{2}m_W}{v}P^{(N)}_\mu\ \bar{\ell}_{L,i}N_R\ W^{-\mu}h + \frac{1}{\sqrt{2}}P^{(h)}_\mu P^{(N)\mu}\ \bar{\nu}_{L,i}N_R\ h\right) \\
& -\frac{\alpha^{(i)}_{L_3}}{\Lambda^2}\Big(i\sqrt{2}vc_W P^{(Z)}_\mu\ \bar{\nu}_{L,i}\sigma^{\mu\nu}N_R\ Z_\nu + i\sqrt{2}vs_W P^{(A)}_\mu\ \bar{\nu}_{L,i}\sigma^{\mu\nu}N_R\ A_\nu \\
& + i2\sqrt{2}m_W\ \bar{\nu}_{L,i}\sigma^{\mu\nu}N_R\ W^+_\mu W^-_\nu + i\sqrt{2}vP^{(W)}_\mu\ \bar{\ell}_{L,i}\sigma^{\mu\nu}N_R\ W^-_\nu \\
& + i4m_W c_W\ \bar{\ell}_{L,i}\sigma^{\mu\nu}N_R\ W^-_\mu Z_\nu + i4m_W s_W\ \bar{\ell}_{L,i}\sigma^{\mu\nu}N_R\ W^-_\mu A_\nu \\
& + i\sqrt{2}P^{(W)}_\mu\ \bar{\ell}_{L,i}\sigma^{\mu\nu}N_R\ W^-_\nu h + i2gc_W\ \bar{\ell}_{L,i}\sigma^{\mu\nu}N_R\ W^-_\nu Z_\mu h \\
& + i2gs_W\ \bar{\ell}_{L,i}\sigma^{\mu\nu}N_R\ W^-_\nu A_\mu h + i\sqrt{2}c_W P^{(Z)}_\mu\ \bar{\nu}_{L,i}\sigma^{\mu\nu}N_R\ Z_\mu h \\
& + i\sqrt{2}s_W P^{(A)}_\mu\ \bar{\nu}_{L,i}\sigma^{\mu\nu}N_R\ A_\mu h + i\sqrt{2}g\ \bar{\nu}_{L,i}\sigma^{\mu\nu}N_R\ W^+_\mu W^-_\nu h\Big) \\
& -\frac{\alpha^{(i)}_{L_4}}{\Lambda^2}\left(\frac{m_Z}{\sqrt{2}}P^{(\bar{\nu})}_\mu\ \bar{\nu}_{L,i}N_R\ Z_\mu + \frac{m_Z}{\sqrt{2}v}(P^{(\bar{\nu})}_\mu - P^{(h)}_\mu)\ \bar{\nu}_{L,i}N_R\ Z^\mu h\right. \\
& + \frac{1}{\sqrt{2}}P^{(h)\mu}P^{(\bar{\nu})}_\mu\ \bar{\nu}_{L,i}N_R\ h - \frac{\sqrt{2}m^2_W}{v}\ \bar{\nu}_{L,i}N_R\ W^{-\mu}W^+_\mu - \frac{m^2_z}{\sqrt{2}v}\ \bar{\nu}_{L,i}N_R\ Z_\mu Z^\mu \\
& - \frac{1}{2}\frac{m^2_Z}{v^2}\ \bar{\nu}_{L,i}N_R\ Z_\mu Z^\mu h - \frac{\sqrt{2}m^2_W}{v^2}\ \bar{\nu}_{L,i}N_R\ W^+_\mu W^{-\mu}h \\
& + m_W P^{(\bar{l})}_\mu W^{-\mu}\ \bar{\ell}_{L,i}N_R\ + \frac{m_W}{v}(P^{(\bar{\ell})}_\mu - P^{(h)}_\mu)W^{-\mu}\ \bar{\ell}_{L,i}N_R\ h \\
& + em_W\ \bar{\ell}_{L,i}N_R\ W^{-\mu}A_\mu + em_Z s_W\ \bar{\ell}_{L,i}N_R\ W^{-\mu}Z_\mu \\
& \left. + \frac{em_Z s_W}{v}\ \bar{\ell}_{L,i}N_R\ Z_\mu W^{-\mu}h + \frac{em_Z c_W}{\sqrt{2}v}\ \bar{\ell}_{L,i}N_R\ A_\mu W^{-\mu}h\right) + h.c.
\end{aligned}
\tag{3.18}
$$

where $P^{(a)}$ is the four-moment of the incoming a-particle and a sum over the family index i is understood again.

The lagrangian terms corresponding to the operators $\mathcal{O}_{NB}$ with coupling α_{L_1}, and $\mathcal{O}_{NW}$ with coupling α_{L_3} have a *tensorial* Dirac structure, given the presence of $\sigma^{\mu\nu}$.

3.4. Bounds on the effective couplings

The effective coupling $\alpha_{\mathcal{J}}^{(i)}$ associated to each effective operator $\mathcal{O}_{\mathcal{J}}$ can be bounded exploiting the existing constraints on the sterile-active neutrino mixings $U_{\ell N}$ in seesaw models I reviewed in sec.2.6.3.

In the effective lagrangian framework we are studying, the heavy Majorana neutrino couples to the three fermion family flavors $i = e, \mu, \tau$ with couplings dependent on the new physics scale Λ and the coefficients $\alpha_{\mathcal{J}}^{(i)}$.

We can interpret the current experimental bounds comparing the effective couplings with the general structure of the interaction between heavy neutrinos with the standard gauge bosons, which I introduced in sec.2.6.1. In the "vanilla" seesaw models, the modified charged-current (2.59) and neutral-current (2.60) are taken into account in the calculation of the different bounds on the mixings $U_{\ell N}$. In the effective theory, we saw the $\mathcal{O}_{N\ell\phi}$ operator induces a lagrangian term in (3.11) which can be directly related to the CC interaction in (2.59):

$$\mathcal{L}_{SVB} \supset -\frac{1}{\Lambda^2}\alpha_W^{(i)}\frac{vm_W}{\sqrt{2}}(\bar{N}_R\gamma^\mu\ell_{R,i})W_\mu^+ + h.c. \quad \mathcal{L}_{CC}^N = -\frac{g}{\sqrt{2}}U_{\ell N}(\bar{N}\gamma^\mu\ell_L)W_\mu^+ + h.c. \tag{3.19}$$

One can then relate the effective coupling $\alpha_W^{(i)}$ with the mixing $U_{\ell N}$ taking

$$\alpha_W^{(i)} \simeq \frac{g\Lambda^2}{vm_W}U_{\ell N} = \frac{2\Lambda^2}{v^2}U_{\ell N}, \tag{3.20}$$

where the second equality follows form (1.45).

This is not the case with the neutral currents in (2.60): the effective operators we are considering do not lead to any lagrangian term (vertex) sharing their Lorentz-Dirac structure, nor at tree, neither at one-loop level. The gauge invariant effective dimension six operators do not lead to a vectorial coupling between the N, ν_L and Z fields. However, as some terms in the one-loop lagrangian in (3.18) contribute to a $N\nu Z$ coupling, in some applications we have calculated explicitly the possible bounds for their couplings, coming from Z decay experiments, although they are suppressed by the $1/16\pi^2$ loop factor.

We then take a conservative approach, and in order to keep the analysis as simple as possible, but with the aim to put reliable bounds on the effective couplings, we relate the mixing between light and heavy neutrinos and the effective couplings as

$$U_{\ell N} \simeq \frac{\alpha v^2}{2\Lambda^2}, \tag{3.21}$$

and we use it to infer bounds on $\alpha_{\mathcal{J}}^{(i)}$ from the existing bounds on $U_{\ell N}$ [15].

In the different applications presented in this thesis we have taken distinct approaches in order to consider the existing bounds for the effective couplings: in our early works we took all the couplings to satisfy the same and most stringent constraints, but in the most recent works we considered bounds on sets of effective couplings depending on their Lorentz-Dirac structure, thus making all the *scalar*, *vectorial* or *tensorial* sets of couplings obey the most stringent bounds found in each case. The details on the treatment made in the different works will be presented in the corresponding chapters.

Electroweak precision data bounds

As I reviewed in sec.2.6.3, there is a stringent set of bounds on the neutrino mixings put by electroweak precision tests as lepton universality, Z decays and lepton flavor violating decays. Following the treatment made in [91, 105, 106], we consider the bounds on the quantities

$$\Omega_{\ell\ell'} = U_{\ell N} U_{\ell' N}, \tag{3.22}$$

and use them to put bounds on the effective couplings, as we explained in the previous section.

For the Lepton-Flavor-Violating processes (LFV), e.g. $\mu \to e\gamma$, which are induced by the quantum effects of the heavy neutrinos, we have several bounds [13, 117–119] but the most restrictive one comes from $Br(\mu \to e\gamma) \leq 5.7\ 10^{-13}$ [13, 98]. This bound is the most stringent for the higher mass range $m_N > m_W$ and imposes $|\Omega_{e\mu}| \leq 0.0001$, which can be translated to the constants α as

$$\Omega_{e\mu} = U_{eN} U_{\mu N} = \left(\frac{\alpha}{2}\frac{v^2}{\Lambda^2}\right)^2 < 0.0001,$$

and for $\Lambda = 1\ TeV$ we have

$$\alpha_{EWPD}^{bound} \leq 0.32\ . \tag{3.23}$$

In the case of the low mass range $m_N < m_Z$ the most stringent bounds come from the DELPHI Collaboration and give $|U_{\ell N}|^2 \leq 5 \times 10^{-3}$, which can be translated to the effective couplings as:

$$\alpha_{Coll}^{bound} \leq 2.3 \tag{3.24}$$

Neutrinoless double beta decay bounds

One common constraint for all our results stems from the neutrinoless double beta decay bounds discussed in sec.2.6.3. The $0\nu\beta\beta$ experiments put the most stringent limits on the mixings U_{eN} for the fist fermion family $i = e$. The four-fermion operators with u and d quarks and the e charged lepton $\mathcal{O}^1_{duNe}$, $\mathcal{O}^1_{LNQd}$, $\mathcal{O}^1_{QuNL}$ and $\mathcal{O}^1_{QNLd}$ -as well as the SVB operator $\mathcal{O}^{(1)}_{N\ell\phi}$- contribute to the $0\nu\beta\beta$-decay process depicted in fig.2.1 via the interactions in fig.3.1.

We take into account the bounds for the $0\nu\beta\beta$-decay following the general treatment made in [120], where an effective interaction Hamiltonian for the $udeN$ interaction is considered:

$$\mathcal{H} = G_{eff}\ \bar{u}\Gamma d\ \ \bar{e}\Gamma N + h.c. \tag{3.25}$$

Here Γ represents a general Lorentz-Dirac structure. We find the G_{eff} constant can be parameterized as depending on the Majorana neutrino mass m_N as

$$G_{eff} \leq A \times 10^{-8} \left(\frac{m_N}{100\ GeV}\right)^{1/2}\ GeV^{-2}, \tag{3.26}$$

where the numerical constant A depends on the nuclear model used and the lifetime for the $0\nu\beta\beta$-decay. We take the most stringent limit $\tau_{0\nu_{\beta\beta}} \geq 1.1 \times 10^{26}$ years obtained by the KamLAND-Zen Collaboration[5] [112].

The operators in fig.3.1 contribute to the effective Hamiltonian (3.25), with $G_{eff} = \frac{\alpha}{\Lambda^2}$, which is related with the mixing angle between light and heavy neutrinos as we stated in (3.21). We find that the value $A = 3.2$ fits very well the bounds obtained for the mixings [93, 122] in the most recent literature.

We can translate the limit coming from G_{eff} on this set of first family operators $\alpha^{(1)}_{\mathcal{O}_{0\nu\beta\beta}}$ which, for $\Lambda = 1$ TeV, is

$$\alpha^{bound}_{0\nu\beta\beta} \leq 3.2 \times 10^{-2} \left(\frac{m_N}{100\ GeV}\right)^{1/2}. \tag{3.27}$$

3.5. Perspectives

The effective operators presented in this chapter lead to a very rich phenomenology: its study in the context of high energy colliders and also in neutrino telescopes constitutes the purpose of the original research presented in this thesis.

I would like to emphasize that the effective operators presented here cover a wide variety of well known renormalizable new physics models as extended scalar and gauge sectors, vector and scalar leptoquarks, heavy fermions, etc. and as discussed in sec.1.5.2 one can try to get a hint of what kind of new physics is responsible for the low energy measured effects by studying their phenomenological implications. In the next chapters I present the contributions we have made during this period towards this direction.

[5] In our first works [2, 4] this limit still came from the GERDA result [121] giving $\tau_{0\nu_{\beta\beta}} \geq 2.1 \times 10^{25}$ years.

Chapter 4

Effective Majorana neutrino decays

I start the presentation of the different results obtained in the study of the phenomenology of Majorana neutrinos in the framework of the effective lagrangian approach introduced in chapter 3. This chapter is devoted to the calculation of the Majorana neutrino decay width and the branching ratios for its different decay modes, introducing the work leading to the publications in [2,3].

4.1. Introduction

The study of sterile Majorana neutrino decays is an issue of great interest in different areas of high energy physics, as the search strategy or the discovery of new effects for heavy neutrinos often rely on their different decay channels to detectable particles. Besides the heavy Majorana neutrino detection in colliders by lepton number violation processes -subject we will address in the following chapters- other kinds of searches exploiting the displaced vertex and delayed photons techniques have been proposed and are taking place at the LHC [123–130] in the framework of "vanilla" and "inverse" Type I seesaw scenarios. Also, searches in neutrino telescopes like IceCube [131,132] have been proposed, and the new decay modes and their relation with the explanation of several anomalies as the sub-horizontal events detected by the neutrino telescope SHALON [133] or the anomaly in the MiniBoone accelerator-neutrino experiment [134] are being investigated [135]. In astrophysical environments, the cosmic and the diffuse supernova neutrino backgrounds can be used to probe possible radiative decays and other decay modes of cosmological interest [136,137].

With these motivations in mind, in this chapter we study the decays of heavy Majorana neutrinos in a general, model-independent approach in the context of an effective theory. This chapter includes the work made in two papers, studying the N decays in two m_N regimes: a first paper [2] restricts to the case of $m_N < m_W$, and a following paper [3] treated all the available decay modes into standard particles.

I will first present the general results we obtained for the decay widths and branching ratios for all possible two-body and tree-body N decays in section 4.2 and our numerical

results for the high mass (sec.4.3.1) and low mass (sec.4.3.2) regimes, explaining how the constraints on the effective couplings are taken into account in each case.

In our work [2] we studied the decay modes of a relatively light Majorana neutrino in the context of the general effective framework. We focused in a mass interval below the standard massive vector bosons mass ($m_N < m_W$) as this reduces the possible decay channels, letting us concentrate on the phenomenology of the neutrino plus photon decay mode. This heavy neutrino decay channel has been introduced as a possible answer to some experimental puzzles, like the MiniBooNE [138, 139] and SHALON [140] anomalies, considering sterile heavy neutrinos created by ν_μ neutral current interactions and decaying radiatively due to a transition magnetic moment [141]. We revisit here the mentioned anomalies in the light of an effective lagrangian description for the heavy Majorana neutrino decays in sec.4.4 and comment on its possible detectability in colliders like the LHC.

4.1.1. Decay widths and branching fractions

In this chapter we deal with the calculation of the decay widths and branching ratios of the possible unpolarized decay modes of a sterile Majorana neutrino. I will now give a brief definition of these observables.

The decay rate (or decay *width*) of an unstable particle into a specified final state of two or more particles is defined as the number of decays per unit time divided by the number of available decaying particles, i.e. the probability per unit time of a particle to decay[1]. The total decay width is the sum of the decay widths of all possible channels:

$$\Gamma_{tot} = \sum_i \Gamma_i. \tag{4.1}$$

The *lifetime* of an unstable particle is the defined as $\tau = (\Gamma_{tot})^{-1}$, and its *half-life* as $\tau \ln(2)$.

The branching fraction or branching ratio for a given decay channel is defined as its decay width divided by the total decay width for the unstable particle:

$$Br(i) = \frac{\Gamma_i}{\Gamma_{tot}}. \tag{4.2}$$

The differential decay width of an unstable particle with 4-momentum p into a final state with k particles of momentum p'_j and phase-space factor $d\Phi_k$ can be calculated as

$$d\Gamma = \frac{1}{2E_p}|\mathcal{M}_{i\to f}|^2 d\Phi_k. \tag{4.3}$$

Here the phase-space $d\Phi_k$ factor is defined as in the appendix A.1. The two-body phase-space and the treatment of resonances A.1.2 are briefly introduced there as a reference to the reader.

[1] In natural units, it is measured in $[s^{-1}] = eV$.

The matrix element $\mathcal{M}_{i\to f}$ gives the transition amplitude between the initial and final state. This is calculated perturbatively with the aid of Feynman diagrams, and depends on the different momenta of the final state particles, to be integrated in order to calculate the decay width. In this work we are considering only the tree-level contributions to the N-decays, taking into account the diagrams shown in the different figures for each possible decay channel, and integrating the phase-space factor in each case. In the case of two-body decays the phase-space can be easily integrated, giving analytic expressions for the decay widths. For three-body decays, the phase-space integration is more involved, and in some cases has to be done numerically, using Monte Carlo techniques. The differential decay widths are usually expressed in terms of a dimensionless variable x representing the quotient between the momenta of one of the product particles and the rest-mass of the decaying particle. Many examples can be seen in specialized textbooks like [142] and for reference I have worked out a detailed calculation of a three-body decay phase-space integration in the appendix A.2.

4.2. N decays

An unstable particle can decay into other particles if the process is kinematically accessible: this requires that at least the sum of the decay products rest-mass must be smaller than the rest-mass of the parent particle.

A heavy Majorana neutrino N with sufficiently high mass m_N can decay to any combination of standard particles[2]. We chose to analyze in two different papers the possible decays of the N: in a first work [2] we studied the possible decay channels for a Majorana neutrino lighter than the W, Z and Higgs bosons mass ($m_N < m_W = 80.4\ GeV$) and focused on its decay modes to fermions and the novel decay channel to an ordinary neutrino and a photon. In a subsequent paper, we completed the calculation including all two-body and three-body decay channels, for a sufficiently heavy N [3].

Both mass regimes are tested by different experiments, and then the experimental bounds we have to take into account for the effective couplings $\alpha_{\mathcal{O}}^{(i)}$ in each case are different. I will comment on the considered bounds for the $\alpha_{\mathcal{O}}^{(i)}$ and how we implement the numerical calculations separately for each case.

4.2.1. Two-body decays

The two-body decay channels for the heavy Majorana neutrino N are shown in fig.4.1. They receive contributions from the lagrangian terms originated in operators involving gauge bosons and the Higgs field presented in (3.7) and (3.9) that lead to the effective lagrangian terms in (3.11) and (3.18).

The analytical expressions obtained for the decay widths of channels $N \to \nu Z$, $N \to l^+W^-$ and $N \to \nu h$ shown in fig.4.1 are:

[2] In processes allowed by conservation laws.

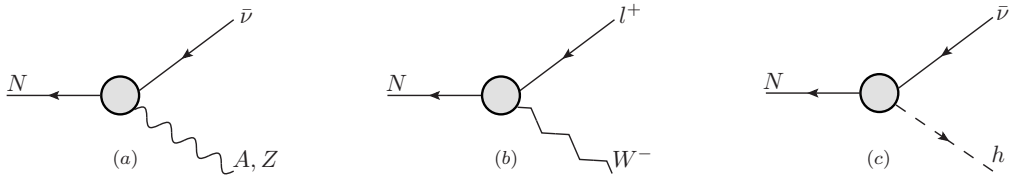

Figure 4.1: Two-body decays with gauge bosons and Higgs field.

$$\begin{aligned}\Gamma^{N\to\nu_i Z} &= \left(\frac{m_N}{128\pi}\right)\left(\frac{m_N}{\Lambda}\right)^4 (1-y_Z)^2\left[(\alpha^{(i)}_{L_4}-\alpha^{(i)}_{L_2})^2(1-y_Z)^2+\right.\\ &8(\alpha^{(i)}_{L_4}-\alpha^{(i)}_{L_2})(\alpha^{(i)}_{L_3}c_W-\alpha^{(i)}_{L_1}s_W)(1-y_Z)\sqrt{y_Z y_v}+\\ &\left.16(2+y_Z)y_V(\alpha^{(i)}_{L_3}c_W-\alpha^{(i)}_{L_1}s_W)^2\right]\end{aligned}$$

with $y_Z = m_Z^2/m_N^2$ and $y_v = v^2/m_N^2$.

$$\Gamma^{N\to l_i W} = \frac{m_N}{32\pi}\left(\frac{m_N}{\Lambda}\right)^4 \alpha^{(i)}_W (1-y_W)^2(1+2y_W)y_v$$

with $y_W = m_W^2/m_N^2$.

$$\Gamma^{(N\to\nu_i h)} = \frac{9m_N}{128\pi}\left(\frac{v}{\Lambda}\right)^4 \alpha^{(i)2}_\phi (1-y_h)$$

with $y_h = m_h^2/m_N^2$.

Finally we have the decay mode to a photon and an ordinary neutrino $N \to \nu A$:

$$\Gamma^{N\to\nu_i A} = \frac{1}{4\pi}\left(\frac{v^2}{m_N}\right)\left(\frac{m_N}{\Lambda}\right)^4 (\alpha^{(i)}_{L_1}c_W + \alpha^{(i)}_{L_3}s_W)^2 \tag{4.4}$$

This decay mode leads to an interesting phenomenology to be discussed in sec.4.4.

It is important to take into account here that the W and h resonant contributions to other decays, as can be seen in figs. 4.5 (a) and (b) were already included in those decays and will not be added to the total width.

4.2.2. Three-body decays

Gauge and Higgs bosons

The three-body decays of the heavy Majorana neutrino N involving gauge bosons and the Higgs field receive contributions from the lagrangians presented in (3.11) and (3.18), whereas the decays to three fermions come also from the operators presented in (3.12).

The effective model we are working with also gives tree-level contributions to four-body decays, but as their contributions are very small -mostly due to the phase-space volume factor, as I comment in the appendix sec. A.1.1- they are not presented in this work.

The three-body decay channels involving gauge bosons and ordinary neutrinos are shown in fig.4.2: (a) and (b) $N \to \nu W^+W^-$, (c) and (d) $N \to \nu ZZ$, and (e) $N \to \nu ZA$. The differential decay rates are expressed in terms of $x = \frac{2p^0}{m_N}$, with p^0 being the energy of the lepton (charged lepton or ordinary neutrino) in the N-rest frame. Detailed examples of this kind of calculations are included in the appendix sec.A.2.

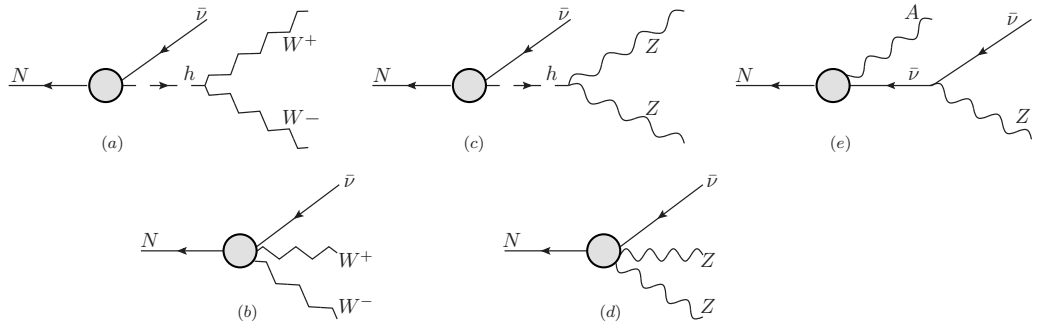

Figure 4.2: Three-body decays with two gauge bosons and ordinary neutrinos.

The analytical expressions for the differential decay widths are:

$$\frac{d\Gamma^{N\to\nu_i W^+W^-}}{dx} = \frac{m_N}{6144\pi^3}\left(\frac{m_N}{\Lambda}\right)^4 \frac{x^2}{(1-x)^2 y_W}((1-x)(1-x-4y_W))^{1/2} \times \Big[16\alpha_{L_3}^{(i)2}(3-x)((1-x)^2+4(1-x)y_W-8y_W^2)+ 3\mid\tilde{\alpha}^{(i)}\mid^2 g^2(1-x)((1-x)^2-4(1-x)y_W+12y_W^2)\Big]$$

where $\tilde{\alpha}^{(i)} = \alpha_{L_4}^{(i)} + \frac{3}{2}\alpha_\phi^{(i)}\frac{y_v}{1-x-y_h+i\sqrt{y_h y_{\Gamma_W}}}$, $y_{\Gamma_W} = \Gamma_W^2/m_N^2$ and $0 \le x \le 1-4y_W$. In this process we discard the $N \to lW$ followed by the $l \to \nu W$ SM vertex contribution, because the amplitude is proportional to the intermediate lepton mass, and thus negligible in comparison with the diagrams shown in fig.4.2 (a) and (b)[3].

[3]These diagram's contributions are a factor of $\frac{m_\ell}{m_N} \lesssim 0.01$ shorter than those shown in fig.4.2 (a) and (b) in the case of tau leptons (which have the bigger mass) for $m_N > 2m_W$.

$$\frac{d\Gamma^{N\to\nu_i ZZ}}{dx} = \frac{m_N}{64\pi^2}\left(\frac{m_N}{\Lambda}\right)^4 \frac{\alpha^{emg}}{s_{2W}^2} y_Z \left[\left(\alpha_{L_4}^{(i)} + \frac{3\alpha_\phi^{(i)} y_v (1-x-y_h)}{(1-x-y_h)^2 + y_h y_{\Gamma_h}}\right)^2 + \left(\frac{3\alpha_\phi^{(i)} y_v \sqrt{y_h y_v}}{(1-x-y_h)^2 + y_h y_{\Gamma_h}}\right)^2\right] \times \frac{x^2}{(1-x)}\left(2 + \frac{(1-x-2y_Z)^2}{4y_Z^2}\right)((1-x-2y_Z)^2 - 4y_Z^2)^{1/2}$$

with $\alpha^{emg} = \frac{e^2}{4\pi}$ being the electromagnetic constant, $y_{\Gamma_h} = \Gamma_h^2/m_N^2$ and $0 \le x \le 1-4y_Z$.

$$\frac{d\Gamma^{N\to\nu_i ZA}}{dx} = \frac{m_N}{32\pi^3}\left(\frac{m_N}{\Lambda}\right)^4 \left(c_W \alpha_{L_1}^{(i)} + s_W \alpha_{L_3}^{(i)}\right)^2 \frac{(1-x+2y_Z)(1-x-y_Z)x^3}{(1-x)^3}.$$

with $0 \le x \le 1-y_Z$.

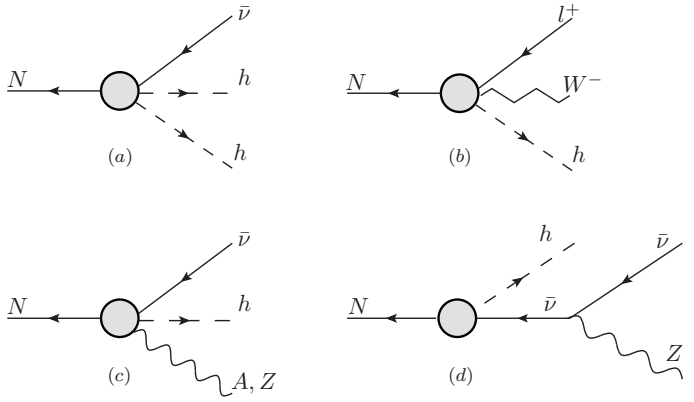

Figure 4.3: Three-body decays with gauge bosons and Higgs field.

The three-body channels with Higgs fields in the final state are shown in fig.(4.3) (a) $N \to \nu hh$, (b) $N \to l^+ W^- h$, (c) $N \to \nu hA$ and (d) $N \to \nu hZ$. The obtained expressions for the decay widths are:

$$\frac{d\Gamma^{N\to\nu_i hh}}{dx} = \frac{18\alpha_W^{(i)2} m_N}{2048\pi^3}\left(\frac{v}{m_N}\right)^2 \left(\frac{m_N}{\Lambda}\right)^4 x^2 \frac{((1-x-2y_h)^2 - 4y_h^2)^{1/2}}{(1-x)}$$

with $0 \le x \le 1-4y_h$.

$$\frac{d\Gamma^{N\to l_i Wh}}{dx} = \frac{m_N \alpha_W^{(i)2}}{768\pi^3}\left(\frac{m_N}{\Lambda}\right)^4 ((1-x-y_h)^2 - 2(1-x+y_h)y_W + 4y_W^2)^{1/2} \times \left[(3-x)\left((1-x-y_h)^2 + y_W^2\right) + (6-3y_h + x(-11+5x+y_h))y_W\right] \frac{x^2}{(1-x)^3},$$

with $0 \leq x \leq 1-(y_h+y_W+2\sqrt{y_h y_W})$.

$$\frac{d\Gamma^{N\to\nu_i Ah}}{dx} = \frac{m_N}{192\pi^3}\left(\frac{m_N}{\Lambda}\right)^4\left(c_W\alpha^{(i)}_{L_1}+s_W\alpha^{(i)}_{L_3}\right)^2\frac{(1-x-y_h)^3x^3}{(1-x)^3}$$

with $0 \leq x \leq 1-y_h$.

$$\begin{aligned}\frac{d\Gamma^{N\to\nu_i Zh}}{dx} &= \frac{9\ m_N\ g^2}{2^{14}\pi^3}\left(\frac{v}{\Lambda}\right)^4\alpha^{(i)2}_{\phi}\times \\ &\left[\frac{(2-x)(1-x+y_h+2y_z)(1-x+y_h-y_z)(x^2-4y_h)^{1/2}}{y_z(1-x+y_h)}\right]\end{aligned}$$

with $2\sqrt{y_h} \leq x \leq 1+y_h-y_z$. This decay width is obtained from the diagram shown in fig.4.3(d), as this contribution involves a tree-level vertex coming from the lagrangian (3.11) and a SM vertex, and is dominant comparing to the one-loop level term coming from the lagrangian (3.18) that would give a vertex as the one shown in fig.4.3 (c).

The three-body decay channels with two gauge bosons and charged leptons in the final state are shown in fig.4.4: $N \to l^+W^-A,Z$. We cannot obtain analytical expressions for these decay widths, and we have done numerical integrations of the phase space in the usual way using the numerical Monte Carlo routine RAMBO [143].

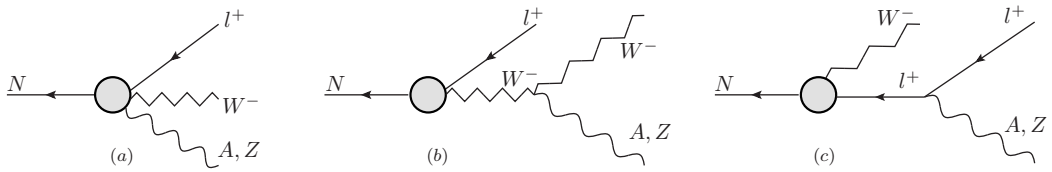

Figure 4.4: Three-body decays with two gauge bosons and charged leptons.

Fermionic three-body decay widths

Some of the three-body decays involving only fermions in the final state come from the four-fermion contact operators presented in (3.8) leading to the tree-level lagrangian in (3.12).

The partial decay widths of a heavy Majorana neutrino N decaying to three fermions were calculated including the contributions in the effective lagrangians (3.11) and (3.12). The decay channels are shown in fig.4.5. As was previously mentioned, the diagrams (a) and (b) show the resonant contributions coming from two-body decays to W and h bosons.

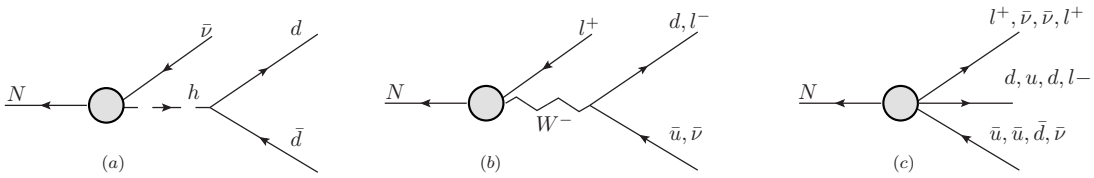

Figure 4.5: Majorana neutrino decaying to three fermions.

The decays to one lepton and two quarks can be written as

$$\begin{aligned}\frac{d\Gamma^{(N\to l^+\bar{u}d)}}{dx} &= \frac{m_N}{512\pi^3}\left(\frac{m_N}{\Lambda}\right)^4 x\frac{(1-x-y_l+y_u)}{(1-x+y_l)^3}\Big\{(1-x+y_l-y_u)\Big[6\alpha_1^{i_u,i_l}x(1-x+y_l)^2\\ &+ 12\alpha_2^{i_u,i_l}(2-x)(1-x+y_l)\sqrt{y_l y_u}+\alpha_3^{i_u,i_l}(2x^3-x^2(5+5y_l+y_u)-4y_l(1+y_l+2y_u)\\ &+ x(3+10y_l+3y_l^2+3y_u+3y_l y_u))\Big]+24\alpha_4^{i_u,i_l}x(1-x+y_l)^2\sqrt{y_l y_u}\Big\} \qquad (4.5)\end{aligned}$$

with $2\sqrt{y_l} < x < 1+y_l-y_u,\ y_l = m_l^2/m_N^2,\ y_u = m_u^2/m_N^2$ and the coefficients $\alpha_{1,..,4}$ take the expressions:

$$\begin{aligned}\alpha_1^{i_u,i_l} &= \left(\alpha_{s_1}^{(i_u)2}+\alpha_{s_2}^{(i_u)2}-\alpha_{s_2}^{(i_u)}\alpha_{s_3}^{(i_u)}\right)\delta^{i_u,i_l}\\ \alpha_2^{i_u,i_l} &= \left(\alpha_{s_1}^{(i_u)}\alpha_W^{(i_l)}\frac{y_W(1-x+y_l-y_W)}{(1-x+y_l-y_W)^2+y_W y_{\Gamma_W}}-\alpha_{s_3}^{(i_u)}\alpha_{V_0}^{(i_u)}\right)\delta^{i_u,i_l}\\ \alpha_3^{i_u,i_l} &= \left(\alpha_{s_3}^{(i_u)2}+4\alpha_{V_0}^{(i_u)2}\right)\delta^{i_u,i_l}+4\alpha_W^{(i_l)2}\frac{y_W^2(1-x+y_l-y_W)}{(1-x+y_l-y_W)^2+y_W y_{\Gamma_W}}\\ \alpha_4^{i_u,i_l} &= \alpha_{s_2}^{(i_u)}\alpha_{V_0}^{(i_u)}\delta^{i_u,i_l}.\end{aligned}$$

$$\begin{aligned}\frac{d\Gamma^{(N\to\nu dd)}}{dx} &= \frac{m_N}{128\pi^3}\left(\frac{m_N}{\Lambda}\right)^4\frac{x^2}{4}\frac{((1-x)(1-x-4y_d))^{1/2}}{(1-x)^2}\times\\ &\Big\{\delta^{i_l,i_d}\alpha_{s_3}^{(i_l)2}(3+x(-5+2x+2y_d))+\\ &6\left(\tilde{\alpha}_1^{i_l,i_d\,2}+\tilde{\alpha}_2^{i_l,i_d\,2}-\delta^{i_l,i_d}\tilde{\alpha}_3^{i_l,i_d}\alpha_{s_3}^{i_l}\right)(1-x)(1-x-2y_d)\Big\}\end{aligned}$$

with $0 < x < 1-4y_d,\ y_d = m_d^2/m_N^2$ and

$$\begin{aligned}\tilde{\alpha}_1^{i_l,i_d\,2} &= \left(\delta^{i_l,i_d}\alpha_{s_2}^{(i_l)}+\alpha_\phi^{(i_l)}c\frac{(1-x-y_h)}{D}\right)^2+\alpha_\phi^{(i_l)2}c^2\frac{y_h y_{\Gamma_h}}{D_h^2}\\ \tilde{\alpha}_2^{i_l,i_d\,2} &= \alpha_\phi^{(i_l)}\frac{c^2}{D_h}\\ \tilde{\alpha}_3^{i_l,i_d} &= \delta^{i_l,i_d}\alpha_{s_2}^{(i_l)}+\alpha_\phi^{(i_l)}\ c\ \frac{(1-x-y_h)}{D_h}\ ,\ y_h = m_h^2/m_N^2\ ,\ y_{\Gamma_h} = \Gamma_h^2/m_N^2\\ D_h &= (1-x-y_h)^2+y_h y_{\Gamma_h}\ ,\ c = \frac{3gv^2 m_d}{4\sqrt{2}m_N^2 m_W}.\end{aligned}$$

$$\frac{d\Gamma^{(N\to\nu uu)}}{dx} = \frac{m_N}{128\pi^3}\left(\frac{m_N}{\Lambda}\right)^4 \tilde{\alpha}^{i_l,i_u\,2}\ \frac{3}{2}x^2\left(1-\frac{4y_u}{(1-x)}\right)^{1/2}(1-x-2y_u)\delta_{i_u,i_l}$$

with $0 < x < 1-4y_u$ and

$$\tilde{\alpha}^{i_l,i_u\,2} = \delta^{i_l,i_u}\alpha_{S_1}^{(i_l)\,2} + 2\alpha_\phi^{(i_l)\,2}\frac{c^2}{D_h}\ ,\ c = \frac{3gv^2m_u}{4\sqrt{2}m_N^2m_W}.$$

The purely leptonic decay gives:

$$\frac{d\Gamma^{(N\to l^+ leptons)}}{dx} = \frac{m_N}{1536\pi^3}\left(\frac{m_N}{\Lambda}\right)^4\frac{(1-x+y_l-y_{l'})^2}{(1-x+y_l)^3}x\left[\alpha_1^{i_l,i_{l'}}P(x)-\alpha_2^{i_l,i_{l'}}R(x)\right]$$

with $2\sqrt{y_l} < x < 1+y_l-y_{l'}$, $y_l = m_l^2/m_N^2$, $y_{l'} = m_l'^2/m_N^2$ and $\alpha_{1,2}$ and the terms $P(x)$, $R(x)$ take the expressions:

$$\begin{aligned}
\alpha_1^{i_l,i_{l'}} &= \alpha_{s_0}^{(i_l)\,2}\,\delta^{i_l,i_{l'}} + \frac{4\alpha_W^{(i_l)\,2}y_W^2}{(1-x+y_l-y_W)^2+y_Wy_{\Gamma_W}}\\
\alpha_2^{i_l,i_{l'}} &= 12\alpha_{s_0}^{(i_{l'})}\alpha_W^{(i_l)}\frac{(1-x+y_l-y_W)}{(1-x+y_l-y_W)^2+y_Wy_{\Gamma_W}}\delta^{i_l,i_{l'}}\\
P(x) &= 2x^3-x^2(5+5y_l+y_{l'})-4y_l(1+y_l+2y_{l'})+x(3+10y_l+3y_l^2+3y_{l'}+3y_ly_{l'})\\
R(x) &= (2-x)(1-x+y_l)(y_ly_{l'})^{1/2}.
\end{aligned}$$

4.3. Numerical results

Besides the values for the standard particles masses and couplings, the numerical values for the N decay widths and branching ratios depend on the m_N mass, on the new physics scale Λ considered, and on the values of the $\alpha_{\mathcal{O}}^{(i)}$ effective couplings. Here we consider the benchmark value $\Lambda = 1\ TeV$.

4.3.1. High m_N range

Regarding the effective couplings, in order to simplify the discussion, for the numerical evaluation we only consider the two following situations. In the numerical set we call **A** the couplings associated to the operators that contribute to the $0\nu\beta\beta$-decay are restricted to the corresponding bound $\alpha_{0\nu\beta\beta}^{bound}$ given and discussed in (3.27) and the other couplings are restricted to the bound determined by the $EWPD$ constraints and given in (3.23) $\alpha_{EWPD}^{bound} = 0.32$. In the case of the set called **B** all the couplings are restricted to the $0\nu\beta\beta$ bound $\alpha_{0\nu\beta\beta}^{bound}$ which is the most stringent. For the one-loop generated operators we consider the coupling constant as $1/(16\pi^2)$ times the corresponding tree-level coupling: $\alpha^{1-loop} = \alpha^{tree}/(16\pi^2)$. Thus, for the operators $\mathcal{O}_{DN}$, $\mathcal{O}_{NW}$ and $\mathcal{O}_{\bar{D}N}$, which contribute to $0\nu\beta\beta$ we have

$$\alpha_{L_2}^{(1)}, \alpha_{L_3}^{(1)}, \alpha_{L_4}^{(1)} \sim \frac{1}{16\pi^2}\alpha_{0\nu\beta\beta}^{bound}$$

for fermions of the first family. For the remaining operators we take

$$\alpha \sim \alpha_{EWPD}^{bound}, \alpha_{0\nu\beta\beta}^{bound}$$

in the sets **A** and **B** respectively.

The numerical results for the Majorana neutrino branching ratios and total decay width are presented in the following. In figs.4.6 and 4.7 we show the results for the branching ratios for the different decay channels found in the previous section. We display the branching ratios as a function of the Majorana neutrino mass m_N calculated for different numerical values of the constants $\alpha_{\mathcal{O}}^{i}$. In all the following results when ordinary neutrinos are present in the final states we sum the contributions of the neutrino and antineutrino channels.

In figure 4.6a we present the branching ratios of the three-fermion and photon-neutrino channels for the couplings set **A**. These are the only kinematically open channels for $m_N < m_W$. One can appreciate here the dominance of the neutrino-photon channel for the lower m_N values.

Figure 4.6b shows the massive gauge and Higgs boson decay channels for the N. The branching ratio for the $N \to \nu h A$ mode is smaller than 1.0×10^{-7} and is not visible in the plot.

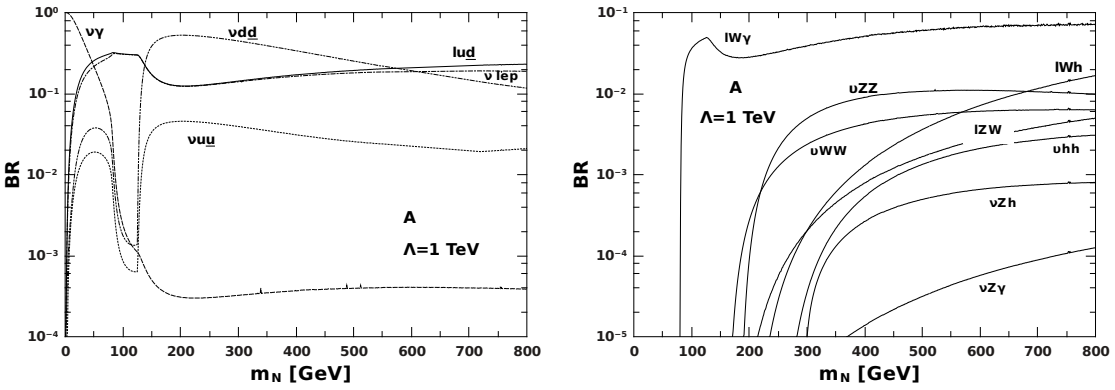

(a) Three fermions and neutrino-photon decay channels.

(b) Massive gauge and Higgs boson decay channels.

Figure 4.6: The branching ratios for the Majorana neutrino decay in the set **A** considering the sum in fermion families.

For completeness we present the branching ratios for the two-body decay channels in fig.4.7. As we explained in the previous section the $N \to \nu h, W$ channels are not included in the total width, as their contribution has already been taken into account in the channels where the W and h bosons participate as intermediate resonant states.

Finally, fig.4.8 shows the total decay width dependence on the mass m_N for both coupling sets considered, and again a sum over families and channels with particles and antiparticles in the final state is performed.

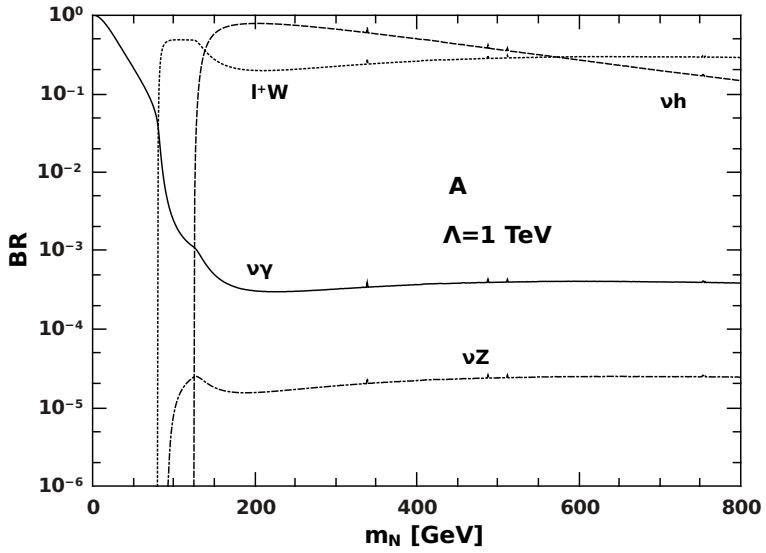

Figure 4.7: The branching ratios for two-body decays considering the sum over families.

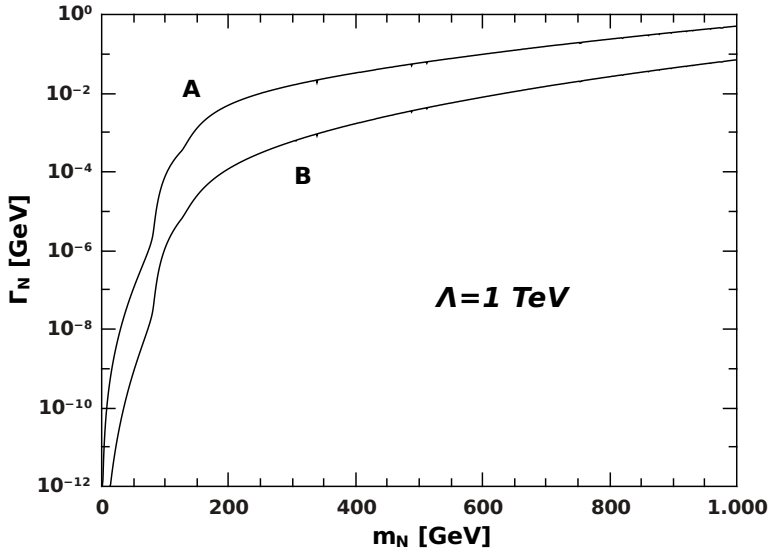

Figure 4.8: Total decay width with coupling constants in the sets **A** and **B** for $\Lambda = 1TeV$.

4.3.2. Low m_N range

As will be explained in sec.4.4, the relevant Majorana neutrino mass range for considering this heavy neutral particle as a solution to the MiniBooNE anomaly is 400 $MeV <$

$m_N < 600\ MeV$ [141]. The experimental bounds for this mass values are exhaustively discussed in [94] and references therein. Taking into account that the MiniBooNE experiment deals with muon-type neutrinos, we now discuss the bounds on the $U_{\mu N}$ mixings, which are not constrained by $0\nu\beta\beta$-decay and are more restrictive than the existing ones for the third fermion family.

It can be seen in the review [94] that the existing bounds for the mixing $U_{\mu N}$ for a mass $m_N \simeq 500\ MeV$ come from beam dump experiments as NuTeV [144], CHARM II [145] and BEBC [146], rare lepton number violating (LNV) meson decays at LHCb [111] and from colliders as those from DELPHI [97]. In the case of the heavy Majorana neutrino with the effective interactions we are considering, the clear dominance of the neutrino plus photon channel found in (4.4) makes the beam dump and rare LNV experiments bounds inapplicable, as this decay mode to invisible particles is not considered in those analyses and can considerably alter the number of events found for N decays inside the detectors [94, 118]. In the light of this argument, we consider the bounds from DELPHI [97] discussed in the previous chapter in sec.3.4 and given in (3.24) $\alpha_{Coll}^{bound} \leq 2.3$.

For completion we have explicitly calculated the bounds that can be inferred from the single $Z \to \nu N$ and pair $Z \to N\ N$ "excited" neutrino production searches at LEP [96]. The first process can be generated by one-loop level effective operators in (3.9) giving the terms in the lagrangian (3.18). As the one-loop level couplings are suppressed by the factor $1/16\pi^2$ the corresponding bound for the couplings $\alpha^{1-loop} v^2/2\Lambda^2$ is absorbed by the $(16\pi^2)^2$ multiplying the bounds, so that the value α_{Coll}^{bound} (3.24) is still more stringent. It is important to mention that other effective operators (four-fermion operators in (3.12)) contribute to the νN and NN production at LEP, but at the Z peak they give less restrictive bounds than α_{Coll}^{bound}. For the decay $Z \to N\ N$ we have a direct contribution from the tree-level operator $\mathcal{O}_{NN\phi}$ giving

$$\Gamma(Z \to NN) = \frac{\alpha_Z^2 c_W^2}{96\pi s_W^2} \left(\frac{v}{\Lambda}\right)^4 m_Z. \tag{4.6}$$

A conservative limit for any m_N mass is obtained from $Br(Z \to NN) Br^2(N \to \nu(\bar{\nu})\gamma) < 5 \times 10^{-5}$ [96]. This result is model-independent and holds for the production of a pair of heavy neutral objects decaying into a photon and a light invisible particle. For the low m_N values considered in this work, we can take $Br(N \to \nu(\bar{\nu})\gamma) \simeq 1$ and the corresponding bound is $\frac{\alpha_Z^2 v^2}{2\Lambda^2} < 3.0 \times 10^{-5}$. This bound is more stringent than the one in (3.24) but it is not taken into account because the corresponding operator does not contribute at tree-level to the N decay in this low m_N range.

For the numerical evaluation we consider again the sets **A** with the bound $\alpha_{0\nu\beta\beta}^{bound}$ on the $0\nu\beta\beta$-decay related operators, and the other couplings restricted to the bound (3.24), $\alpha_{Coll}^{bound} \leq 2.3$. For the set **B** and the 1-loop generated operators we take the same values we considered in sec.4.3.1.

In fig.4.9 we show the results for the Majorana neutrino decay presented in sec.4.2, for the low m_N mass range shown. Figure 4.9a shows the branching ratio as a function of the Majorana neutrino mass m_N. The decay is calculated for different values of the constants $\alpha_{\mathcal{O}}^i$. We show the branching ratios for both sets **A** and **B**. It can be seen

that for low masses the dominant channel is the decay of N to a photon and a neutrino. Figure 4.9b shows the total decay width dependence on the mass for both coupling sets considered.

Taking the values of the couplings $\alpha^{(i)}$ to be equal for every family i and also for every tree-level coupling α^{tree} and taking the one-loop generated couplings as $\alpha^{1-loop} = \alpha^{tree}/16\pi^2$ we derived an approximated expression for the ratio between the widths $\Gamma(N \to \nu(\bar{\nu})A)$ in (4.4) and $\Gamma(N \to l^+\bar{u}d)$ in (4.5):

$$\frac{\Gamma^{(N\to\nu(\bar{\nu})A)}}{\Gamma^{(N\to l^+\bar{u}d)}} \to \frac{2}{15\pi}\left(\frac{v}{m_N}\right)^2 (c_W + s_W)^2 . \tag{4.7}$$

This limiting value explains the behavior found in figs.4.9 and 4.6a for low Majorana neutrino masses, showing the neutrino plus photon decay channel is clearly dominating. This is an interesting fact since we have a new source of photons, leading to a very rich phenomenology discussed in the next section.

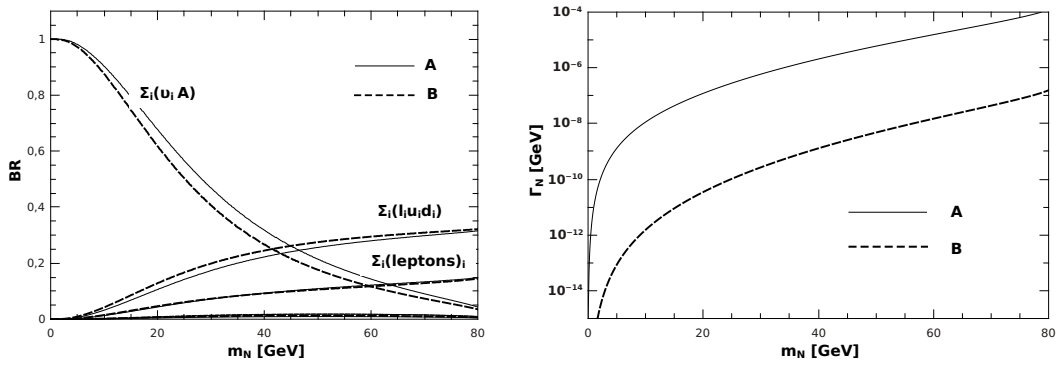

(a) (b)

Figure 4.9: (a)The branching ratios for the Majorana neutrino decay with coupling constants in the set **A** (solid lines) and set **B** (dashed lines). Only the charged anti-lepton channels are plotted. The unlabeled curves correspond to the decay $N \to \nu uu$ and $N \to \nu dd$. (b) Total width for the two combinations of coupling constants defined in the text (set **A** and set **B**) and $\Lambda = 1$ TeV.

4.4. Application to neutrino-related questions

Searches for heavy neutrinos rely on their possibility to decay to detectable particles. The interpretation of the corresponding results for such searches requires a model for the decay of the heavy neutrino. Several explanations to different kind of experimental puzzles seem related to weakly interacting neutral particles, like new neutrinos. In particular the MiniBooNE [138] anomaly or the observation of sub-horizontal air-showers by

the Cherenkov telescope SHALON [140] have possible explanations by long lived neutral particles like the one studied in this work.

The MiniBooNE neutrino oscillation experiment at Fermilab was built to search for $\nu_\mu \to \nu_e$ conversion in order to confirm or refute the previous results of the LSND oscillation experiment at Los Alamos, which were inconsistent with global neutrino oscillation data [147] existing at the time. The MiniBooNE experiment detects the appearance of electron-like neutrinos ν_e in a beam originally consisting in muon neutrinos ν_μ, pointing the ν_μ beam into a detector filled with mineral oil in which Cherenkov radiation from charged particles is detected by photomultipliers[4]. The MiniBooNE anomaly consists in an unexplained excess of low energy electron-like events in charged-current quasi-elastic ν_e events over the expected standard neutrino interactions that would be given by considering the charged-current standard interactions shown in (1.58) [138, 139].

This excess of electron-like events could be caused by the decay of a heavy neutrino. This solution was proposed by Gninenko [141] in a model with a sterile neutrino mixed with the standard neutrinos by a matrix $U_{\mu N}$. He finds that an N neutrino with

$$\begin{aligned} &400\ MeV < m_N < 600\ MeV \\ &10^{-3} < |U_{\mu N}|^2 < 4 \times 10^{-3} \\ &10^{-11} s < \tau_N < 10^{-9} s \end{aligned} \tag{4.8}$$

could explain the anomaly, as the excess of electron-like events appearing in the ν_μ beam could be caused by the decay of a heavy neutrino with a radiative dominant decay mode $N \to \nu\gamma$, where the final photon would be converted into an e^+e^- pair with a small opening angle, indistinguishable from an electron in the detector. This is called a *converted* photon. The pair (detected by its Cherenkov radiation) would be counted as coming from the charged-current interaction produced by a ν_e appearing in the beam from $\nu_\mu \to \nu_e$ oscillation and contribute to the registered ν_e excess.

The Gninenko analysis is based on the assumption that the heavy neutrino radiative decay is dominant. The effect of the mentioned strong radiative decay is the flux attenuation by N decay and then the decrease of the signal events in the detector. The consequences are less restrictive bounds on $|U_{\mu N}|^2$ [94, 118], as we explained in sec.4.3.2. The proposal is then that the excess of events observed by MiniBooNE could originate from converted photons and not from electrons truly coming from ν_e charged-current interactions. The future experiment MicroBooNE will provide a test to this proposal, as it will be able to separate photons from electrons or positrons [148, 149].

In the context of the effective interactions considered in this work, one has to check if the $N \to \nu A$ is the dominant decay, by comparing the decay of N to pions, which is the correct hadronic final state for the low masses studied here. We have found that the

[4]The detection principle is similar to the one presented for the IceCube telescope in the appendix C.3.1.

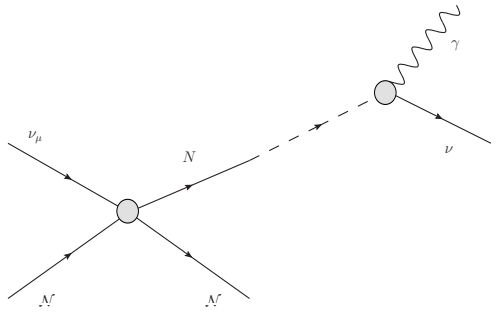

Figure 4.10: Production process of extra neutrino N by effective interactions and their subsequent decay.

corresponding decay is mainly given by

$$\Gamma^{N\to l_i^+\pi^-} = \frac{G_F^2}{8\pi}\left(\frac{\alpha_W^{(i)}}{2\Lambda^2}\right)^2 f_\pi^2 m_N^3\left[(1-\frac{m_l^2}{m_N^2})^2-\frac{m_\pi^2}{m_N^2}\left(1+\frac{m_l^2}{m_N^2}\right)\right]\times \sqrt{\left(1+\frac{m_l^2}{m_N^2}-\frac{m_\pi^2}{m_N^2}\right)^2-4\frac{m_l^2}{m_N^2}}, \tag{4.9}$$

with G_F being the Fermi and f_π the pion-decay constants[5].

In the mass range proposed in [141] we find that the ratio of the branching ratios for the different decay channels is $Br(N\to l_i^+\pi)/Br(N\to\nu(\bar{\nu})A)\simeq 8\times 10^{-6}$ and $Br(N\to leptons)/Br(N\to\nu(\bar{\nu})A)\simeq 4\times 10^{-6}$ thus confirming the dominance of the radiative decay $N\to\nu A$.

The heavy neutrino N could be directly produced by the ν_μ in neutrino-nucleon reactions by the effective operators $\mathcal{O}_{QuNL}$, $\mathcal{O}_{LNQd}$ and $\mathcal{O}_{QNLd}$, with the subsequent decay and photon conversion as we show in fig. 4.10.

The excess of ν_e events is related to the relative magnitude between the Standard Model Neutral Current (SM-NC) $\nu_\mu\mathcal{N}\to\nu_\mu\mathcal{N}$ process and the effective NC-like N production $\nu_\mu\mathcal{N}\to N\mathcal{N}$ being $\mathcal{N}$ a nucleon. For the effective operators we have a 4-fermion contribution with intensity α/Λ^2 and for the SM-NC $g^2/(4m_W^2)$. Then the amplitude ratio is $\mathcal{K}=\alpha v^2/2\Lambda^2$ and the N production is weighed by the factor $\mathcal{K}^2=(\alpha v^2/2\Lambda^2)^2$ relative to the SM-NC ν_μ scattering. The constant $\mathcal{K}^2$ plays the role of the mixing matrix $U_{\mu N}^2$ in the Gninenko [141] work, and then the value $U_{\mu N}^2$ found in (4.8) is consistent with the allowed value by the collider bound in (3.24) [103].

The constraint for the lifetime of the heavy neutrino in (4.8) must also be fulfilled in order to consider the N effective radiative decay as an alternative explanation for the MiniBooNE anomaly. In fig.4.11 we show the lifetime τ_N as a function of m_N for the sets **A** and **B** and for $\Lambda=1$ TeV. In the case of $\Lambda>1$ TeV the allowed region is upwards the curves. Thus, we can see a region compatible with set **A** where $\tau_N<10^{-9}\,s$ as in the solution proposed by Gninenko.

[5]Their current experimental values are $G_F=1.166\times 10^{-5}\ GeV$ and $f_\pi\sim 130\ MeV$.

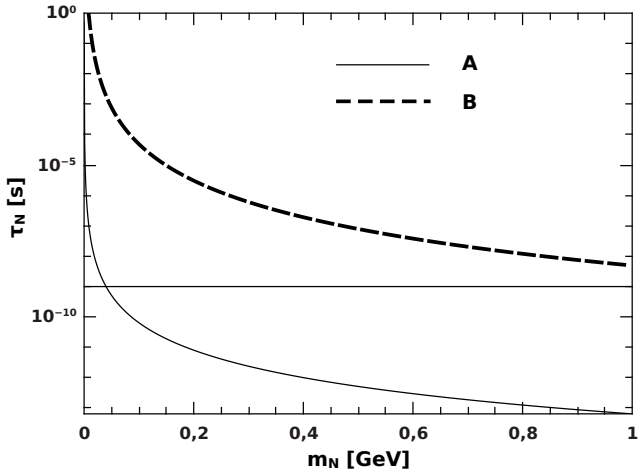

Figure 4.11: N lifetime as a function of its mass for the sets of coupling constants labeled **A** and **B** for $\Lambda = 1\ TeV$. For $\Lambda > 1\ TeV$ the values allowed for the lifetime correspond to the region upwards the curves. The horizontal solid line corresponds to the limit value found in the Gninenko solution for the MiniBooNE anomaly ($\tau_N < 10^{-9} s$).

As was previously mentioned, this kind of neutral particle which decays dominantly to a neutrino and a photon could be the explanation for several sub-horizontal air-shower events detected by the Cherenkov telescope SHALON [140]. The SHALON mirror telescope is a gamma-ray telescope located in the Tien-Shan mountains Astronomical Observatory in Kazakhstan, that detects the Cherenkov radiation produced by cosmic rays in the atmosphere. The analysis of the signal at different zenith angles has included observations from the sub-horizontal direction ($\theta = 97°$). This inclination defines an Earth skimming trajectory with 7 km of air and around 1000 km of rock in front of the telescope. In [140] they claim to have detected five air-showers of TeV energies coming from the sub-horizontal direction, which is a configuration where the signal from cosmic rays is expected to be zero. In the cited work the authors propose that the solution could be a neutral and then penetrating long-lived massive particle able to cross 1000 km of rock and decay within the 7 km of air in front of the telescope, with the same properties of those found by Gninenko in his analysis of the MiniBooNE anomaly.

In fig. 4.12 we show the decay length as a function of the heavy neutrino mass for different energies and couplings in the sets **A** and **B**. We can see that there is a region of the parameter space which could possibly explain the SHALON observations with a $l_{decay} \sim 1000\ km$.

Long-lived neutral particles: detectability

To conclude, a few words about the detectability of this particle in colliders like the LHC. Searches for neutral long-lived particles as the heavy neutrino proposed by [141]

have been studied in the context of τ^- rare decays [135]. The authors propose to search for events with two vertices, featuring the production and decay of the unstable neutrino N. The use of displaced vertices has also been proposed to search for sterile neutrinos at the LHC [124, 127] for N decaying to leptons and quarks or purely leptonically. Early displaced vertices searches are reviewed in [150].

As we have shown, for the N masses considered in this work the dominant decay is the radiative $N \to \nu\gamma$ channel, which can be observed by the signature of an isolated electromagnetic cluster together with missing transverse energy:

$$\gamma + E_T^{miss} \tag{4.10}$$

where the photon originates in a displaced vertex.

New physics searches involving such final states have been performed at the LHC [126, 151] and it has been suggested that this signal could be enhanced with the combined use of missing transverse momentum plus photons and displaced vertices searching techniques [128, 152]. The use of this technique will allow to probe parts of the parameter space which are inaccessible by other methods. The use of displaced vertices has the advantage that for decay lengths of the order of very roughly $L \in (10^{-3} - 1)\ m$, there is little standard model background. We find that decay lengths as the above mentioned for masses between $1 - 30\ GeV$ are possible in this model as we show in fig.4.12b for the sets **A** and **B** in the region between the horizontal lines.

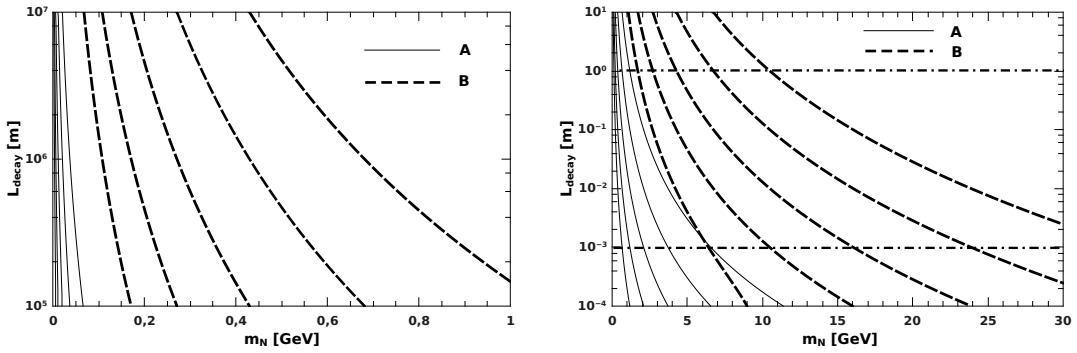

(a) N Decay Length (b) N Decay Length (higher masses)

Figure 4.12: Decay length for different neutrino energies as a function of the neutrino mass for the coupling constant sets **A** (solid lines) and **B** (dashed lines) for $\Lambda = 1$ TeV. The energies, $E = 10^n$ GeV, vary from left to right with increasing n (1-5). For $\Lambda > 1$ TeV the decay length corresponds to the top right region from the curves.

4.5. Summary and perspectives

Searches for heavy neutrinos often rely on the possibility that they may decay to detectable particles. The interpretation of the corresponding results of such searches

requires a model for the heavy neutrino decay. In this chapter we calculated the different decay modes and branching ratios for heavy sterile Majorana neutrinos in an effective approach for its interactions. Depending on the Majorana neutrinos mass scale, the decay can have effects on different physical contexts like solar/astrophysical neutrinos, collider searches like those taking place at the LHC, neutrino experiments as OPERA, MiniBoone, SHALON, etc. We presented the analytical results for the dominant channels, discussed the existing bounds taken into account for the effective couplings, and displayed the different branching ratios and the total decay width for the heavy sterile neutrino considered.

For a relatively light heavy Majorana neutrino (with $m_N < m_W$) we find that for masses below approximately 30 GeV the dominant channel is the neutrino plus photon mode: $N \to \nu A$. With this decay mode in mind, we explored the plausibility of considering it as an explanation for the MiniBooNE and SHALON anomalies. We checked that in the effective model the radiative decay is dominant respect to the lepton plus pion mode, and leads to values of the effective couplings α which are consistent with the mixing value $|U_{\mu N}|^2$ found by Gninenko [141] and with collider bounds [97]. Moreover, we showed that the Majorana neutrino lifetime also fits the limits in [141]. This kind of weakly interacting long-lived particle has also been proposed as an explanation for sub-horizontal events in the SHALON telescope [140], and we find the N decay length is compatible with the proposed explanation for part of our parameter space. This kind of particle could also be searched for in the LHC, with the use of the displaced vertices technique, with little standard model background. We will explore more concretely this possibility in chapter 6, where we study the N phenomenology in the LHC.

In the following chapters I continue presenting the results we obtained studying the possible production of Majorana neutrinos in ep and pp colliders.

Chapter 5

Majorana neutrinos production at the LHeC

In this chapter I present our first work on the collider phenomenology given by the effective lagrangian for the Majorana neutrinos considered in this thesis. This work leads to the publication in [4].

The basic concepts on collider phenomenology are presented in an appendix B. These include the definition of scattering cross sections, a brief introduction on detectors, and the most important definitions of kinematical variables to take into account when studying physics in collider environments.

5.1. Introduction

In the case that heavy neutrinos do exist, present and future experiments will be capable of determining their Dirac or Majorana nature. In particular, the production of Majorana neutrinos via e^+e^-, $e^-\gamma$, $\gamma\gamma$ and hadronic collision have been extensively investigated in the past [15–23, 153–156].

In this chapter we study the possibility for an e^-p collider at CERN (LHeC: Large Hadron electron Collider [157]) in order to produce clear signatures of Majorana neutrinos in the context of interactions coming from an effective lagrangian approach. We study the lepton number violating reaction $e^-p \to l_j^+ + 3jets$[1] ($l_j \equiv e, \mu, \tau$) which receives contributions from the diagrams depicted in fig.5.1. We have not considered the pure leptonic decay channels because they involve light neutrinos that escape detection, in which case the Majorana nature of the heavy neutrinos would have no effect on the signal, since we should be able to know whether the final state contains neutrinos or anti-neutrinos.

The lepton number violating process studied here was previously investigated in [158, 159] for the Type I seesaw mechanism, focusing on the DESY experiment and extended

[1]The *jet* definition is given in B.2.3: it can be taken as the sequel of an outgoing quark, after hadronization.

to LEP and the LHC. Recent studies of the seesaw model at lepton-proton colliders like the proposed LHeC were performed in [160, 161].

The principal advantage of electron-proton collisions with respect to proton-proton colliders is the cleanness of the signal. In the case of the LHeC, the leptonic number violation by two units is ensured by the presence of a final anti-lepton. Conversely, LNV detection in hadron colliders implies tagging two leptons of the same sign in the final state, together with a higher number of jets, making the signal more challenging to search for.

5.2. Scattering amplitudes

In order to study the production on Majorana neutrinos N in an electron-proton collider we calculate the scattering cross-section for a process where an electron encounters a "parton" (quark) constituent of the proton, producing an N. This kind of processes are commonly treated in introductory quantum field theory and particle physics books under the name *deep inelastic scattering*. The general kinematical treatment of parton-model collisions in the case of hadron colliders is introduced in the appendix B.2.3 and can be found useful in this easiest case.

The production process for an N out of the scattering of an electron and a light quark inside the proton can take place by an effective vertex (I) in fig.5.1, which receives contributions form the four-fermion interactions we obtained in (3.12), and the SM $ud\bar{W}$ vertex together with the WlN vertex in[2] (3.11). The decay vertex (II) also receives contributions from the same operators.

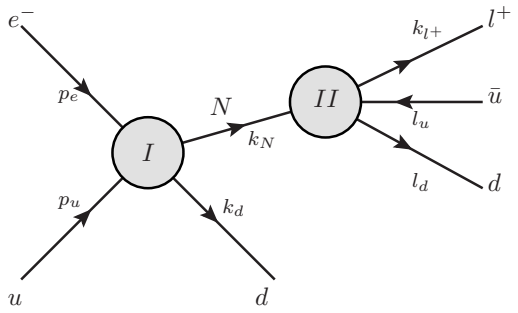

Figure 5.1: Diagrams contributing to the production of Majorana neutrinos in ep colliders.

We calculate the cross-section for the production of the Majorana neutrino according to the processes shown in fig.5.1. I write here only the lagrangian terms contributing to

[2] These are the ones depicted in fig.3.1, contributing to $0\nu\beta\beta$-decay.

the studied process, which come from the lagrangian terms in (3.11) and (3.12)

$$\mathcal{L}_{eff}^{tree} = \frac{1}{\Lambda^2}\left\{-\frac{m_W v}{\sqrt{2}}\alpha_W^{(i)}\, W^{\dagger\,\mu}\,\overline{N}_R\gamma_\mu e_{R,i} + \alpha_{V_0}^{(i)}\bar{d}_{R,i}\gamma^\mu u_{R,i}\overline{N}_R\gamma_\mu e_{R,i} + \right.$$
$$\left.\alpha_{S_1}^{(i)}\bar{d}_{L,i}u_{R,i}\overline{N}e_{L,i} - \alpha_{S_2}^{(i)}\bar{e}_{L,i}N_R\bar{u}_{L,i}d_{R,i} + \alpha_{S_3}^{(i)}\bar{u}_{L,i}N_R\bar{e}_{L,i}d_{R,i}\right\} + ... + h.c. \quad (5.1)$$

Taking the center of mass energy $\sqrt{s} = \sqrt{4E_eE_p}$, $\hat{\sigma}$ to be the parton level scattering cross-section, and with x the usual deep inelastic scaling variable, defined respectively as in secs. B.2.1 and B.2.3, we obtain the cross-section

$$\sigma(ep \to l^+ + 3jets) = \sum_i \int_{m_N^2/s}^1 dx f_i(x)\hat{\sigma}_i(xs) \quad (5.2)$$

where $i = 1$ corresponds to the channel $eu \to Nd$ and $i = 2$ to the crossed channel $e\bar{d} \to N\bar{u}$ obtained by the crossing symmetry. The function $f_1(x)$ represents the $u(x)$ parton distribution function[3] (PDF), $f_2(x)$ the one for $\bar{d}(x)$ and the parton level cross-section is

$$\hat{\sigma}_i(xs) = \int (2\pi)^4\delta^{(4)}(p_e + p_u - \sum_{j=1,4} k_j)\overline{|M_{(i)}|^2}\prod_{j=1,4}\frac{d^4k_j}{2\pi^3}\ . \quad (5.3)$$

The squared scattering amplitudes in the *narrow width approximation* (reviewed in sec.A.1.2) are:

$$\overline{|M_{(i)}|}^2 = \left(\frac{\pi}{4m_N\Gamma_N\hat{s}}\right)\delta(k_N^2 - m_N^2)|\Lambda_{(I),i}|^2(|\Lambda_{(II)}^{(+)}|^2 + |\Lambda_{II}^{(-)}|^2) \quad (5.4)$$

where

$$\begin{aligned}
|\Lambda_{(I),1}|^2 &= \frac{4}{\Lambda^2}\left[4(\alpha_{S_2}(\alpha_{S_2} - \alpha_{S_3}) + \alpha_{S_1}^2)(k_d\cdot p_u)(k_N\cdot p_e) + \right.\\
&\quad (4\alpha_W^2|\Pi_W^{(2)}|^2 + \alpha_{S_3}(\alpha_{S_3} - \alpha_{S_2}))(k_d\cdot p_e)(k_N\cdot p_u)\\
&\quad \left.+(\alpha_{S_3}\alpha_{S_2} + 4\alpha_{V_0}^2)(k_d\cdot k_N)(p_e\cdot p_u)\right]\\
|\Lambda_{(II)}^{(-)}|^2 &= \frac{16}{\Lambda^4}\left[|\Pi_W^{(2)}|^2\alpha_W^2(k_N\cdot l_u)(k_{l^+}\cdot l_d) + \alpha_{V_0}^2(k_N\cdot l_d)(k_{l^+}\cdot l_u)\right]\\
|\Lambda_{(II)}^{(+)}|^2 &= \frac{4}{\Lambda^4}\left[(\alpha_{S_1}^2 + \alpha_{S_2}^2 - \alpha_{S_2}\alpha_{S_3})(l_u\cdot l_d)(k_{l^+}\cdot k_N) + \right.\\
&\quad \left.(\alpha_{S_3}^2 - \alpha_{S_2}\alpha_{S_3})(k_{l^+}\cdot l_d)(l_u\cdot k_N) + \alpha_{S_2}\alpha_{S_3}(l_u\cdot k_{l^+})(l_d\cdot k_N)\right] \quad (5.5)
\end{aligned}$$

with $\Pi_W^{(1)} = m_W^2/(-2(p_u\cdot k_d) - m_W^2)$, $\Pi_W^{(2)} = m_W^2/(2(l_u\cdot l_d) - m_W^2)$. The final leptons can be either of e^+, μ^+ or τ^+ since this is allowed by the interaction lagrangian (5.1).

[3] A plot of the x-dependence of the proton PDFs can be found in fig. B.1.

All these possible final states are clear signals for intermediary Majorana neutrinos, thus we sum the cross-section over the flavors of the final leptons.

The total width (Γ_N) for the Majorana neutrino decay we used for the numerical results in this work is the one calculated in [155], only taking into account the fermionic decays shown in sec.4.2.2, which are dominant in the Majorana neutrino mass region considered.

5.3. Numerical Results

For the numerical study we assume an LHC-like beam of protons with an energy of 7 TeV, while examining two choices for the electron beam. We consider a low energy scenario with an electron beam of $E_e = 50\ GeV$ (Scenario 1), and other high energy scenario with $E_e = 150\ GeV$ (Scenario 2). For each experimental setup we assume a baseline integrated luminosity[4] of $L = 100\ \text{fb}^{-1}$ which is close to the values discussed for the LHeC proposal [157].

The branching ratios, cross sections and discovery regions for the Majorana neutrino in the effective lagrangian approach considered in this chapter depend on the quotient of the coupling constants $\alpha_{\mathcal{J}}^{(i)}$, associated with the operators in (5.1), and the new physics scale Λ squared i.e. $\kappa_{\mathcal{J}}^{(i)} = \alpha_{\mathcal{J}}^{(i)}/\Lambda^2$, in addition to the Majorana neutrino mass m_N. The considered operators are bounded by LEP and low energy data and we have also taken into account the bounds on the operators which come from the $0\nu_{\beta\beta}$-decay.

We start this section discussing the SM backgrounds, the LEP, low-energy data and $0\nu_{\beta\beta}$-decay bounds, before showing our results for the scattering cross-section for the process $e^- p \to l_j^+ + 3jets$, the different distributions and cuts implemented, and the Majorana neutrino discovery regions for both considered scenarios.

Standard Model background

The considered signal, being a lepton number violating process, is strictly forbidden in the SM, assuming that baryon number is also preserved, as we already discussed in sec.1.4.4. In fact, the SM background will always involve additional light neutrinos that escape the detectors and generate missing energy. This fact makes the signal very clean and difficult to mimic by SM processes.

As was pointed out in [160], the dominant background comes from W production, with its subsequent decay into charged leptons l^+ (e^+, μ^+, τ^+). In particular, the process $e^- p \to e^- l^+ jjj\nu$ is not distinguished from the signal if the outgoing electron is lost in the beamline. This process is dominated by the exchange of an almost real photon with a very collinear outgoing electron ($p\gamma \to l^+ jjj\nu$). This last process, convoluted with the parton distribution function ($p_{\gamma/e}$) representing the probability of finding a photon inside an electron, is found to be the major contribution to W production. The simulation of

[4]The instantaneous luminosity is the number of particles passing each other per unit time through unit transverse area at the interaction point. The reaction rate, i.e. the number of scattering events per unit time is directly proportional to the luminosity: $R(s) = \sigma(s)L$.

the background processes was done using the program CalcHep [162]. In section 5.3.1 we discuss different cuts that can be made in the phase space to increase the sensitivity and improve the signal to background relation.

Effective couplings bounds

The heavy Majorana neutrino couples to the three flavor families with couplings $\kappa_{\mathcal{J}}^{(i)} = \alpha_{\mathcal{J}}^{(i)}/\Lambda^2$.

From the electroweak precision tests bounds discussed in sec.3.4, considering the most stringent bound in [13] and for a generic new physics scale Λ we have

$$\kappa_{EWPD}^{bound} = \alpha_{EWPD}^{bound}/\Lambda^2 \leq 0.32/\Lambda^2. \tag{5.6}$$

By the time this work was published, the neutrinoless double beta decay bounds were still constrained by the results from the GERDA Collaboration [121], giving:

$$\kappa_{0\nu\beta\beta} = \frac{\alpha_{0\nu\beta\beta}}{\Lambda^2} \leq 7.8 \times 10^{-8} \left(\frac{m_N}{100GeV}\right)^{1/2} \; TeV^{-2}, \tag{5.7}$$

so this numerical value is the one used in defining our benchmark effective coupling sets, as I explain in the following.

Signal Cross section

We have already discussed in the previous section that some of the operators that contribute to the $0\nu_{\beta\beta}$-decay may be strongly constrained. Therefore, for studying the Majorana neutrino production cross-section in ep colliders and the following decay $N \to l^+ + 2jets$ we analyze two situations: in **Set I** we consider the case where the effective couplings for the operators that do not contribute to neutrinoless decay take all the same value $\alpha = 1$. In **Set II** we consider all those effective couplings to be equal and limited by the neutrinoless double beta decay bound (5.7).

In fig.5.2a we show the results for the cross-section, as a function of the Majorana neutrino mass m_N, for the considered electron beam energies: $E_e = 50\ GeV$ (Scenario 1) and $E_e = 150\ GeV$ (Scenario 2) for both Sets **I** and **II**. We have considered $\sqrt{s} < \Lambda$ in order to ensure the validity of the effective lagrangian approach. We display here the results for $\Lambda = 2500\ GeV$.

The phase space integration of the squared amplitude is made generating the final momenta with the Monte Carlo routine RAMBO [143]. This allows us to make the distributions and necessary cuts in the phase space to study the possibility of discovering Majorana neutrino effects.

5.3.1. Distributions and Kinematical Cuts

The dominant backgrounds for the studied process have been analyzed in [160]. In particular they conclude that a cut that could be effective to separate signal and background is to reject events where the outgoing l^+ does not have a minimum transverse

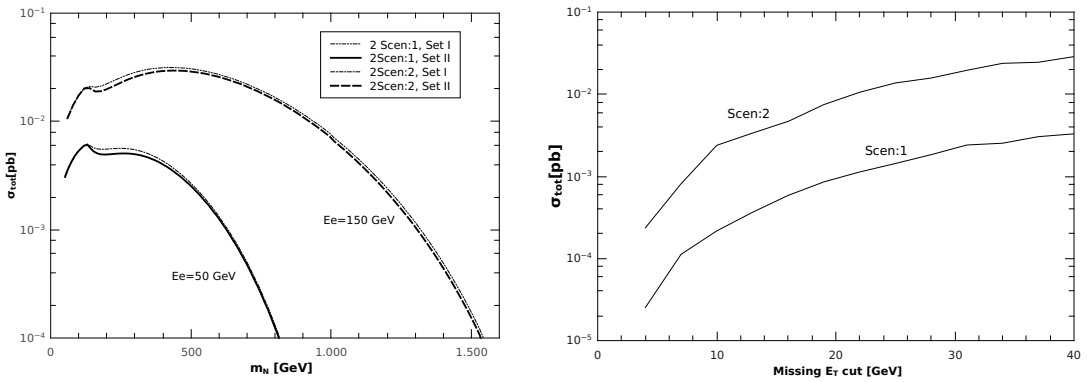

(a) Signal cross-section. (b) Background E_T dependence.

Figure 5.2: Cross section for the process $ep \to NX$ with N decaying according to Ref. [155] (a) and Background dependence with missing E_T (b).

momentum[5]. On the other hand, as the signal only includes visible particles and the background includes at least one neutrino, another possible cut is imposing an upper bound on the missing transverse energy. We follow this approach and implement the mentioned cuts. In fig.5.2b we show the behavior of the background with the maximum missing energy E_T for the scenarios where $E_e = 50\ GeV$ (Scenario 1) and $E_e = 150$GeV (Scenario 2). A cut of $E_{T,max} \leq 10\ GeV$, which is a reasonable value for the detector resolution, has not appreciable effects on the signal but significantly reduces the background.

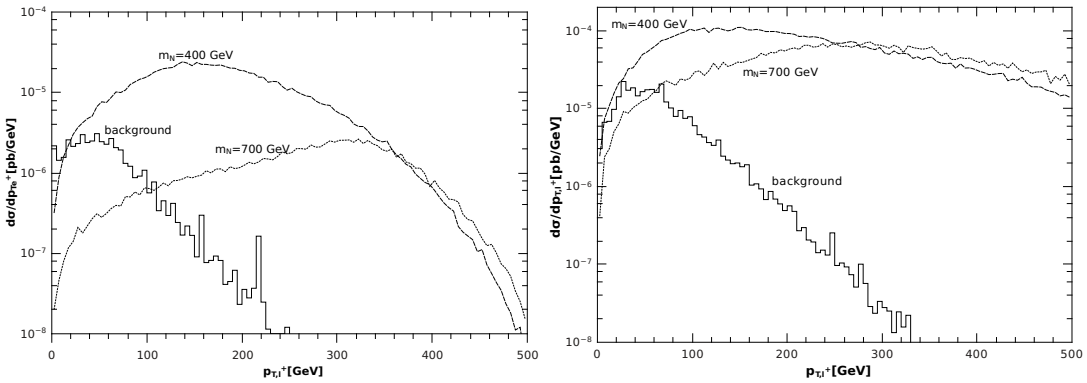

(a) Scenario 1 (b) Scenario 2

Figure 5.3: Differential cross-section of signal and background in function of transverse momentum p_{T,l^+}. The cut in missing E_T is included.

[5]The transverse momentum p_T is defined in (B.6), and missing transverse momentum and energy in (B.9).

In fig.5.3 we show the differential cross-section for the background and the signal for different values of the Majorana mass as a function of the transverse momentum p_{T,l^+} of the anti-lepton. In this figures the cut on the missing energy E_T has already been included. As it can be appreciated, the background is mostly concentrated at low values of p_{T,l^+}, and a cut imposed on p^{min}_{T,l^+} could be effective to improve the signal/background relation.

Finally, in fig.5.4 we show a plot comparing the magnitude of the signal for different values of the Majorana neutrino mass (solid lines), and the background for different $E_{T,max}$ cuts (dashed lines), depending on the p^{min}_{T,l^+} cut imposed. In both figures the arrows indicate the value of the cuts used in the analysis: we impose $p_{T,l^+} \geq 90\ GeV$ and $E_{T,miss} \leq 10\ GeV$ in order to reduce the background without appreciably decreasing the signal.

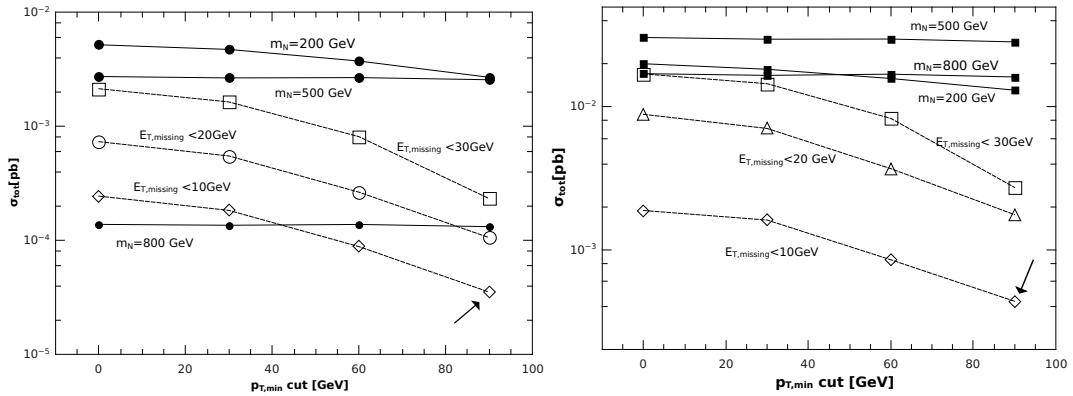

(a) Scenario 1 (b) Scenario 2

Figure 5.4: Comparison between signal and background for different Majorana neutrino masses, cut in missing E_T and the transversal momentum of the final lepton p_{T,l^+}. The solid lines show the cross section for the signal, and the dotted lines, for the background. The arrows indicate the cuts and backgrounds used in the analysis.

5.3.2. Discovery Regions

In order to investigate the possibility of detection of Majorana neutrinos in the process under consideration, we study the region (discovery region) where the signal can be separated from the background with a statistical significance higher than 5σ. We use the method of the *effective significance* described in [163,164]. There they show that the effective significance is well approximated by

$$\mathcal{S} = 2(\sqrt{n_s + n_b} - \sqrt{n_b}) - k(\alpha) \tag{5.8}$$

with k(α)=1.28 for $\alpha = 0.1$ where $1 - \alpha$ is the probability of measuring a number of events bigger than a value n_0, such that the probability (β) that the Standard Model

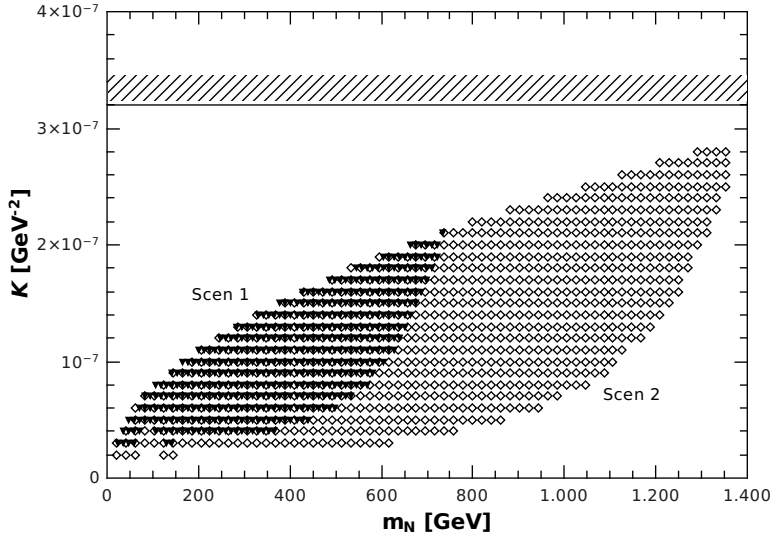

Figure 5.5: Majorana neutrino discovery regions at $5\,\sigma$ in the κ, m_N plane. The horizontal line represents the low-energy and LEP limits discussed in sec. 5.3.

reproduces such number is rather small, $\beta < 3 \times 10^{-7}$ for $\mathcal{S} > 5$ (5σ-test). In (5.8) $n_s = L\sigma_s$ and $n_b = L\sigma_b$ are the number of events for signal and backgrounds, being L the luminosity.

In fig.5.5 we show the discovery regions for different values of the Majorana neutrino mass m_N, and the quotient $\kappa_{\mathcal{J}}^{(i)} = \alpha_{\mathcal{J}}^{(i)}/\Lambda^2$. As we explained in sec.5.3, we consider the case in which all the $0\nu\beta\beta$ contributing coupling constants $\alpha_{\mathcal{J}}^{(i)}$ (generically α) are non-zero and equal, so that $\kappa \leq \kappa_{0\nu\beta\beta}$ in (5.7). The figure shows that Majorana neutrinos of masses up to near 700 GeV for Scenario 1 and 1300 GeV for Scenario 2 may be detected.

The maximum allowed value for the Majorana neutrino mass corresponds to the intersection between the $0\nu\beta\beta$ bound (5.7) and the contour of level five for the surface $\mathcal{S}$ (5.8), this is: $\mathcal{S}(m_N, \Lambda) = 5$. The last equation can be written as $\alpha_{0\nu\beta\beta}/\Lambda^2 \approx f(m_N)$ where f is a function of m_N and the collider energy, but independent of Λ. Thus, the intersection and then the maximum possible value for m_N is almost independent of the new physics scale Λ[6].

Systematic uncertainties are hard to estimate without a detailed reconstruction of the detector, but they are expected to be around a few percent [165]. However, the influence of the background systematic uncertainties in the result is small, because the background itself is small. In the case of the signal we have calculated the modifications for the discovery region if the number of events for the signal is changed by $\pm 30\%$. The results are shown in fig.5.6, showing no appreciable change in the region.

[6] Provided thet the signal is larger than the background.

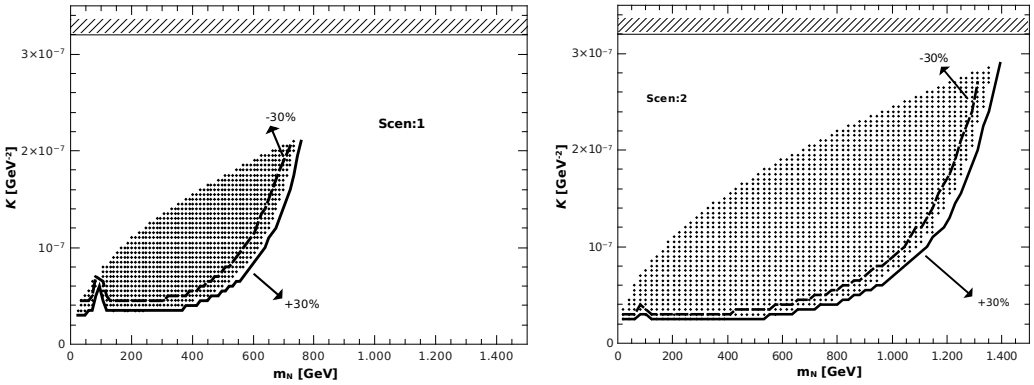

(a) Scenario 1 (b) Scenario 2

Figure 5.6: Sensitivity of the discovery regions to a $\pm 30\%$ change in the number of signal events.

5.4. Summary and perspectives

In order to investigate the possibilities for discovering Majorana neutrinos in an $e^- p$ collider at CERN (LHeC), we have calculated the cross-section for the lepton number violating process $e^- p \to l_j^+ + 3jets$ in an effective lagrangian approach, complementing previous analyses for this facility involving typical seesaw scenarios.

While models like the minimal seesaw mechanism lead to the decoupling of the heavy Majorana neutrinos, predicting unobservable LNV, the effective lagrangian framework considered in this work parameterizes the new physics effects in a model independent way, enabling the occurrence of sizable LNV signals for effective couplings $\alpha_{\mathcal{J}}^{(i)}$ of order one.

We have calculated the total unpolarized cross-section $\sigma(e^- p \to l_j^+ + 3jets)$ for different values of m_N, the effective couplings $\alpha_{\mathcal{J}}^{(i)}$ and the new physics scale Λ, and implemented cuts in the phase space that can help to enhance the signal to background relation. We obtained the Majorana neutrino discovery regions at 5σ statistical significance, combining the effect of the SM backgrounds with the most restrictive $0\nu_{\beta\beta}$-decay bounds for the effective couplings.

Our analysis shows that the LHeC facility could discover Majorana neutrinos with masses lower than 700 GeV and 1300 GeV with a 7 TeV proton beam, and electron beams of $E_e = 50$ GeV and $E_e = 150$ GeV respectively. Thus, we find lepton-proton colliders could provide a new probe of the Majorana nature of neutrinos, shedding light on this fundamental unsolved issue in particle physics.

I now move on to introduce our study of the possible Majorana neutrino phenomenology in the CERN Large Hadron Collider (LHC).

Chapter 6

Not-that-heavy Majorana neutrino signals at the LHC

In this chapter I present our work on the LHC phenomenology for the effective lagrangian approach introduced in chapter 3. This chapter is based in the preprint [5], currently under revision.

We consider the possibility of Majorana neutrinos production at the Large Hadron Collider (LHC) by studying the $pp \to l_i^+ l_j^+ + 2\ jets$ ($l_j \equiv e, \mu$) process which, due to leptonic number violation, is a clear signature for intermediate Majorana neutrino contributions, as we studied in chapter 2. Majorana neutrinos with masses of a few GeV are long-lived neutral particles. Following the ideas in sec.4.4 we take advantage of its measurable decay length: in the same-sign dilepton channel (ss-dilepton), we exploit this fact imposing cuts that help in rejecting the SM background, and analyze the distribution corresponding to the angle between the final leptons in the lab frame, using a forward-backward-like asymmetry to study the effects of the different gauge invariant operators. We also study the $pp \to l_i^+ \nu\gamma$ process, which is dominant for low m_N masses if tensorial one-loop generated new physics contributions are present. This channel could be observed at the LHC with the aid of non-pointing photons observables and cuts on the displacement between the prompt lepton and the photon.

6.1. Introduction

The inquiry on the Majorana nature of neutrinos has led to dedicated searches for evidence of lepton number violation (LNV) at hadron colliders in the very well known same-sign dilepton channel $pp \to l_i^+ l_j^+ + 2\ jets$ [15, 17, 21, 23, 106, 119, 166–173], and recently including new production mechanisms [174–176]. Also, the chances to discover heavy Majorana neutrinos in e^+e^-, e^-p, $e^-\gamma$ and $\gamma\gamma$ colliders have been studied [4, 16, 19, 95, 153–155, 159, 160, 177]. Searches for heavy Majorana neutrinos in the ss-dilepton channel are currently being performed at the LHC [178–182].

The effective model we are working with [15] has been tested in the LHC [181, 182] for Majorana neutrino masses above 100 GeV in events with high transverse momentum

objects including two reconstructed leptons and jets, for $\sqrt{s} = 7\ TeV$. The data are found to be in agreement with the expected SM background, leading to limits in the effective couplings and new physics scale for some selected operators. If this kind of sterile neutrino exists for $m_N < m_W$, the produced jets in the final state $l_i^+ l_j^+ + 2\ jets$ may not pass the cuts required to reduce backgrounds, as pointed out, for example, in [183].

Indeed, for masses m_N around a few GeV the Majorana neutrino we are considering behaves as a long-lived neutral particle, with a measurable decay length, as we showed in fig.4.12. This gives us a new means for probing the effective new physics at this lower mass scale, taking advantage of displaced vertices techniques. Recent works use displaced vertices for studying heavy sterile neutrinos in the LHC [124,127,130,172,184] and future colliders [129, 185].

In our previous work [2] presented in chapter 4, we found that for $m_N \lesssim 30\ GeV$ the dominant neutrino plus photon $N \to \nu\gamma$ decay channel is given by the contribution of effective tensorial operators generated at one-loop in the unknown underlying ultraviolet theory. As this channel cannot shed light on the Majorana or Dirac nature of heavy neutrinos, we first tackle the LNV same-sign dilepton signals for low Majorana neutrino masses neglecting the contribution of the one-loop generated operators. This enables us to test the capability to discern between the different gauge invariant operators contribution to the $pp \to l_i^+ l_j^+ + 2\ jets$ process, using a forward-backward like asymmetry, and imposing displaced-vertices cuts that reject the SM background.

In spite of not being a LNV signal, a study of the dominant neutrino plus photon decay channel is included in this chapter, motivated by the finding that long-lived neutral radiatively decaying particles like the Majorana neutrino N could explain the MiniBooNE [138, 139] and SHALON [140] anomalies [2], following sterile neutrino explanations for these experimental puzzles [141] as we saw in sec 4.4. The radiative $N \to \nu\gamma$ channel can be observed by the signature of an isolated electromagnetic cluster together with missing transverse energy, where the photon originates in a displaced vertex[1]. New physics searches involving displaced photons and missing transverse energy have been performed at the LHC [123, 151], mainly dedicated to SUSY searches, and searches with the same final state: lepton, photon and missing E_T [186].

Again, as I mentioned in chapter 5, the basic concepts on particle detection and kinematical variables for hadron colliders are introduced and discussed in the appendix B, and the reader is referred there for many definitions not included in the text.

6.2. Effective model

In this chapter we study the well known same-sign dilepton Majorana neutrino signal $pp \to l_i^+ l_j^+ jj$ schematically depicted in fig.6.2, and the new $pp \to l_i^+ \nu\gamma$ neutrino plus photon channel shown in fig.6.7. The relevant effective lagrangian terms contributing to the studied processes are discussed in the following.

[1] Hence the name non-pointing photon.

For the production vertex I in figs.6.2 and 6.7, and the decay vertex II in fig.6.2, we have tree-level generated contributions from the effective lagrangian coming from the operators in (3.7), related to the spontaneous symmetry breaking process, and four-fermion contributions from the operators in (3.8):

$$\mathcal{L}_{eff}^{tree} = \frac{1}{\Lambda^2}\left\{-\frac{m_W v}{\sqrt{2}}\alpha_W^{(i)}\, W^{\dagger\,\mu}\,\overline{N}_R\gamma_\mu e_{R,i} + \alpha_{V_0}^{(i)}\bar{d}_{R,i}\gamma^\mu u_{R,i}\overline{N}_R\gamma_\mu e_{R,i} + \right.$$
$$\left.\alpha_{S_1}^{(i)}\bar{d}_{L,i}u_{R,i}\overline{N}e_{L,i} - \alpha_{S_2}^{(i)}\bar{e}_{L,i}N_R\bar{u}_{L,i}d_{R,i} + \alpha_{S_3}^{(i)}\bar{u}_{L,i}N_R\bar{e}_{L,i}d_{R,i}\right\} + ... + h.c. \quad (6.1)$$

where the sum over the families i is understood and the constants $\alpha_{\mathcal{J}}^{(i)}$ are associated to specific operators according to sec.3.3.

For the $N \to \nu\gamma$ decay vertex II in fig.6.7 the considered lagrangian terms are generated by one-loop level tensorial operators in (3.18):

$$\mathcal{L}_{eff}^{1-loop} = \frac{-i\sqrt{2}v}{\Lambda^2}(\alpha_{L_1}^{(i)}c_W + \alpha_{L_3}^{(i)}s_W)(P_\mu^{(A)}\ \bar{\nu}_{L,i}\sigma^{\mu\nu}N_R\ A_\nu) + ... + h.c. \quad (6.2)$$

where $-P^{(A)}$ is the four-momentum of the outgoing photon and a sum over the family index i is understood again. The coupling constants $\alpha_{L_{1,3}}^{(i)}$ are associated to the specific operators:

$$\alpha_{L_1}^{(i)} = \alpha_{NB}^{(i)},\ \ \alpha_{L_3}^{(i)} = \alpha_{NW}^{(i)}.$$

The effective operators can be classified by their structure into *scalar*, *vectorial* and *tensorial*. The scalar and vectorial operators contributing to the studied processes are those appearing in (6.1) with couplings named $\alpha_{S_{1,\ 2,\ 3}}$ and $\alpha_{W,\ V_0}$ respectively. They play a role in the production and decay vertices for the $pp \to l_i^+ l_j^+ + 2\ jets$ process, and only in the production vertex for the $l_i^+\nu\gamma$ channel. The one-loop tensorial operators in (6.2) drive the $N \to \nu\gamma$ decay[2].

6.2.1. Effective coupling bounds summary

As I introduced in sec.3.4, in order to put reliable bounds for the effective couplings, we take into account existing experimental constraints on sterile-active neutrino mixings, relating the U_{lN} mixings in Type-I seesaw models with our effective couplings by the relation (3.21)

$$U_{lN}^2 \simeq \left(\frac{\alpha v^2}{2\Lambda^2}\right)^2. \quad (6.3)$$

For the couplings involving the first fermion family the most stringent are the $0\nu\beta\beta$-decay bounds obtained by the KamLAND-Zen Collaboration [112] which give us an upper limit $\alpha_{0\nu\beta\beta}^{bound} \leq 3.2\times 10^{-2}\left(\frac{m_N}{100\ GeV}\right)^{1/2}$ for $\Lambda = 1\ TeV$.

[2]Equations (6.1) and (6.2) show explicitly only the lagrangian terms contributing to the studied processes.

Concerning the second fermion family, for sterile neutrino masses $2\ GeV \lesssim m_N \lesssim 10\ GeV$ the upper limits come from the DELPHI Collaboration [97] leading to the value $\alpha^{bound}_{DELPHI} \lesssim 2.3$. In the lower mass region the kinematic searches we commented in sec. 2.6.3 also give competitive constraints. The Belle [110] and LHCb [111] Collaborations find upper bounds in the $2\ GeV \lesssim m_N \lesssim 5\ GeV$ region. However, it must be taken into account that these results depend heavily on the considered decay modes for the sterile N [187–191]. The bound from Belle is still the most stringent, giving a value $\alpha^{bound}_{Belle} \lesssim 0.3$.

For higher masses in the range $m_W \lesssim m_N$ the upper limits come from electroweak precision data (EWPD) and radiative lepton flavor violating (LFV) decays as $\mu \to e\gamma$ [13,93,98,104] giving a bound $\alpha^{bound}_{EWPD} \leq 0.32$.

In order to simplify the discussion, for the numerical evaluation we only consider the most stringent bounds, taking the couplings associated to the operators that contribute to the $0\nu\beta\beta$-decay for the first family as restricted by the corresponding bound $\alpha^{bound}_{0\nu\beta\beta}$, and the other constants are restricted to the value $\alpha^{bound} \leq 0.3$. For the 1-loop generated operators we consider the coupling constant as $1/(16\pi^2)$ times the corresponding tree-level coupling: $\alpha^{1-loop} = \alpha^{tree}/(16\pi^2)$. Thus, for example, for the operator $\mathcal{O}_{NW}$, which contributes to $0\nu\beta\beta$-decay we have

$$\alpha^{(1)}_{L_3} = \frac{1}{16\pi^2}\alpha^{bound}_{0\nu\beta\beta}.$$

6.2.2. Low m_N kinematic features

As we mentioned in the introduction, Majorana neutrinos with masses of a few GeV are found to be long-lived neutral particles that could be searched for in the LHC with displaced vertices techniques. In this chapter we exploit this long decay length in order to search for the production of Majorana neutrinos.

In higher m_N regions the same-sign dilepton (l^+l^+jj) signal has been thoroughly studied in colliders and, as we mentioned in the introduction, this signal has been studied in the effective framework we consider here [15], and searched for in the LHC [181,182] for m_N above $100\ GeV$. Up to now, all LHC searches for heavy Majorana neutrinos [178–182] in these final states are performed without considering the possibility of a sufficiently long heavy neutrino lifetime making the decay vertex to be displaced from the production point.

The decay length of the Majorana neutrino, and its flight direction in the lab frame can be determined as:

$$\vec{l}_N = \frac{\vec{k}_N}{|\vec{k}_N|}\tau_N \ \beta_N = \frac{\vec{k}_N}{|\vec{k}_N|}\frac{\left((E_N/m_N)^2 - 1\right)^{1/2}}{\Gamma_N}. \tag{6.4}$$

Here k_N is the N momentum, τ_N is its lifetime, and β_N is the N speed in units of the speed of light. $E_N^2 = |\vec{k}_N|^2 + m_N^2$ and Γ_N is the N decay width.

In order to make a preliminary survey we study the same-sign dileptons plus jets and the lepton and neutrino plus photon channels making a parton level Monte Carlo

simulation with the RAMBO [143] routine. The effective new physics energy scale Λ in (3.4) is taken to be $\Lambda = 1\ TeV$ and the c.m. energy of the hard processes $\sqrt{s} \leq \Lambda$ to insure the validity of the effective lagrangian approach. The numerical values for the effective couplings are taken as explained in sec.6.2.1. In this work we only consider Majorana neutrinos with masses $m_N \lesssim 10\ GeV$ because these are the values leading to an N decay length -and thus a vertex displacement- measurable in the LHC. This was shown in chapter 4. In figure 4.12b we found that the decay length of the Majorana neutrinos, for energies $E_N \leq 5\ GeV$, lies in the detectable range $(10^{-3} - 1)\ m$ in the LHC for masses[3] $m_N \lesssim 10\ GeV$.

The measurable decay length of the few-GeV mass Majorana neutrino will be exploited by considering two distinct observables: for the ss-dilepton signal, we find that the vertex displacement can be measured by obtaining the distance between the traces (in the detector lab frame) of both outgoing leptons, a prompt one coming from the N production vertex, and the other originated in the decay vertex. For the neutrino plus photon channel, we consider the distance between the prompt outgoing lepton and the displaced photon traces, and also the non-pointing photon observables defined in recent new physics searches in ATLAS [123, 151].

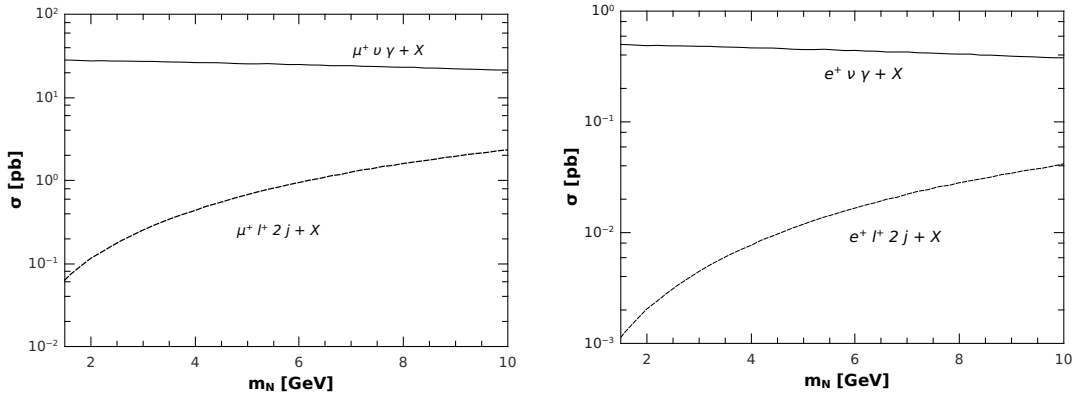

(a) Anti-muon channel.

(b) Positron channel.

Figure 6.1: Total cross sections for the $pp \to l^+\nu\gamma + X$ and $pp \to l^+l^+ + 2\ j + X$ processes.

In the effective framework we are working with, the dominant decay channel in the few-GeV m_N mass region is the $N \to \nu\gamma$ channel. Considering on shell N production, the cross-section for the ss-dilepton process can be written in the narrow width approximation as the product of the production cross-section by the decay channel branching ratio: $\sigma(pp \to lljj) \simeq \sigma(u\bar{d} \to lN)Br(N \to ljj)$. Taking into account non-zero values for the

[3]for the couplings set **A** which is the one corresponding to the numerical values considered in this work.

scalar, vectorial and tensorial couplings, the cross sections for the l^+l^+jj and the $l^+\nu\gamma$ final states are shown in fig.6.1, for the final prompt anti-muon (a) and positron (b) channels, respectively.

The radiative N-decay channel completely dominates the low mass region and is driven by tensorial one-loop operators. Then, for the study of the LNV same-sign dileptons plus jets signal, we fix the one-loop generated couplings to zero $\alpha^{1-loop} = 0$. This allows us to focus our interest in distinguishing the effects of the vectorial and scalar operators on the signal, as it is not sensitive to the tensorial operators effect.

In fig.6.1 one can also appreciate the diminishing effect of the $\alpha^{bound}_{0\nu\beta\beta}$ value on the $l^+ = e^+$ channel: the cross-section for the second family $l^+ = \mu^+$ is appreciably higher, due to the more relaxed bound α^{bound}_{Belle}.

6.3. Same sign dilepton signal

For calculating the scattering cross-section of the $pp \to l^+N \to l^+l^+jj$ process, we consider the hard scattering of quark partons inside the colliding protons in the LHC beams. The hard scattering of protons is studied in detail in the appendix B. There it is argued that due to the dependence of the parton distribution functions of valence quarks inside the proton on the scaling momentum fraction x shown in fig. B.1, one can consider, in a first approximation, the parton hard scatterings we take into account in the diagrams in fig.6.2.

Thus, using the effective lagrangian in (6.1), we calculate the cross-section for the production of the Majorana neutrino for the $u\bar{d}$ hard process.

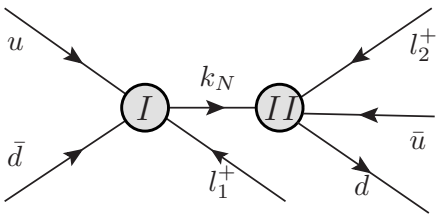

Figure 6.2: Diagrams contributing to the process $pp \to l^+l^+jj$.

Considering that the leading contribution to the process takes place when the Majorana neutrino is produced as a resonance, we can treat it in the narrow width approximation studied in sec. A.1.2. Then the corresponding amplitude for the process can be

written as the product of the production and decay amplitudes (see (A.12)):

$$\begin{aligned}\mathcal{M} \quad &= \frac{-im_N}{\Lambda^4} P_N(k_N^2)\Big\{\Pi_W(q_2^2)\alpha_W^{(i)}\,\bar{u}(l_u)\gamma_\nu P_R v(l_d)\bar{u}(l_2)\gamma^\nu + \alpha_{V_0}^{(i)}\,\bar{u}(l_u)\gamma_\nu P_L v(l_d)\bar{u}(l_2)\gamma^\nu \\ &+\alpha_{S_1}^{(i)}\,\bar{u}(l_u)P_R v(l_d)\bar{u}(l_2) - \alpha_{S_2}^{(i)}\,\bar{u}(l_u)P_L v(l_d)\bar{u}(l_2) + \alpha_{S_3}^{(i)}\,\bar{u}(l_2)P_L v(l_d)\bar{u}(l_u)\Big\} \\ &\times\Big\{-\Pi_W(q_1^2)\alpha_W^{(i)}\,\gamma_\mu P_R v(l_1)\bar{v}(p_d)\gamma^\mu P_L u(p_u) + \alpha_{V_0}^{(i)}\,\gamma_\mu P_R v(l_1)\bar{(}p_d)\gamma^\mu P_R u(p_u) \\ &+\alpha_{S_1}^{(i)}\,P_L v(l_1)\bar{v}(p_d)P_R u(p_u) - \alpha_{S_2}^{(i)}\,P_L v(l_1)\bar{v}(p_d)P_L u(p_u) \\ &+\alpha_{S_3}^{(i)}\,P_L u(p_u)\bar{v}(p_d)P_L v(k_1)\Big\}, \end{aligned} \tag{6.5}$$

where l_1 and l_2 are the four-momenta of the final leptons, p_u and p_d are the four-momenta of the initial quarks and, l_u and l_d stand for the four-momenta of the final quarks. The W propagator is encoded in Π_W:

$$\Pi_W(q^2) = \frac{m_W^2}{q^2 - m_W^2}, \quad q_1 = p_u + p_d, \quad q_2 = l_u + l_d, \tag{6.6}$$

and k_N is the four-momentum of the intermediate Majorana neutrino, and its propagator contribution is written as in (A.12):

$$P_N(k_N^2) = \frac{1}{(k_N^2 - m_N^2)^2 + (m_N\Gamma_N)^2}. \tag{6.7}$$

Taking the center of mass energy $\sqrt{s} = 14$ TeV, $\hat{\sigma}$ and $\hat{s}$ to be the parton level scattering cross-section and squared center of mass energy, and x_1 and x_2 the scaling fractions for the initial partons u and $\bar{d}$ respectively, we obtain

$$\sigma(pp \to l^+l^+ + 2jets) = \int_{x_m}^1 \int_{x_m/x_1}^1 dx_1 dx_2 (f_u(x_1) f_{\bar{d}}(x_2) + f_u(x_2) f_{\bar{d}}(x_1))\hat{\sigma}_i(x_1 x_2 s) \tag{6.8}$$

where the minimum value for x_1 and x_2 is $x_m = m_N^2/s$ and the function $f_q(x)$ represents the $q(x)$ parton distribution function (PDF), as in sec.B.2.1. The parton level scattering cross-section is written as usually[4]:

$$\hat{\sigma}_i(\hat{s} = x_1 x_2 s) = \int \frac{\overline{|\mathcal{M}|^2}}{2\hat{s}} d\Phi_4, \tag{6.9}$$

with $\mathcal{M}$ in (6.5), the four particle phase-space in (A.1) and m_p the proton mass.

In view of the discussion given in the introduction, we study the few-GeV m_N region for the ss-dilepton signal taking into account the separate effects of the scalar and vectorial operators, neglecting the tensorial operators contribution. To see the effects from the scalar operators we set the coupling constants corresponding to the vector operators

[4]The definition is given in (B.2).

α_W and α_{V_0} equal to zero. Similarly, to study the contribution from the class of vector operators we set the couplings α_{S_1}, α_{S_2} and α_{S_3} equal to zero. Throughout this section we present our numerical results summing over the final leptons possibilities ($l_1^+ l_2^+ = e\mu$, μe, ee, $\mu\mu$).

As the considered signal is a LNV process, it is strictly forbidden in the SM, and the background always involves additional light neutrinos in the final state that escape the detectors as missing energy. The SM backgrounds have been extensively discussed in the literature [23, 106, 119, 173], and in recent experimental searches [178, 179].

The background for these searches can be classified into prompt leptons, charge-flip opposite-sign dileptons and misidentified leptons. The first are SM events resulting in two genuine same-sign leptons. These include the following processes. Diboson production (WZ, ZZ) giving ss-dileptons when both Z and W decay leptonically and one lepton from Z decay cannot be isolated or is missed out of the detector coverage. Also, $t\bar{t}$-plus boson ($t\bar{t}W$, $t\bar{t}W$, $t\bar{t}Z$) processes contributing to the signal when the tops decay hadronically and the bosons decay leptonically. Triboson ($W^\pm W^\pm W^\mp$) and double W-sstrahlung ($WWjj$) as well as double parton scattering ($qq' \to W$). The charge-flip events originate in opposite-sign dileptons signals in which an electron undergoes bremsstrahlung in the tracker volume and the associated photon converts into a e^+e^- pair. Here the opposite sign electron can be misidentified as the primary electron if it carries a large fraction of the original electron's energy. This effect is negligible for muons. The last group includes objects misidentified as prompt leptons, originated in B-hadrons decays[5], light quark or gluon jets and photon conversions, and mainly $t\bar{t}$ in which a top quark yields a prompt isolated lepton ($t \to Wb \to l\nu b$) and the other same charge lepton arises from b quark decay or a jet misidentified as an isolated prompt lepton. This is the dominant background for the $m_N < m_W$ region [106, 178] and it cannot be easily eliminated in the few-GeV m_N region, as the cuts imposed on the final leptons p_T in order to reject those coming from b decays can also affect the signal. Distributions on the invariant mass of the $l_2^+ jj$ system $M(l_2^+ jj) \sim m_N$ could help to distinguish the signal from backgrounds [171, 183].

Taking into account the vertex displacement could help to reduce the background, and this is why we study this very interesting feature for the low mass region. Recent LHC searches exploiting the long-lived particles displaced vertex feature in final states with charged leptons and jets [125, 192–194] originally intended for SUSY particles [195] are currently being used for studying models with right handed massive neutrinos [130].

We calculate the distance between the traces of the charged leptons, which, almost always, is different from zero since the vertices are displaced. A sketch in fig. 6.3a shows the $L^{l^+l^+}$ distance definition.

In our parton level Monte Carlo numerical simulation the distance between the straight line containing the flight direction of the prompt lepton produced in the primary vertex and the one for the displaced secondary lepton can be found as the length of the segment orthogonal to and crossing both traces: $\hat{n}_{l_1^+}$ and $\hat{n}_{l_2^+}$ in fig.6.3a. This line

[5] The B-hadrons are those containing b quarks.

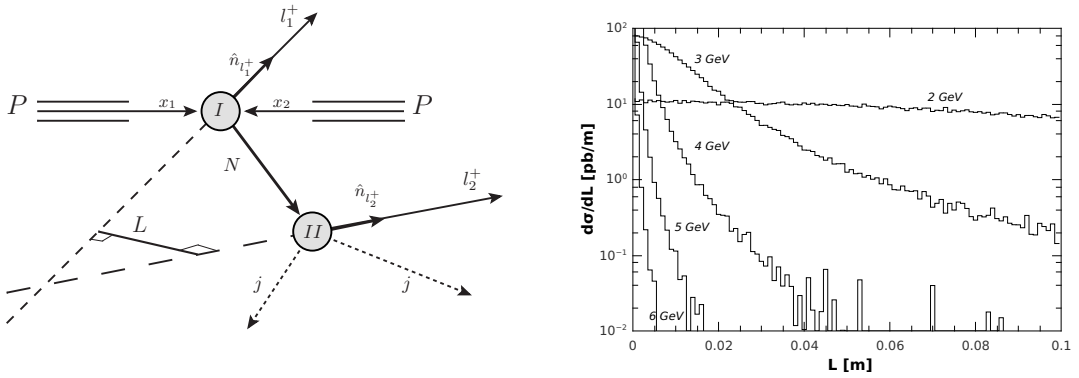

(a) Schematic representation of the distance $L^{l^+l^+}$ between the final leptons directions

(b) Differential $L^{l^+l^+}$ distribution for different m_N values. Scalar and vectorial operators are included.

Figure 6.3: $L^{l^+l^+}$ definition and differential distribution.

has the direction of the unit vector $\hat{n} = \hat{n}_{l_1^+} \times \hat{n}_{l_2^+} / |\hat{n}_{l_1^+} \times \hat{n}_{l_2^+}|$ and the distance $L^{l^+l^+}$ can be calculated as $L^{l^+l^+} = \hat{n} \cdot \vec{l}_N$, with the definition given in (6.4).

The distribution of the signal distances between the lepton's fly directions is shown in fig.6.3b for various few-GeV m_N masses. In order to reject the prompt ss-dilepton background, we set this cut up to $L^{l^+l^+} = 1\ mm$, which is approximately the precision of the detector, discarding events for which the distance between the traces of the final leptons is less than 1 mm. In this way, we conveniently eliminate the background, since the distance between the traces would be zero if this final state (up to additional non-detectable neutrinos) comes from standard interactions. In fig.6.4 we show the scalar and

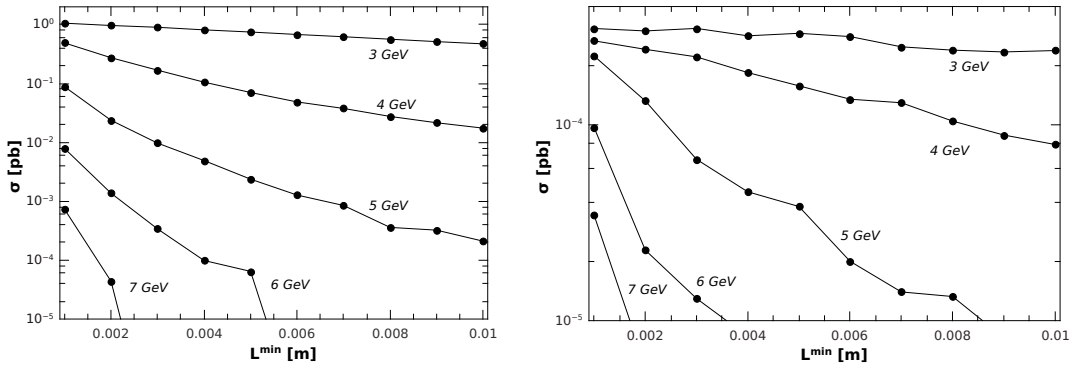

(a) Vectorial

(b) Scalar

Figure 6.4: Contribution of the vectorial and scalar operators to the cross-section for different m_N values as a function of the cut in $L^{l^+l^+}_{min}$.

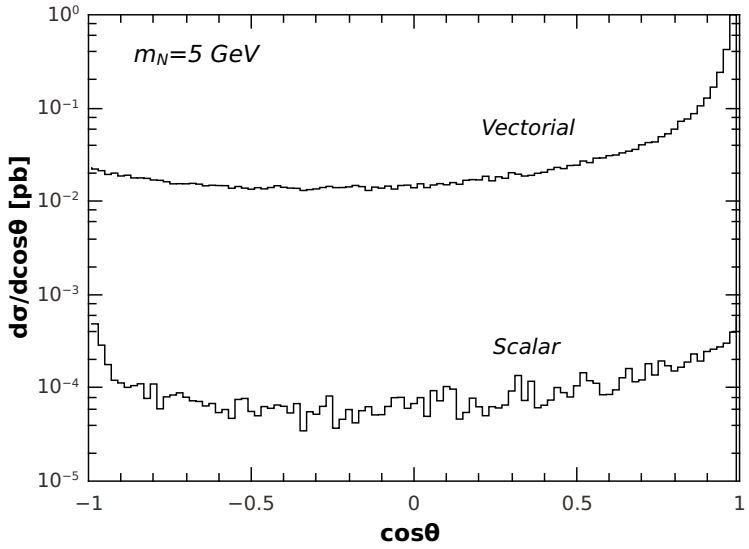

Figure 6.5: Angular distribution of the final leptons for $m_N = 5$ GeV and for the contribution of the vectorial and scalars operators.

vectorial operators contribution to the ss-dilepton cross-section, for different m_N values, as a function of the cut in the minimal displacement distance $L_{min}^{l^+l^+}$.

Once the displacement between the Majorana production and decay vertices is used to reduce the background in the few-GeV m_N region, we are interested in testing the separated contributions of the vectorial and scalar operators to the process, in order to obtain information about the new physics behind these effects.

Using the angular distribution $d\sigma/d\cos\theta$ where θ is the angle between the outgoing leptons tracks in the lab frame, we construct a forward-backward-like asymmetry $A_{FB}^{l^+l^+}$ as a function of the number of events in each hemisphere:

$$A_{FB}^{l^+l^+} = \frac{N_+ - N_-}{N_+ + N_-} \tag{6.10}$$

where N_+ is the number of events $0 \leq \theta \leq \pi/2$ and N_- is the number of events with $\pi/2 \leq \theta \leq \pi$. This asymmetry does not require the prompt lepton assignment needed for calculating the usual A_{FB} for the underlying production process $pp \to l^+N$, also avoiding the identical colliding beams problem [15].

As can be seen in fig.6.5, where we show the angular distribution for a mass of $m_N = 5\ GeV$, the contributions from both the scalar and vector operators lead to an unbalance. In order to estimate the chances of disentangling the contributions corresponding to the scalar and vector classes of operators, we study the angular asymmetry $A_{FB}^{l^+l^+}$, taking

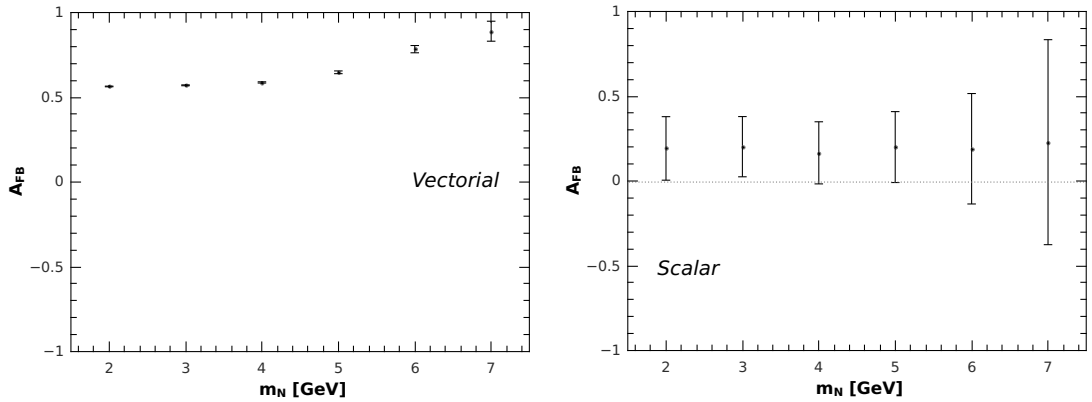

(a) Contribution of the Vectorial Operators. (b) Contribution of the Scalar Operators.

Figure 6.6: Asymmetry in the angular distribution between the final leptons, with the errors estimates as defined in the text.

into account the error

$$\Delta A_{FB}^{l^+l^+} = \sqrt{\left(\frac{\partial A_{FB}^{l^+l^+}}{\partial N_+}\right)^2 (\Delta N_+)^2 + \left(\frac{\partial A_{FB}^{l^+l^+}}{\partial N_-}\right)^2 (\Delta N_-)^2}. \tag{6.11}$$

Assuming the number of events to be Poisson distributed, we write

$$\Delta N_+ = \sqrt{N_+} \text{ and } \Delta N_- = \sqrt{N_-}$$

and a straightforward calculation leads to

$$\Delta A_{FB}^{l^+l^+} = \sqrt{\frac{1-(A_{FB}^{l^+l^+})^2}{N_+ + N_-}}. \tag{6.12}$$

The results for the $A_{FB}^{l^+l^+}$ observable for the vectorial and scalar operators cases are shown in figs.6.6a and 6.6b. We find that for the scalar set of operators the asymmetry is compatible with zero, but the vectorial set shows a clear effect, different from zero, by several standard deviations. All the figures include the $L_{min}^{l^+l^+} > 1\ mm$ cut.

6.4. Prompt lepton and displaced photon plus missing $\mathbf{E_T}$ signal

As we found in chapter 4, the $N \to \nu\gamma$ decay channel dominates the low m_N region and is driven by one-loop generated tensorial operators. If one includes these in the N decay width calculation, this decay mode would overshadow the ss-dilepton signal. So in

the case that new physics involving tensorial modes is present, in this section we explore the chances to observe the $pp \to l^+\nu\gamma$ process in the LHC.

The cross-section for the production and decay of the heavy Majorana neutrino hard process we study can be written as:

$$\hat{\sigma}_{u\bar{d}\to l^+\nu\gamma}(\hat{s}) = \int \frac{1}{2\hat{s}} \overline{|\mathcal{M}|}^2 d\Phi_3$$

Here the squared scattering amplitude in the narrow width approximation is

$$\overline{|\mathcal{M}|}^2 = \frac{\pi}{2\Gamma_N m_N} \delta(k_N^2 - m_N^2) |\mathcal{M}^I|^2 |\mathcal{M}^{II}|^2$$

with the amplitude for the production vertex I in fig.6.7 being

$$\begin{aligned} |\mathcal{M}^I|^2 &= \frac{4}{\Lambda^4}\Big[(l_1.k_N)(p_d.p_u)[\alpha_{S_1}^{(i)2} + \alpha_{S_2}^{(i)}(\alpha_{S_2}^{(i)} - \alpha_{S_3}^{(i)})] \\ &\quad +(l_1.p_u)(p_d.k_N)[\alpha_{S_2}^{(i)}\alpha_{S_3}^{(i)} + 4\alpha_{V_0}^{(i)2}] \\ &\quad +(l_1.p_d)(p_u.k_N)[\alpha_{S_3}^{(i)}(\alpha_{S_3}^{(i)} - \alpha_{S_2}^{(i)}) + 4\alpha_W^{(i)2}|\Pi_W|^2]\Big] \end{aligned} \tag{6.13}$$

(i is the family index for the final charged anti-lepton l_1^+) and the amplitude for the decay vertex II being

$$|\mathcal{M}^{II}|^2 = \frac{16v^2}{\Lambda^4}\Big[(k.p)^2(\alpha_{L_1}^{(j)}c_W + \alpha_{L_3}^{(j)}s_W)^2\Big] \tag{6.14}$$

where $j = 1, 2$ is the family index for the final neutrino.

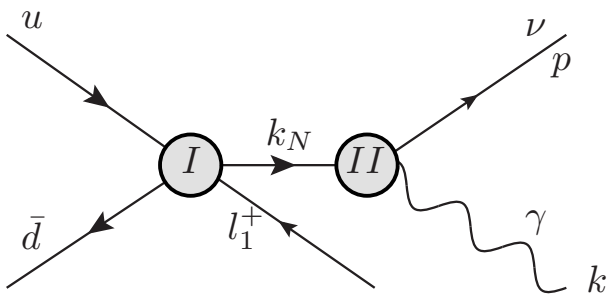

Figure 6.7: Schematic momenta in Eqs.(6.13) and (6.14).

The background for the $l^+\nu\gamma$ final state has been studied in SUSY searches in events with a photon, a lepton and missing transverse momentum at the LHC [186] for high momentum regions and considering signals where all final particles are produced promptly. It is classified as misidentified photons or leptons and SM-electroweak background. The first arises when electrons or jets are misidentified as photons and comes from events

where a photon converts into an e^+e^- pair and an electron fails to register track seeds due to detector inefficiencies, or a jet is misidentified as a photon when a large fraction of its energy is carried by mesons decaying into photons. Misidentified leptons are reconstructed leptons not arising from W or Z boson decays, and come primarily from heavy-flavor quark decays and hadrons misidentified as leptons. The SM-electroweak background is dominated by $Z, W-\gamma$ events that have the same signature as the signal events: a photon, a lepton and missing transverse energy (E_T^{miss}) from neutrinos. In the case of the dominant SM-electroweak background, leptons arise mostly from $W \to \nu l$ decays, and the E_T^{miss} peaks nearly at $m_W/2$. In our case, for few-GeV m_N this background could be reduced imposing a cut on the $\nu-\gamma$ system transverse mass $M_T \lesssim m_N$ as defined in [186]. Also, the invariant mass[6] of the $e\gamma$ system can be required to be different from the nominal Z boson mass, to reduce the background in the $l^+ = e^+$ channel.

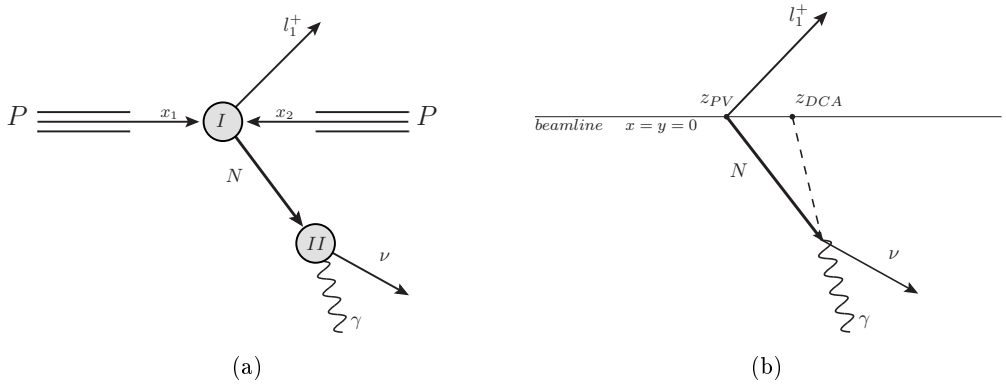

Figure 6.8: Schematic representation of the $pp \to l^+\nu\gamma$ process and the z_{DCA} observable.

For our signal, the smoking gun for the production and flight of the N is its decay length, that leads to a finite separation between the primary and secondary vertex. We are mostly interested in exploiting this distinctive displaced vertex feature, in this case measuring the distance between the prompt lepton track and the displaced photon flight direction, in order to reduce the backgrounds in the low m_N region.

In the LHC, observables using non-pointing photons have been defined and new physics searches were performed involving photons originating from a displaced vertex due to the decay of a long-lived particle into a photon and an invisible particle. This non-pointing photons and E_T^{miss} final state searches [123,151] are oriented to the discovery of long-lived SUSY particles, but as it is the case for this work, they could also serve to the purpose of discovering heavy Majorana neutrinos as well. The analysis technique developed exploits the capabilities of the ATLAS electromagnetic calorimeter to make precise measurements of the flight direction of photons. This direction can be determined by measuring precisely the lateral and the longitudinal positions of the photon-originated

[6] The invariant and transverse mass variables are defined in the appendix sec.B.2.3.

shower in the front and middle layers of the EM calorimeter. The variable used as a measure of the degree of non-pointing of the photon is called z_{DCA}, the difference between the z coordinate of the photon extrapolated back to its distance of closest approach (DCA) to the beamline (i.e. $x = y = 0$) and z_{PV}, the z coordinate of the primary vertex [196], as can be seen in fig.6.8.

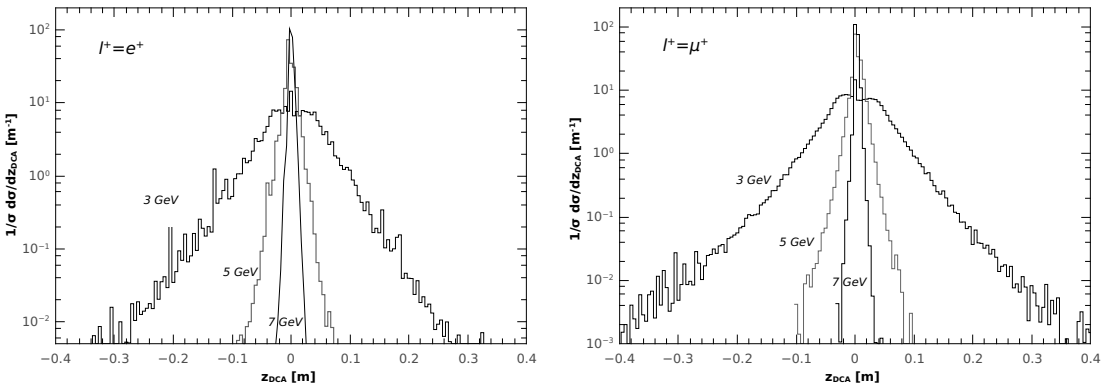

(a) (b)

Figure 6.9: z_{DCA} distribution for the $l^+\nu\gamma$ channel, for different m_N values.

The distance of closest approach of the displaced photon can be calculated using the decay length of the Majorana neutrino defined in (6.4). Taking $z_{PV} = 0$, in fig.6.9 we plot the normalized differential cross-section as a function of the distance of closest approach z_{DCA} for the $l^+ = e^+, \mu^+$ channels.

We find our signal leads to z_{DCA} values comparable to those measured in ATLAS [123, 151] (for a very different studied signal consisting of a diphoton final state) and could be searched for, with the aid of other m_N-dependent mentioned cuts suitable for our signal's final state.

Indeed, as suggested in sec.6.3, cuts on the displacement distance $L^{l^+\gamma}$ between the prompt lepton and the displaced photon traces could also be implemented, helping to reduce the backgrounds. In fig.6.10 we show the normalized differential cross-section of the signal for the $l^+ = e^+, \mu^+$ channels as a function of the displacement distance $L^{l^+\gamma}$ defined equivalently as in sec.6.3, for different Majorana neutrino masses.

We find that a cut $L^{l^+\gamma} > 10mm$ would not seriously affect our signal in both flavor charged lepton channels, for m_N up to 5 GeV.

6.5. Final remarks and perspectives

In this chapter we studied the effects of a heavy sterile Majorana neutrino in the processes $pp \to l_i^+ l_j^+ jj$ and $pp \to l_i^+ \nu\gamma$ in the LHC, modeling the N interactions with the standard particles by the effective lagrangian studied in chapter 3. As the effective model we consider has already been tested in the LNV ss-dilepton signal for Majorana

masses over a hundred GeV, and in fact the model predicts that a low mass N behaves as a long-lived neutral particle with a detectable decay length, in this chapter we focus on the complementary study of the ss-dilepton channel for low m_N, using displaced vertices observables to diminish the backgrounds. As for a few-GeV m_N masses the dominant decay channel for the N is $N \to \nu\gamma$, driven by tensorial one-loop generated operators, for the study of the ss-dilepton signal we assume the new physics does not involve tensorial contributions, and study the differences between the vectorial and scalar operators using a forward-backward-like asymmetry in the angle between the outgoing leptons. Making a statistical analysis we find the contributions from the two operators groups could be distinguished, and the vectorial operators give an asymmetry clearly distinct from zero. Including all the operator's contributions we study the dominant low m_N regime $pp \to l_i^+ \nu\gamma$ process, finding the signal distribution in the non-pointing photon observable z_{DCA} could allow for the discovery of the signal in the LHC, with the aid of cuts in the displacement between the prompt lepton and the outgoing photon to reject the backgrounds.

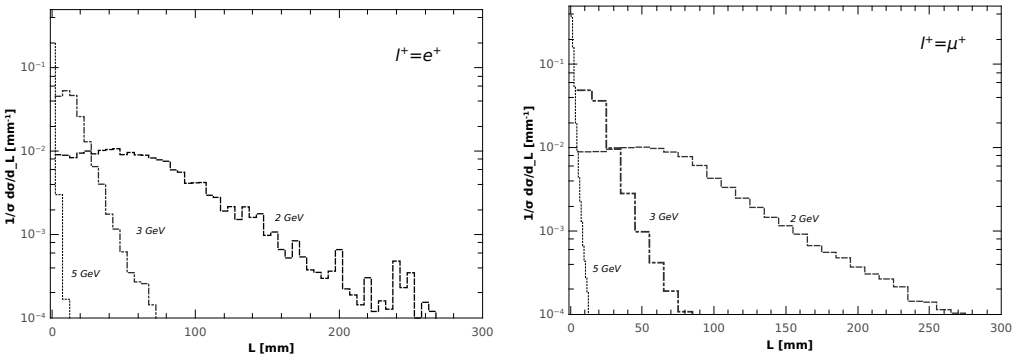

(a) (b)

Figure 6.10: $L^{l^+\gamma}$ differential distribution for the $l^+\nu\gamma$ channel, for different m_N values.

Our findings suggest to deepen this preliminary parton level study in order to accurately model the signals and backgrounds in the LHC with Monte Carlo simulations including hadronization and detector simulation techniques. The not-that-heavy Majorana neutrinos could be discovered at the LHC in the case the triggers and analyses for Run II dedicated searches keep reconstruction thresholds sufficiently low to efficiently tag displaced vertices form signal processes.

Chapter 7

Effects of Majorana Physics on the UHE ν_τ Flux Traversing the Earth

Neutrino astrophysics is the newest frontier in the field, and neutrino telescopes will map out the sky in the following years, probing further back in time and deeper into the ultra high energy astrophysical neutrino sources. In this chapter I present a study on the phenomenology of the effective Majorana neutrino model we are working with in connection to neutrino astrophysics, searching for the possibility to detect its effects in the IceCube neutrino telescope: a huge array in the south pole, covering 1 km^3 of ice with photomultipliers that detect the Cherenkov radiation of charged particles produced by incoming high energy neutrinos. A brief introduction on the IceCube experiment, its detection principles, the relevant observables, and the incident neutrino fluxes on the Earth can be found in the appendix C.

In this chapter we study the effects produced by sterile Majorana neutrinos on the ν_τ flux traversing the Earth, considering the interaction between the Majorana neutrinos and the standard matter as modeled by the effective lagrangian introduced in chapter 3. The surviving tau-neutrino flux is calculated using transport equations that take into account the Majorana neutrino production and decay. We compare our results with the pure SM interactions, computing the surviving flux for different values of the effective lagrangian couplings, considering the detected flux by IceCube for an operation time of ten years, and Majorana neutrinos with mass m_N near the tau lepton mass m_τ. This chapter is based on the paper [6].

7.1. Introduction

The discovery of neutrino flavor oscillations still remains as one of the most compelling evidence for physics beyond the SM. While many proposals have been posed to explain the tiny ordinary neutrino masses, the seesaw mechanism stays as one of the most straightforward ideas for solving the neutrino mass problem, as we saw in chapter 2. This mechanism introduces right-handed sterile neutrinos that can have a Majorana mass term leading to the tiny known masses for the standard neutrinos, as long as the

Yukawa couplings between the right-handed Majorana neutrinos and the standard ones remain small, and this fact leads to the decoupling of the Majorana neutrinos, due to a negligible left-right neutrino mixing U_{lN}. Thus, as suggested in [15], the detection of Majorana neutrinos (N) would be a signal of physics beyond the minimal seesaw mechanism, and its interactions could be better described in a model-independent approach based on an effective theory, considering a scenario with only one Majorana neutrino N and negligible mixing with the ν_L, as we introduced in chapter 3.

On the other hand, in the recent years the observation of ultra high energy (UHE) astrophysical neutrinos in the IceCube telescope [197], with a yet unknown specific origin, energy spectral shape and flavor composition, as well as the non-finding of tau-neutrinos in still primary searches performed within these data [198], raise the question on tau-neutrino detection in neutrino telescopes.

Moreover -as we introduced in chapter 4- anomalies found in short baseline (SBL) neutrino oscillation experiments like LSND and MiniBoone [138,139,147,199] have driven the introduction of light, almost sterile neutrinos which mix poorly with the known light mass states and could help to accommodate the oscillation data introducing a third mass splitting. The IceCube Collaboration has searched for these sterile neutrinos [200] probing light sterile neutrino $3+1$ models [201,202] and recently led to new bounds for the sterile-active muon-neutrino mixing.

As the mixing parameters for the second fermion family with a sterile Majorana neutrino $\nu_\mu - \nu_s$ are strongly constrained within the framework of $3+1$ scenarios [93,203], and motivated by the lack of tau-neutrinos in the UHE cosmic flux in IceCube, in this chapter we study the possibilities that UHE tau-neutrinos from astrophysical sources may provide a signature for Majorana neutrino production by giving a surviving flux after traversing the Earth which may differ from the standard one. In particular the non-observation of ν_τ going up signal could be a manifestation of a sterile neutrino modifying the ν_τ flux.

We study the possibility that the existence of Majorana neutrinos coupled to the tau-neutrinos modifies their interactions with nucleons in matter, and thus change the surviving ν_τ flux after traversing the Earth. We have studied the bounds on the effective Majorana neutrino coupling strengths obtained from different experimental data, and we find these couplings can have appreciable effects on the ν_τ flux attenuation at high energies. This fact may have an impact on the detection of astrophysical ν_τ flux. IceCube has recently analyzed high energy neutrino events [204, 205], and found, although with large uncertainty, consistency with equal fractions of all flavors, but without including a specific tau-neutrino identification algorithm. If ν_τ events are finally found, due to the increase of detection time augmenting the statistics, then the data can be used to place bounds on the heavy Majorana neutrino effects we are showing in this chapter.

Many recent papers have studied the IceCube UHE astrophysical events with explanations involving dark matter models with right-handed neutrinos [206–209] and non-standard effective interactions [210], and also the chances to probe sterile- tau-neutrino mixings have been considered [211]. The effects of dark matter and new physics on ν_τ propagation has been studied by our research group in [212–214].

In sec.7.3.1 we discuss the relevant processes and the results obtained for the cross-sections and decay rates. In Sec.7.3.2, we review the passage of high energy tau-neutrinos through the Earth using transport equations including the effects of Majorana neutrinos. We solve these equations taking into account the neutral-current regeneration and the regeneration by the decay of the Majorana neutrino, for different values of ζ which, as we will define in the next section, is a combination of the effective couplings and the energy scale associated with the new interactions. This enables us to compare the surviving flux with the one obtained using SM physics only. In particular we go to a Majorana mass region where the effective couplings are less constrained, maximizing the effect on the survival flux. Finally, in sec.7.4 we present the results and in sec.7.5 a short discussion with our conclusions.

7.2. Effective model summary

In order to study the effects on the ν_τ propagation through the Earth due to the existence of Majorana neutrinos N, we consider the dominant processes responsible for the change in the ν, τ and N fluxes. Besides the SM processes involving ordinary neutrinos, we have new contributions related with the production and scattering of the Majorana neutrinos N interacting with matter nucleons ($\mathcal{N}$):

$$\nu\mathcal{N} \to NX, \qquad N\mathcal{N} \to lX, \qquad N\mathcal{N} \to \nu X, \qquad N\mathcal{N} \to NX. \tag{7.1}$$

As we studied in chapter 3, the effective lagrangian terms contributing to this processes are mainly four-fermion interactions in (3.12) and those mediated by W and Z exchange, combining the SM electroweak charged and neutral-current vertices in (1.56) and (1.61) with the SVB lagrangian terms

$$\mathcal{L}_{SVB}^{tree} = \frac{1}{\Lambda^2}\left\{\alpha_Z(\bar{N}_R\gamma^\mu N_R)\left(\frac{vm_Z}{2}Z_\mu\right) - \alpha_W^{(i)}(\bar{N}_R\gamma^\mu l_{R,i})\left(\frac{vm_W}{\sqrt{2}}W_\mu^+\right) + \cdots + h.c.\right\}.$$

In this chapter we make a change in our four-fermion effective couplings, allowing for family mixing, in order to probe the interactions between the Majorana neutrino N and first family quarks u, d in matter nuclei in the Earth, the tau lepton and tau-neutrinos and how their fluxes are modified. Thus, we allow for family mixing in the interactions involving two or more SM leptons, writing the corresponding effective couplings in (3.12) as $\alpha^{(i,j)}$, with the indices i, j representing the three different lepton families.

Also, we will take into account the Majorana neutrino decay contribution to the different fluxes. For the low Majorana neutrino mass region, the dominant decay was found to be $N \to \gamma\,\nu$, as we saw in chapter 4. For completeness we include in fig.7.1 a plot with the N branching ratios in the low mass region, where the numerical values for the coupling constants are those given in (7.16).

The shown reactions (7.1) contribute to the transport equations to be presented in sec.7.3, where the relative relevance of the different terms for the considered mass region will be discussed.

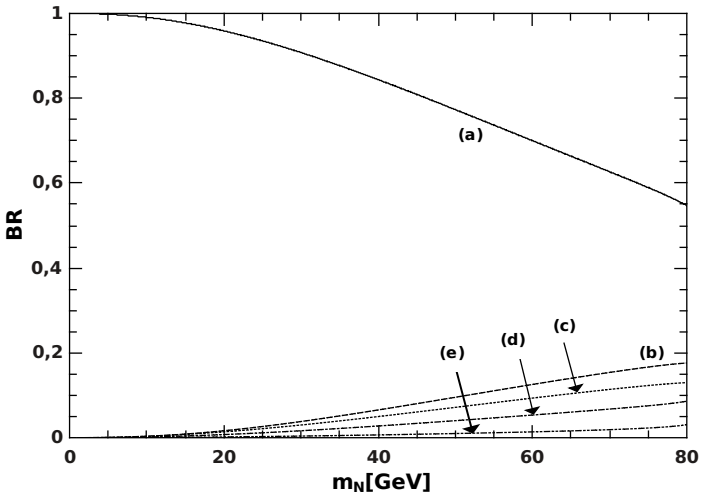

Figure 7.1: Branching ratios for the Majorana neutrino decay channels in the low mass region. The labels represent the decays (a) $N \to \nu_i\gamma$, (b) $N \to d\bar{d}\nu_i(\bar{\nu}_i)$, (c) $N \to u\bar{u}\nu_i(\bar{\nu}_i)$, (d) $N \to leptons$ and (e) $N \to u\bar{d}l_i$. Here we sum in families for $i = 1 - 3$.

Experimental bounds on the effective couplings

As we discussed in sec.3.4, the current experimental bounds on the U_{lN} mixings can be re-interpreted in terms of the effective couplings considering a particular combination of the couplings and the new physics scale Λ which we call $\zeta_{\mathcal{O}}$:

$$\zeta_{\mathcal{O}} = \left(\frac{\alpha_{\mathcal{O}} v^2}{2\Lambda^2}\right)^2 \tag{7.2}$$

where $v = 250$ GeV represents the Higgs field vacuum expectation value.

For our analysis in this chapter we will consider the three sets of operators called $\mathcal{O}_{SVB}$, $\mathcal{O}_{4-f}$, $\mathcal{O}_{1-loop}$, defined as the sets of couplings coming from operators in each set, as we introduced them in sec.3.3, and the existent bounds on their values. In this chapter we refine our treatment, calculating explicitly the contributions from different experiments to the values of the couplings in the three sets of effective operators. We found that for a Majorana neutrino with mass near the tau lepton mass value $m_N \sim m_\tau$ the bounds on the couplings allow for a sizable effect on the tau-neutrino surviving flux Φ_{ν_τ}, as we will show in the following.

The couplings ζ_{SVB} can be bounded taking into account LEP and τ lepton universality tests results. We consider the LEP bounds on single $Z \to \nu N$ and pair $Z \to N\ N$ sterile neutrino production searches [96]. Conservative limits for any m_N mass [96] are

$$Br(Z \to NN)Br^2(N \to \nu(\bar{\nu})\gamma) < 5 \times 10^{-5} \tag{7.3}$$

$$Br(Z \to \nu N)Br(N \to \nu(\bar{\nu})\gamma) < 2.7 \times 10^{-5}. \tag{7.4}$$

This results are model-independent and hold for the production of a single and a pair of neutral objects decaying into a photon and a light invisible particle. For the decay

Process / Coupling	ζ_{SVB}	ζ_{4-f}	ζ_{1-loop}
$Z \to NN$ †	$< 7.56 \times 10^{-4}$	-	-
$e^+e^- \to \nu N$ †	-	$< 2.85 \times 10^{-1}$	-
$e^+e^- \to NN$ †	-	$< 2.63 \times 10^{-1}$	-
$Z \to \nu N$ †	-	-	$< 6.75 \times 10^{-4}$

Table 7.1: Experimental bounds on the effective couplings.
†LEP Ref. [96].

$Z \to N\ N$ we have a direct contribution from the tree level operator $\mathcal{O}_{NN\phi}$, giving

$$\Gamma(Z \to NN) = \frac{1}{24\pi}\left(\frac{\alpha_Z v^2}{2\Lambda^2}\right)^2 \frac{m_Z^3}{v^2}. \tag{7.5}$$

For the low m_N values considered here, we can take $Br(N \to \nu(\bar{\nu})\gamma) \simeq 1$ and then the corresponding bound is

$$\zeta_Z < 7.56 \times 10^{-4}. \tag{7.6}$$

The process $Z \to \nu N$ has no contributions from the operators $\mathcal{O}_{SVB}$.

Another observable that can put restrictive bounds on the $\mathcal{O}_{SVB}$ is the universality test from the τ-decay, in the mass range $m_\mu \leq m_N \leq m_\tau$. Following [93] we define the quotient R_τ in the effective model as

$$\begin{aligned} R_\tau^{eff} &= \frac{\Gamma(\tau \to \nu_\tau(N) + e\bar{\nu}_e)}{\Gamma(\mu \to \nu_\mu + e\bar{\nu}_e)} = \frac{\Gamma(\tau \to \nu_\tau + e\bar{\nu}_e) + \Gamma(\tau \to N + e\bar{\nu}_e)}{\Gamma(\mu \to \nu_\mu + e\bar{\nu}_e)} \\ &= \left(\frac{m_\tau}{m_\mu}\right)^5 \left(\frac{g(y_\tau)}{g(y_\mu)} + \frac{h(y_N, \zeta_{S0}, \zeta_W)}{8g(y_\mu)}\right) \end{aligned} \tag{7.7}$$

The function $g(x) = 1 - 8x + 8x^3 - x^4 - 12x^2\ln(x)$ is the SM result for the $\tau \to \nu_\tau + e\nu_e$ and $\mu \to \nu_\mu + e\nu_e$ decays, with $y_\tau = (m_e/m_\tau)^2$ and $y_\mu = (m_e/m_\mu)^2$ respectively. The $\tau \to N + e\nu_e$ process receives $\mathcal{O}_{4-f}$ and $\mathcal{O}_{SVB}$ contributions, encoded in the function

$$\begin{aligned} h(y_N, \zeta_{S0}, \zeta_W) &= (1 - y_N^2)(9\zeta_{S0}(1 + y_N^2) + 12\ \zeta_{S0}(y_N - 1)^2 + 2\zeta_W(y_N^2 - 8y_N + 1)) \\ &\quad +12\ y_N\ \ln(y_N)(3\zeta_{S0} - 2\zeta_W) \end{aligned} \tag{7.8}$$

with $y_N = (m_N/m_\tau)^2$. The observed value for the quotient is $R_\tau^{obs} = (1.349 \pm 0.004) \times 10^6$ [93,107]. This imposes stringent bounds on both the SVB ζ_W and the four-fermion ζ_{S0} couplings, but if we take the mass of the sterile N to be right below m_τ, these bounds can be relaxed because the partial decay width is kinematically canceled.

We study now the case of the effective four-fermion interactions. Here we have again contributions to the LEP process $e^-e^+ \to \nu N$ and $e^-e^+ \to NN$ but in this case without the Z resonance, and then we expect weaker bounds than those imposed on the ζ_{SVB} couplings.

We consider first the reaction $e^+e^- \to \nu N$ calculated at the Z-pole

$$\sigma_{\nu N} = \frac{12\pi}{m_Z^2} Br(Z \to e^+e^-) Br(Z \to \nu N) \tag{7.9}$$

where $Br(Z \to e^+e^-) \simeq 3.4 \times 10^{-2}$ and the upper bound for the branching ratio for the channel $Z \to \nu N$ obtained from (7.4) is $Br(Z \to \nu N) \leq 2.7 \times 10^{-5}$ [96]. Thus, we have

$$\sigma_{\nu N} \lesssim 4.1 \times 10^{-9} GeV^{-2} \tag{7.10}$$

and, as the four-fermion contribution to the cross-section is

$$\sigma_{\nu N} = \left(\frac{\alpha_{S_0} v^2}{2\Lambda^2}\right)^2 \frac{m_Z^2}{48\pi v^4}$$

the bound for the corresponding coupling is $\zeta_{S0} \leqslant 2.85 \times 10^{-1}$.

On the other hand, we have the reaction $e^-e^+ \to NN$ with the bound obtained by LEP and shown in (7.3). Using the general expression for the cross-section at the Z-pole

$$\sigma_{NN} = \frac{12\pi}{m_Z^2} Br(Z \to e^+e^-) Br(Z \to NN)$$

and in the low mass limit where $Br(N \to \nu(\bar{\nu})\gamma) = 1$ we have

$$\sigma_{NN} \lesssim 8.2 \times 10^{-9}\ GeV^{-2}. \tag{7.11}$$

In the effective theory we are considering, the operators that contribute to the Majorana neutrino pair production are the four-fermion operators $\mathcal{O}_{LN}$, $\mathcal{O}_{eNN}$ and $\mathcal{O}_{LNN}$ and the corresponding cross sections are

$$\sigma^{NN} = \left(\frac{\alpha_{\mathcal{O}} v^2}{2\Lambda^2}\right)^2 \frac{m_Z^2}{b_{\mathcal{O}} \pi v^4}, \tag{7.12}$$

where $b_{eNN} = 24$, $b_{LNN} = 24$ and $b_{LN} = 96$. Thus, using (7.11) the most restrictive bound obtained is $\zeta_{4-f} \lesssim 2.63 \times 10^{-1}$.

In the case of one-loop operators we have contributions to the Z-decay $Z \to \nu N$

$$\Gamma(Z \to \nu N) = \left(\frac{\alpha^{1-loop} v^2}{2\Lambda^2}\right)^2 \frac{(c_W - s_W)^2}{6\pi} \frac{m_Z^3}{v^2} \tag{7.13}$$

and with the experimental bound for the Branching ratio [96]

$$Br(Z \to \nu N) = \frac{\Gamma(Z \to \nu N)}{\Gamma(Z \longrightarrow all)} \lesssim 2.7 \times 10^{-5} \tag{7.14}$$

we obtain $\Gamma(Z \to \nu N) \leq 6.7 \times 10^{-5}\ GeV$, and thus

$$\zeta_{1-loop} = \left(\frac{\alpha^{1-loop} v^2}{2\Lambda^2}\right)^2 \lesssim 6.75 \times 10^{-4}. \tag{7.15}$$

For the Lepton-Flavor-Violating processes e.g. $\mu \to e\gamma$, $\mu \to e^+e^-e$ and $\tau \to e^+e^-e$ induced by the quantum effect of the heavy neutrinos, we have very weak bounds for $m_N < m_W$ [13, 95]. As we already discussed in sec.4.3.2 and sec.6.2.1 there is a clear dominance of the neutrino plus photon decay channel. From fig.7.1 we can conclude that the beam-dump and rare LNV experiments bounds are inapplicable, beacuse this decay mode to invisible particles is not considered in those analyses and it can considerably alter the number of events found for N decays inside the detectors [93, 94].

The results on the bounds for the different sets of coupling constants $\zeta_{\mathcal{O}}$ are summarized in table 7.1. In consequence, for the Majorana neutrino mass around m_τ we can avoid the most stringent bounds, and we will consider for simplicity the following set of limits for the operators of the respective sets:

$$\begin{aligned} \zeta_{SVB} &\lesssim 7.6 \times 10^{-4} \\ \zeta_{4-fermion} &\lesssim 2.7 \times 10^{-1} \\ \zeta_{1-loop} &\lesssim 7.0 \times 10^{-4}. \end{aligned} \tag{7.16}$$

7.3. Neutrino propagation through the Earth

7.3.1. Relevant processes

In this section we study the different reactions taking place in the transport of tau-neutrinos in their journey through the Earth. We classify the produced effects as absorption and regeneration processes.

Absorption effects are all the processes that take out of the flux tau-neutrinos of energy E, and regeneration effects are those adding tau-neutrinos with energy E to the flux. We must consider that beside ordinary neutrinos we have Majorana neutrinos and tau-leptons produced by the former when they pass through the Earth.

The standard interactions of ordinary neutrinos with the nucleons $\mathcal{N}$ forming the Earth are $\nu_\tau \mathcal{N} \to l^\pm X$ and $\nu_\tau \mathcal{N} \to \nu_\tau X$. Here the charged-current and neutral-current reactions contribute to the absorption effects of ordinary tau-neutrinos and neutral-current reactions contribute to the regeneration effects as we will discuss in the next section.

The production of Majorana neutrinos is driven by the collision of ordinary neutrinos with nucleons in the Earth, $\nu_\tau \mathcal{N} \to NX$. This reaction absorbs ordinary tau-neutrinos producing Majorana neutrinos.

Next, we have to take into account the interaction of Majorana neutrinos with the nucleons forming the Earth, $N\mathcal{N} \to NX$, $N\mathcal{N} \to l^\pm X$ and $N\mathcal{N} \to \nu_\tau X$. In the same way as for the ordinary neutrinos, these reactions produce absorption effects of Majorana neutrinos, as well as regeneration effects for ordinary neutrinos and charged leptons.

Finally we have the Majorana neutrino dominant decay: $N \to \nu\ \gamma$ causing Majorana neutrino absorption and ordinary neutrino regeneration, and the standard τ-decay leading to τ absorption and ν_τ regeneration.

As we will discus in the next section, only some processes are relevant for the ν_τ propagation in the Earth. We do not show explicitly expressions for the different cross-sections because it is a standard calculation. We prefer to show the results as plots for the interaction and decay lengths for the SM scatterings $\nu_\tau \mathcal{N} \to lX$, $\nu_\tau \mathcal{N} \to \nu_\tau X$, the τ-decay, the Majorana production process $\nu_\tau \mathcal{N} \to NX$, and the N-decay, as they give the relevant contributions to the transport equations. In the case of Majorana interactions the dominant contribution is given by the four-fermion operators $\mathcal{O}_{4-f}$.

These lengths are defined in terms of the associated process cross-sections as:

$$\begin{aligned} L_{\rm int}^{\rm tot,SM}(E) &= \frac{1}{\langle\rho_n\rangle(\sigma^{\nu\mathcal{N}\to l^+X} + \sigma^{\nu\mathcal{N}\to\nu X})} \\ L_{\rm int}^{\rm Maj}(E) &= \frac{1}{\langle\rho_n\rangle\sigma^{\nu\mathcal{N}\to NX}} \\ L_{\rm decay}^{\tau-{\rm decay}}(E) &= \frac{1}{\langle\rho_n\rangle\Sigma_\tau} \\ L_{\rm decay}^{\rm N-decay}(E) &= \frac{1}{\langle\rho_n\rangle\Sigma_N}. \end{aligned} \tag{7.17}$$

Here $\langle\rho_n\rangle$ is the average number density of nucleons along the column depth on the path with inclination θ with respect to the nadir direction, as it will be shown in (7.32). The number density is defined as $\rho_n = N_A\rho$ where N_A is the Avogadro constant and ρ is the Earth mass density. The decay functions $\Sigma_{N\ (\tau)}$ are defined in (7.27).

In fig.7.2 we show the corresponding interaction and decay lengths, along the nadir direction, as a fraction of the Earth radius, when the couplings take the upper values shown in (7.17).

In order to take into account the contribution of the N decay to the regeneration through the $N \to \nu_\tau\gamma$ channel, we follow the approach of Gaisser [215], which is developed in the appendix sec.C.4. We also take into account the regeneration effects coming from the τ-decay according to expressions obtained by Gaisser [215] and also shown in [216]. In fig.7.2b we show for comparison the interaction length for the other interactions involved.

In the following section we will discuss the relative importance between the different contributions to the ν_τ propagation.

7.3.2. Surviving neutrino flux

The neutrinos traveling through the Earth may suffer charged-current (CC) and neutral-current (NC) interactions with the nucleons in their path (see [217, 218] and references therein). Neutrino oscillation within the Earth can be neglected for energies higher than 1 TeV [219][1].

As we mentioned above, the change in neutrino flux $\Phi_{\nu_\tau}(E,\chi)$ as it traverses the Earth can be divided into two effects: absorption and regeneration. In the SM we have the total cross-section $\sigma_{{\rm tot}\ \nu_\tau}^{\rm SM}(E) = \sigma_{\rm CC}(E) + \sigma_{\rm NC}(E)$, which represents a probability of

[1] This is because the oscillation length (2.7) is greater than the Earth's diameter for energies above this value.

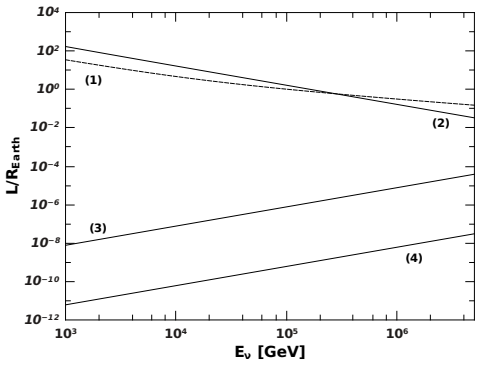

(a) Interaction lengths: (1) for the SM ν_τ scattering process ($L_{int}^{tot,SM}$), (2) for the Majorana production process $\nu_\tau \mathcal{N} \to NX$ relevant for the ν_τ absorption (L_{int}^{Maj}). Decay lengths: (3) for the lepton τ, $L_{decay}^{\tau-decay}$ and (4) for the Majorana neutrino N, $L_{decay}^{N-decay}$.

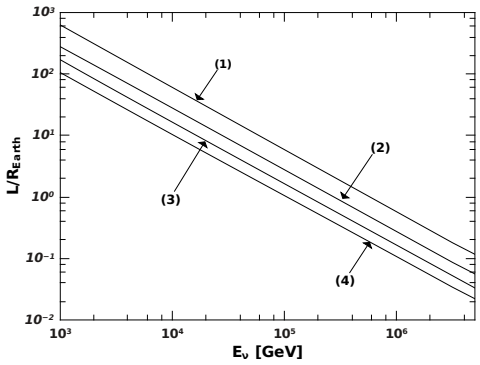

(b) Interaction lengths for different Majorana neutrino processes: (1) $N\mathcal{N} \to lX$, (2) $N\mathcal{N} \to \nu_\tau X$, (3) $\nu_\tau \mathcal{N} \to NX$ and (4) $N\mathcal{N} \to NX$.

Figure 7.2: Comparison between the interaction and decay lengths for different neutrino energies as a fraction of the Earth radius.

CC or NC standard tau-neutrino interactions. When neutrinos pass through an amount of matter $d\chi = \rho_n(z)dz$ in a distance dz along the neutrino beam path, where $\rho_n(z)$ is the Earth's number density, the change in the flux $\Phi_{\nu_\tau}(E,\chi)$ due only to absorption is proportional to $\Phi_{\nu_\tau}(E,\chi)$ and to the cross-section:

$$\frac{d\Phi_{\nu_\tau}(E,\chi)}{d\chi} = -\sigma^{\rm SM}_{{\rm tot}\ \nu_\tau}(E)\Phi_{\nu_\tau}(E,\chi). \tag{7.18}$$

Here $\chi(z)$ is the amount of material found up to a depth z, that is,

$$\chi(z) = \int_0^z dz' \rho_n(z'), \tag{7.19}$$

where the number density is the Avogadro constant times the density, $\rho_n(z') = N_A\rho(z')$.

In order to consider the complete transport effect for UHE neutrinos, we have to add to (7.18) the effect of regeneration, which accounts for the possibility that neutrinos of energies $E' > E$ may end up with energy E due to NC interactions with the nucleons, adding neutrinos to the flux of energy E. Then the SM transport equation for neutrinos reads

$$\frac{\partial\Phi_{\nu_\tau}(E,\chi)}{\partial\chi} = -\sigma^{\rm SM}_{{\rm tot}\ \nu_\tau}(E)\Phi_{\nu_\tau}(E,\chi) + \int_0^1 \frac{dy}{(1-y)}\Phi_{\nu_\tau}\left(E/(1-y),\chi\right)\frac{d\sigma^{\nu_\tau\mathcal{N}\to\nu_\tau X}(E,y)}{dy}. \tag{7.20}$$

Here the usual change of variables $y = (E' - E)/E'$ has been made.

On the other hand, taking into account the sterile Majorana neutrinos production and decay processes, we have new contributions to the absorption and regeneration effects on the ν_τ-flux. Also, if we consider the ν_τ transport, it is important to take into account the transport of the τ lepton which regenerates the ν_τ by τ-decay. In the same way, the Majorana neutrino decay can regenerate the ν_τ flux. So in principle one needs to simultaneously solve a system of three coupled integro-differential equations:

$$\begin{aligned}\frac{\partial\Phi_{\nu_\tau}(E,\chi)}{\partial\chi} &= -\sigma^{\rm t}_{\nu_\tau}(E)\Phi_{\nu_\tau}(E,\chi) + \sigma^{\rm t}_{\nu_\tau}(E)\int_0^1 \frac{dy}{(1-y)}\Phi_{\nu_\tau}(E_y,\chi)K^{\rm NC}_{\nu_\tau}(E,y) \\ &+ \sigma^{\rm t}_{\tau}(E)\int_0^1 \frac{dy}{(1-y)}\Phi_{\tau}(E_y,\chi)K^{\rm cc}_{\tau}(E,y) + \sigma^{\rm t}_{N}(E)\int_0^1 \frac{dy}{(1-y)}\Phi_{N}(E_y,\chi)K^{{\rm N}\mathcal{N}\to\nu_\tau{\rm X}}_{N}(E,y) \\ &+ \Sigma_{\tau}(E)\int_0^1 \frac{dy}{(1-y)}\Phi_{\tau}(E_y,\chi)K^{\rm dec}_{\tau}(E,y) + \Sigma_{N}(E)\int_0^1 \frac{dy}{(1-y)}\Phi_{N}(E_y,\chi)K^{\rm dec}_{N}(E,y)\end{aligned} \tag{7.21}$$

$$\begin{aligned}&\frac{\partial\Phi_{\tau}(E,\chi)}{\partial\chi} = -\sigma^{\rm t}_{\tau}(E)\Phi_{\tau}(E,\chi) - \Sigma_\tau\Phi_\tau(E,\chi) + \frac{d}{dE}(E\beta(E)\Phi_\tau(E)) + \\ &\sigma^{\rm t}_{\tau}(E)\int_0^1 \frac{dy}{(1-y)}\Phi_{\tau}(E_y,\chi)K^{\rm NC}_{\tau}(E,y) + \sigma_{\nu_\tau}(E)\int_0^1 \frac{dy}{(1-y)}\Phi_{\nu_\tau}(E_y,\chi)K^{\rm cc}_{\nu_\tau}(E,y) \\ &+\sigma_N(E)\int_0^1 \frac{dy}{(1-y)}\Phi_{N}(E_y,\chi)K^{{\rm N}\mathcal{N}\to\tau{\rm X}}_{N}(E,y)\end{aligned} \tag{7.22}$$

$$\begin{aligned}\frac{\partial\Phi_N(E,\chi)}{\partial\chi} &= -\sigma^{\rm t}_N(E)\Phi_N(E,\chi) - \Sigma_N(E)\Phi_N(E,\chi) \\ &+ \sigma^{\rm t}_{\nu_\tau}(E)\int_0^1 \frac{dy}{(1-y)}\Phi_{\nu_\tau}(E_y,\chi)K^{\nu_\tau\mathcal{N}\to{\rm NX}}_{\nu_\tau}(E,y) \\ &+ \sigma^{\rm t}_{\tau}(E)\int_0^1 \frac{dy}{(1-y)}\Phi_{\tau}(E_y,\chi)K^{\tau\mathcal{N}\to{\rm NX}}_{\tau}(E,y) \\ &+ \sigma^{\rm t}_{N}(E)\int_0^1 \frac{dy}{(1-y)}\Phi_{N}(E_y,\chi)K^{{\rm N}\mathcal{N}\to{\rm NX}}_{N}(E,y)\end{aligned} \tag{7.23}$$

In (7.21) the right hand side terms correspond to the absorption, neutral-current regeneration, charged-current regeneration by τ interaction, regeneration by Majorana neutrino interaction, and regeneration by τ and N decays.

Equation (7.22) corresponds to the τ transport with absorption by interaction and decay, and regeneration by τ neutral-current, ν_τ charged-current and by the interaction of Majorana neutrinos through the $N\mathcal{N} \to \tau X$ reaction. The third term represents the energy loss due to electromagnetic interactions.

In eq.(7.23) we have absorption terms by interaction and by N decay. The other terms represent the N-flux regeneration by the ν_τ, τ and N interactions with nucleons.

In the above equations the cross-sections in the absorption by interaction terms are

$$\sigma^{\rm t}_{\nu_\tau}(E) \;=\; \sigma^{\rm SM}_{{\rm tot}\ \nu_\tau}(E) + \sigma^{\nu_\tau\mathcal{N}\to NX}_{\nu_\tau}(E) \tag{7.24}$$

and $\sigma^{\rm t}_N(E)$ and $\sigma^{\rm t}_\tau(E)$ include all the Majorana neutrino interactions in (7.1).

The different cross-section regeneration kernels are

$$\begin{aligned}
K^{\rm NC}_{\nu_\tau}(E,y) &= \frac{1}{\sigma^{\rm t}_{\nu_\tau}(E)}\frac{d\sigma^{\nu_\tau\mathcal{N}\to\nu_\tau X}(E_y,y)}{dy}\\
K^{\rm CC}_{\tau}(E,y) &= \frac{1}{\sigma^{\rm t}_{\tau}(E)}\frac{d\sigma^{\tau\mathcal{N}\to\nu_\tau X}(E_y,y)}{dy}\\
K^{{\rm N}\mathcal{N}\to\nu_\tau{\rm X}}_{N}(E,y) &= \frac{1}{\sigma^{\rm t}_{N}(E)}\frac{d\sigma^{N\mathcal{N}\to\nu_\tau X}(E_y,y)}{dy}\\
K^{\rm NC}_{\tau}(E,y) &= \frac{1}{\sigma^{\rm t}_{\tau}(E)}\frac{d\sigma^{\tau\mathcal{N}\to\tau X}(E_y,y)}{dy}\\
K^{\rm CC}_{\nu_\tau}(E,y) &= \frac{1}{\sigma^{\rm t}_{\nu_\tau}(E)}\frac{d\sigma^{\nu_\tau\mathcal{N}\to\tau X}(E_y,y)}{dy}\\
K^{{\rm N}\mathcal{N}\to\tau{\rm X}}_{N}(E,y) &= \frac{1}{\sigma^{\rm t}_{N}(E)}\frac{d\sigma^{N\mathcal{N}\to\tau X}(E_y,y)}{dy}\\
K^{\nu_\tau\mathcal{N}\to{\rm NX}}_{\nu_\tau}(E,y) &= \frac{1}{\sigma^{\rm t}_{\nu_\tau}(E)}\frac{d\sigma^{\nu_\tau\mathcal{N}\to NX}(E_y,y)}{dy}\\
K^{\tau\mathcal{N}\to{\rm NX}}_{\tau}(E,y) &= \frac{1}{\sigma^{\rm t}_{\tau}(E)}\frac{d\sigma^{\tau\mathcal{N}\to NX}(E_y,y)}{dy}\\
K^{{\rm N}\mathcal{N}\to{\rm NX}}_{N}(E,y) &= \frac{1}{\sigma^{\rm t}_{N}(E)}\frac{d\sigma^{N\mathcal{N}\to NX}(E_y,y)}{dy}
\end{aligned} \tag{7.25}$$

with $E_y = E' = E/(1-y)$.

The decay kernels for the Majorana neutrino N or τ-lepton are calculated in the appendix sec.C.4 and in [216] respectively:

$$K^{\rm dec}_{N(\tau)}(E,y) \;=\; (1-y)\frac{dn_{N(\tau)}(1-y)}{dy} \tag{7.26}$$

and the decay-length functions are

$$\Sigma_{N(\tau)}(E) = \left(\frac{E}{m_{N(\tau)}}\langle\rho_n\rangle T_{N(\tau)}\right)^{-1} \tag{7.27}$$

where $T_{N(\tau)} = (\Gamma^{tot}_{rest\ N(\tau)})^{-1}$ is the $N(\tau)$ lifetime in its rest frame, with

$$\Gamma^{tot}_{rest\ N} = \frac{1}{4\pi}\left[\sum_{i=1}^{3}\left(\alpha^i_{L_1}c_W + \alpha^i_{L_3}s_W\right)^2\right]\frac{v^2}{m_N}\left(\frac{m_N}{\Lambda}\right)^4 \tag{7.28}$$

as for the N low mass range the dominant decay is $N \to \nu\gamma$.

Some of the terms in the equations above can be neglected in the considered energy range. The τ and N interactions are neglected against their decays. The τ interactions begin to be dominant at an energy around $E_{\nu_\tau} = 10^8\ GeV$ [216]. For the N interactions, the contributions of the different processes are compared in fig.7.2 as a plot for the ratio between the interaction and decay lengths and the Earth radius. We neglect the regeneration terms coming from the τ and N interactions, which are proportional to the τ and N flux, in comparison with those due to NC interactions of ν_τ and those originated in the τ and N decay. Under these conditions, for the ν_τ transport equation (7.21) we take into account the absorption and neutral-current regeneration terms and the regeneration by τ and N-decay. For the τ-transport equation, we consider absorption by τ-decay and regeneration by ν_τ scattering by nucleons, which is the source of the appereance of τ leptons. In the case of the Majorana neutrino transport equation, absorption by N-decay and also regeneration by ν_τ scattering by nucleons are included, the last process being the source for the N-flux.

Finally, the equations we need to solve are

$$\begin{aligned}\frac{\partial\Phi_{\nu_\tau}(E,\chi)}{\partial\chi} &= -\sigma^{\rm t}_{\nu_\tau}(E)\Phi_{\nu_\tau}(E,\chi) + \sigma^{\rm t}_{\nu_\tau}(E)\int_0^1\frac{dy}{(1-y)}\Phi_{\nu_\tau}(E_y,\chi)K^{\rm NC}_{\nu_\tau}(E,y)\\ &+ \Sigma_\tau(E)\int_0^1\frac{dy}{(1-y)}\Phi_\tau(E_y,\chi)K^{\rm dec}_\tau(E,y)\\ &+ \Sigma_N(E)\int_0^1\frac{dy}{(1-y)}\Phi_N(E_y,\chi)K^{\rm dec}_N(E,y)\end{aligned} \tag{7.29}$$

$$\frac{\partial\Phi_\tau(E,\chi)}{\partial\chi} = -\Sigma_\tau(E)\Phi_\tau(E,\chi) + \sigma^{\rm t}_{\nu_\tau}(E)\int_0^1\frac{dy}{(1-y)}\Phi_{\nu_\tau}(E_y,\chi)K^{\rm CC}_{\nu_\tau}(E,y) \tag{7.30}$$

$$\frac{\partial\Phi_N(E,\chi)}{\partial\chi} = -\Sigma_N(E)\Phi_N(E,\chi) + \sigma^{\rm t}_{\nu_\tau}(E)\int_0^1\frac{dy}{(1-y)}\Phi_{\nu_\tau}(E_y,\chi)K^{\nu_\tau\mathcal{N}\to{\rm NX}}_N(E,y) \tag{7.31}$$

The system of transport equations (7.29)-(7.31) must be solved with the initial conditions $\Phi_{\nu_\tau}(E,\chi=0) = \Phi^0_{\nu_\tau}(E,\theta)$, $\Phi_\tau(E,\chi=0) = 0$ and $\Phi_N(E,\chi=0) = 0$, where $\Phi^0_{\nu_\tau}(E,\theta)$ is the initial neutrino flux, as introduced in the appendix sec.C.2.

Taking the column depth on the path with inclination θ respective to the nadir direction taken from the down-going normal to the neutrino telescope as $\mathcal{T}(\theta)$:

$$\mathcal{T}(\theta) = \chi(2R\cos\theta) = \int_0^{2R\cos\theta}\rho_n(z)dz,$$

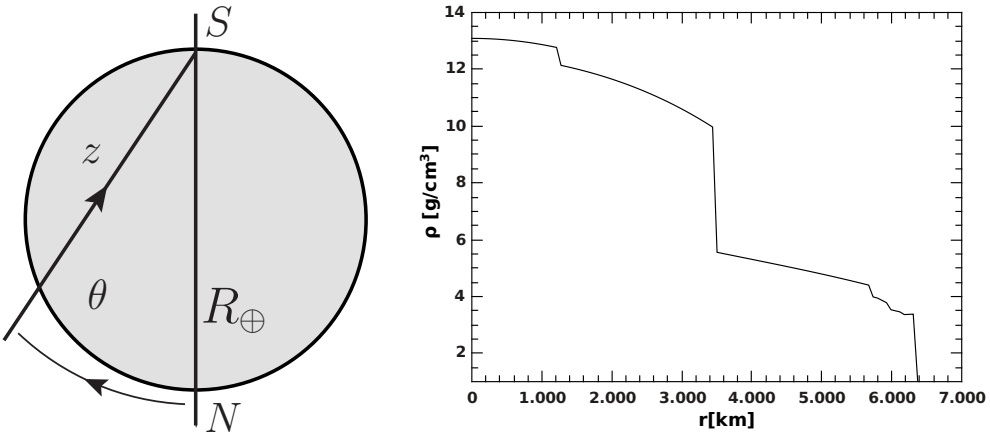

(a) (b)

Figure 7.3: (a) The nadir angle θ, and the traversed matter distance $z = 2R\cos(\theta)$. (b) Earth density as given by the PREM [220].

with R as the Earth radius, we define $\langle \rho_n \rangle$ as the average number density along the column,

$$\langle \rho_n(\theta) \rangle = \frac{\mathcal{T}(\theta)}{2R\cos\theta}. \tag{7.32}$$

The Earth density is given by the Preliminary Reference Earth Model (PREM) [220]. In fig.7.3b we present the Earth density profile.

In accordance with [221], and following the treatment in [213, 216, 222], we solve eqs. (7.30) and (7.31) considering the terms dependent of the ν_τ flux $\Phi_{\nu_\tau}(E, \chi)$ as non-homogeneities, and replace those solutions in (7.29), dividing by $\Phi_{\nu_\tau}(E, \chi)$. Then we make an approximation, taking the fluxes quotient (7.35) as the ones solving the corresponding homogeneous equations [221]. Finally, we write the solution for the surviving τ-neutrino flux traversing a path of length $\mathcal{T}(\theta)$ through the Earth in terms of $\sigma_{\text{eff}}(E, \mathcal{T}(\theta))$ as

$$\Phi_{\nu_\tau}(E, \mathcal{T}(\theta)) = \Phi_{\nu_\tau}(E, 0) \exp[-\sigma_{\text{eff}}(E, \mathcal{T}(\theta))\mathcal{T}(\theta)], \tag{7.33}$$

with

$$\begin{aligned}\sigma_{\rm eff}(E,\mathcal{T}(\theta)) &= \sigma^t_{\nu_\tau}(E)-\sigma^t_{\nu_\tau}(E)\int_0^1 dy\xi(E,y)K^{\rm NC}_{\nu_\tau}(E,y)\mathcal{D}(E_y,E)\\ &- \int_0^1 dydy'\xi(E,y)\xi(E_y,y')\frac{\Sigma_\tau(E)K^{\rm dec}_\tau(E,y)\sigma^t_{\nu_\tau}(E_y)K^{\rm CC}_\tau(E_y,y')}{\Delta_\tau(E_y,E_{yy'})}\\ &\quad(\mathcal{D}(E_{yy'},E)-\mathcal{D}_\tau(E_y,E))\\ &- \int_0^1 dydy'\xi(E,y)\xi(E_y,y')\frac{\Sigma_N(E)K^{\rm dec}_N(E,y)\sigma^t_{\nu_\tau}(E_y)K^{\nu_\tau\mathcal{N}\to{\rm NX}}_{\nu_\tau}(E_y,y')}{\Delta_N(E_y,E_{yy'})}\\ &\quad(\mathcal{D}(E_{yy'},E)-\mathcal{D}_N(E_y,E)).\end{aligned} \tag{7.34}$$

Here $E_{yy'}=E/((1-y)(1-y'))$ and the flux quotients are

$$\xi(E,y)=\frac{1}{(1-y)}\frac{\Phi^0_{\nu_\tau}(E_y)}{\Phi^0_{\nu_\tau}(E)}\,,\qquad \xi(E_y,y')=\frac{1}{(1-y')}\frac{\Phi^0_{\nu_\tau}(E_{yy'})}{\Phi^0_{\nu_\tau}(E)} \tag{7.35}$$

with

$$\begin{aligned}\mathcal{D}(E_1,E_2) &= \frac{[1-\exp(-\Delta(E_1,E_2)\mathcal{T}(\theta))]}{\Delta(E_1,E_2)\mathcal{T}(\theta)}\,,\quad \Delta(E_1,E_2)=\sigma^t_{\nu_\tau}(E_1)-\sigma^t_{\nu_\tau}(E_2)\\ \mathcal{D}_\tau(E_1,E_2) &= \frac{[1-\exp(-\Delta_\tau(E_1,E_2)\mathcal{T}(\theta))]}{\Delta_\tau(E_1,E_2)\mathcal{T}(\theta)}\,,\quad \Delta_\tau(E_1,E_2)=\Sigma_\tau(E_1)-\sigma^t_{\nu_\tau}(E_2)\\ \mathcal{D}_N(E_1,E_2) &= \frac{[1-\exp(-\Delta_N(E_1,E_2)\mathcal{T}(\theta))]}{\Delta_N(E_1,E_2)\mathcal{T}(\theta)}\,,\quad \Delta_N(E_1,E_2)=\Sigma_N(E_1)-\sigma^t_{\nu_\tau}(E_2).\end{aligned}$$

7.4. Numerical results

In this section we present our results assuming a Majorana neutrino contribution with $m_N\sim m_\tau$. In order to obtain numerical results for the surviving ν_τ flux including Majorana neutrino effects, we consider a particular choice for the effective coupling constants ζ, with the upper values presented in (7.16). Also, for the initial ν_τ flux we have considered the best fit of IceCube $\Phi^0_{\nu_\tau}=2.3\times10^{-18}(E/100TeV)^{-2.6}\ GeV^{-1}\ cm^{-2}\ s^{-1}\ sr^{-1}$ [204, 205].

The idea is to see whether the effect of the Majorana neutrinos modifies the ν_τ surviving flux and to what extent it should be distinguishable from the standard surviving flux when a detection is performed in a neutrino telescope, which will clearly depend on the uncertainty involved.

First, in fig.7.4, we compare the surviving ν_τ flux with Majorana neutrino effects, taking into account both absorption and regeneration, with the SM prediction. In fig.7.4a, we show the comparison with the SM, showing the quotient $R^{SM}(\theta,E_{\nu_\tau})=\Phi_{\nu_\tau}/\Phi^{SM}_{\nu_\tau}$ for different nadir angles θ. We also include a figure (fig.7.4b) with the quotient between the surviving flux and the initial flux, $R^0(\theta,E_{\nu_\tau})=\Phi_{\nu_\tau}/\Phi^0_{\nu_\tau}$.

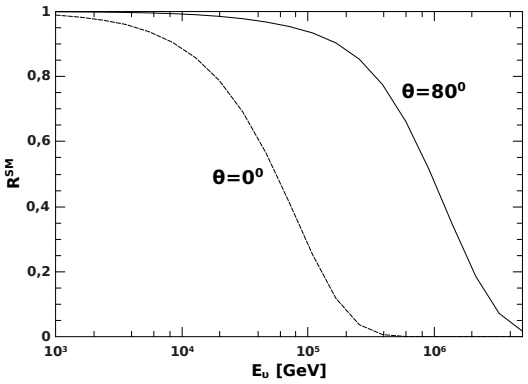

(a) The quotient $R^{SM}(\theta, E_{\nu_\tau}) = \Phi_{\nu_\tau}(\theta, E)/\Phi^{SM}_{\nu_\tau}(\theta, E)$ for different nadir angles. $\Phi_{\nu_\tau}(E, \theta)$ includes SM and Majorana neutrino effects.

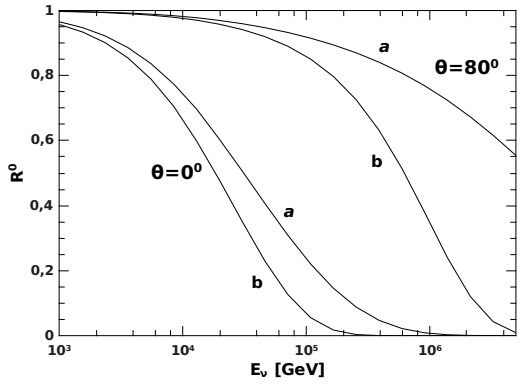

(b) The quotient $R^0(\theta, E_{\nu_\tau}) = \Phi_{\nu_\tau}(\theta, E)/\Phi^0_{\nu_\tau}(E)$ for different nadir angles. For the curve labeled **a** $\Phi_{\nu_\tau}(E, \theta)$ is the SM flux after traversing the Earth. The curve labeled **b** also includes the Majorana neutrino effects. $\Phi^0_{\nu_\tau}(E, \theta)$ is the initial flux arriving to the Earth's surface.

Figure 7.4: Ratio between ν_τ fluxes for different angles.

In order to calculate the capability of IceCube to detect the effects of Majorana neutrinos physics, we have considered an approximated number of events[2] as given by

$$N = n_T \int dt \int d\Omega \int dE\ \Phi_{\nu_\tau}(E, \theta)\ \sigma^{CC}_{\nu_\tau}(E) \tag{7.36}$$

where n_T is the number of target nucleons in the effective volume, and $\sigma^{CC}_{\nu_\tau}$ is the charged-current cross-section, adequate in order to consider ν_τ double-bang[3] events. The function $\Phi_{\nu_\tau}(E, \theta)$ is the τ-neutrino flux in the vicinity of the detector. We consider the number of events in the region $0° < \theta < 60°$ around the nadir direction, for an observation time of 10 years. We have taken the energy interval binning as $\Delta log_{10} E = 0.25$. To appreciate the size of the effect of Majorana neutrino production, we consider the percentage deviation between the non-standard and the SM event numbers ($\Delta_\% = 100 \times (N_{\rm SM} - N_{\rm Maj})/N_{\rm SM}$), with $N_{\rm Maj}$ the number of events including the Majorana neutrino effects, and we compare it with the percentage relative error ($\delta_\% = 100/\sqrt{N_{\rm SM}}$) for Poisson distributed events. The results are shown in fig.7.5a for different values of the dominant coupling ζ_{4-f}. The solid circles indicate the center of each energy bin. We consider the variations in this effective coupling due to the dominant contribution of the four-fermion interactions to the deviation in the Φ_{ν_τ} flux. As we can see from this figure, there is a region in the parameter space where the effect of Majorana neutrinos would be distinguishable from the SM background, i.e. the percentage deviation $\Delta_\%$ is bigger than the SM error $\delta_\%$.

[2]The definition of this observable is given in the appendix sec.C.1.1.

[3]The double-bang topology is defined in the appendix sec. C.3.1.

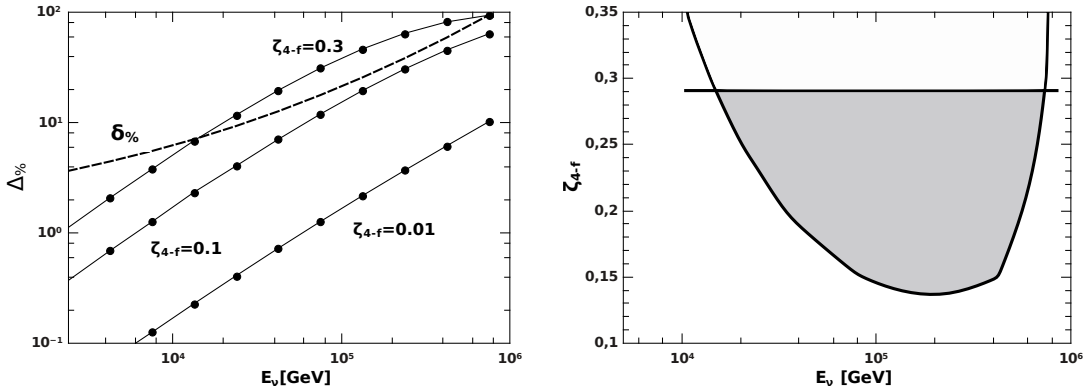

(a) Percentage deviation of the number of events ($\Delta_{\%}$) and comparison with SM statistical error ($\delta_{\%}$) for different values of the four-fermion couplings ζ_{4-f}. The solid circles indicate the center of the considered energy bin.

(b) Region in the (E_ν, ζ_{4-f}) plane where the studied effects could have impact. The region is limited by the curve where the percentage deviation $\Delta_{\%}$ equals the SM error $\delta_{\%}$ and a horizontal line which is the upper bound for the four-fermion coupling in Table 7.1.

Figure 7.5: Parameter-space region where the studied effects could have an impact in IceCube observations.

In fig.7.5b we show the region in the (E_ν, ζ_{4-f}) plane where the phenomena studied could have a detectable impact. The region is limited by the curve for which $\Delta_{\%}$ equals the SM error $\delta_{\%}$ and the horizontal straight line, representing the upper bound for the four-fermion coupling. As the Majorana effects decrease with lower energy, higher values for the ζ_{4-f} coupling are allowed. On the other hand, due to the spectral index (-2.6), the incident flux strongly decreases with growing energy, and this reduces the number of events, thus increasing the SM error. This gives bigger values for the effective coupling at higher energies, in order to have $\Delta_{\%} = \delta_{\%}$.

7.5. Final remarks

We have studied how the production of sterile Majorana neutrinos would affect the attenuation of cosmic ν_τ neutrinos when they pass through the Earth. For the propagation, we considered a system of transport equations for ordinary and Majorana neutrinos and the τ charged lepton, presenting our results for the flux attenuation with and without Majorana effects, and we show the percentage deviation between the SM flux and the flux with Majorana attenuation. Our results can serve as a complementary tool to explore the effects of sterile neutrino physics, by directly studying the effects of UHE neutrino interactions with the nucleons of the Earth using neutrino telescopes. Over the coming years, new neutrino telescopes are planned to be working in the Northern hemisphere. In particular the European project KM3NeT [223–225], originated from the projects ANTARES, NEMO, and NESTOR will be installed in the Mediterranean sea

with an instrumented volume of several cubic kilometers. This telescope along with the Baikal-GVD upgrade [226, 227] will improve the statistics, increasing the significance of the observations to bound new physics effects as the ones we discussed in this chapter.

Chapter 8

Conclusions and perspectives

This thesis was dedicated to the study of distinct phenomenological consequences of the introduction of an effective lagrangian approach to model the interactions of a heavy sterile Majorana neutrino. We consider that the sterile N interacts with the light neutrinos by higher dimension effective operators, and take this interaction to be dominant in comparison with the mixing through the Yukawa couplings, in contrast to the usual viewpoint in which the mixing with the standard neutrinos is assumed to govern the N production and decay mechanisms.

The lagrangian parameterizes the effects of new physics beyond the SM by a set of dimension 6 operators constructed with the SM and the Majorana neutrino fields as effective degrees of freedom, satisfying the standard $SU(2)_L \times U(1)$ gauge symmetry. This offers a model-independent and broader view of the kind of physics leading to massive neutrinos and lepton number violation phenomena.

The aim of the thesis was to study the possibility to produce and discover Majorana neutrinos through lepton number violating signals in high energy colliders and also to explore the possible effects of the existence of Majorana neutrinos in the propagation of tau-neutrinos through the Earth, which can be detected in neutrino telescopes.

We calculated the total decay width and branching ratios for the Majorana neutrino in two distinct mass regimes: first restricting ourselves to a mass region below the SM weak bosons mass: $m_N < m_W$ [2], which reduces the possible decay channels, and for a broader mass interval $m_N < 1\ TeV$ in [3], where the decay width to known particles was obtained. For the lower mass region, we found the neutrino plus photon decay channel $N \to \nu\gamma$ is clearly dominating. This decay mode is due to tensorial terms in the effective lagrangian, which are generated at one-loop in the unknown underlying full theory. This kind of radiative neutrino decay modes have been invoked in the literature [141] as an answer to the puzzle posed by the MiniBoone oscillation experiment results [138, 139], which do not fit in the three-neutrino oscillations framework. We found that the excess encountered by MiniBoone in $\nu_\mu \to \nu_e$ conversion could be explained by the existence of Majorana neutrinos with a dominant radiative decay mode in which the final photon would be converted into an e^+e^- pair with a small opening angle, indistinguishable from an electron in the detector, which fakes a signal not coming from ν_e charged-current

interactions. Also, this kind of neutrino could explain the appearance of unexpected sub-horizontal air-shower events in the SHALON telescope [140]. This results were presented in chapter 4.

The production of Majorana neutrinos in high energy colliders was studied in chapters 5 and 6. In a first work [4] we investigated the possibility of detecting Majorana neutrinos at the Large Hadron-electron Collider (LHeC), an electron-proton collision mode at CERN, studying the $l_j^+ + 3jets$ ($l_j \equiv e, \mu, \tau$) final states which are, due to leptonic number violation, a clear signature for intermediate Majorana neutrino contributions. We presented our results for the total cross section as a function of the Majorana neutrino mass, the effective couplings and the new physics scale in the effective lagrangian. We also showed the possible discovery region as a function of the Majorana neutrino mass and the effective couplings values. Our results showed that the LHeC may be able to discover Majorana neutrinos with masses lower than 700 GeV and 1300 GeV for electron beams settings of energies $E_e = 50$ GeV and $E_e = 150$ GeV, respectively.

In the case of the LHC [5] we studied the well known same-sign dilepton signal $pp \to l_i^+ l_j^+ + 2\ jets$ ($l_j \equiv e, \mu$). As Majorana neutrinos with masses of a few GeV are long-lived neutral particles, we took advantage of their measurable decay length, exploiting this fact to impose cuts that help reject the SM background. We used a forward-backward-like asymmetry in the distribution of the angle between both final leptons, in order to distinguish the effects of vectorial and scalar operators. For the scalar contributions, the asymmetry is found to be compatible with zero, but in the case of vector operators, we found a clear non-zero contribution. We also studied the $pp \to l_i^+ \nu\gamma$ process, which is dominant for low m_N masses if tensorial one-loop generated new physics contributions are present. We found the signal distribution in the non-pointing photon observable z_{DCA} [123, 151] could allow for the discovery of the signal in the LHC, with the aid of cuts in the displacement between the prompt lepton and the outgoing photon to reject the backgrounds.

Finally, our work on the effects of the existence of a Majorana neutrino on the ν_τ propagation in the Earth [6] was presented in chapter 7. This effect could be measured in the IceCube neutrino telescope as a deviation for the number of ν_τ detected events from the SM-only expectations. The surviving tau-neutrino flux was calculated using transport equations including Majorana neutrino production and decay. We compared our results with the pure SM interactions, computing the surviving flux for different values of the effective lagrangian couplings, considering the detected flux by IceCube for an operation time of 10 years, and Majorana neutrinos with mass m_N near the m_τ mass. We showed the region in the (E_ν, ζ_{4-f}) plane where the Majorana physics effects could be detectable by the IceCube experiment.

Regarding our working perspectives, in the case of the study of the Majorana neutrino phenomenology for the same-sign-dilepton and displaced-photon signals in the LHC studied in chapter 6, an interesting and challenging task is to be able to give quantitative predictions for the experiment's sensitivity to these signals. Our next goal is to be able to simulate signal and SM background events in a format that allows us to implement

kinematical cuts in the final phase-space, in order to perform a detailed study of the efficiency of our studied signal, in a similar fashion to what we did in chapter 5. This is a much more involved task for proton-proton collision simulations, due to QCD and electromagnetic showering effects related to the process in which our theoretical final-state partons, leptons and photons actually convert into the observed particles in the LHC detectors.

During the years of this thesis work, the big experimental collaborations in the LHC and theoretical research groups in the associated universities have developed very sophisticated software for the numerical simulation of scattering events in the LHC, comprising a coherent set of physics models for the evolution from a few-body hard-scattering process to a complex multi-particle final state, including the parton's hadronization process, and the development of decay showers for leptons and photons after the primary collision, between other features as detector simulation. The use of this kind of software allows for passing from purely theoretical predictions from distinct new physics models, to concrete simulated events, bringing them closer to the format in which truly experimental data are analyzed in new physics searches.

Our current working perspective is to implement the Majorana neutrino effective lagrangian model in the software package FeynRules [228, 229] and move ahead to interphase it with sophisticated Monte Carlo event generators as MadGraph5_aMC@NLO [230] in order to simulate our signal. Then, we plan to implement the simulation of showers for leptons and photons in the final states, as well as the hadronization into jets of the outgoing quarks using programs like Pythia [231, 232]. The aim is to be able to make precise numerical predictions, regarding the implementation of the displaced vertices observables in the fashion we presented in our analyses for the LHC in chapter 6, and include the reconstruction efficiencies for the displaced vertices observables, which would need a detector simulation to be correctly taken into account.

The use of this simulation software will allow us to broaden our research. One possible direction is to deepen the study of the phenomenology of the Majorana neutrino effective lagrangian we studied in this thesis in order to include new signals in new experimental facilities and also perform more dedicated studies on the possible constraints to the effective couplings.

The program of experimental research in neutrino physics extends beyond 2030. In the coming years a wealth of new data is expected from the energy, intensity and cosmic frontiers. This new information is expected to shed light on the fundamental aspects of neutrino physics: the nature -Dirac or Majorana- of massive neutrinos, the status of CP symmetry in the lepton sector and the baryon asymmetry of matter, the absolute neutrino mass scale, the origin of the observed patterns of the neutrino masses and mixing, and, eventually, on the mechanism of neutrino mass generation. Just as the past history of neutrinos physics has been full of surprises, I look forward for more!

Appendix A

Kinematics and phase-space

In this appendix I introduce the basic tools for the calculation of the decay rates and scattering cross-sections presented in chapters 4, 5 and 6. It includes a discussion on final state phase-space integrations and basic kinematical definitions, which can be found in the PDG review [1].

A.1. Phase-space

The Lorentz-invariant phase-space element for an n-particle final state can be written as

$$d\Phi_n \equiv (2\pi)^4 \ \delta^4 \left(P - \sum_{i=1}^{n} p_i \right) \prod_{i=1}^{n} \frac{1}{(2\pi)^3} \frac{d^3\vec{p}_i}{2E_i}. \tag{A.1}$$

The δ^4 imposes the constraint on the phase-space by the four-momentum conservation of the initial state total momentum P. The phase-space factor gives the properly normalized "number of final states" to have final particle's momenta $\vec{p'_j}$ in a volume element $d^3p'_1, ..., d^3p'_k$ around $(\vec{p'_1}, ..., \vec{p'_k})$. Each final state particle satisfies an on-shell condition $p_i^2 = m_i^2$ and the total c.m. energy squared is $s = P^2 = \left(\sum_{i=1}^{n} p_i\right)^2$.

The phase-space element for one-particle final state is

$$d\Phi_1 \equiv (2\pi) \ \frac{d^3\vec{p}_1}{2E_1} \delta^4(P - p_1) = \pi |\vec{p}_1| d\vec{p}_1 \delta^3(\vec{P} - \vec{p}_1) = \frac{2\pi}{s} \ \delta(1 - \frac{m_1}{\sqrt{s}}). \tag{A.2}$$

Here the variable E_1 has been integrated out, which leads to $E_1^{cm} = \sqrt{s}$ in the c.m. frame. The coefficient of the phase-space element is called "phase-space volume" after integrating out all the variables. Here it is 2π for one-particle final state in our convention.

A.1.1. Two-body kinematics

For a two-particle final state with the momenta $\vec{p}_1$, $\vec{p}_2$ respectively, the Lorentz-invariant phase-space element is given by

$$d\Phi_2 \equiv \frac{1}{(2\pi)^2}\,\delta^4\left(P-p_1-p_2\right)\frac{d^3\vec{p}_1}{2E_1}\frac{d^3\vec{p}_2}{2E_2} = d\Omega_{cm}\frac{\lambda^{1/2}(s,m_1^2,m_2^2)}{32\pi^2 s}.$$

where the "two-body kinematic function" is defined as

$$\lambda(x,y,z) = (x-y-z)^2 - 4yz = x^2+y^2+z^2-2xy-2xz-2yz. \tag{A.3}$$

The two-body phase-space element is dimensionless, and thus no dimensionful variables remain unfixed. The two-body phase-space weight is constant and the magnitudes of the energy-momentum of the two particles are fully determined by the four-momentum conservation. As we mentioned in the introduction for the case of the beta nuclear decay, in two-body final states the particle energy spectrum is monochromatic. So in the c.m. frame the momenta and energies are fixed to

$$|\vec{p}_1| = |\vec{p}_2| = \frac{\lambda^{1/2}(s,m_1^2,m_2^2)}{2\sqrt{s}},\ E_1^{cm} = \frac{s+m_1^2-m_2^2}{2\sqrt{s}},\ E_2^{cm} = \frac{s+m_2^2-m_1^2}{2\sqrt{s}},$$

While the momentum magnitude is the same for the two daughter particles in the parent rest-frame, the more massive the particle is, the larger its energy is.

From (A.2) and (A.3) one can see that the phase-space volume of two particles is scaled down with respect to that of one particle by a factor

$$\frac{d\Phi_2}{s\ d\Phi_1} \approx \frac{1}{(4\pi)^2}. \tag{A.4}$$

One can roughly consider that the phase-space volume with each additional final-state particle (properly normalized by the dimensionful unit s) scales down by this similar factor. This explains why most of the time the three-body decays have lower widths than two-body decays, and so on. It is interesting to note that it is just like the scaling factor with each additional loop integral.

A recursion relation can be written in order to decompose the n-body phase-space into phase-spaces of less particles:

$$\begin{aligned} d\Phi_n(P;p_1,...,p_n) &= d\Phi_{n-1}(P;p_1,...,p_{n-1,n})\times \\ &\quad d\Phi_2(p_{n-1,n};p_{n-1},p_n)\frac{dm_{n-1,n}^2}{2\pi}, \end{aligned} \tag{A.5}$$

with $m_{n-1,n}^2 = m_{n-1}^2 + m_n^2$.

This recursion relation is particularly useful to write the intermediate mass integral for a resonant state (see next section).

A.1.2. Breit-Wigner resonance and the narrow width approximation (NWA)

The propagator contribution of an unstable particle of mass m_V and total width Γ_V is written as

$$R(s) = \frac{1}{(s - m_V^2)^2 + \Gamma_V^2 m_V^2}. \tag{A.6}$$

This is the Breit-Wigner Resonance.

Consider a very general case of a virtual particle V^* in an intermediate state,

$$a \to bV^* \to b\ p_1 p_2. \tag{A.7}$$

An integral over the virtual mass can be obtained by the reduction formula in the last section (A.5). Together with kinematical considerations, the resonant integral reads

$$\int_{(m_*^{min})^2=(m_1+m_2)^2}^{(m_*^{max})^2=(m_a-m_b)^2} dm_*^2. \tag{A.8}$$

The integral is rather singular near the resonance. Thus a variable change is effective for the practical purpose,

$$\tan\theta = \frac{m_*^2 - m_V^2}{\Gamma_V m_V}, \tag{A.9}$$

resulting in a flat integrand over θ

$$\int_{(m_*^{min})^2}^{(m_*^{max})^2} \frac{dm_*^2}{(m_*^2 - m_V^2)^2 + \Gamma_V^2 m_V^2} = \int_{\theta^{min}}^{\theta^{max}} \frac{d\theta}{\Gamma_V m_V}, \tag{A.10}$$

where $\theta = \tan^{-1}(m_*^2 - m_V^2)/\Gamma_V m_V$. In the limit

$$(m_1 + m_2) + \Gamma_V \ll m_V \ll m_a - \Gamma_V, \tag{A.11}$$

then $\theta^{min} \to -\pi$ and $\theta^{max} \to 0$. This is the condition for the narrow-width approximation (NWA) [233]:

$$\frac{1}{(m_*^2 - m_V^2)^2 + \Gamma_V^2 m_V^2} \approx \frac{\pi}{\Gamma_V m_V}\ \delta(m_*^2 - m_V^2). \tag{A.12}$$

The NWA allows to neglect non-resonant as well as non-factorizable amplitude contributions, thus leading to significant simplifications for calculations.

The phase-space recursion in (A.5) together with the narrow width approximation in (A.12) allows us to write the partial decay width of an unstable particle decaying as in (A.7) as the product of the first decay width and the branching fraction for the considered V decay channel:

$$\Gamma(a \to bV^* \to b\ p_1 p_2) \sim \Gamma(a \to bV).Br(V \to b\ p_1 p_2) \tag{A.13}$$

with V being the real boson.

A.2. Three-body decay phase-space integration

Let us examine here the phase-space integration for three-body decays, as those presented in chapter 4. In order to fix ideas, consider the decay $N \to \ell\ 1\ 2$ depicted in fig.A.1.

Recalling section 4.1.1 we see the differential decay width in this case is written

$$d\Gamma^{N\to\ell\ 1\ 2} = \frac{1}{2E_N}(2\pi)^4\delta^4(q-p-p_1-p_2)|\mathcal{M}|^2\frac{d^3p}{(2\pi)^3 2p^0}\frac{d^3p_1}{(2\pi)^3 2p_1^0}\frac{d^3p_2}{(2\pi)^3 2p_2^0}.$$

As is customary, we choose to integrate over the $p_{1,2}$ momenta, and define the variable $x = \frac{2p^0}{m_N}$, where p^0 is the lepton's energy in the c.m. frame. There the N is at rest, and its energy is $E_N = m_N$. Taking $d^3\vec{p} = 4\pi|\vec{p}|^2 d\vec{p}$ and $|\vec{p}|^2 = (p^0)^2 - m_\ell^2$ we can write

$$\frac{d\Gamma^{N\to\ell\ 1\ 2}}{dx} = \frac{m_N}{4(2\pi)^4}\left(\frac{x^2}{4} - y_\ell\right)\int\frac{d^3\vec{p_1}}{2p_1^0}\int\frac{d^3\vec{p_2}}{2p_2^0}|\mathcal{M}|^2\delta^4(q-p-p_1-p_2) \qquad \text{(A.14)}$$

where $y_\ell = m_\ell^2/m_N^2$.

For each decay process, the squared matrix element $|\mathcal{M}|^2$ will depend on the distinct scalar products $q\cdot p_1,\ q\cdot p_2,\ (q\cdot p_1)(q\cdot p_2),\ (p_1\cdot p_2)$ or the identity matrix. Then we will encounter the following integrals:

$$\begin{aligned}
I &= \int\frac{d^3\vec{p_1}}{2p_1^0}\int\frac{d^3\vec{p_2}}{2p_2^0}\delta^4(q-p-p_1-p_2)\\
I_{i,\,\alpha} &= \int\frac{d^3\vec{p_1}}{2p_1^0}\int\frac{d^3\vec{p_2}}{2p_2^0}p_{i\alpha}\delta^4(q-p-p_1-p_2) \qquad i=1,2\\
I_{ij,\,\alpha\beta} &= \int\frac{d^3\vec{p_1}}{2p_1^0}\int\frac{d^3\vec{p_2}}{2p_2^0}p_{i\alpha}p_{j\beta}\delta^4(q-p-p_1-p_2) \qquad i,j=1,2. \qquad \text{(A.15)}
\end{aligned}$$

These are manifestly Lorentz-covariant, due to the invariance of the δ^4 and the relation

$$\frac{d^3\vec{q}}{2q^0} = \int d^4q\,\delta(q^2-m_q^2)\Theta(q^0).$$

When integrating over p_1 and p_2, due to the momentum-conservation delta, the integrals in (A.15) will only depend on the four-momentum $k = q-p = p_1+p_2$.

In order to show an example of the general procedure, let's calculate explicitly the integral I_1^α. It will be needed when integrating the terms where the scalar product $q.p_1$ appears. The integral will be written

$$q_\alpha I_1^\alpha = \int\frac{d^3\vec{p_1}}{2p_1^0}\int\frac{d^3\vec{p_2}}{2p_2^0}\ q_\alpha p_1^\alpha\ \delta^4(q-p-p_1-p_2).$$

As I_1^α will only depend on $k^\alpha = (q-p)^\alpha$ we proceed making the ansatz $k_\alpha I_1^\alpha = Ak^2$, with A being some constant. As $k^2 > 0$ we can move to a reference frame where the four-momentum k takes the form $k = \tilde{k} = (\tilde{k}^0, \vec{0})$, so that $\tilde{k}_0\tilde{I}_1^0 = A\tilde{k}^2 = Ak^2$.

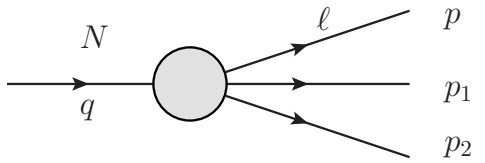

Figure A.1: Three-body decay $N \to \ell\ 1\ 2$. Particle 1 (2) has four-momentum p_1 (p_2) and mass m_1 (m_2). The lepton ℓ has four-momentum p and mass m_ℓ. The decaying particle N has four-momentum q and mass m_N.

The expression for $\tilde{I}_1^0$ is

$$\tilde{I}_1^0 = \int \frac{d^3\vec{p_1}}{2p_1^0} \int \frac{d^3\vec{p_2}}{2p_2^0} p_1^0 \delta^4(\tilde{k} - p_1 - p_2),$$

where the delta function can be factorized as $\delta^4(\tilde{k} - p_1 - p_2) = \delta(\vec{p_1} + \vec{p_2})\delta(p_1^0 + p_2^0 - \tilde{k}^0)$. Writing $|\vec{p}_{1,2}|^2 = (p_{1,2}^0)^2 - m_{1,2}^2$ we find

$$\begin{aligned} \tilde{I}_1^0 &= \int \frac{d^3\vec{p_1}}{4} \int \frac{d^3\vec{p_2}}{p_2^0} \delta(\vec{p_1} + \vec{p_2})\delta(p_1^0 + p_2^0 - \tilde{k}^0) \\ &= \frac{1}{4} \int d^3\vec{p_1} \int \frac{d^3\vec{p_2}}{\sqrt{|\vec{p_2}|^2 + m_2^2}} \delta(\vec{p_1} + \vec{p_2})\delta(p_1^0 + \sqrt{|\vec{p_2}|^2 + m_2^2} - \tilde{k}^0). \end{aligned}$$

When integrating over $\vec{p_2}$, we substitute $|\vec{p_2}| = |\vec{p_1}|$ and we are left with

$$\tilde{I}_1^0 = \frac{1}{4} \int \frac{d^3\vec{p_1}}{\sqrt{|\vec{p_1}|^2 + m_2^2}} \delta(p_1^0 + \sqrt{|\vec{p_1}|^2 + m_2^2} - \tilde{k}^0).$$

A last step, putting $|\vec{p}_1|^2 = (p_1^0)^2 - m_1^2$ and $d^3\vec{p}_1 = 4\pi|\vec{p}_1|^2 d|\vec{p}_1| = 4\pi\sqrt{(p_1^0)^2 - m_1^2}\, p_1^0 dp_1^0$ allows ws to write everything in terms of p_1^0:

$$\tilde{I}_1^0 = \pi \int \frac{\sqrt{(p_1^0)^2 - m_1^2}}{\sqrt{(p_1^0)^2 - m_1^2 + m_2^2}}\ p_1^0\ dp_1^0 \delta(p_1^0 + \sqrt{(p_1^0)^2 - m_1^2 + m_2^2} - \tilde{k}^0).$$

The delta function can be rewritten using the property $\delta(f(x)) = \sum_i \frac{\delta(x - x_i)}{|f'(x_i)|}$, with $f(x_i) = 0$. So imposing $f(p_1^0) = 0$ leads us to the value $p_1^0 = \frac{(\tilde{k}^0)^2 + m_1^2 - m_2^2}{2\tilde{k}^0}$ and the derivative is

$$\frac{df}{dp_1^0} = \frac{\sqrt{(p_1^0)^2 - m_1^2 + m_2^2} + p_1^0}{\sqrt{(p_1^0)^2 - m_1^2 + m_2^2}}.$$

Finally the integral can be written as

$$\tilde{I}_1^0 = \pi \int \frac{\sqrt{(p_1^0)^2 - m_1^2}}{\sqrt{(p_1^0)^2 - m_1^2 + m_2^2} + p_1^0}\ p_1^0\ dp_1^0 \delta\left(p_1^0 - \frac{(\tilde{k}^0)^2 + m_1^2 - m_2^2}{2\tilde{k}^0}\right),$$

and thus

$$\begin{aligned}\tilde{I}_1^0 &= \frac{\pi}{\tilde{k}^0}\left(\frac{(\tilde{k}^0)^2+m_1^2-m_2^2}{2\tilde{k}^0}\right)\left(\frac{((\tilde{k}^0)^2+m_1^2-m_2^2)^2}{4(\tilde{k}^0)^2}-m_1^2\right)^{1/2}\\ &= \frac{\pi}{4\tilde{k}^0}\left(\frac{(\tilde{k}^0)^2+m_1^2-m_2^2}{(\tilde{k}^0)^2}\right)\left(((\tilde{k}^0)^2+m_1^2+m_2^2)^2-4(\tilde{k}^0)^2m_1^2\right)^{1/2}.\end{aligned}$$

Recalling that $\tilde{k}_0\tilde{I}_1^0 = A\tilde{k}^2 = Ak^2$ and in this frame $(\tilde{k}^0)^2 = k^2$, we change back to k and find the constant

$$A = \frac{1}{k^2}\frac{\pi}{4}\left(\frac{k^2+m_1^2-m_2^2}{k^2}\right)\left((k^2-m_1^2-m_2^2)^2-4m_1^2m_2^2\right)^{1/2}.$$

This finally leads us to the integral

$$\begin{aligned}I_1^\alpha &= \int\frac{d^3\vec{p_1}}{2p_1^0}\int\frac{d^3\vec{p_2}}{2p_2^0}p_1^\alpha\ \delta^4(q-p-p_1-p_2)\\ &= \frac{\pi}{4}\left(\frac{k^2+m_1^2-m_2^2}{k^4}\right)\left((k^2-m_1^2-m_2^2)^2-4m_1^2m_2^2\right)^{1/2}k^\alpha. \qquad \text{(A.16)}\end{aligned}$$

Performing a similar calculation, the integral $I_{12,\ \alpha\beta}$ in (A.15) can be obtained making the ansatz $I_{12,\ \alpha\beta} = Bk^2g_{\alpha\beta} + Ck_\alpha k_\beta$, with B, C constant. Since the variables p_1 and p_2 are integrated over, only the second rank tensors $g_{\alpha\beta}$ and $k_\alpha k_\beta$ can occur in the result. Then we can construct the following invariants:

$$\begin{aligned}g^{\alpha\beta}I_{12,\ \alpha\beta} &= (4B+C)k^2\\ k^\alpha k^\beta I_{12,\ \alpha\beta} &= (B+C)k^4. \qquad \text{(A.17)}\end{aligned}$$

We can calculate explicitly the invariants in (A.17)

$$\begin{aligned}g^{\alpha\beta}I_{12,\ \alpha\beta} &= \int\frac{d^3\vec{p_1}}{2p_1^0}\int\frac{d^3\vec{p_2}}{2p_2^0}p_{1\alpha}\ p_2^\alpha\ \delta^4(q-p-p_1-p_2)\\ k^\alpha k^\beta I_{12,\ \alpha\beta} &= \int\frac{d^3\vec{p_1}}{2p_1^0}\int\frac{d^3\vec{p_2}}{2p_2^0}(p_1\cdot k)(p_2\cdot k)\ \delta^4(q-p-p_1-p_2)\end{aligned}$$

going again to the reference frame where $k = \tilde{k} = (\tilde{k}^0, \vec{0})$ and performing the integrals, which allow us to calculate the constants B and C.

The final result is given by

$$\begin{aligned}I_{12,\ \alpha\beta} &= \frac{\pi}{24}\left[1-\frac{(m_1+m_2)^2}{k^2}\right]^{1/2}\left[1-\frac{(m_1-m_2)^2}{k^2}\right]^{1/2}\\ &\times\ \left[g_{\alpha\beta}k^2\left(1-\frac{(m_1+m_2)^2}{k^2}\right)+2k_\alpha k_\beta\left(1+\frac{m_1^2+m_2^2}{k^2}-2\frac{(m_1^2-m_2^2)^2}{k^4}\right)\right]\\ &\times\ \Theta(k^2-(m_1+m_2)^2) \qquad \text{(A.18)}\end{aligned}$$

where the step-function assures four-momentum conservation. The other integrals in (A.15) can be obtained in a similar fashion.

The integration over the x variable in (A.14) has to be done between the kinematically allowed limits. If we analyze the situation in the rest-frame of the decaying particle N, where its four-momentum is $q = (m_N, \vec{0})$ so that $k^2 = m_N^2 + m_\ell^2 - 2m_N\, p^0$, we have

$$x = 1 + y_\ell - \frac{k^2}{m_N^2}.$$

The minimal value of k^2 occurs when the particles 1 and 2 are produced at rest, so

$$k^2_{min} = m_1^2 + m_2^2 \qquad \text{and} \qquad x_{max} = 1 + y_\ell - \frac{k^2_{min}}{m_N^2} = 1 + y_\ell - (y_1 + y_2)$$

with $y_{1,2} = m_{1,2}^2/m_N^2$. On the other hand, the maximum value of k^2 occurs when p^0 is minimal. This is when the lepton is produced at rest: $p^0_{min} = m_\ell$. This gives us

$$k^2_{max} = m_N^2 + m_\ell^2 - 2m_N p^O_{min} = (m_N - m_\ell)^2 \;\text{ and }\; x_{min} = 1 + y_\ell - \frac{k^2_{min}}{m_N^2} = 2\frac{m_\ell}{m_N}.$$

Thus, the integration interval for x is

$$2\sqrt{y_\ell} \leq x \leq 1 + y_\ell - y_1 - y_2. \tag{A.19}$$

Appendix B

Collider phenomenology

In this appendix I collect the basic concepts on collider phenomenology used in chapters 5 and 6. They are mostly based on the notes [234] and the textbook [235].

B.1. Scattering cross-sections

If we collide two beams made of particles with momenta $p_{1,2}$ and masses $m_{1,2}$, the differential scattering cross-section is the number of collision events leading to a particular final state of n particles with momenta p'_k $(k = 1, ..., n)$ divided by the flux of particles in collision. After the proper normalization of states and the flux, it can be written, for two incident beams with collinear momenta $\vec{p_1}$ and $\vec{p_2}$ as:[1]

$$d\sigma_{coll} = \frac{|\mathcal{M}_{i\to f}|^2}{4\sqrt{(p_1.p_2)^2 - m_1^2 m_2^2}} d\Phi_n. \tag{B.1}$$

Here, the phase-space factor $d\Phi_n$, defined as in (A.1), includes a momentum conservation delta $\delta^4(P - \sum_{i=1}^n p'_k)$ and gives the properly normalized "number of final states" to have final particle's momenta $\vec{p'_k}$ in a volume element $d^3p'_1, ..., d^3p'_n$ around $(\vec{p'_1}, ..., \vec{p'_n})$, given the incoming momenta $P = p_1 + p_2$. The matrix element $\mathcal{M}_{i\to f}$ gives, as in sec.4.1.1, the transition amplitude between the specific initial and final states.

Using the Mandelstam variable $s \equiv (p_1 + p_2)^2$ and the λ function defined in (A.3), the total cross-section can be put in the usual form

$$\sigma(s) = \int d\sigma_{coll} = \int \frac{d\Phi_n}{2\sqrt{\lambda(s, m_1^2, m_2^2)}} |\mathcal{M}_{i\to f}|^2, \tag{B.2}$$

where the integration takes place over the whole phase-space.

B.2. Hadron colliders

A collider like the LHC at CERN performs proton-proton collisions. Protons are hadrons composed by quarks and gluons (partons), which are the fundamental degrees of

[1] This is the situation in the laboratory and the center of mass (c.m.) reference frames.

freedom participating in strong interactions at high energies. I review here the treatment of parton collisions.

B.2.1. Hard scattering of partons

The QCD factorization theorem states that the cross-sections for high energy hadronic reactions with a large momentum transfer can be factorized into a parton-level "hard scattering" convoluted with the parton distribution functions (PDFs). A parton distribution function can be defined as the probability density for finding a parton with a certain momentum fraction x at a factorization scale Q^2.

For scattering of two hadrons A and B to produce a final state F the cross-section can be formally written as a sum over the sub-process cross-sections from the contributing partons

$$\sigma(AB \to F\ X) = \sum_{a,b} \int dx_1 dx_2\ P_{a/A}(x_1, Q^2) P_{b/B}(x_2, Q^2)\ \hat{\sigma}(ab \to F), \tag{B.3}$$

where X is the inclusive scattering remnant, and Q^2 is the factorization scale (or the typical momentum transfer) in the hard scattering process, much larger than the QCD scale $\Lambda^2_{QCD} \approx (200\ \text{MeV})^2$. The parton-level hard scattering cross-section can be calculated perturbatively, while the parton distribution functions parameterize the non-perturbative aspects of the collision and can only be obtained by some ansatz and by fitting the data.

Fig. B.1 shows the parton momentum distributions versus the energy fractions x, taking the CTEQ-5 parton distribution set [236], which is the one used in the calculations in this thesis. In the figure the QCD factorization scale is chosen to be Q^2=10 GeV^2 and 10^4 GeV^2 in the two panels, respectively. It is important to notice that the valence quarks u_v, d_v, as well as the gluons carry a large momentum fraction, typically $x \sim 0.08 - 0.3$, and the "sea quarks" ($\bar{u} = u_{sea}, \bar{d} = d_{sea}, s, c, b$) are concentrated in small x values, and are significantly enhanced at higher Q^2. This implies that heavy objects near the energy threshold are more likely produced by valence quarks, and higher energy processes (compared to the mass scale of the parton-level subprocess) are more dominantly mediated via sea quarks and gluons.

B.2.2. Particle detection at colliders

A modern particle detector is an electronic complex, which typically consists of a secondary displaced vertex detector, a charge-tracking system, electromagnetic calorimetry, hadronic calorimetry and a muon chamber, etc. The detection of the different particles is based on their interactions with the matter of which the detectors are made. A simplified layout is shown in fig. B.2.

The theoretical calculations are made considering the fundamental degrees of freedom in the lagrangian, namely the quarks, leptons, gauge bosons, etc. But most of them are not the particles directly "seen" in the detectors. Heavy particles like Z, W, t will

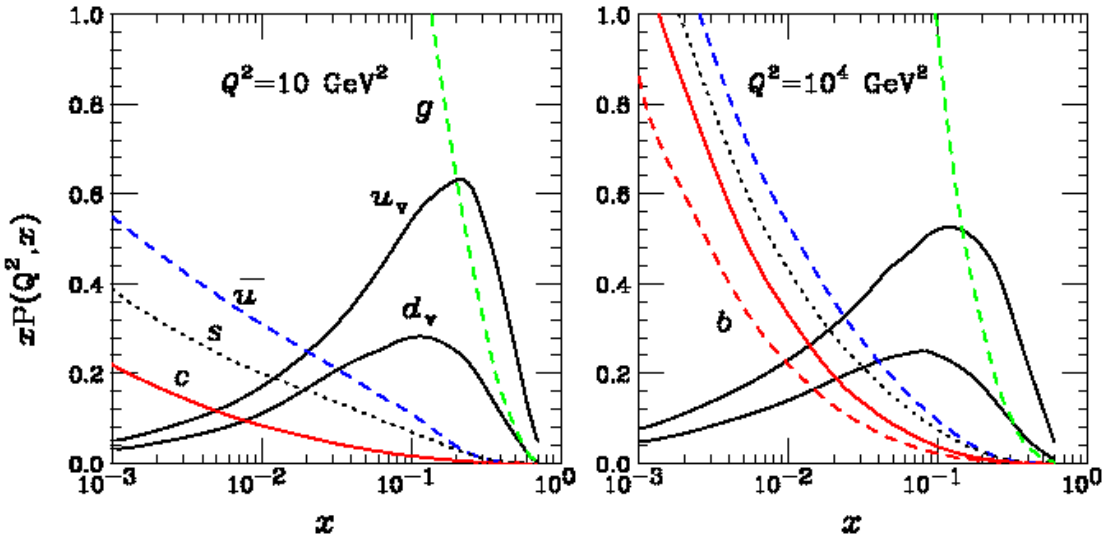

Figure B.1: Parton momentum distributions for the proton versus their energy fraction x at two different factorization scales, from CTEQ-5 [236].

promptly decay to leptons and quarks, with a lifetime $1/\Gamma \sim 1/(2\text{ GeV}) \approx 3.3 \times 10^{-25}$ s. Other quarks will *fragment* into color-singlet hadrons due to QCD confinement at a time scale of $t_h \sim 1/\Lambda_{QCD} \approx 1/(200\text{ MeV}) \approx 3.3 \times 10^{-24}$ s. The individual hadrons left after fragmentation may behave rather differently in the detector depending on their interactions with matter and their lifetimes. The clusters of hadrons formed from the outgoing quarks from the hard scattering event are identified as *jets*. Stable particles such as p, $\bar{p}$, $e^{\pm}$, γ will show up in the detector as energy deposit in the hadronic and electromagnetic calorimeters or as charge tracks in the tracking system.

Depending on their lifetime, particles behave in the detector in different ways.

- Quasi-stable: fast-moving particles of a life-time $\tau > 10^{-10}$ s can be considered quasi-stable. Those include the weak-decay particles like the neutral hadrons $n, \Lambda, K^0_L, ...$ and charged particles $\mu^{\pm}$, $\pi^{\pm}, K^{\pm}, ...$

- Short-lived resonances: particles undergoing a decay of typical electromagnetic or strong strength, such as $\pi^0, \rho^{0,\pm}...$ and very massive particles like $Z, W^{\pm}, t$ will decay "instantaneously". They can only be "seen" from their decay products and hopefully via a reconstructed resonance.

- Displaced vertex: particles of a lifetime $\tau \sim 10^{-12}$ s, such as $B^{0,\pm}$, $D^{0,\pm}$, $\tau^{\pm}$, may travel a distinguishable distance ($c\tau \sim 100$ μm.) before decaying into charged tracks, and thus result in a displaced secondary vertex.

- Things not "seen": those that do not participate in electromagnetic nor strong interactions, but long-lived as least like the quasi-stable particles will escape from

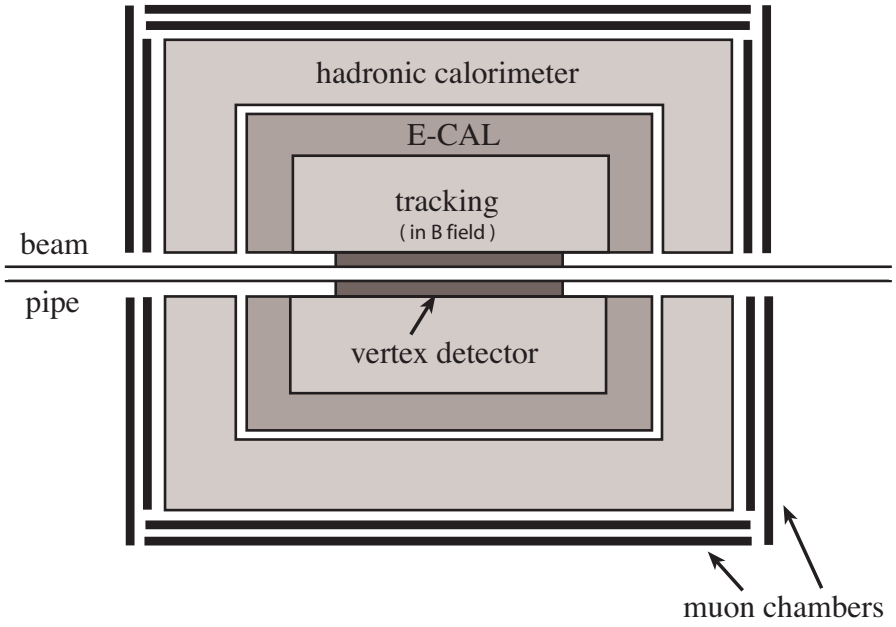

Figure B.2: Modern multi-purpose detector at colliders [234].

detection, such as the neutrinos ν. Their presence can be inferred from the measure of *missing energy*, as we will see soon.

The different parts of the detector and the electronic system allow to measure the energy, momentum, and other particle's properties, and record the events data.

- Tracking: the tracking chamber determines the trajectories of traversing charged particles and their electromagnetic energy loss. When combined with a magnetic field they can be used to measure a charged particle's momentum, by measuring the trajectory's curvature.

- Electromagnetic calorimeter: high energy electrons and photons lead to cascade electromagnetic showers due to bremsstrahlung and pair production. The ECAL measures this energy deposit.

- Hadron calorimeter: The HCAL measures the showers of subsequent hadrons developed from the high energy incident hadrons (the jets).

- Triggering: The trigger is the decision-making process to keep or reject events to be recorded. It can be designed with many criteria: particle identification, multiplicity, kinematics, event topology, etc.

B.2.3. Kinematics at hadron colliders

In performing parton model calculations for hadronic collisions like in (B.3) the partonic c.m. frame is not the same as the hadronic c.m. frame, e. g. the lab frame for the collider. Let's consider a collision between two hadrons A and B with four-momenta $P_A = (E_A, 0, 0, p_A)$ and $P_B = (E_A, 0, 0, -p_A)$ in the lab frame. The two partons participating in the subprocess have momenta $p_1 = x_1 P_A$ and $p_2 = x_2 P_B$. The fractions x_1 and x_2 are called *scaling* variables. The parton system moves in the lab frame with a four-momentum

$$P_{cm} = [(x_1 + x_2)E_A,\ 0,\ 0,\ (x_1 - x_2)p_A] \quad (E_A \approx p_A), \tag{B.4}$$

or with a speed $\beta_{cm} = (x_1 - x_2)/(x_1 + x_2)$, or with a rapidity $y_{cm} = \frac{1}{2} \ln \frac{x_1}{x_2}$.

Let's consider a final state particle of momentum $p^\mu = (E, \vec{p})$ in the lab frame. Since the c.m. frame of the two colliding partons is *a priori* undetermined with respect to the lab frame, the scattering polar angle θ in these two frames is not a good observable to describe theory and the experiment. This is why one needs to define kinematical variables that are invariant under unknown longitudinal boosts.

Transverse momentum and the azimuthal angle

Since the ambiguous motion between the parton c.m. frame and the hadron lab frame is along the longitudinal beam direction ($\vec{z}$), variables involving only the transverse components are invariant under longitudinal boosts. It is convenient to write the phase-space element in cylindrical coordinates as

$$\frac{d^3\vec{p}}{E} = dp_x dp_y \frac{dp_z}{E} = p_T dp_T d\phi\ \frac{dp_z}{E}, \tag{B.5}$$

where ϕ is the azimuthal angle about the $\vec{z}$ axis, and

$$p_T = \sqrt{p_x^2 + p_y^2} = p \sin\theta \tag{B.6}$$

is the transverse momentum. Both p_T and ϕ are boost-invariant, and so is dp_z/E.

The invariant mass variable

Consider an unstable particle V produced by $a + b$ and decaying to $1 + 2 + ... + n$. One can find this particle by discovering a resonant signal in the $s = (p_a + p_b)^2$ channel. For a weakly coupled particle $\Gamma_V \ll M_V$ and according to the Breit-Wigner resonance (A.6), the amplitude develops a kinematical peak near the pole mass value at

$$(p_a + p_b)^2 = (\ \sum_i^n p_i\ )^2 \approx M_V^2. \tag{B.7}$$

This is called the invariant mass, and is the most effective observable for discovering a resonance if either the initial momenta or the final momenta can be fully reconstructed.

The transverse mass variable

When the momenta of the outgoing particles cannot be fully reconstructed, as is the case with final-state neutrinos, one needs to define new suitable variables. An important example of a two-body decay in this thesis is the pure leptonic decay $W \to e\nu$. The invariant mass of the leptonic system is

$$m_{e\nu}^2 = (E_e + E_\nu)^2 - (\vec{p}_{eT} + \vec{p}_{\nu T})^2 - (p_{ez} + p_{\nu z})^2. \tag{B.8}$$

The neutrino cannot be directly observed by the detector and only its transverse momentum can be inferred by the imbalance of the observed momenta,

$$\vec{\not{p}_T} = -\sum \vec{p_T}(observed), \tag{B.9}$$

called missing transverse momentum, identified as $\not{p}_T = p_{\nu T}$. Missing transverse energy is similarly defined, and $\not{E}_T = E_\nu$.

In the case of final states with neutrinos, we find the invariant mass variable cannot be reconstructed, so one needs to ignore the (unknown) longitudinal motion of the leptonic system (or in this example the W boson) and define a transverse mass of the system [237]

$$\begin{aligned} m_{e\nu T}^2 &= (E_{eT} + E_{\nu T})^2 - (\vec{p}_{eT} + \vec{p}_{\nu T})^2 \\ &\approx 2\vec{p}_{eT} \cdot \vec{p}_{\nu T} \approx 2E_{eT}\not{E}_T\ (1 - \cos\phi_{e\nu}), \end{aligned} \tag{B.10}$$

where $\phi_{e\nu}$ is the opening angle between the electron and the neutrino in the transverse plane. When a W boson is produced with no transverse motion $E_{eT} = \not{E}_T = m_{e\nu T}/2$. The transverse mass variable is invariant under longitudinal boosts, and it reaches the maximum $m_{e\nu T} = m_{e\nu}$, for $p_{ez} = p_{\nu z}$, so that there is no longitudinal motion for the electron and the neutrino when boosting to the W-rest frame. In general,

$$0 \leq m_{e\nu T} \leq m_{e\nu}. \tag{B.11}$$

The Breit-Wigner resonance at $m_{e\nu} = m_W$ naturally leads to a kinematical peak near $m_{e\nu T} \approx m_W$. In the narrow width approximation (sec.A.1.2), $m_{e\nu T}$ is cut off sharply at m_W. In practice, the distribution extends beyond m_W because of the finite width Γ_W.

Appendix C

Neutrino telescopes phenomenology

In this appendix I collect some basic concepts on neutrino astronomy, which are used in chapter 7. It reviews the relevant observables in neutrino telescopes, the detection principles and the incident neutrino fluxes on the Earth.

C.1. Observables

The relevant observable in neutrino telescopes is the number of detected neutrinos, identifying their flavors, incoming direction and energies, in order to do neutrino astronomy and to learn about the neutrino-nucleon interaction cross-sections, where the new physics could be encoded.

The number of detected neutrinos depends on the number of target nucleons in the detector volume, the neutrino-nucleon interaction cross-section, and the neutrino flux reaching the detector.

The aim of our work in chapter 7 will be to probe the effects on the neutrino fluxes propagating through the Earth, due to the change in the interaction cross-sections produced by the existence of the Majorana neutrino N with the effective interactions introduced in chapter 3.

C.1.1. Number of events

As will be explained in sec.C.3.1, the IceCube neutrino telescope experiment detects the Cherenkov light produced by charged leptons created by neutrinos arriving into the detector volume via the charged- and neutral-current interactions studied in sec.1.4.3.

To first approximation, a neutrino of energy E incident on a side of area $A = L^2$ will be detected provided it interacts with some nucleon $\mathcal{N}$ within the detector volume, i.e. within the instrumented distance L (here we think of an L^3 instrumented volume). The probability for that interaction to occur can be given as

$$P(E) = 1 - e^{\frac{-L}{\lambda(E)}} \simeq \frac{L}{\lambda(E)} \tag{C.1}$$

where the neutrino mean free path[1] in the ice is $\lambda(E) = (\rho_{ice} N_A \sigma_{\nu\mathcal{N}}(E))^{-1}$, with $\rho_{ice} = 0.9\ gr\ cm^{-3}$, the Avogadro constant given as $N_A = 6.022 \times 10^{23}\ gr^{-1}$ and $\sigma_{\nu\mathcal{N}}(E)$ is the neutrino-nucleon cross-section at energy E.

If a neutrino flux $\Phi(E)$ (neutrinos per GeV per cm^2 per second) crosses a detector area $A(E)$, then the number of events produced (with an energy detection threshold E_{th}) in an operation time T, can be taken as:

$$N_{events} = T \int_{E_{th}} A(E) P(E) \Phi(E) dE \simeq T \int_{E_{th}} A(E) L\ \rho_{ice} N_A \sigma_{\nu\mathcal{N}}(E)\ \Phi(E) dE, \quad \text{(C.2)}$$

where one identifies the "effective" detector volume $V_{eff} = A(E)L$ [238]. Depending on the neutrino's energy considered, and on the neutrino flavor one is interested in detecting, the effective volume can be taken equal to the instrumented volume (meaning the volume covered by the photomultipliers) or more, as will be discussed in sec.C.3.1.

As we will be interested in counting the tau-neutrinos flux traversing the Earth, we will need to take into account the amount of matter traversed by the neutrinos in their journey. That quantity is related to the nadir angle of detection θ as schematically shown in fig.7.3a.

Then we write the number of events after an operation time T as

$$N_{events} = T\ n_T \int d\Omega \int dE\ \Phi(E, \theta)\ \sigma_{\nu\mathcal{N}}(E) \quad \text{(C.3)}$$

taking n_T as the number of target nucleons in the effective detector volume considered ($n_T = V_{eff} \rho_{ice} N_A$). The "surviving" flux $\Phi(E, \theta)$ (neutrinos per $GeV\ cm^2\ sr\ s$) reaching the telescope's volume at angle θ with an energy E will be our quantity of interest, as it depends on the distinct interactions the neutrinos encounter while traveling through the Earth, and on regeneration effects, as well as on the incident neutrino flux on the Earth from the atmosphere and outer space, as I will discuss in the next section.

In chapter 7 we are interested in the tau-neutrino flux ϕ_{ν_τ} detected in the IceCube telescope. As will be seen in the following, the atmospheric ν_τ sources are very feeble and the only efficient ν_τ source is the oscillation over cosmic distances of the ν_e and ν_μ produced in astrophysical sources.

C.2. Incident neutrino fluxes

The incident neutrino flux on the Earth comes from various origins, and I will give a very brief introduction on the subject in this section.

C.2.1. High energy cosmic rays

Cosmic rays (CR) are particles hitting the Earth, mostly composed by ionized nuclei (90% protons, 9% alpha particles and the remaining 1% are heavy nuclei).

[1] Or interaction length.

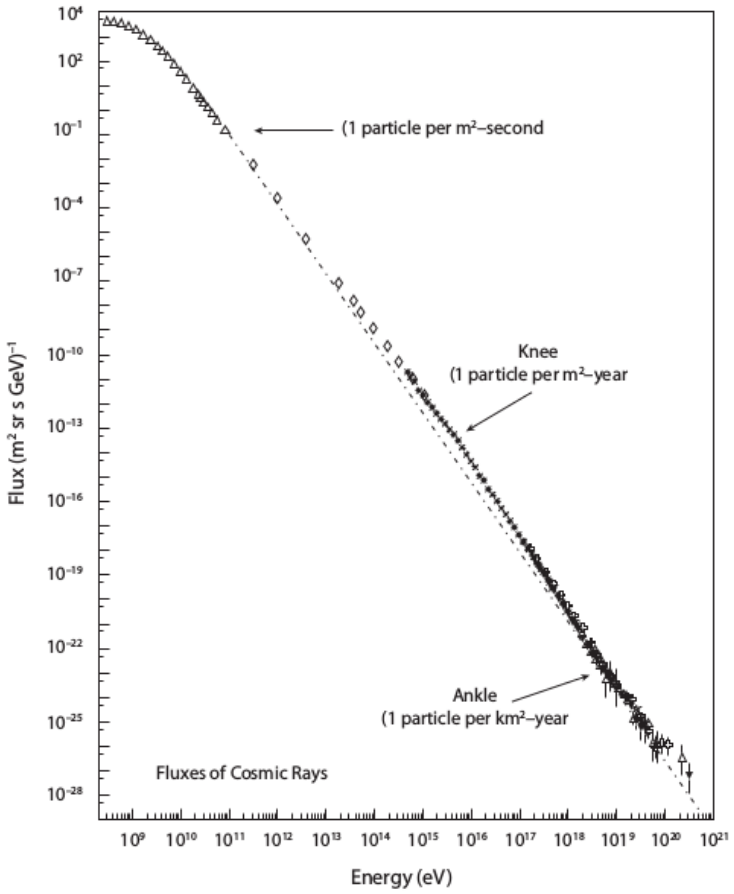

Figure C.1: Cosmic rays flux versus energy. Taken from [239].

The spectrum of cosmic rays has been well measured up to energies near 10^{20} eV (10^{8} TeV in the laboratory frame) where the experiments become limited by poor statistics. The spectrum consists of a series of power laws that change at energies called as the "knee" and "ankle" as shown in fig.C.1.

Below the knee, it is believed particles can be accelerated principally by supernova remnants (SNR) in our galaxy. The shock fronts powered by supernova explosions propagate into the interstellar medium, and by repeated scattering processes across the shock front particles can gain energy (this is called "first-order Fermi acceleration"). Between the knee and the ankle, the CR origin is less known, and the prevailing explanations claim they have an extra-galactic origin, possibly gamma ray bursts (GRB) or active galactic nuclei (AGN). Beyond the ankle, in the ultra-high energy zone, the cosmic rays are believed to be mostly protons (or nuclei) with energies above an EeV, of extra-galactic origin, given that the gyro-radius of the proton exceeds the size of the galaxy.

Waxman-Bahcall diffuse neutrino flux

High-energy neutrino production is thought to be associated with the interactions of high-energy protons that produce energetic charged pions by $p\gamma$ or by $p\bar{p}$ interactions. In sources that are optically thin to meson-nucleon interactions, the $\pi^+ \to \mu^+\nu_\mu$ decays and subsequent $\mu^+ \to e^+\nu_e\,\bar{\nu}_\mu$ decays (and corresponding π^- decay chain) lead to high-energy neutrinos. Assuming that the ultra-high energy cosmic rays are extragalactic protons and lose their energy in interactions producing pions, as the ones above, Waxman and Bahcall (WB) [240,241] estimated a neutrino flux from astrophysical sources to be

$$E_\nu^2\Phi_{WB} \equiv E_\nu^2\Phi_\nu \lesssim 2\times 10^{-8}\ GeV\ cm^{-2}\ sr^{-1}\ s^{-1}. \tag{C.4}$$

Cosmogenic neutrino flux

Over a $50\times 10^{18}\ eV$ ($50\ EeV$) energy threshold, the cosmic ray protons will undergo inelastic interactions, mainly $p\gamma \to \Delta^+ \to n\pi^+$ and $p\pi^0$ on the cosmic microwave background (CMB). This threshold is known as the Greisen-Zatsepin-Kuzmin energy (E_{GZK}) [242,243]. At these energies the gyro-radius of a proton in the galactic magnetic field is larger than the size of the galaxy, and therefore it is expected that these cosmic ray protons are of extra-galactic origin. Since the attenuation caused by this reaction has a length scale of about 50 Mpc [2], a strong suppression in the cosmic ray spectrum is expected above E_{GZK} ("the GZK cut"). The decays of charged pions produced in the GZK process are a source of cosmogenic neutrinos, predicted by Berezinski and Zatsepin (BZ) [244].

Both cosmogenic and Waxman-Bahcall fluxes are considered to arrive at the Earth with a 1 : 1 : 1 (electron: muon: tau) flavor composition, due to oscillation during the traveled distances.

Atmospheric neutrinos

The interactions of cosmic rays with the nucleons $\mathcal{N}$ in the atmosphere produce pions and kaons that decay to ν_μ, ν_e and their anti-neutrinos:

$$\begin{aligned} p\,\mathcal{N} &\to \pi^+(K^+...) \to \nu_\mu\mu^+ \to \nu_\mu e^+\nu_e\bar{\nu}_\mu \\ n\,\mathcal{N} &\to \pi^-(K^-...) \to \bar{\nu}_\mu\mu^- \to \bar{\nu}_\mu e^-\bar{\nu}_e\nu_\mu. \end{aligned} \tag{C.5}$$

On average there are twice as many ν_μ as ν_e at GeV energies, although the ν_e tend to be at somewhat lower energies since they are produced only on a secondary decay. These are called "conventional" atmospheric neutrinos. This flux is negligible for neutrino energies over $10^5\ GeV$.

The atmospheric neutrino flux is well understood: the normalizations are known to 20% or better, and ratios of fluxes are known to 5%. For energies beyond $10^5\ GeV$, there are also neutrinos coming from charmed and bottom mesons decays, which can

[2] $50\ Mpc \sim 150\times 10^{22} m$.

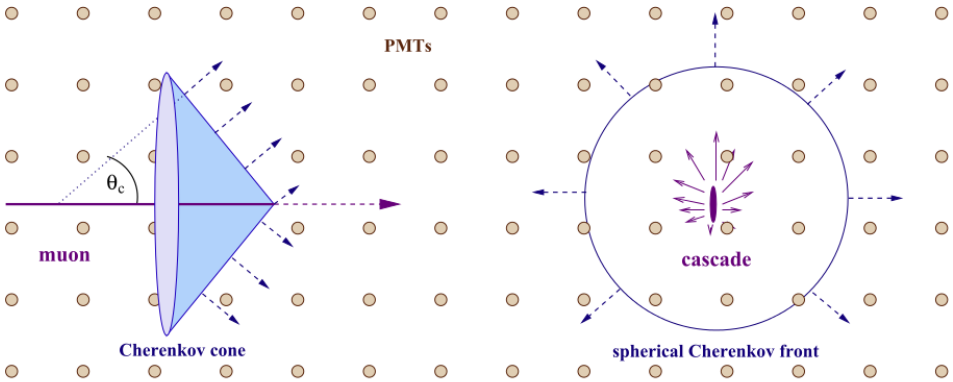

Figure C.2: Detection principles for muon tracks (left) and cascades (right) in underwater/ice detectors. Taken from [246].

produce tau-neutrinos (in a ten times smaller rate than muon neutrinos). This is called the "prompt" flux [60, 245].

The flavor ratio of conventional atmospheric neutrinos before oscillation is $1 : 2 : 0$ (electron: muon: tau). The flux of tau-neutrinos from atmospheric neutrino oscillation on the baseline of the Earth's diameter peaks near 25 GeV, which is much lower than the PeV energy at which IceCube can identify tau-neutrinos. The prompt neutrino flux has a nonzero tau-neutrino component, but the prompt tau-neutrino flux is an order of magnitude lower than the prompt muon-neutrino flux, and is below IceCube's sensitivity.

C.3. IceCube telescope

The IceCube neutrino detector is located at the Amundsen-Scott South Pole Station near the geographic South Pole. The detector instruments one cubic kilometer of antarctic ice with 86 electrical cables, called strings, deployed on a hexagonal grid one square kilometer in area. Each string contains 60 Digital Optical Modules (DOMs) deployed between 1450 m and 2450 m deep. The DOM is a glass pressure vessel containing a 10-inch photomultiplier tube (PMT) with digitizing and time stamping electronics, and 12 LED flashers for in situ calibration. Eight of the strings near the center form the DeepCore sub-detector, with closer string-to-string and DOM-to-DOM spacing than the rest of the IceCube strings. The IceCube construction was complete as of December 2010, and its primary goal is to detect astrophysical neutrinos from potential cosmic ray acceleration sites such as active galactic nuclei, gamma ray bursts and supernovae.

C.3.1. Detection principles

IceCube is sensitive to all three flavors of neutrinos. When a neutrino interacts with a nucleus in the ice, the DOMs detect the Cherenkov light deposited by the interaction

and by the daughter particles. The amount of light and arrival time at each DOM are used to reconstruct the properties of the neutrino. In the case of a charged-current (CC) interaction, the neutrino flavor determines the event topology.

A muon-neutrino CC interaction inside or near the detector's instrumented volume results in a muon which deposits a "track" of light in the detector's PMTs as the muon passes through. An electron-neutrino CC interaction, as well as a neutral-current interaction of any flavor, results in a spherical "cascade" of light centered on the interaction point, since the electron quickly interacts with surrounding matter, as is shown in fig.C.2.

Muons from cosmic ray air showers dominate the background in the southern hemisphere sky, which is above IceCube's horizon. These muons appear as down going tracks which originate outside of the instrumented volume. Muons cannot penetrate the Earth, so the neutrinos produced in cosmic ray interactions are the background from the northern hemisphere sky.

Tau neutrinos detection topologies

A tau-neutrino CC interaction above about 1 PeV in energy may produce a "double-bang" signal; this happens when the initial cascade from the CC interaction producing a tau lepton and the final cascade from the tau decay can be resolved by IceCube. The two cascades would be connected by a track associated with the tau lepton. However, it is likely that only one of the cascades is fully contained in the detector, as shown in fig.C.3, where several additional tau-neutrino signals are shown. These are explained in detail in the following [247].

The signal topology for a τ lepton produced by a ν_τ CC interaction depends on the energy. One can write the tau decay length as $l_\tau \sim 50\ m \times (\frac{E_\tau}{10^6\ GeV})$. Thus, for energies beyond 20 PeV the tau lepton saturates the detector size. Depending on the energy of the produced tau lepton, its production or decay vertices can be observed, or both. As the tau lepton can decay leptonically through the channels $\tau \to e\bar{\nu}_e\nu_\tau$ ($\sim 18\%$) or $\tau \to \mu\bar{\nu}_\mu\nu_\tau$ ($\sim 18\%$) or mostly hadronically to neutral and charged pions and kaons ($\sim 64\%$), the topology of the produced events will also depend on the tau decay modes.

In the "double-bang" topology, an hadronic shower occurs when the tau is produced by CC interactions, then it travels a certain distance within the detector, and decays producing another shower, 82% of the time if it decays to e or hadronically. The "lollipop" topology occurs when the tau is produced outside the instrumented volume, and the penetrating track along with the decay shower are detected. The inverse is called "popillol" topology. A "sugardaddy" topology occurs when the tau is created outside the detector, but decays into a muon inside the detector, and the muon track is recorded. The only topology that is a clear signal of tau-neutrinos, almost without background, is the double-bang.

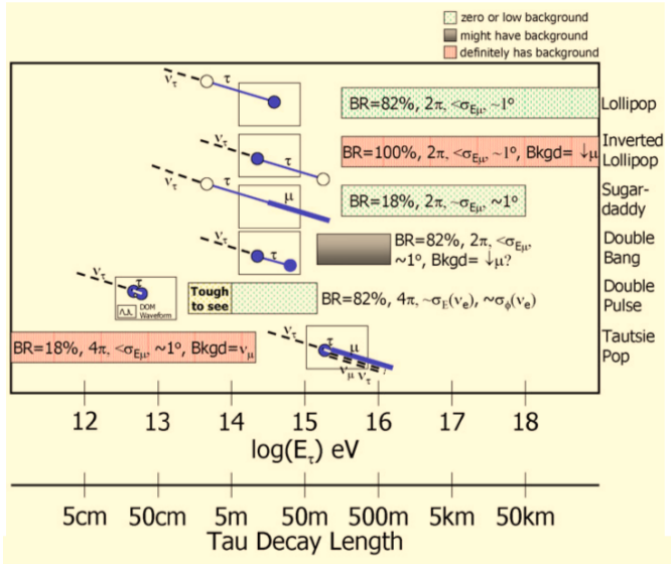

Figure C.3: Summary of ν_τ channels possibly accessible to IceCube, shown as a function of energy and approximate tau decay length, with indications of background level, acceptance, angular and energy resolutions, and specific anticipated background. Taken from [247].

C.4. N decay in the laboratory

Here in this section we follow the development shown in the book of T.K. Gaisser [215], in our case for the $N \to \gamma\nu$ decay, used in chapter 7. First we obtain the N decay width in its rest frame, and then boost the result to the laboratory frame. In the N rest frame we have the following expression:

$$\frac{1}{\Gamma_{\rm rest}} \frac{d\Gamma_{\rm rest}}{dx\, d\cos\theta_\nu} = 2\left(f_0(x) - P f_1(x)\cos\theta_\nu\right), \tag{C.6}$$

where θ_ν is the direction of motion of the final ν taken from the Majorana neutrino N moving direction, and $P = \cos\theta_P$ where θ_P is the angle between the Majorana neutrino spin direction in its rest frame, and its moving direction seen from the laboratory frame. The variable x represents the quotient between the final neutrino energy in the rest frame of the N and the mass of the Majorana neutrino: $x = k^0/m_N$. The functions $f_0(x)$ and $f_1(x)$ are

$$f_0(x) = x(1-x)\delta(x-1/2)$$

$$f_1(x) = x^2\delta(x-1/2), \tag{C.7}$$

To obtain the corresponding expression in the laboratory frame, we make the appropriate Lorentz transformations. Denoting by E_ν and E_N the laboratory energies of the final

neutrino and the Majorana neutrino, respectively, we have

$$z = x(1 - \beta_N \cos\theta_\nu), \tag{C.8}$$

with $z = E_\nu/E_N$ and $\beta_N = \sqrt{1 - {m_N}^2/E_N^2} \simeq 1$.

We implement the Lorentz transformation with the help of the δ-function, yielding

$$\frac{1}{\Gamma_{\rm LAB}} \frac{d\Gamma_{\rm LAB}}{dz\, dx\, d\cos\theta_\nu} = 2\left(f_0(x) - P f_1(x)\cos\theta_\nu\right)\delta\left[z - x\left(1 + \beta_N \cos\theta_\nu\right)\right], \tag{C.9}$$

where $P = +1$ for the right-handed Majorana neutrinos.

We first integrate over θ_ν and next we integrate over x in the interval (x_{min}, x_{max}) with $x_{min} = z/(1+\beta_N)$ and $x_{max} = min(1, z/(1-\beta_N))$, obtaining

$$\frac{1}{\Gamma_{LAB}} \frac{d\Gamma_{LAB}}{dz} = 2(1-z)\Theta(1/2 - x(z)_{min})\Theta(x(z)_{max} - 1/2). \tag{C.10}$$

For the low mass range considered in this work the clearly dominant decay channel is the neutrino plus photon mode, and $\Gamma^{\rm tot}_{LAB}(E) = \sum_{i=e,\mu,\tau} \Gamma^{N\to\nu_i\gamma}_{LAB}(E)$. Then we consider the ν_τ decay channel, leading to the final ν_τ neutrinos distribution in the laboratory frame:

$$\frac{1}{\Gamma^{tot}_{LAB}(E)} \frac{d\Gamma^{N\to\nu_\tau\gamma}_{LAB}}{dz} \equiv \frac{dn(z)}{dz}. \tag{C.11}$$

Thus, after the indicated integrations in the evolution equations, the useful expression that we obtain is

$$\frac{dn(z)}{dz} = \frac{dn(1-y)}{dy} = \frac{2}{3}y. \tag{C.12}$$

Here $y \equiv (1 - z)$.

Bibliography

[1] C. Patrignani *et al.* (Particle Data Group), *Review of Particle Physics*, Chin. Phys. **C40**, 100001 (2016).

[2] L. Duarte, J. Peressutti and O. A. Sampayo, *Majorana neutrino decay in an Effective Approach*, Phys. Rev. **D92**, 093002 (2015), arXiv:1508.01588 [hep-ph].

[3] L. Duarte, I. Romero, J. Peressutti and O. A. Sampayo, *Effective Majorana neutrino decay*, Eur. Phys. J. **C76**, 453 (2016), arXiv:1603.08052 [hep-ph].

[4] L. Duarte, G. A. González-Sprinberg and O. A. Sampayo, *Majorana neutrinos production at LHeC in an effective approach*, Phys. Rev. **D91**, 053007 (2015), arXiv:1412.1433 [hep-ph].

[5] L. Duarte, J. Peressutti and O. A. Sampayo, *Not-that-heavy Majorana neutrino signals at the LHC* (2016), arXiv:1610.03894 [hep-ph].

[6] L. Duarte, I. Romero, G. Zapata and O. A. Sampayo, *Effects of Majorana Physics on the UHE ν_τ Flux Traversing the Earth*, Eur. Phys. J. **C77**, 68 (2017), arXiv:1609.07661 [hep-ph].

[7] S. M. Bilenky, *Neutrino. History of a unique particle*, Eur. Phys. J. **H38**, 345 (2013), arXiv:1210.3065 [hep-ph].

[8] P. Minkowski, *$\mu \to e\gamma$ at a rate of one out of 1-billion muon decays?*, Phys.Lett. **B67**, 421 (1977).

[9] M. Gell-Mann, P. Ramond and R. Slansky, *Complex Spinors and Unified Theories*, Conf.Proc. **C790927**, 315 (1979), arXiv:1306.4669 [hep-th].

[10] T. Yanagida, *Horizontal Symmetry and Masses of Neutrinos*, Prog.Theor.Phys. **64**, 1103 (1980).

[11] R. N. Mohapatra and G. Senjanovic, *Neutrino Mass and Spontaneous Parity Violation*, Phys.Rev.Lett. **44**, 912 (1980).

[12] A. Pilaftsis, *Radiatively induced neutrino masses and large Higgs neutrino couplings in the standard model with Majorana fields*, Z. Phys. **C55**, 275 (1992), arXiv:hep-ph/9901206 [hep-ph].

[13] D. Tommasini, G. Barenboim, J. Bernabeu and C. Jarlskog, *Nondecoupling of heavy neutrinos and lepton flavor violation*, Nucl.Phys. **B444**, 451 (1995), arXiv:hep-ph/9503228 [hep-ph].

[14] J. Gluza, *On teraelectronvolt Majorana neutrinos*, Acta Phys. Polon. **B33**, 1735 (2002), arXiv:hep-ph/0201002 [hep-ph].

[15] F. del Aguila, S. Bar-Shalom, A. Soni and J. Wudka, *Heavy Majorana Neutrinos in the Effective Lagrangian Description: Application to Hadron Colliders*, Phys.Lett. **B670**, 399 (2009), arXiv:0806.0876 [hep-ph].

[16] E. Ma and J. T. Pantaleone, *Heavy Majorana neutrino production*, Phys.Rev. **D40**, 2172 (1989).

[17] A. Datta, M. Guchait and A. Pilaftsis, *Probing lepton number violation via Majorana neutrinos at hadron supercolliders*, Phys.Rev. **D50**, 3195 (1994), arXiv:hep-ph/9311257 [hep-ph].

[18] J. Gluza and M. Zralek, *CP violation in the heavy neutrinos production process* $e + e- \to N(1)N(2)$, Phys.Rev. **D51**, 4707 (1995), arXiv:hep-ph/9409224 [hep-ph].

[19] A. Hofer and L. Sehgal, *Pair production and correlated decay of heavy Majorana neutrinos in e+ e- collisions*, Phys.Rev. **D54**, 1944 (1996), arXiv:hep-ph/9603240 [hep-ph].

[20] G. Cvetic, C. Kim and C. Kim, *Heavy Majorana neutrinos at e+ e- colliders*, Phys.Rev.Lett. **82**, 4761 (1999), arXiv:hep-ph/9812525 [hep-ph].

[21] J. Almeida, F.M.L., Y. D. A. Coutinho, J. A. Martins Simoes and M. do Vale, *On a signature for heavy Majorana neutrinos in hadronic collisions*, Phys.Rev. **D62**, 075004 (2000), arXiv:hep-ph/0002024 [hep-ph].

[22] G. Belanger, F. Boudjema, D. London and H. Nadeau, *Inverse neutrinoless double beta decay revisited*, Phys.Rev. **D53**, 6292 (1996), arXiv:hep-ph/9508317 [hep-ph].

[23] A. Atre, T. Han, S. Pascoli and B. Zhang, *The Search for Heavy Majorana Neutrinos*, JHEP **0905**, 030 (2009), arXiv:0901.3589 [hep-ph].

[24] K. N. Abazajian *et al.*, *Light Sterile Neutrinos: A White Paper* (2012), arXiv:1204.5379 [hep-ph].

[25] M. E. Peskin and D. V. Schroeder, *An Introduction to quantum field theory*, Reading, USA: Addison-Wesley (1995) 842 p(1995).

[26] M. Maggiore, *A Modern introduction to quantum field theory*, Oxford University Press **Oxford Series in Physics, 12.** (2005).

[27] L. Alvarez-Gaume and M. A. Vazquez-Mozo, *An invitation to quantum field theory*, Lect. Notes Phys. **839**, 1 (2012).

[28] S. Willenbrock, *Physics in D=4. Proceedings, Theoretical Advanced Study Institute in elementary particle physics, TASI 2004, Boulder, USA, June 6-July 2, 2004*, 3 (2004), arXiv:hep-ph/0410370 [hep-ph].

[29] A. Pich, *Proceedings, High-energy Physics. Proceedings, 18th European School (ESHEP 2010): Raseborg, Finland, June 20 - July 3, 2010*, 1 (2012), arXiv:1201.0537 [hep-ph].

[30] R. N. Mohapatra and P. B. Pal, *Massive Neutrinos in Physics and Astrophysics.Third Edition.*, World Sci. Lect. Notes Phys.72.

[31] J. Goldstone, *Field Theories with Superconductor Solutions*, Nuovo Cim. **19**, 154 (1961).

[32] Y. Nambu, *Quasiparticles and Gauge Invariance in the Theory of Superconductivity*, Phys. Rev. **117**, 648 (1960).

[33] J. Goldstone, A. Salam and S. Weinberg, *Broken Symmetries*, Phys. Rev. **127**, 965 (1962).

[34] F. Englert and R. Brout, *Broken Symmetry and the Mass of Gauge Vector Mesons*, Phys. Rev. Lett. **13**, 321 (1964).

[35] P. W. Higgs, *Spontaneous Symmetry Breakdown without Massless Bosons*, Phys. Rev. **145**, 1156 (1966).

[36] G. Guralnik, C. Hagen and T. Kibble, *Global Conservation Laws and Massless Particles*, Phys. Rev. Lett. **13**, 585 (1964).

[37] T. Kibble, *Symmetry breaking in nonAbelian gauge theories*, Phys. Rev. **155**, 1554 (1967).

[38] Y. Nambu, *Axial vector current conservation in weak interactions*, Phys. Rev. Lett. **4**, 380 (1960).

[39] S. Glashow, *Partial Symmetries of Weak Interactions*, Nucl. Phys. **22**, 579 (1961).

[40] S. Weinberg, *A Model of Leptons*, Phys. Rev. Lett. **19**, 1264 (1967).

[41] A. Salam, *Elementary Particle Theory* (N. Svartholm .Alquimistand Wiksells, Stockholm, 1968) p. 367.

[42] G. 't Hooft, *Renormalization of Massless Yang-Mills Fields*, Nucl. Phys. **B33**, 173 (1971).

[43] N. Cabibbo, *Unitary Symmetry and Leptonic Decays*, Phys. Rev. Lett. **10**, 531 (1963).

[44] M. Kobayashi and T. Maskawa, *CP Violation in the Renormalizable Theory of Weak Interaction*, Prog. Theor. Phys. **49**, 652 (1973).

[45] S. Glashow, J. Iliopoulos and L. Maiani, *Weak Interactions with Lepton-Hadron Symmetry*, Phys. Rev. **D2**, 1285 (1970).

[46] S. L. Adler, *Axial vector vertex in spinor electrodynamics*, Phys. Rev. **177**, 2426 (1969).

[47] J. S. Bell and R. Jackiw, *A PCAC puzzle: pi0 –> gamma gamma in the sigma model*, Nuovo Cim. **A60**, 47 (1969).

[48] K. G. Wilson, *Renormalization group and critical phenomena. 1. Renormalization group and the Kadanoff scaling picture*, Phys. Rev. **B4**, 3174 (1971).

[49] K. G. Wilson, *Renormalization group and critical phenomena. 2. Phase space cell analysis of critical behavior*, Phys. Rev. **B4**, 3184 (1971).

[50] K. G. Wilson, *The renormalization group and critical phenomena*, Rev. Mod. Phys. **55**, 583 (1983).

[51] C. P. Burgess, *Introduction to Effective Field Theory*, Ann. Rev. Nucl. Part. Sci. **57**, 329 (2007), arXiv:hep-th/0701053 [hep-th].

[52] J. Wudka, *Proceedings, 7th Mexican Workshop on Particles and Fields (MWPF 1999): Merida, Mexico, November 10-17, 1999*, AIP Conf. Proc. **531**, 81 (2000), [,81(1999)], arXiv:hep-ph/0002180 [hep-ph].

[53] A. Pich, *Probing the standard model of particle interactions. Proceedings, Summer School in Theoretical Physics, NATO Advanced Study Institute, 68th session, Les Houches, France, July 28-September 5, 1997. Pt. 1, 2*, 949 (1998), arXiv:hep-ph/9806303 [hep-ph].

[54] S. Weinberg, *Baryon and Lepton Nonconserving Processes*, Phys. Rev. Lett. **43**, 1566 (1979).

[55] W. Buchmuller and D. Wyler, *Effective Lagrangian Analysis of New Interactions and Flavor Conservation*, Nucl. Phys. B **268**, 621 (1986).

[56] B. Grzadkowski, M. Iskrzynski, M. Misiak and J. Rosiek, *Dimension-Six Terms in the Standard Model Lagrangian*, JHEP **1010**, 085 (2010), arXiv:1008.4884 [hep-ph].

[57] C. Giunti and C. W. Kim, *Fundamentals of Neutrino Physics and Astrophysics*, Oxford, UK: Univ. Pr. 710 p(2007).

[58] B. Kayser, F. Gibrat-Debu and F. Perrier, *The Physics of massive neutrinos*, World Sci. Lect. Notes Phys. **25**, 1 (1989).

[59] S. M. Bilenky and C. Giunti, *Neutrinoless Double-Beta Decay: a Probe of Physics Beyond the Standard Model*, Int. J. Mod. Phys. **A30**, 1530001 (2015), arXiv:1411.4791 [hep-ph].

[60] V. Barger, D. Marfatia and K. Whisnant, *The physics of neutrinos* (Princeton Univ. Pr., Princeton, USA, 2012) ISBN 9780691128535, `http://press.princeton.edu/titles/9913.html`.

[61] C. L. Cowan, F. Reines, F. B. Harrison, H. W. Kruse and A. D. McGuire, *Detection of the free neutrino: A Confirmation*, Science **124**, 103 (1956).

[62] G. Danby, J. M. Gaillard, K. A. Goulianos, L. M. Lederman, N. B. Mistry, M. Schwartz and J. Steinberger, *Observation of High-Energy Neutrino Reactions and the Existence of Two Kinds of Neutrinos*, Phys. Rev. Lett. **9**, 36 (1962).

[63] B. Pontecorvo, *Mesonium and anti-mesonium*, Sov. Phys. JETP **6**, 429 (1957), [Zh. Eksp. Teor. Fiz.33,549(1957)].

[64] B. Pontecorvo, *Inverse beta processes and nonconservation of lepton charge*, Sov. Phys. JETP **7**, 172 (1958), [Zh. Eksp. Teor. Fiz.34,247(1957)].

[65] Z. Maki, M. Nakagawa and S. Sakata, *Remarks on the unified model of elementary particles*, Prog. Theor. Phys. **28**, 870 (1962).

[66] R. Davis, Jr., D. S. Harmer and K. C. Hoffman, *Search for neutrinos from the sun*, Phys. Rev. Lett. **20**, 1205 (1968).

[67] J. N. Bahcall, *Solar neutrinos. I: Theoretical*, Phys. Rev. Lett. **12**, 300 (1964).

[68] J. N. Bahcall, N. A. Bahcall and G. Shaviv, *Present status of the theoretical predictions for the Cl-36 solar neutrino experiment*, Phys. Rev. Lett. **20**, 1209 (1968).

[69] V. N. Gribov and B. Pontecorvo, *Neutrino astronomy and lepton charge*, Phys. Lett. **B28**, 493 (1969).

[70] Q. R. Ahmad *et al.* (SNO), *Measurement of the rate of* $\nu_e + d \rightarrow p + p + e^-$ *interactions produced by* ^8B *solar neutrinos at the Sudbury Neutrino Observatory*, Phys. Rev. Lett. **87**, 071301 (2001), arXiv:nucl-ex/0106015 [nucl-ex].

[71] Q. R. Ahmad *et al.* (SNO), *Measurement of day and night neutrino energy spectra at SNO and constraints on neutrino mixing parameters*, Phys. Rev. Lett. **89**, 011302 (2002), arXiv:nucl-ex/0204009 [nucl-ex].

[72] Q. R. Ahmad *et al.* (SNO), *Direct evidence for neutrino flavor transformation from neutral current interactions in the Sudbury Neutrino Observatory*, Phys. Rev. Lett. **89**, 011301 (2002), arXiv:nucl-ex/0204008 [nucl-ex].

[73] K. S. Hirata *et al.* (Kamiokande-II), *Proceedings: Workshop on Elementary Particle Picture of the Universe, 2nd, Tsukuba, Japan, Feb 4-6, 1988*, Phys. Lett. **B205**, 416 (1988), [447(1988)].

[74] K. S. Hirata *et al.* (Kamiokande-II), *Observation of a small atmospheric muon-neutrino / electron-neutrino ratio in Kamiokande*, Phys. Lett. **B280**, 146 (1992).

[75] D. Casper *et al.*, *Measurement of atmospheric neutrino composition with IMB-3*, Phys. Rev. Lett. **66**, 2561 (1991).

[76] R. Becker-Szendy *et al.*, *A Search for muon-neutrino oscillations with the IMB detector*, Phys. Rev. Lett. **69**, 1010 (1992).

[77] Y. Fukuda *et al.* (Super-Kamiokande), *Measurement of the flux and zenith angle distribution of upward through going muons by Super-Kamiokande*, Phys. Rev. Lett. **82**, 2644 (1999), arXiv:hep-ex/9812014 [hep-ex].

[78] Y. Fukuda *et al.* (Super-Kamiokande), *Evidence for oscillation of atmospheric neutrinos*, Phys. Rev. Lett. **81**, 1562 (1998), arXiv:hep-ex/9807003 [hep-ex].

[79] V. N. Aseev *et al.* (Troitsk), *An upper limit on electron antineutrino mass from Troitsk experiment*, Phys. Rev. **D84**, 112003 (2011), arXiv:1108.5034 [hep-ex].

[80] P. A. R. Ade *et al.* (Planck), *Planck 2015 results. XIII. Cosmological parameters*, Astron. Astrophys. **594**, A13 (2016), arXiv:1502.01589 [astro-ph.CO].

[81] B. Pontecorvo, *Neutrino Experiments and the Problem of Conservation of Leptonic Charge*, Sov. Phys. JETP **26**, 984 (1968), [Zh. Eksp. Teor. Fiz.53,1717(1967)].

[82] S. M. Bilenky and B. Pontecorvo, *Lettere Nuovo Cimento 17 (1976) 569-574, In *Pontecorvo, B.: Selected scientific works* 321-326*, Lett. Nuovo Cim. **17**, 569 (1976).

[83] J. Schechter and J. W. F. Valle, *Neutrino Masses in SU(2) x U(1) Theories*, Phys. Rev. **D22**, 2227 (1980).

[84] E. Ma, *Pathways to naturally small neutrino masses*, Phys. Rev. Lett. **81**, 1171 (1998), arXiv:hep-ph/9805219 [hep-ph].

[85] M. Magg and C. Wetterich, *Neutrino Mass Problem and Gauge Hierarchy*, Phys. Lett. **B94**, 61 (1980).

[86] T. P. Cheng and L.-F. Li, *Neutrino Masses, Mixings and Oscillations in SU(2) x U(1) Models of Electroweak Interactions*, Phys. Rev. **D22**, 2860 (1980).

[87] G. Lazarides, Q. Shafi and C. Wetterich, *Proton Lifetime and Fermion Masses in an SO(10) Model*, Nucl. Phys. **B181**, 287 (1981).

[88] R. N. Mohapatra and G. Senjanovic, *Neutrino Masses and Mixings in Gauge Models with Spontaneous Parity Violation*, Phys. Rev. **D23**, 165 (1981).

[89] R. Foot, H. Lew, X. G. He and G. C. Joshi, *Seesaw Neutrino Masses Induced by a Triplet of Leptons*, Z. Phys. **C44**, 441 (1989).

[90] G. Altarelli and F. Feruglio, *Neutrino masses and mixings: A theoretical perspective*, Phys. Rept. **320**, 295 (1999).

[91] F. del Aguila, J. A. Aguilar-Saavedra and R. Pittau, *Elementary particle physics. Proceedings, Corfu Summer Institute, CORFU2005, Corfu, Greece, September 4-26, 2005*, J. Phys. Conf. Ser. **53**, 506 (2006), arXiv:hep-ph/0606198 [hep-ph].

[92] T. Asaka, S. Blanchet and M. Shaposhnikov, *The nuMSM, dark matter and neutrino masses*, Phys. Lett. **B631**, 151 (2005), arXiv:hep-ph/0503065 [hep-ph].

[93] A. de Gouvêa and A. Kobach, *Global Constraints on a Heavy Neutrino*, Phys. Rev. **D93**, 033005 (2016), arXiv:1511.00683 [hep-ph].

[94] F. F. Deppisch, P. S. Bhupal Dev and A. Pilaftsis, *Neutrinos and Collider Physics*, New J. Phys. **17**, 075019 (2015), arXiv:1502.06541 [hep-ph].

[95] S. Antusch and O. Fischer, *Testing sterile neutrino extensions of the Standard Model at future lepton colliders*, JHEP **05**, 053 (2015), arXiv:1502.05915 [hep-ph].

[96] D. Decamp *et al.* (ALEPH), *Searches for new particles in Z decays using the ALEPH detector*, Phys. Rept. **216**, 253 (1992).

[97] P. Abreu *et al.* (DELPHI), *Search for neutral heavy leptons produced in Z decays*, Z. Phys. **C74**, 57 (1997), [Erratum: Z. Phys.C75,580(1997)].

[98] F. del Aguila, J. de Blas and M. Perez-Victoria, *Effects of new leptons in Electroweak Precision Data*, Phys. Rev. **D78**, 013010 (2008), arXiv:0803.4008 [hep-ph].

[99] P. Langacker and D. London, *Lepton Number Violation and Massless Nonorthogonal Neutrinos*, Phys.Rev. **D38**, 907 (1988).

[100] E. Nardi, E. Roulet and D. Tommasini, *Global analysis of fermion mixing with exotics*, Nucl. Phys. **B386**, 239 (1992).

[101] E. Nardi, E. Roulet and D. Tommasini, *New neutral gauge bosons and new heavy fermions in the light of the new LEP data*, Phys. Lett. **B344**, 225 (1995), arXiv:hep-ph/9409310 [hep-ph].

[102] E. Nardi, E. Roulet and D. Tommasini, *Limits on neutrino mixing with new heavy particles*, Phys.Lett. **B327**, 319 (1994), arXiv:hep-ph/9402224 [hep-ph].

[103] S. Bergmann and A. Kagan, *Z - induced FCNCs and their effects on neutrino oscillations*, Nucl.Phys. **B538**, 368 (1999), arXiv:hep-ph/9803305 [hep-ph].

[104] E. Fernandez-Martinez, J. Hernandez-Garcia and J. Lopez-Pavon, *Global constraints on heavy neutrino mixing*, JHEP **08**, 033 (2016), arXiv:1605.08774 [hep-ph].

[105] F. del Aguila and J. Aguilar-Saavedra, *l W nu production at CLIC: A Window to TeV scale non-decoupled neutrinos*, JHEP **0505**, 026 (2005), arXiv:hep-ph/0503026 [hep-ph].

[106] F. del Aguila, J. A. Aguilar-Saavedra and R. Pittau, *Heavy neutrino signals at large hadron colliders*, JHEP **10**, 047 (2007), arXiv:hep-ph/0703261 [hep-ph].

[107] K. Olive *et al.* (Particle Data Group), *Review of Particle Physics*, Chin.Phys. **C38**, 090001 (2014).

[108] R. E. Shrock, *New Tests For, and Bounds On, Neutrino Masses and Lepton Mixing*, Phys. Lett. **B96**, 159 (1980).

[109] R. E. Shrock, *General Theory of Weak Leptonic and Semileptonic Decays. 1. Leptonic Pseudoscalar Meson Decays, with Associated Tests For, and Bounds on, Neutrino Masses and Lepton Mixing*, Phys. Rev. **D24**, 1232 (1981).

[110] D. Liventsev *et al.* (Belle), *Search for heavy neutrinos at Belle*, Phys. Rev. **D87**, 071102 (2013), arXiv:1301.1105 [hep-ex].

[111] R. Aaij *et al.* (LHCb), *Search for Majorana neutrinos in $B^- \to \pi^+\mu^-\mu^-$ decays*, Phys. Rev. Lett. **112**, 131802 (2014), arXiv:1401.5361 [hep-ex].

[112] A. Gando *et al.* (KamLAND-Zen), *Search for Majorana Neutrinos near the Inverted Mass Hierarchy Region with KamLAND-Zen*, Phys. Rev. Lett. **117**, 082503 (2016), [Addendum: Phys. Rev. Lett.117,no.10,109903(2016)], arXiv:1605.02889 [hep-ex].

[113] K. S. Babu and C. N. Leung, *Classification of effective neutrino mass operators*, Nucl. Phys. **B619**, 667 (2001), arXiv:hep-ph/0106054 [hep-ph].

[114] A. de Gouvea and J. Jenkins, *A Survey of Lepton Number Violation Via Effective Operators*, Phys. Rev. **D77**, 013008 (2008), arXiv:0708.1344 [hep-ph].

[115] A. Aparici, K. Kim, A. Santamaria and J. Wudka, *Right-handed neutrino magnetic moments*, Phys. Rev. **D80**, 013010 (2009), arXiv:0904.3244 [hep-ph].

[116] C. Arzt, M. Einhorn and J. Wudka, *Patterns of deviation from the standard model*, Nucl.Phys. **B433**, 41 (1995), arXiv:hep-ph/9405214 [hep-ph].

[117] S. Antusch and O. Fischer, *Non-unitarity of the leptonic mixing matrix: Present bounds and future sensitivities*, JHEP **10**, 94 (2014), arXiv:1407.6607 [hep-ph].

[118] M. Drewes and B. Garbrecht, *Experimental and cosmological constraints on heavy neutrinos* (2015), arXiv:1502.00477 [hep-ph].

[119] D. Alva, T. Han and R. Ruiz, *Heavy Majorana neutrinos from $W\gamma$ fusion at hadron colliders*, JHEP **02**, 072 (2015), arXiv:1411.7305 [hep-ph].

[120] R. Mohapatra, *Particle physics implications of neutrinoless double beta decay*, Nucl.Phys.Proc.Suppl. **77**, 376 (1999), arXiv:hep-ph/9808284 [hep-ph].

[121] C. Macolino (GERDA), *Results on neutrinoless double beta decay from GERDA Phase I*, Mod.Phys.Lett. **A29**, 1430001 (2014), arXiv:1312.0562 [hep-ex].

[122] A. Faessler, M. González, S. Kovalenko and F. Šimkovic, *Arbitrary mass Majorana neutrinos in neutrinoless double beta decay*, Phys. Rev. **D90**, 096010 (2014), arXiv:1408.6077 [hep-ph].

[123] G. Aad *et al.* (ATLAS), *Search for nonpointing photons in the diphoton and E_T^{miss} final state in $\sqrt{s} = 7$ TeV proton-proton collisions using the ATLAS detector*, Phys. Rev. **D88**, 012001 (2013), arXiv:1304.6310 [hep-ex].

[124] J. C. Helo, M. Hirsch and S. Kovalenko, *Heavy neutrino searches at the LHC with displaced vertices*, Phys. Rev. **D89**, 073005 (2014), arXiv:1312.2900 [hep-ph].

[125] G. Aad *et al.* (ATLAS), *Search for massive, long-lived particles using multitrack displaced vertices or displaced lepton pairs in pp collisions at $\sqrt{s} = 8$ TeV with the ATLAS detector*, Phys. Rev. **D92**, 072004 (2015), arXiv:1504.05162 [hep-ex].

[126] G. Aad *et al.* (ATLAS), *Search for new phenomena in events with a photon and missing transverse momentum in pp collisions at $\sqrt{s} = 8$ TeV with the ATLAS detector*, Phys. Rev. **D91**, 012008 (2015), [Erratum: Phys. Rev.D92,no.5,059903(2015)], arXiv:1411.1559 [hep-ex].

[127] A. M. Gago, P. Hernández, J. Jones-Pérez, M. Losada and A. M. Briceño, *Probing the Type I Seesaw Mechanism with Displaced Vertices at the LHC*, Eur. Phys. J. **C75**, 470 (2015), arXiv:1505.05880 [hep-ph].

[128] S. Biswas, J. Chakrabortty and S. Roy, *Multi-photon signal in supersymmetry comprising non-pointing photon(s) at the LHC*, Phys. Rev. **D83**, 075009 (2011), arXiv:1010.0949 [hep-ph].

[129] S. Antusch, E. Cazzato and O. Fischer, *Displaced vertex searches for sterile neutrinos at future lepton colliders*, JHEP **12**, 007 (2016), arXiv:1604.02420 [hep-ph].

[130] B. Batell, M. Pospelov and B. Shuve, *Shedding Light on Neutrino Masses with Dark Forces*, JHEP **08**, 052 (2016), arXiv:1604.06099 [hep-ph].

[131] G. Pagliaroli, A. Palladino, F. L. Villante and F. Vissani, *Testing nonradiative neutrino decay scenarios with IceCube data*, Phys. Rev. **D92**, 113008 (2015), arXiv:1506.02624 [hep-ph].

[132] M. Masip and P. Masjuan, *Heavy-neutrino decays at neutrino telescopes*, Phys. Rev. **D83**, 091301 (2011), arXiv:1103.0689 [hep-ph].

[133] M. Ross-Lonergan, *Proceedings, Topical Research Meeting on Prospects in Neutrino Physics (NuPhys2013)*, J. Phys. Conf. Ser. **598**, 012028 (2015).

[134] M. Masip, P. Masjuan and D. Meloni, *Heavy neutrino decays at MiniBooNE*, JHEP **01**, 106 (2013), arXiv:1210.1519 [hep-ph].

[135] C. Dib, J. C. Helo, M. Hirsch, S. Kovalenko and I. Schmidt, *Heavy Sterile Neutrinos in Tau Decays and the MiniBooNE Anomaly*, Phys. Rev. **D85**, 011301 (2012), arXiv:1110.5400 [hep-ph].

[136] G. L. Fogli, E. Lisi, A. Mirizzi and D. Montanino, *Neutrino physics and astrophysics. Proceedings, 21st International Conference, Neutrino 2004, Paris, France, June 14-19, 2004*, Nucl. Phys. Proc. Suppl. **143**, 505 (2005).

[137] S.-H. Kim, K.-i. Takemasa, Y. Takeuchi and S. Matsuura, *Search for Radiative Decays of Cosmic Background Neutrino using Cosmic Infrared Background Energy Spectrum*, J. Phys. Soc. Jap. **81**, 024101 (2012), arXiv:1112.4568 [hep-ph].

[138] A. A. Aguilar-Arevalo *et al.* (MiniBooNE), *A Search for electron neutrino appearance at the* $\Delta m^2 \sim 1eV^2$ *scale*, Phys. Rev. Lett. **98**, 231801 (2007), arXiv:0704.1500 [hep-ex].

[139] A. A. Aguilar-Arevalo *et al.* (MiniBooNE), *Unexplained Excess of Electron-Like Events From a 1-GeV Neutrino Beam*, Phys. Rev. Lett. **102**, 101802 (2009), arXiv:0812.2243 [hep-ex].

[140] V. G. Sinitsyna, M. Masip and V. Y. Sinitsyna, *Proceedings, 17th International Symposium on Very High Energy Cosmic Ray Interactions (ISVHECRI 2012)*, EPJ Web Conf. **52**, 09010 (2013).

[141] S. N. Gninenko, *The MiniBooNE anomaly and heavy neutrino decay*, Phys. Rev. Lett. **103**, 241802 (2009), arXiv:0902.3802 [hep-ph].

[142] W. Greiner and B. Muller, *Gauge theory of weak interactions*, Berlin, Germany: Springer (1993) 308 p. (Theoretical physics, 5)(1993).

[143] R. Kleiss, W. J. Stirling and S. Ellis, *A New Monte Carlo Treatment of Multiparticle Phase Space at High-energies*, Comput.Phys.Commun. **40**, 359 (1986).

[144] A. Vaitaitis *et al.* (NuTeV, E815), *Search for neutral heavy leptons in a high-energy neutrino beam*, Phys. Rev. Lett. **83**, 4943 (1999), arXiv:hep-ex/9908011 [hep-ex].

[145] P. Vilain *et al.* (CHARM II), *Search for heavy isosinglet neutrinos*, Phys. Lett. **B343**, 453 (1995), [Phys. Lett.B351,387(1995)].

[146] A. M. Cooper-Sarkar *et al.* (WA66), *Search for Heavy Neutrino Decays in the BEBC Beam Dump Experiment*, Phys. Lett. **B160**, 207 (1985).

[147] A. Aguilar-Arevalo *et al.* (LSND), *Evidence for neutrino oscillations from the observation of anti-neutrino(electron) appearance in a anti-neutrino(muon) beam*, Phys. Rev. **D64**, 112007 (2001), arXiv:hep-ex/0104049 [hep-ex].

[148] H. Chen *et al.* (MicroBooNE), *Proposal for a New Experiment Using the Booster and NuMI Neutrino Beamlines: MicroBooNE* (2007).

[149] V. Papavassiliou (MicroBooNE), *Proceedings, 24th International Conference on Neutrino physics and astrophysics (Neutrino 2010): Athens, Greece, June 14-19, 2010*, Nucl. Phys. Proc. Suppl. **229-232**, 472 (2012).

[150] P. W. Graham, D. E. Kaplan, S. Rajendran and P. Saraswat, *Displaced Supersymmetry*, JHEP **07**, 149 (2012), arXiv:1204.6038 [hep-ph].

[151] G. Aad *et al.* (ATLAS), *Search for nonpointing and delayed photons in the diphoton and missing transverse momentum final state in 8 TeV pp collisions at the LHC using the ATLAS detector*, Phys. Rev. **D90**, 112005 (2014), arXiv:1409.5542 [hep-ex].

[152] Y. Cui and B. Shuve, *Probing Baryogenesis with Displaced Vertices at the LHC*, JHEP **02**, 049 (2015), arXiv:1409.6729 [hep-ph].

[153] J. Peressutti, O. Sampayo and J. I. Aranda, *Signatures for Majorana neutrinos in e- gamma collider*, Phys.Rev. **D64**, 073007 (2001), arXiv:hep-ph/0105162 [hep-ph].

[154] J. Peressutti and O. Sampayo, *Signals for Majorana neutrinos in a gamma gamma collider*, Phys.Rev. **D67**, 017302 (2003), arXiv:hep-ph/0211355 [hep-ph].

[155] J. Peressutti, I. Romero and O. A. Sampayo, *Majorana Neutrinos Production at NLC in an Effective Approach*, Phys.Rev. **D84**, 113002 (2011), arXiv:1110.0959 [hep-ph].

[156] J. Peressutti and O. A. Sampayo, *Majorana neutrinos in e γ colliders from an effective Lagrangian approach*, Phys. Rev. **D90**, 013003 (2014).

[157] O. Bruening and M. Klein, *The Large Hadron Electron Collider*, Mod.Phys.Lett. **A28**, 1330011 (2013), arXiv:1305.2090 [physics.acc-ph].

[158] G. Ingelman and J. Rathsman, *Heavy Majorana neutrinos at e p colliders*, Z.Phys. **C60**, 243 (1993).

[159] W. Buchmuller and C. Greub, *Heavy Majorana neutrinos in electron - positron and electron - proton collisions*, Nucl.Phys. **B363**, 345 (1991).

[160] C. Blaksley, M. Blennow, F. Bonnet, P. Coloma and E. Fernandez-Martinez, *Heavy Neutrinos and Lepton Number Violation in lp Colliders*, Nucl.Phys. **B852**, 353 (2011), arXiv:1105.0308 [hep-ph].

[161] H. Liang, X.-G. He, W.-G. Ma, S.-M. Wang and R.-Y. Zhang, *Seesaw Type I and III at the LHeC*, JHEP **1009**, 023 (2010), arXiv:1006.5534 [hep-ph].

[162] A. Belyaev, N. D. Christensen and A. Pukhov, *CalcHEP 3.4 for collider physics within and beyond the Standard Model*, Comput.Phys.Commun. **184**, 1729 (2013), arXiv:1207.6082 [hep-ph].

[163] S. Bityukov and N. Krasnikov, *On the observability of a signal above background*, Nucl.Instrum.Meth. **A452**, 518 (2000).

[164] I. V. Narsky, *Estimation of upper limits using a Poisson statistic*, Nucl.Instrum.Meth. **A450**, 444 (2000), arXiv:hep-ex/9904025 [hep-ex].

[165] J. Abelleira Fernandez *et al.* (LHeC Study Group), *A Large Hadron Electron Collider at CERN: Report on the Physics and Design Concepts for Machine and Detector*, J.Phys. **G39**, 075001 (2012), arXiv:1206.2913 [physics.acc-ph].

[166] W.-Y. Keung and G. Senjanovic, *Majorana Neutrinos and the Production of the Right-handed Charged Gauge Boson*, Phys. Rev. Lett. **50**, 1427 (1983).

[167] D. A. Dicus, D. D. Karatas and P. Roy, *Lepton nonconservation at supercollider energies*, Phys. Rev. **D44**, 2033 (1991).

[168] O. Panella, M. Cannoni, C. Carimalo and Y. N. Srivastava, *Signals of heavy Majorana neutrinos at hadron colliders*, Phys. Rev. **D65**, 035005 (2002), arXiv:hep-ph/0107308 [hep-ph].

[169] S. Kovalenko, Z. Lu and I. Schmidt, *Lepton Number Violating Processes Mediated by Majorana Neutrinos at Hadron Colliders*, Phys. Rev. **D80**, 073014 (2009), arXiv:0907.2533 [hep-ph].

[170] A. Das and N. Okada, *Improved bounds on the heavy neutrino productions at the LHC*, Phys. Rev. **D93**, 033003 (2016), arXiv:1510.04790 [hep-ph].

[171] C. O. Dib and C. S. Kim, *Discovering sterile Neutrinos ligther than M_W at the LHC*, Phys. Rev. **D92**, 093009 (2015), arXiv:1509.05981 [hep-ph].

[172] E. Izaguirre and B. Shuve, *Multilepton and Lepton Jet Probes of Sub-Weak-Scale Right-Handed Neutrinos*, Phys. Rev. **D91**, 093010 (2015), arXiv:1504.02470 [hep-ph].

[173] S. Chakdar, K. Ghosh, V. Hoang, P. Q. Hung and S. Nandi, *The search for electroweak-scale right-handed neutrinos and mirror charged leptons through like-sign dilepton signals*, Phys. Rev. **D95**, 015014 (2017), arXiv:1606.08502 [hep-ph].

[174] A. Das, P. Konar and S. Majhi, *Production of Heavy neutrino in next-to-leading order QCD at the LHC and beyond*, JHEP **06**, 019 (2016), arXiv:1604.00608 [hep-ph].

[175] C. Degrande, O. Mattelaer, R. Ruiz and J. Turner, *Fully-Automated Precision Predictions for Heavy Neutrino Production Mechanisms at Hadron Colliders*, Phys. Rev. **D94**, 053002 (2016), arXiv:1602.06957 [hep-ph].

[176] P. S. B. Dev, A. Pilaftsis and U.-k. Yang, *New Production Mechanism for Heavy Neutrinos at the LHC*, Phys. Rev. Lett. **112**, 081801 (2014), arXiv:1308.2209 [hep-ph].

[177] S. Bray, J. S. Lee and A. Pilaftsis, *Heavy Majorana neutrino production at e- gamma colliders*, Phys.Lett. **B628**, 250 (2005), arXiv:hep-ph/0508077 [hep-ph].

[178] V. Khachatryan *et al.* (CMS), *Search for heavy Majorana neutrinos in $e^{\pm}e^{\pm}$+ jets and $e^{\pm}$ $\mu^{\pm}$+ jets events in proton-proton collisions at $\sqrt{s} = 8$ TeV*, JHEP **04**, 169 (2016), arXiv:1603.02248 [hep-ex].

[179] V. Khachatryan *et al.* (CMS), *Search for heavy Majorana neutrinos in $\mu^{\pm}\mu^{\pm}$+ jets events in proton-proton collisions at $\sqrt{s} = 8$ TeV*, Phys. Lett. **B748**, 144 (2015), arXiv:1501.05566 [hep-ex].

[180] G. Aad *et al.* (ATLAS), *Search for heavy Majorana neutrinos with the ATLAS detector in pp collisions at $\sqrt{s} = 8$ TeV*, JHEP **07**, 162 (2015), arXiv:1506.06020 [hep-ex].

[181] G. Aad *et al.* (ATLAS Collaboration), *Inclusive search for same-sign dilepton signatures in pp collisions at $\sqrt{s} = 7$ TeV with the ATLAS detector*, JHEP **1110**, 107 (2011), arXiv:1108.0366 [hep-ex].

[182] G. Aad *et al.* (ATLAS Collaboration), *Search for heavy neutrinos and right-handed W bosons in events with two leptons and jets in pp collisions at $\sqrt{s} = 7$ TeV with the ATLAS detector*, Eur.Phys.J. **C72**, 2056 (2012), arXiv:1203.5420 [hep-ex].

[183] C. O. Dib, C. S. Kim, K. Wang and J. Zhang, *Distinguishing Dirac/Majorana Sterile Neutrinos at the LHC*, Phys. Rev. **D94**, 013005 (2016), arXiv:1605.01123 [hep-ph].

[184] D. G. Cerdeño, V. Martín-Lozano and O. Seto, *Displaced vertices and long-lived charged particles in the NMSSM with right-handed sneutrinos*, JHEP **05**, 035 (2014), arXiv:1311.7260 [hep-ph].

[185] A. Blondel, E. Graverini, N. Serra and M. Shaposhnikov (FCC-ee study Team), *Proceedings, 37th International Conference on High Energy Physics (ICHEP 2014): Valencia, Spain, July 2-9, 2014*, Nucl. Part. Phys. Proc. **273-275**, 1883 (2016), arXiv:1411.5230 [hep-ex].

[186] V. Khachatryan *et al.* (CMS), *Search for supersymmetry in events with a photon, a lepton, and missing transverse momentum in pp collisions at $\sqrt{s} = 8$ TeV*, Phys. Lett. **B757**, 6 (2016), arXiv:1508.01218 [hep-ex].

[187] B. Shuve and M. E. Peskin, *Revision of the LHCb Limit on Majorana Neutrinos*, Phys. Rev. **D94**, 113007 (2016), arXiv:1607.04258 [hep-ph].

[188] G. Cvetic and C. S. Kim, *Rare decays of B mesons via on-shell sterile neutrinos*, Phys. Rev. **D94**, 053001 (2016), arXiv:1606.04140 [hep-ph].

[189] D. Milanes, N. Quintero and C. E. Vera, *Sensitivity to Majorana neutrinos in $\Delta L = 2$ decays of B_c meson at LHCb*, Phys. Rev. **D93**, 094026 (2016), arXiv:1604.03177 [hep-ph].

[190] S. Mandal and N. Sinha, *Favoured B_c Decay modes to search for a Majorana neutrino*, Phys. Rev. **D94**, 033001 (2016), arXiv:1602.09112 [hep-ph].

[191] C. Dib and C. S. Kim, *Remarks on the lifetime of sterile neutrinos and the effect on detection of rare meson decays $M^+ \to M' - \ell^+\ell^+$*, Phys. Rev. **D89**, 077301 (2014), arXiv:1403.1985 [hep-ph].

[192] V. Khachatryan *et al.* (CMS), *Search for Displaced Supersymmetry in events with an electron and a muon with large impact parameters*, Phys. Rev. Lett. **114**, 061801 (2015), arXiv:1409.4789 [hep-ex].

[193] V. Khachatryan *et al.* (CMS), *Search for long-lived particles that decay into final states containing two electrons or two muons in proton-proton collisions at $\sqrt{s} = 8$ TeV*, Phys. Rev. **D91**, 052012 (2015), arXiv:1411.6977 [hep-ex].

[194] G. Aad *et al.* (ATLAS), *Proceedings, Meeting of the APS Division of Particles and Fields (DPF 2015): Ann Arbor, Michigan, USA, 4-8 Aug 2015*, Phys. Rev. **D92**, 012010 (2015), arXiv:1504.03634 [hep-ex].

[195] J. A. Evans and J. Shelton, *Long-Lived Staus and Displaced Leptons at the LHC*, JHEP **04**, 056 (2016), arXiv:1601.01326 [hep-ph].

[196] N. Nikiforou, *Search for Non-Pointing Photons in the Diphoton and Missing Transverse Energy Final State in 7 TeV pp Collisions Using the ATLAS Detector*, Ph.D. thesis, Columbia U. (2014-02-26), `http://inspirehep.net/record/1296368/files/594721125_CERN-THESIS-2014-011.pdf`

[197] M. G. Aartsen *et al.* (IceCube), *Observation of High-Energy Astrophysical Neutrinos in Three Years of IceCube Data*, Phys. Rev. Lett. **113**, 101101 (2014), arXiv:1405.5303 [astro-ph.HE].

[198] M. G. Aartsen *et al.* (IceCube), *Search for Astrophysical Tau Neutrinos in Three Years of IceCube Data*, Phys. Rev. **D93**, 022001 (2016), arXiv:1509.06212 [astro-ph.HE].

[199] G. Mention, M. Fechner, T. Lasserre, T. A. Mueller, D. Lhuillier, M. Cribier and A. Letourneau, *The Reactor Antineutrino Anomaly*, Phys. Rev. **D83**, 073006 (2011), arXiv:1101.2755 [hep-ex].

[200] M. G. Aartsen *et al.* (IceCube), *Searches for Sterile Neutrinos with the IceCube Detector*, Phys. Rev. Lett. **117**, 071801 (2016), arXiv:1605.01990 [hep-ex].

[201] H. Nunokawa, O. L. G. Peres and R. Zukanovich Funchal, *Probing the LSND mass scale and four neutrino scenarios with a neutrino telescope*, Phys. Lett. **B562**, 279 (2003), arXiv:hep-ph/0302039 [hep-ph].

[202] J. Kopp, P. A. N. Machado, M. Maltoni and T. Schwetz, *Sterile Neutrino Oscillations: The Global Picture*, JHEP **05**, 050 (2013), arXiv:1303.3011 [hep-ph].

[203] G. H. Collin, C. A. Argüelles, J. M. Conrad and M. H. Shaevitz, *First Constraints on the Complete Neutrino Mixing Matrix with a Sterile Neutrino*, Phys. Rev. Lett. **117**, 221801 (2016), arXiv:1607.00011 [hep-ph].

[204] M. G. Aartsen *et al.* (IceCube), *Flavor Ratio of Astrophysical Neutrinos above 35 TeV in IceCube*, Phys. Rev. Lett. **114**, 171102 (2015), arXiv:1502.03376 [astro-ph.HE].

[205] M. G. Aartsen *et al.* (IceCube), *A combined maximum-likelihood analysis of the high-energy astrophysical neutrino flux measured with IceCube*, Astrophys. J. **809**, 98 (2015), arXiv:1507.03991 [astro-ph.HE].

[206] M. Re Fiorentin, V. Niro and N. Fornengo, *A consistent model for leptogenesis, dark matter and the IceCube signal*, JHEP **11**, 022 (2016), arXiv:1606.04445 [hep-ph].

[207] P. S. B. Dev, D. Kazanas, R. N. Mohapatra, V. L. Teplitz and Y. Zhang, *Heavy right-handed neutrino dark matter and PeV neutrinos at IceCube*, JCAP **1608**, 034 (2016), arXiv:1606.04517 [hep-ph].

[208] M. Chianese and A. Merle, *A Consistent Theory of Decaying Dark Matter Connecting IceCube to the Sesame Street* (2016), arXiv:1607.05283 [hep-ph].

[209] S. M. Boucenna, M. Chianese, G. Mangano, G. Miele, S. Morisi, O. Pisanti and E. Vitagliano, *Decaying Leptophilic Dark Matter at IceCube*, JCAP **1512**, 055 (2015), arXiv:1507.01000 [hep-ph].

[210] M. C. Gonzalez-Garcia, M. Maltoni, I. Martinez-Soler and N. Song, *Non-standard neutrino interactions in the Earth and the flavor of astrophysical neutrinos*, Astropart. Phys. **84**, 15 (2016), arXiv:1605.08055 [hep-ph].

[211] A. Esmaili, F. Halzen and O. L. G. Peres, *Exploring $\nu_\tau - \nu_s$ mixing with cascade events in DeepCore*, JCAP **1307**, 048 (2013), arXiv:1303.3294 [hep-ph].

[212] M. M. Reynoso, I. Romero and O. A. Sampayo, *Excited neutrino production by ultrahigh energy neutrinos traversing the Earth*, Phys. Rev. **D86**, 113012 (2012).

[213] M. M. Reynoso, I. Romero and O. A. Sampayo, *Leptoquark effects on ν_τ propagation in the Earth*, Eur. Phys. J. **C73**, 2417 (2013).

[214] M. M. Reynoso and O. A. Sampayo, *Propagation of high-energy neutrinos in a background of ultralight scalar dark matter*, Astropart. Phys. **82**, 10 (2016), arXiv:1605.09671 [hep-ph].

[215] T. K. Gaisser, *Cosmic rays and particle physics*, Cambridge, UK: Univ. Pr. 279 p(1990), http://www.cambridge.org/uk/catalogue/catalogue.asp?isbn=0521326672.

[216] S. I. Dutta, M. H. Reno and I. Sarcevic, *Tau neutrinos underground: Signals of muon-neutrino —> tau neutrino oscillations with extragalactic neutrinos*, Phys. Rev. **D62**, 123001 (2000), arXiv:hep-ph/0005310 [hep-ph].

[217] A. Nicolaidis and A. Taramopoulos, *Shadowing of ultrahigh-energy neutrinos*, Phys. Lett. **B386**, 211 (1996), arXiv:hep-ph/9603382 [hep-ph].

[218] M. M. Reynoso and O. A. Sampayo, *On neutrino absorption tomography of the earth*, Astropart. Phys. **21**, 315 (2004), arXiv:hep-ph/0401102 [hep-ph].

[219] J. Kwiecinski, A. D. Martin and A. M. Stasto, *Penetration of the earth by ultrahigh-energy neutrinos predicted by low x QCD*, Phys. Rev. **D59**, 093002 (1999), arXiv:astro-ph/9812262 [astro-ph].

[220] A. M. Dziewonski and D. L. Anderson, *Preliminary reference Earth model*, Physics of the Earth and Planetary Interiors **25**, 297 (1981), ISSN 0031-9201, http://www.sciencedirect.com/science/article/pii/0031920181900467.

[221] P. Jain, S. Kar, D. W. McKay, S. Panda and J. P. Ralston, *Angular dependence of neutrino flux in KM**3 detectors in low scale gravity models*, Phys. Rev. **D66**, 065018 (2002), arXiv:hep-ph/0205052 [hep-ph].

[222] S. Iyer, M. H. Reno and I. Sarcevic, *Searching for muon-neutrino —> tau-neutrino oscillations with extragalactic neutrinos*, Phys. Rev. **D61**, 053003 (2000), arXiv:hep-ph/9909393 [hep-ph].

[223] M. Spurio (KM3NeT), *Proceedings, 3rd Roma International Conference on Astro-Particle Physics (RICAP 11)*, Nucl. Instrum. Meth. **A692**, 53 (2012).

[224] F. Di Capuafor the KM3NeT Collaboration, *Proceedings, 24th Conference on High Energy Physics (IFAE 2015): Rome, Italy, April 8-10, 2015*, Nuovo Cim. **C39**, 241 (2016).

[225] P. Piattelli, *Proceedings, 34th International Cosmic Ray Conference (ICRC 2015): The Hague, The Netherlands, July 30-August 6, 2015*, PoS **ICRC2015**, 1158 (2016).

[226] A. V. Avrorin *et al.*, *Proceedings, 3rd Roma International Conference on Astro-Particle Physics (RICAP 11)*, Nucl. Instrum. Meth. **A692**, 46 (2012).

[227] B. Shaybonov, *Proceedings, 34th International Cosmic Ray Conference (ICRC 2015): The Hague, The Netherlands, July 30-August 6, 2015*, PoS **ICRC2015**, 1165 (2016).

[228] A. Alloul, N. D. Christensen, C. Degrande, C. Duhr and B. Fuks, *FeynRules 2.0 - A complete toolbox for tree-level phenomenology*, Comput. Phys. Commun. **185**, 2250 (2014), arXiv:1310.1921 [hep-ph].

[229] C. Degrande, C. Duhr, B. Fuks, D. Grellscheid, O. Mattelaer and T. Reiter, *UFO - The Universal FeynRules Output*, Comput. Phys. Commun. **183**, 1201 (2012), arXiv:1108.2040 [hep-ph].

[230] J. Alwall, R. Frederix, S. Frixione, V. Hirschi, F. Maltoni, O. Mattelaer, H. S. Shao, T. Stelzer, P. Torrielli and M. Zaro, *The automated computation of tree-level and next-to-leading order differential cross sections, and their matching to parton shower simulations*, JHEP **07**, 079 (2014), arXiv:1405.0301 [hep-ph].

[231] T. Sjöstrand, S. Ask, J. R. Christiansen, R. Corke, N. Desai, P. Ilten, S. Mrenna, S. Prestel, C. O. Rasmussen and P. Z. Skands, *An Introduction to PYTHIA 8.2*, Comput. Phys. Commun. **191**, 159 (2015), arXiv:1410.3012 [hep-ph].

[232] T. Sjostrand, S. Mrenna and P. Z. Skands, *PYTHIA 6.4 Physics and Manual*, JHEP **05**, 026 (2006), arXiv:hep-ph/0603175 [hep-ph].

[233] C. F. Uhlemann and N. Kauer, *Narrow-width approximation accuracy*, Nucl. Phys. **B814**, 195 (2009), arXiv:0807.4112 [hep-ph].

[234] T. Han, *Physics in D >= 4. Proceedings, Theoretical Advanced Study Institute in elementary particle physics, TASI 2004, Boulder, USA, June 6-July 2, 2004*, 407 (2005), arXiv:hep-ph/0508097 [hep-ph].

[235] V. D. Barger and R. J. N. Phillips, *Collider Physics*, Redwood City, USA: Addison-Wesley, Frontiers in Physics **71**, 592 (1987).

[236] H. L. Lai, J. Huston, S. Kuhlmann, J. Morfin, F. I. Olness, J. F. Owens, J. Pumplin and W. K. Tung (CTEQ), *Global QCD analysis of parton structure of the nucleon: CTEQ5 parton distributions*, Eur. Phys. J. **C12**, 375 (2000), arXiv:hep-ph/9903282 [hep-ph].

[237] V. D. Barger, A. D. Martin and R. J. N. Phillips, *11th International Symposium on Lepton and Photon Interactions at High Energies Ithaca, New York, August 4-9, 1983*, Z. Phys. **C21**, 99 (1983).

[238] F. Halzen, *Astroparticle physics with high energy neutrinos: from amanda to icecube*, Eur. Phys. J. **C46**, 669 (2006), arXiv:astro-ph/0602132 [astro-ph].

[239] J. W. Cronin, S. P. Swordy and T. K. Gaisser, *Cosmic rays at the energy frontier*, Sci. Am. **276**, 32 (1997).

[240] E. Waxman and J. N. Bahcall, *High-energy neutrinos from astrophysical sources: An Upper bound*, Phys. Rev. **D59**, 023002 (1999), arXiv:hep-ph/9807282 [hep-ph].

[241] J. N. Bahcall and E. Waxman, *High-energy astrophysical neutrinos: The Upper bound is robust*, Phys. Rev. **D64**, 023002 (2001), arXiv:hep-ph/9902383 [hep-ph].

[242] K. Greisen, *End to the cosmic ray spectrum?*, Phys. Rev. Lett. **16**, 748 (1966).

[243] G. T. Zatsepin and V. A. Kuzmin, *Upper limit of the spectrum of cosmic rays*, JETP Lett. **4**, 78 (1966), [Pisma Zh. Eksp. Teor. Fiz.4,114(1966)].

[244] V. S. Berezinsky and G. T. Zatsepin, *Cosmic neutrinos of superhigh energy*, Yad. Fiz. **11**, 200 (1970).

[245] E. Reya and J. Rodiger, *Signatures of cosmic tau-neutrinos*, Phys. Rev. **D72**, 053004 (2005), arXiv:hep-ph/0505218 [hep-ph].

[246] U. F. Katz and C. Spiering, *High-Energy Neutrino Astrophysics: Status and Perspectives*, Prog. Part. Nucl. Phys. **67**, 651 (2012), arXiv:1111.0507 [astro-ph.HE].

[247] D. F. Cowen (IceCube), *TeV particle astrophysics. Proceedings, 2nd Workshop, Madison, USA, August 28-31, 2006*, J. Phys. Conf. Ser. **60**, 227 (2007).